**FIRAT UNIVERSITY**
**GRADUATE SCHOOL OF NATURAL AND APPLIED SCIENCES**
**TÜRKİYE**

# SYNTHESIS, THERMAL AND ELECTROCHEMICAL PROPERTIES OF 2-MERCAPTOBENZOTHIAZOLE AND 8-HYDROXYQUINOLINE, AND 4-HYDROXYPHENYLACETAMIDE SUBSTITUTED PHTHALOCYANINE COMPLEXES

**Othman Abdulrahman Hamad JUKL**

Doctoral Thesis

DEPARTMENT OF CHEMISTRY

OCTOBER 2024

**FIRAT UNIVERSITY**
**GRADUATE SCHOOL OF NATURAL AND APPLIED SCIENCES**
**TÜRKİYE**

Department of Chemistry

Doctoral Thesis

# SYNTHESIS, THERMAL AND ELECTROCHEMICAL PROPERTIES OF 2-MERCAPTOBENZOTHIAZOLE AND 8- HYDROXYQUINOLINE, AND 4-HYDROXYPHENYLACETAMIDE SUBSTITUTED PHTHALOCYANINE COMPLEXES

Author
**Othman Abdulrahman Hamad JUKL**

Supervisor
Prof. Dr. Sinan SAYDAM

OCTOBER 2024
ELAZIG

**FIRAT UNIVERSITY**
**GRADUATE SCHOOL OF NATURAL AND APPLIED SCIENCES**
**TÜRKİYE**

Department of Chemistry

Doctoral Thesis

| | |
|---|---|
| Title: | Synthesis, Thermal and Electrochemical Properties of 2-Mercaptobenzothiazole and 8- Hydroxyquinoline, and 4-Hydroxyphenylacetamide Substituted Phthalocyanine Complexes |
| Author: | Othman Abdulrahman Hamad JUKL |
| Submission Date: | 01 September 2024 |
| Defense Date: | 03 October 2024 |

# THESIS APPROVAL

This thesis, which was prepared according to the thesis writing rules of the Graduate School of Natural and Applied Sciences, Fırat University, was evaluated by the committee members who have signed the following signatures and was unanimously approved after the defense exam made open to the academic audience.

*Signature*

| | | |
|---|---|---|
| Supervisor: | Prof. Dr. Sinan SAYDAM<br>Firat University, Faculty of Science | Approved |
| Chair: | Prof. Dr. Dursun ÖZER<br>Fırat University, Faculty of Engineering | Approved |
| Member: | Prof. Dr. Mustafa SÜLÜ<br>Inönü University, Faculty of Science and Arts | Approved |
| Member: | Prof. Dr. Ahmet Orhan GÖRGÜLÜ<br>Marmara University, Faculty of Science | Approved |
| Member: | Assoc. Prof. Dr. Kenan KORAN<br>Fırat University, Faculty of Science | Approved |

This thesis was approved by the Administrative Board of the Graduate School on

..... / ..... / 20 .....

*Signature*

Prof. Dr. Burhan ERGEN
Director of the Graduate School

# DECLARATION

I hereby declare that I wrote this Doctoral Thesis titled “Synthesis, Thermal and Electrochemical Properties of 2-Mercaptobenzothiazole and 8- Hydroxyquinoline, and 4-Hydroxyphenylacetamide Substituted Phthalocyanine Complexes” in consistent with the thesis writing guide of the Graduate School of Natural and Applied Sciences, Firat University. I also declare that all information in it is correct, that I acted according to scientific ethics in producing and presenting the findings, cited all the references I used, express all institutions or organizations or persons who supported the thesis financially. I have never used the data and information I provide here in order to get a degree in any way.

03 October 2024

**Othman Abdulrahman Hamad JUKL**

# PREFACE

Phthalocyanines are a class of macrocyclic compounds that have a total of 18 π electrons, in the central macrocyclic ring which are spread out or delocalized. The macrocyclic ring is composed of four iminoisoindoline groups. Phthalocyanines have interesting electronic structures, remarkable stability, and physical and chemical properties, which make these compounds have the potential to be used in many different technological fields.

For everybody, writing a thesis on any topic or field is rather stressful. Being student preparing a report on the particular issue, I embraced it with difficulties, opportunities, and also got success in the end submitting the thesis.

First of all, I would like to thank almighty Allah for helping me to finish my thesis on the phthalocyanine complex we have to work on this project carefully. Nevertheless, it would not have been possible without the wonderful support of my family, so I would like to sincerely thank all of them.

Especially thanks to Prof. Dr. Sinan SAYDAM for their direction and continuous supervision, as well as for giving the required information about the project to finish it. This research would not have been only somewhat successful without his kind supervision and direction. Our discussions which are very countless helped me understand the direction and the importance of the research work. His direction and supervision helped to shape this research to be finished flawlessly at every stage of the research.

I wish to thank the staff members of the chemistry department, with special thanks to Doç. Dr. Kenan KORAN, Doç. Dr. Fatih BİRYAN and Prof. Dr. Hülya TUNCER, for the help given to me during experimental work especially thermal analysis and NMR spectrum of the samples.

Last but not least, my sincere thanks and appreciation also go to my parents, my family especially my mother, brothers and sisters, and all my friends who directly or indirectly helped me, from the beginning until the finish of the assignments.

**Othman Abdulrahman Hamad JUKL**

ELAZIG, 2024

# LIST OF CONTENTS

# ABSTRACT

## Synthesis, Thermal and Electrochemical Properties of 2-Mercaptobenzothiazole and 8- Hydroxyquinoline, and 4-Hydroxyphenylacetamide Substituted Phthalocyanine Complexes

**Othman Abdulrahman Hamad JUKL**

Doctoral Thesis

FIRAT UNIVERSITY
Graduate School of Natural and Applied Sciences

Department of Chemistry

October 2024, Page: xviii + 147

Phthalocyanines are aromatic macrocyclic compounds made up of four iminoisoindoline groups in the center of macrocycle that have a total of 18 π electrons. Phthalocyanine compounds have many interesting properties and applications because of electronic structures, high thermal stability, and physical and chemical properties, therefore these compounds have the potential to be used in several different technological fields.

In this study, 4-nitrophthalonitrile synthesized first from phthalimide and then the reaction of 2-mercaptobenzothiazole, 8-hydroxyquinoline, and 4-Hydroxyacetamitade afforded the three different new phthalonitrile ligands, namely (4-(benzo[d]thiazol-2-ylthio)phthalonitrile, 4-(quinolin-8-yloxy)phthalonitrile, and 2-(4-(3,4-dicyanophenoxy) phenyl)acetamide). Next, phthalocyanine complexes of first row transition metals synthesized from these ligands (CrPc, FePc, CoPc, NiPc, CuPc, ZnPc, and H2Pc) including unmetalled phthalocyanine compounds

Characterization of synthesized compounds performed with numerous spectroscopic methods, such as 1H NMR, 13C NMR, UV-Vis, FT-IR spectroscopy, and elemental analysis, was also used to analyze the structures of the synthesized compounds. The metal phthalocyanine complexes' UV-visible absorption spectra revealed a prominent Q band that more around 660-680 nm. Thermogravimetric (TG) and Differential Thermogravimetric (DTG) analysis revealed that phthalocyanine complexes MPc (M= Cr, Fe, Co, Ni, Cu, and Zn ) and metal-free phthalocyanines, were stable (up to 200 °C) throughout a broad temperature range (weight loss starting at 200 and more weight loss between 300-600 °C). Electrochemical properties of synthesized phthalocyanine compounds performed using cyclic (CV) and square wave (SWV)voltammetry. It was observed that all of the phthalocyanine compounds showed characteristic electrochemical redox waves of the central macrocyclic ring and in the case of redox-active metal phthalocyanine complexes showed the additional redox wave representing metal oxidation and reduction. Generally, phthalocyanine rings have four reductions and two oxidation potentials in the electrochemical windows of the solvent. In most cases we have observed all of the redox potentials of the phthalocyanine complexes in DMF and reported ferrocene/ferrocenium sudo reference electrode.

**Keywords:** Phthalocyanine, 2-Mercaptobenzothiazole, 8-Hydroxyquinoline, 4-Hydroxyphenylacetamide, Thermal Analysis, and Electrochemistry.

# ÖZET

## 2-Merkaptobenzotiyazol, 8- Hidroksikinolin ve 4-Hidroksifenilasetamid, Sübstitüe Ftalosiyanin Komplekslerinin Sentezi, Termal ve Elektrokimyasal Öezllikleri

**Othman Abdulrahman Hamad JUKL**

Doktora Tezi

FIRAT ÜNİVERSİTESİ
Fen Bilimleri Enstitüsü

Kimya Anabilim Dalı

Ekim 2024, Sayfa: xviii + 147

Ftalosiyanin bileşikleri, merkez halkada toplam 18 π elektron bulunduran dört iminoizoindolin grubundan oluşmuş aromatik makrosiklik bileşiklerdir. Ftalosiyanin bileşikleri, elektronik yapıları, yüksek termal kararlılıkları ve fiziksel ve kimyasal özellikleri sebebi ile birçok ilginç özelliğe ve uygulamalara sahip olduğu için, ftalosiyanin bileşiklerin birçok farklı teknolojik alanda kullanılma potansiyeli vardır.

Bu çalışmada, ilk önce ftalimidden çıkılarak 4-nitroftalonitril sentezi gerçekleştirildi. Takiben 4-Nitroftalonitril ile 2-merkaptobenzotiyazol, 8-hidroksikinolin ve 4-Hidroksiasetamitatın reaksiyonu sonucu, üç farklı yeni ftalonitril bilelşiği (ligandı) Sentezlendi, (4-(benzo[d]tiazol-2-iltiyo)ftalonitril, 4-(kinolin-8-iloksi)ftalonitril ve 2-(4-(3,4-disiyanofenoksi) fenil)asetamid).

Daha sonra, bu ligandlün ile birinci sıra geçiş metal tuzlarının ($Cr^{+2}$, $Fe^{+2}$, $Co^{+2}$, $Ni^{+2}$, $Cu^{+2}$, $Zn^{+2}$) susuz ortamda etkileştirilmesi ile bu metallere ait ftalosiyanin kompleksleri sentezlendi (CrPc, FePc, CoPc, NiPc, CuPc, ZnPc). Sentezlenen bileşiklerin karakterizasyonu, 1H NMR, 13C NMR, UV-Vis, FT-IR spektroskopisi ve element analizi gibi enstrümental analiz yöntemleri gerçekleştirildi.

Metal ftalosiyanin komplekslerinin UV-görünür bölge absorpsiyon spektrumlarında 660-680 nm bölgesinde ftalosiyanin bileşiklerine ait karekteristik Q bandı görülmektedir. Termogravimetrik (TG) ve Diferansiyel Termogravimetrik (DTG) analizler sonuçları, ftalosiyanin komplekslerinin MPc (M: Cr, Fe, Co, Ni, Cu ve Zn) geniş bir sıcaklık aralığında (200 -600 °C) kararlı olduğunu, 200 °C'ye kadar bozunmadan kaldığını ortaya koymuştur. Sentezlenen ftalosiyanin bileşiklerinin elektrokimyasal özellikleri, dönüşümlü (CV) ve kare dalga (SWV) voltametre kullanılarak gerçekleştirildi. Sentezlenen bütün ftalosiyanin bileşiklerinin Merkez aromatik makrosiklik halkaya ait karakteristik elektrokimyasal redoks dalgalarını gösterdiği ve redoks aktif metal ftalosiyanin komplekslerinde ise metale ait yükseltgenme ve indirgenme reaksiyonlarına ait ek redoks dalgaları da gözlenmiştir. Genel olarak, ftalosiyanin bileşikleri çözücünün elektrokimyasal pencere aralığına bağlı olarak dört indirgenme ve iki oksidasyon potansiyeline sahiptir. Sentezlenmiş olan ftalosiyanin bileşiklerinin biri hariç DMF'deki ftalosiyanin komplekslerine ait dört indirgenme potansiyelleri gözlenirken, iki kompleks hariç oksidasyon potensiyelleri gözlenmiş ve ferrosen/ferrosenyum sudo referans elektroduna karşı rapor edilmiştir.

**Anahtar Kelimeler:** Ftalosiyanin, 2-Merckaptobenzotiyazol, 8-Hydroksikinolin, 4-Hidroksifenilasetamid, Termal Analiz, Elektrokimya.

# LIST OF FIGURES

Page

# LIST OF TABLES

# LIST OF APPENDICES

# SYMBOLS AND ABBREVIATIONS

## Abbreviations

Pc : Phthalocyanine
Pcs : Phthalocyanines
DBPC : 2,6-di-tert-butyl-p-cresol
DMSO : Dimethyl sulfoxide
Pc : Phthalocyanine
Pcs : Phthalocyanines
CrPc : Chrome phthalocyanine
FePc : Iron phthalocyanine
$Fc/Fc^{+}$ : Ferrocene/Ferrocenium ion
CuPc : Copper phthalocyanine
ZnPc : Zinc phthalocyanine
CoPc : Cobalt phthalocyanine
NiPc : Nickel phthalocyanine
$H_2Pc$ : Metal free phthalocyanine
MPc : Metal phthalocyanine
NPN : Nitro phthalonitrile
NIR : Near Infrared
PDT : Photodynamic therapy
DMF : Dimethylformamide
DMSO : Dimethyl sulfoxide
THF : Tetrahydrofuran
DBN : 1,8-diazabicyclo-5-ene
DBU : 1,8-diazabicyclo(5,4,0)undec-7-ene
FT-IR : Fourier-transform infrared spectroscopy
UV-vis : Ultraviolet visible spectroscopy
NMR : Nuclear magnetic resonance
HOMO : Highest occupied molecular orbital
LUMO : Lowest unoccupied molecular orbital
DSSCs : Dye-sensitized solar cells
CV : Cyclic voltammetry
SWV : Square wave voltammetry
DTG : Differential Thermogravimitric analysis
TG : Thermogravimetric analysis
TBAFB : Tetra butyl ammonium tetrafluoroborate
GC : Glassy carbon
M. Wt. : Molecular weight
cm : Centimeter
L : Litter
nm : Nanometre
mL : Milliliter
g : Gram
mol : Mole
h : Hour
°C : Celsius, Degree Centigrade

PS : Photosensitizer
SPc : Superphthalocyanine
SubPc : Subphthalocyanines
Re : Reduction
Ox : Oxidation
Mr : Metal Reduction
Mo : Metal Oxidation

# 1. INTRODUCTION

In navigating the vast landscape of phthalocyanine research, there are a variety of objectives. The aim of this research is to synthesize novel phthalocyanine complexes and investigate thermal, spectroscopic, and electrochemical properties that contribute to scientific knowledge. This involves the synthesis of new phthalocyanine compounds, and characterization fundamentals, and helps to find new applications field of technology.

## 1.1. Coordination Compound

One of the most stunning and fascinating features of chemistry, is coordination chemistry, in particular, the spectrum of colors that compounds may have [1]. Coordination chemistry has a wide range of applications in various fields, including chemistry and industry. They are essential in catalysis, materials science, and the study of many biological processes. Additionally, many brightly colored compounds and pigments are coordination complexes, making them of interest in the field of dyes and pigments. Throughout medical history, metal-based coordination compounds have been utilized to treat a wide range of illnesses, including cancer [2]. Therefore this section will discuss the metal-ligand bonding, coordination compounds, and coordination geometries [3, 4].

Coordination compounds, also known as coordination complexes, are classes of compounds in chemistry that consist of a central metal atom or ion bonded to surrounding molecules or ions, known as ligands [5]. Ligands have one or more lone pairs of electrons that can be donated to the metal atom, forming coordinate covalent bonds. Ligands can be classified as monodentate, bidentate, or polydentate [6]. The arrangement of ligands around the central metal atom is described by the coordination geometries, which include octahedral, tetrahedral, square planar, and more [7-9]. Depending on the charges of the central atom and the ligands, the coordinated species may have a positive, neutral, or negative charge. The total number of ligands bonded to the metal atom is referred to as the coordination number [10]. The coordination number of the central metal atom is the number of bonds it forms with the ligands, the common coordination numbers include 4, 6, and 8. [7].

Around the start of the 18$^{th}$ century, the renowned painter Diesbach developed the first coordination compound which is known as Prussian blue or $KFe[Fe(CN)_6]$. Different oxidation state forms a distinct geometric shape, such as a tetrahedral, square planner, octahedral, etc. [11]. Alfred Werner, in 1893, provided the definitive explanation for these compounds. He proposed the idea of secondary valence, or residual valence, for the metals, suggesting that these valences exist alongside the more familiar primary valence [10].

The bonding of ligand molecules with a metal in some cases results in tension and deformation. The effects of extremely short and long bonds, as well as severe angular distortions, on reactivities, coordination complex stabilities, electronic and spectra, and reduction potentials, are analyzed using data from many concrete examples, such as cobalt(III), cobalt(II), iron(III) and iron(II) hexaamines, and copper(II) and copper(I). [12]. There are several different configurations that meet the basic geometric criteria for nitrogen to operate as a bond donor in organic and coordination compounds containing nitrogen such as Porphyrins and Phthalocyanines. The structure of Cu(II) complexes with N-heterocyclic ligands, for instance, revealed the presence of bonds of the -N=N-, -C=N-, and -C-N- types [13]. Phthalocyanines are flexible chemical dyes that may be functionalized with various kinds of substituents at their periphery or inner core to obtain cationic, anionic, or neutral ligands [14].

There are three different hypotheses that attempt to describe the characteristics of the coordinate bond. They are the crystal field theory, the valence bond theory, and the molecular orbital theory. Linus Pauling is widely credited as the creator of the valence bond theory of metal complexes. According to this model, a covalent bond forms when a ligand's pair of electrons enters the hybridized atomic orbitals of the metal [10, 15]. The molecular orbital theory is now the most prominent model for the chemical bonds.

## 1.2. Phthalocyanines Overview

Phthalocyanines (Pcs) are large organic aromatic macrocyclic compounds [16, 17] with 18π delocalized conjugate electron system [18, 19], comprising four isoindole units connected by nitrogen atoms in a two-dimensional ring structure [20, 21]. These compounds are often associated with porphyrins due to their structural resemblance, [22] possessing the basic porphyrin ring structure [23]. The chemical formula of unsubstituted phthalocyanine is ($C_{32}H_{18}N_8$) [24], shown in **Figure 1.1**.

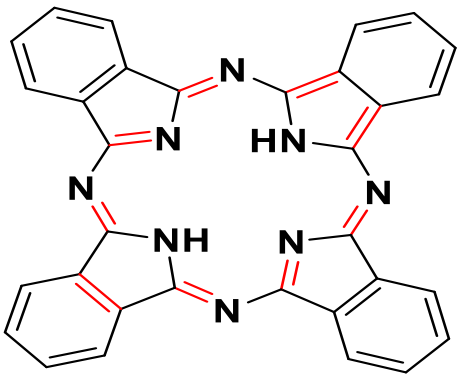


**Figure 1.1.** Phthalocyanine structure.

Pcs are large, planar systems [25] containing 16-membered (8 carbons and 8 nitrogen) molecules with a highly conjugated π-electron system [26, 27]. These nitrogen-rich, redox-active conjugated macrocycles are an important class of compounds that have a wide range of metal-based applications due to the great stability they provide to the metal ion through their rigid N4-coordination site [28]. The highly conjugated molecular structure of Pcs gives them distinctive spectra and electrical properties [29]. The core cavity of Pc can accommodate around seventy different elements, and the physical or chemical characteristics of Pc are sensitive to the nature of the core metal cation in the center of phthalocyanines [30-32]. It is well known that the variety of electron-donating and electron withdrawing substituents added to the aromatic macrocycle affect the physical and chemical characteristics of metal phthalocyanines as well as the central metal ions [33]. In recent decades, Pcs have attracted significant interest [28], as they can form coordination complexes with the vast majority of elements and typically exhibit very vivid colors. Numerous pc derivatives, most of which have a blue-green hue, have been produced, although Pc with various colors in general other than blue and green are rare [34].

Generally, Pcs are poorly soluble in many organic solvents [22, 34, 35], and have no solubility in water [36], due to their high inclination to aggregate as a consequence of interactions between their π-electron systems [34]. Once they are being aggregated, Pc molecules become very responsive to the effects of polar solvents [29]. However, it is possible to increase their solubility in a wide variety of organic solvents by substituting various groups into the Pc macrocycle at either peripheral or non-peripheral position [35, 37]. Their spectroscopic, photophysical, photochemical, and electrochemical properties that are degraded due to aggregation affected by influenced by factors such as concentration, solvent composition, substituents, metal ions, and temperature [34, 38]. Also, Pcs are employing both structural elements and pigments due to their thermal and chemical stability, increased electron transfer rate, and ring interchangeability as they are just a few of the unique features of Pcs. Some Pcs, including copper Pcs and cobalt Pcs, are named for their respective core elements, suggesting that the material's properties vary with their composition [39].

In most cases, Pcs are thermally stable up to ~400 ºC in a vacuum and are solid at room temperature. Additionally, they are resistant to strong acids [40, 41]. Diamagnetic ion complexes of phthalocyanines are considered more promising photosensitizers than their metal-free counterparts [42]. It is well-known that Pcs and porphyries are effective oxygen reduction catalysts, and may serve as low-cost alternatives to platinum [43, 44] for fuel cell applications. Furthermore, Pcs have the ability to change conductivity by adjusting the distance between hopping sites [45]. Absorption peaks at about 400 and 700 nm are quite prominent due to π to π* transitions [41, 46].

In recent years, Pcs have emerged as a critical component in a variety of emerging technologies, including photodynamic therapy, liquid crystals, solar cells, gas sensors, and electrochemical sensors [47]. The chemical, photophysical, and photochemical properties of these

materials make them useful in a wide variety of technological applications, from chemical sensors to medicinal applications including photodynamic therapy (PDT) as well as antifungal, antioxidant, and antibacterial compounds [48]. Pcs are excellent candidates for large-scale applications due to their intense absorption in the near-infrared (NIR) and red region of spectroscopic radiations, reversible redox chemistry with a large number of substituents and a metal center, and high fluorescence quantum yields [47]. Modifying the central metal atom and locations of substituents on the macrocycle ligands are well-known methods of fine-tuning the electrochemical and spectroscopic properties of phthalocyanine derivatives [49].

Since their discovery at the turn of the twentieth century, metal phthalocyanines (MPcs) have played a significant role in advancing research across scientific fields; including molecular electronics [50]. As shown in **Figure 1.2**.

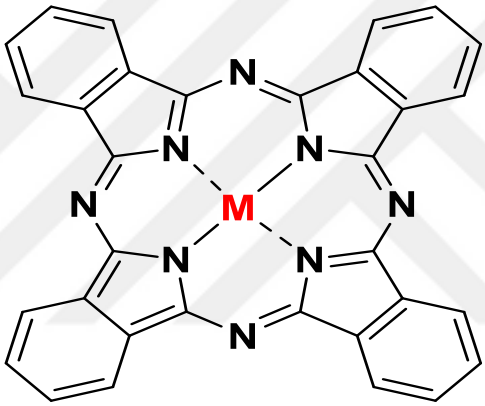


**Figure 1.2.** Metal Phthalocyanine structure.

Numerous studies have been conducted on phthalocyanine with a wide variety of metal ions and peripheral (β) and non-peripheral (α) position substituents. Binuclear double-decker, clamshell, polynuclear, and dendritic phthalocyanine have all been synthesized, and their characteristics have been described. Ball-type phthalocyanine is a relatively new form of Pcs that has received much attention in recent years [51]. In their simplest form, MPc ($C_{32}H_{18}N_8M$) consists of four isoindole groups linked by nitrogen atoms to create an 18π-electron ring structure, with two covalent connections and two coordination bond chelating a metal or metalloid core [52]. As shown in **Figure 1.3.**

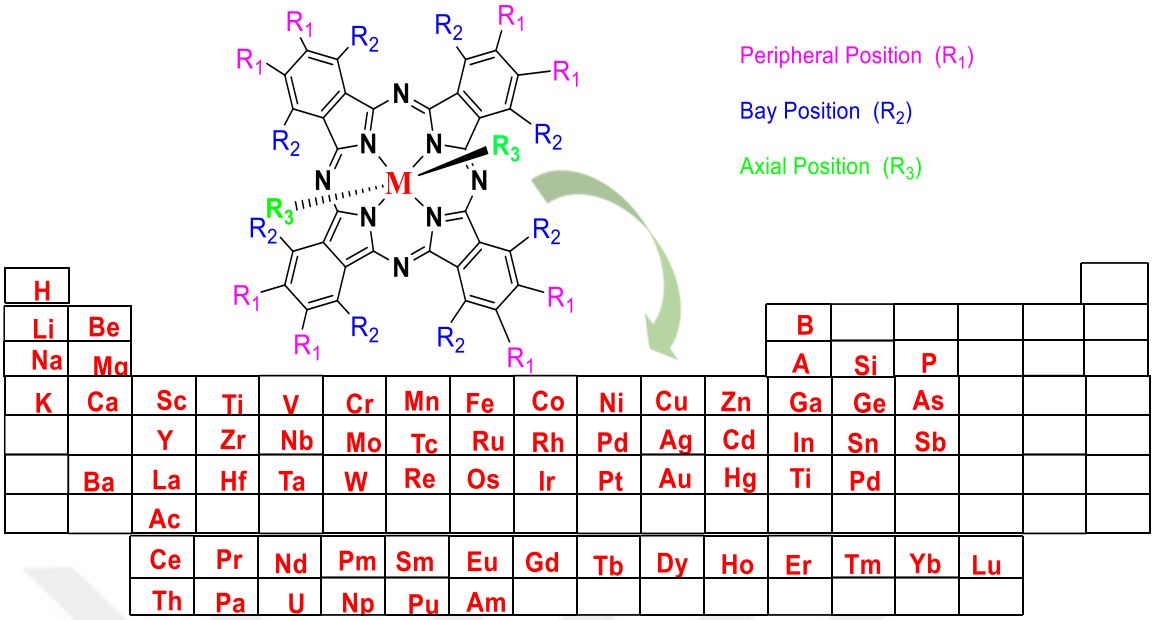


**Figure 1.3.** Schematic diagram of MPc structure with elements that form phthalocyanine complexes.

Phthalocyanines are an attractive option for the initial π-π* transition on the MPc [53], due to their high absorption, Q-band, ranging from 600 to 800 nm accounted for by a second π-π* transition, with relatively low absorption Soret band ranging from 300 to 500 nm [52, 54, 55]. The absorption spectra of MPcs are shown in **Figure 1.4 a, b**, with a strong band at 670 nm (Q-band) and a weak band near 350 nm (Soret or B-band) corresponding to the HOMO-LUMO π-π* transitions in the visible range. These structures often have high molar absorption coefficients resulting from the high degree of conjugation. The necessary electrochemical and spectroscopic traits may be achieved by modifying the Pc macro ring (α or β position), changing the central metal atom, or adding an axial ligand to the central metal atom [56].

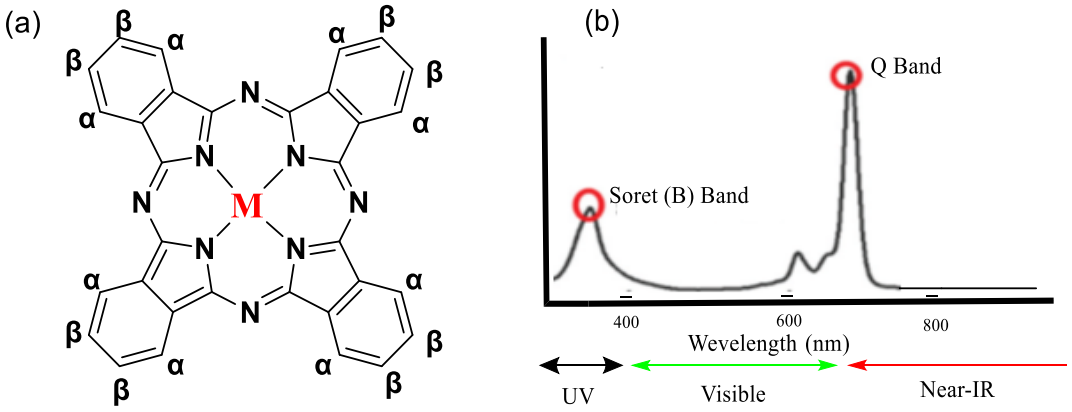


**Figure 1.4.** Molecular structure (a) and absorption spectrum (b) of MPc.

## 1.3. A Brief History of Phthalocyanine

The first synthesis of phthalocyanines started a new field of study for scientists across various fields of science [47]. The name Pc is derived from the Greek words for rock oil (naphtha) and dark blue (cyanine). Diesbach and Van Der Weid accidentally founded Pcs in the early 19$^{th}$ century [27, 57, 58], exactly discovered in 1907 [57, 59]. During the Synthesis of 2-Cyanobemzamide by heating o-dibromo benzene with copper cyanide in pyridine at 200 ºC, a blue-colored insoluble substance was produced [57, 60]. However, its structure remained unclear until at that time [27]. Twenty years later, in 1927, Disbach and his colleague successfully synthesized copper phthalocyanine from 1,2-dibromobenzene [60, 61]. Additionally, Scottish Dyes, Ltd. of Grangemouth, Scotland, synthesized a new iron Pc at around the same time. An unexpected blue-green impurity was found in phthalic anhydride and phthalimide which was produced commercially from ammonia. It was later determined that this impurity formed when phthalimide reacted with iron, resulting in a highly persistent, insoluble pigment. The structure of phthalimide is illustrated. Phthalimide structure is shown in **Figure 1.5**. Linstead and his team defined the nomenclature and structure of Pc for the first time between 1928 and 1933, as they categorized these macrocyclic compounds as a new class of organic molecules [27, 59]. Their structure was fully clarified after 1928 as they began to have economic significance. Pcs have a long history of use as pigments and dyes [58]. In 1935, an English firm began industrial production of CuPc as a blue pigment, followed by others in Germany and the United States [60].

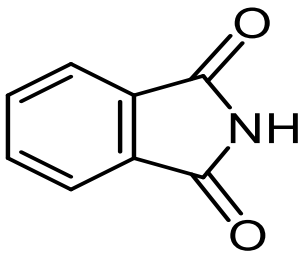


**Figure 1.5.** Phthalimide structure.

The chemical structure of Pc was fully elucidated between 1930 and 1950, During this period their X-ray spectra, absorption spectra, oxidation and reduction properties, catalytic characteristics, magnetic properties, photoconductivity, and many other physical properties were studied. This research confirmed that Pcs, like porphyrins, are highly colorful aromatic complexes with 18-π electrons [62]. Before 1960, Pcs were the only known class of synthesized macro cyclic ligands with such high conjugation [62]. However, since the late 1980s, significant advances have been made in the synthesis of low-symmetry phthalocyanine structures. The selective production of low symmetry free complexes was first described by Kobayashi et al. in 1990 [63].

## 1.4. Structure of Phthalocyanines and Nomenclature

In general, phthalocyanines have structural similarities with other macrocyclic pigments, particularly the with the porphyrin. These macrocycles are characterized by a fundamental structure made of four pyrrole like subunits connected circularly by methine or azamethine bridges, to create a ring with 16 atoms. The conjugated base of phthalocyanines ($H_2Pc$) contains pyrrole-like rings that are structurally similar to isoindole [57], as shown in **Figure 1.6**.

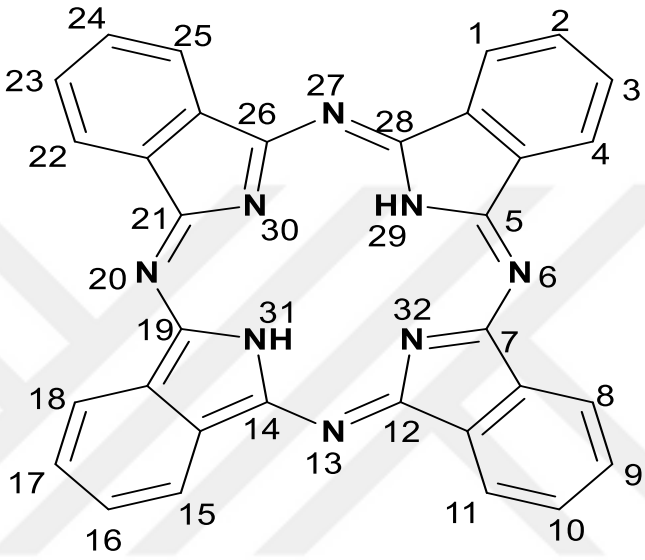


**Figure 1.6.** Structure of basic phthalocyanine with IUPAC nomenclature, reproduced from Ref.

Pcs are a type of macrocyclic compound with bivalent, tetradentate, planar, conjugated 18π electron aromatic ring structures, on the other hand, include four phenylene rings and four aza (—N=C—) groups attached to the carbon of the pyrrole unit through four aza bridges [62, 64]. As shown in **Figure 1.7.**

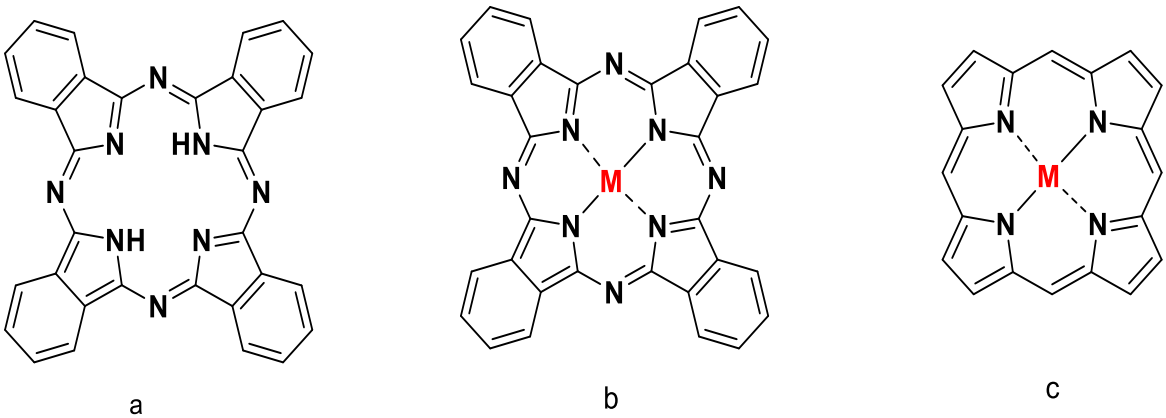


**Figure 1.7.** Metal-free phthalocyanine ($H_2Pc$) (a), metal phthalocyanine(M-Pc) (b), porphyrins (c).

Phthalocyanines, which are structurally linked to the porphyrins, are more stable than porphyrins and offer appropriate characteristics for photodynamic therapy by absorbing visible light, while porphyrins primarily absorb light around 400 nm, Pcs absorbing light at much longer wavelengths [65, 66]. The numbering and naming of Pcs is given in **Figure 1.8**.

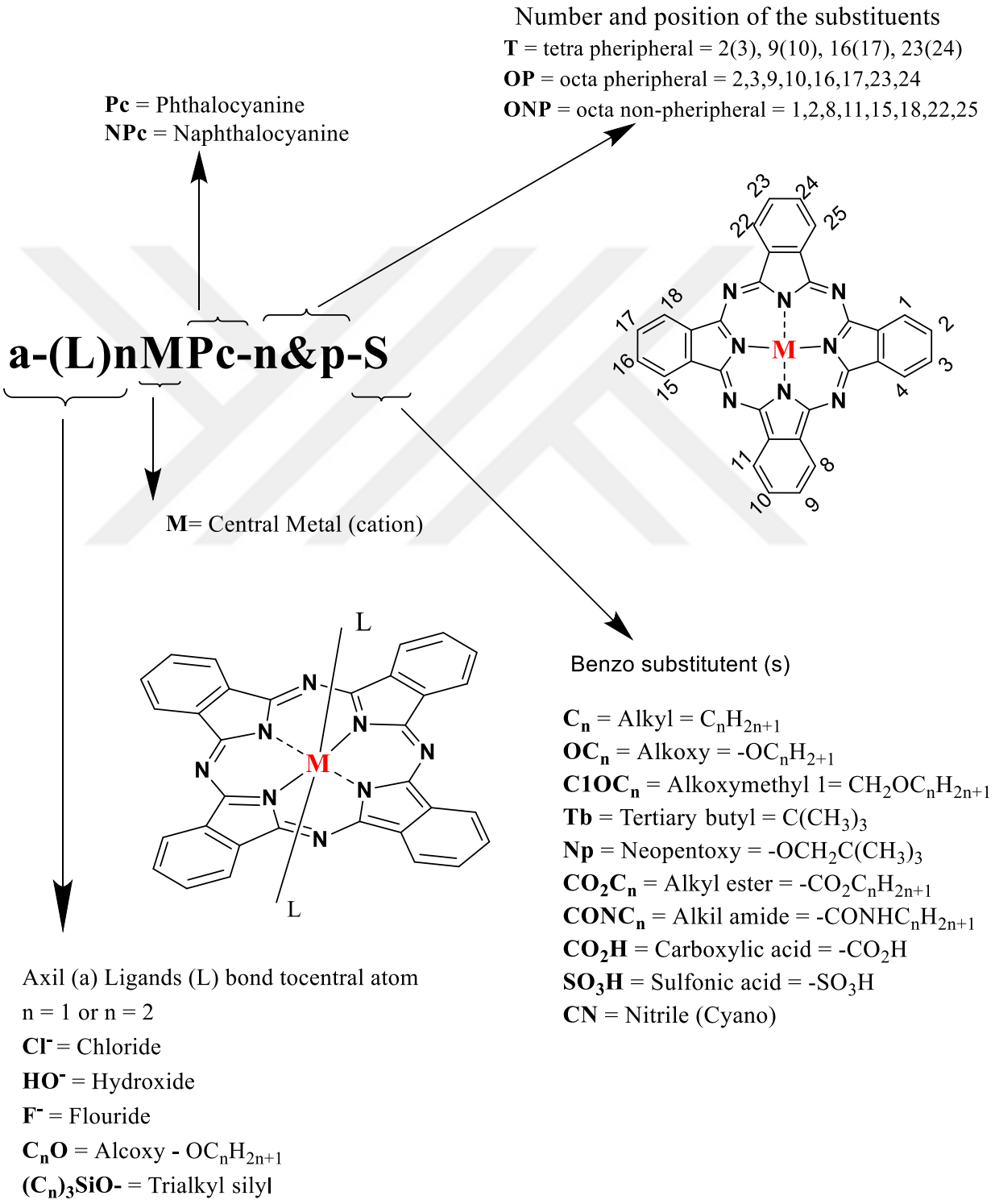


**Figure 1.8.** Notation and naming of Pcs. [62, 67].

## 1.5. Applications of Phthalocyanines.

After the synthesis of Pc complexes in the early 20th century, it has been found that there are numerous applications [29]. These complexes have been widely employed in various fields due to their excellent electronic, and physicochemical properties, as well as their stability [47, 68, 69].

The application of MPc depends on the kind of central metal present, the redox activity of that metal, and the functional groups attached to it. By introducing or removing functional groups with different excitation characteristics from the metal phthalocyanine backbone, their photochemical and photophysical properties can be altered [70, 71].

Pcs have been used in a wide range of technological, industrial, and medical applications, including chemical sensors [47, 58, 68, 72-74], biological applications [40, 68], optical data storage [26, 74], catalysts [51, 70, 71, 75-78], semiconductors [73, 79, 80], photodynamic therapy, and more [58, 74, 81]. Several investigations on the in vitro biological activities of Pcs [68, 82], including antioxidant, antibacterial, [40, 68], enzyme inhibition [68, 83], DNA interaction, and anticancer effects [68, 83], have been described [68].

In recent years, MPcs have gained significant interest due to their affordability [84], chemical and thermal stability, and ease of production [84, 85]. Their usefulness has been demonstrated in several fields, including dye solar cells [51, 84, 85], photosensitizers [27, 71, 78, 81, 86], photocatalysis [27, 53], pigment and dye production [84, 87, 88], drug delivery [83, 84], photodynamic treatment [26, 35, 81, 83, 86, 89], and catalysis [27, 53, 58, 88]. As a result of their low production costs, ease of manufacturing [84], and chemical and thermal stability [82, 84, 90]. MPcs are also used in liquid crystal materials [26, 47, 78, 91], electronic materials [53], and for coating various carbon substrates to enhance electrical conductivity and create unique active sites [92]. Notably, the use of Pcs as metal clusters in the creation of $CO_2$ electrocatalysts proved very fruitful. Copper, in particular, has been favored over other metals due to the unique ability to create valuable $C_2$ or higher carbon compounds [93].

### 1.5.1. Pigments and Dyes Applications.

There are two primary categories of colorants: dyes and pigments. A pigment is an inorganic or organic colorant that cannot be dissolved in water, while a dye is soluble in water or other solvents [61, 94]. The photophysical and photochemical properties of dyes, which are aromatic macrocycles with vivid green or blue-green hues, are of great interest [95, 96]. MPcs are an interesting and versatile family of organic functional dyes and pigments [76]. For a long time, phthalocyanines have been the go-to blue pigment for applications like road signs and bullet trains due to their low production costs, high durability, and resistance to fading. [97].

Copper phthalocyanine has been recognized as one of the most significant and earliest industrial pigments and dyes among phthalocyanines [98, 99]. This structure imparts their characteristic blue or green color [87, 100], making them particularly suitable for dyeing strong and large-sized materials. They are commonly utilized in the production of polyester fibers, polyacrylonitrile, and notably in the manufacturing of nylon. Additionally, they are employed for dyeing cellulose-based substrates such as paper and cotton [98, 99]. CuPcs also have other applications, in paints, inks, coatings, plastics, and textiles, known for their excellent lightfastness, chemical stability, and strong coloring power [87, 100]. Thus, phthalocyanine pigments are used to color the majority of blue and green automobiles, especially sports cars and vehicles. In recent years. Pcs have also found widespread usage in cutting-edge technological fields [61].

Copper phthalocyanine is inherently blue and exists in several polymorphic forms, with α and β being the most common. The metastable α form, which is a redder blue than the β form, is preferred for paints. In contrast, the stable polymorph, which is the greenish-blue β form, is ideal for inks used in labeling. Fully halogenated (often chlorinated) copper phthalocyanines are commonly used to make green pigments [61]. CuPc is depicted in **Figure 1.9**. was initially produced on an industrial scale in 1953 under the trade name Monastral blue. To enhance the brightness of the copper phthalocyanine pigment, the technique of dissolving and reprecipitating it in sulfuric acid was employed to produce α-form particles. This method increased the solubility of copper phthalocyanine derivatives that contained more than one sulfo group, as reported in the synthesis [67].

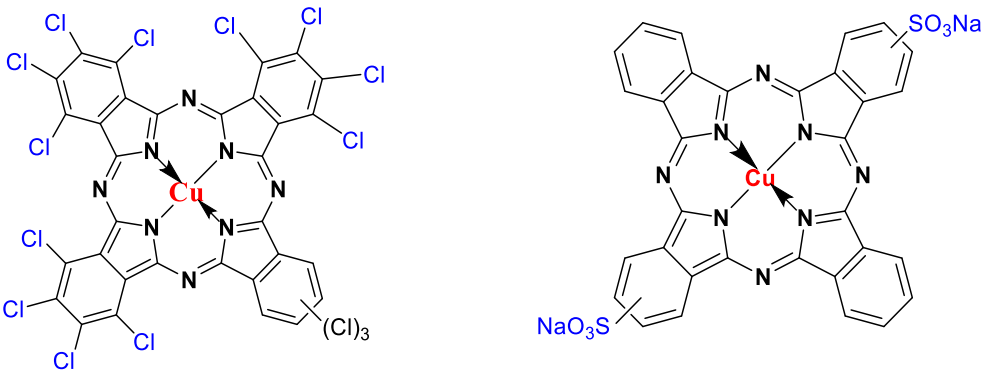


**Figure 1.9.** Copper phthalocyanine pigment and dyes.

Copper phthalocyanine pigments are commonly used in inkjet printers to produce vibrant and high-quality prints. These pigments offer several advantages that make them suitable for inkjet inks: Color Stability, Lightfastness, water fastness, and wide color gamut. It's important to note that, other pigment types such as carbon black and dyes are also utilized in ink formulations to achieve specific color requirements and performance characteristics. In the late 1980s, the first-

generation inkjet printers utilized nonstandard dyes specifically refined for inkjet printing to meet the specific requirements of early inkjet technology [26, 101]. As shown in **Figure 1.10**.

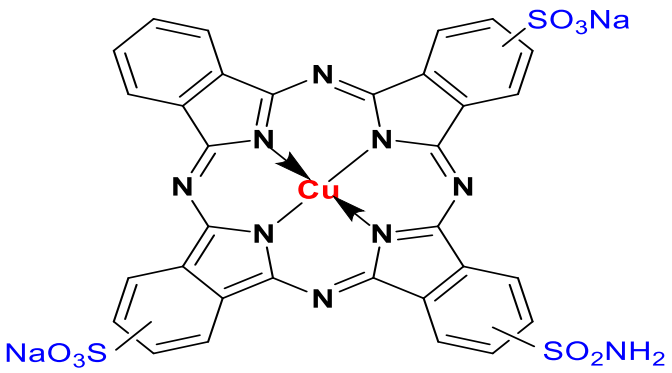


**Figure 1.10.** Copper phthalocyanine for Inkjets printers.

### 1.5.2. Electrophotography Application.

Phthalocyanine compounds have significant applications in electrophotography, the technology behind modern laser printers and photocopiers, as well as Photosensitive drum coating, charge generation layer, toner pigment, and charge transport layer [102]. They exhibit desirable electrical and optical properties, making them suitable for generating and transporting charge carriers in electrophotographic systems [103]. Phthalocyanines have been extensively used in these materials, and technologies, such as amorphous silicon, organic photoconductors, and newer generations of toner formulations, have also emerged and gained significance in this field [102].

Phthalocyanines are widely recognized for their role in laser printing and photocopying technology. They are essential chemicals in both the photoconductor and image forming processes, enabling the creation of visible images on the substrate surface. Among various types of Pcs, the titanyl oxy phthalocyanine type titanium (IV) polymorph, stands out as the most effective material for generating the latent image in modern laser printers [104] [105]. As shown in **Figure 1.11**.

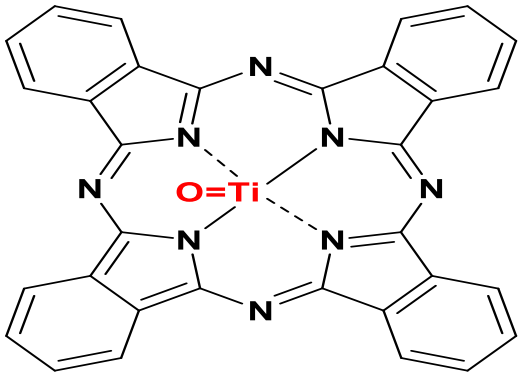


**Figure 1.11**. Titanyloxy phthalocyanine.

### 1.5.3. Optical Data Storage Applications.

Phthalocyanines have also found applications in optical data storage [26]. The optical constants of thin films provide valuable insights into the materials' microscopic characteristics, making their determination crucial. El-Nahass et al. studied the effect of film thickness on the optical absorbance of metal-free phthalocyanine ($H_2Pc$) films. Recent studies have also analyzed the impact of film thickness on the structural and optical properties of InPcCl and $Na_2Pc$ thin films. Optical phase transitions were inferred indirectly [20].

In optical computing technology, digital data is conveyed in the form of pits on the surface of an optical disk or through a circular track on the disk's surface using a laser beam. As the brightness of the reflected light from the pits varies, a low-power laser detector "reads" these pits and converts them into electrical impulses. The CD-ROM (compact disk read-only memory) format contains text, sound, and pictures; the WORM (write-once, read-many) format allows data to be saved once and read multiple times; and the latest disks are fully rewritable, representing the most up-to-date method for creating compact discs [106]. As shown in **Figure 1.12**.

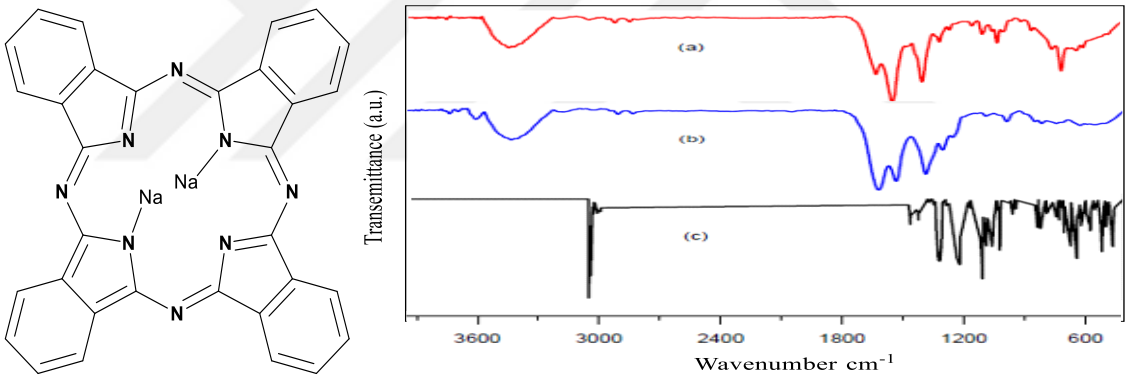


**Figure 1.12.** Schematic diagram of $Na_2Pc$ molecule and FT-IR spectra of $Na_2Pc$ (a) powder, (b) films, (c) calculated.

The optical bandgap between the HOMO and LUMO levels explains the charge transfer interaction inside the molecule. The HOMO-LUMO electronic transition energy was determined using the GGA-RPBE function and DNP basis set, as shown in **Figure 1.13**. $Na_2Pc$ has a HOMO value of 4.945 eV and a LUMO value of 3.642 eV, resulting in an energy difference of 1.303 eV. A smaller energy gap may be attributed to a stronger charge transfer interaction [20].

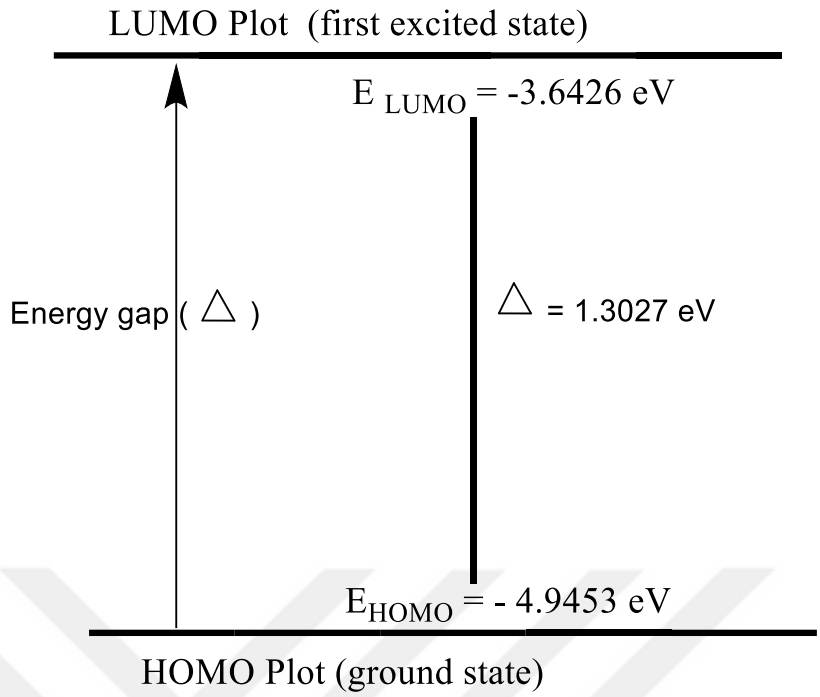


**Figure 1.13.** Frontier molcular orbital of $Na_2Pc$ molcule.

### 1.5.4. Phthalocyanines in organic light emitting devices Applications.

Phthalocyanines have gained significant attention for their applications in organic light emitting devices (OLEDs). OLEDs are a type of display technology that utilizes thin organic layers to emit light when an electric current is applied. Phthalocyanines offer several advantages as materials for OLEDs, including high stability, strong absorption in the visible spectrum, and excellent charge transport properties [107]. It is well known that phthalocyanines, such as metal-free phthalocyanine ($PcH_2$), copper phthalocyanine (PcCu), and oxo-titanium (IV) phthalocyanine ($PcTiO_3$), have excellent thermal and chemical stability, as shown in **Figure 1.14**. They undergo partial oxidation when exposed to oxidizing agents like iodine or atmospheric oxygen, with the latter causing an intrinsic doping effect [108]. This phenomenon enhances the stability and conductivity of phthalocyanines, which could be beneficial for OLEDs [107]. Pcs can also adjust conductivity by changing the number of hops between nodes. Several experiments investigating the impact of compression on the conductivity of Pc under isothermal conditions have provided convincing evidence of this phenomenon [45].

Overall, Pc provides a versatile platform for various roles in OLEDs including hole and electron transport, light emission, sensitization, and doping. Their unique properties make them promising candidates for the development of efficient and stable organic light-emitting devices [109].

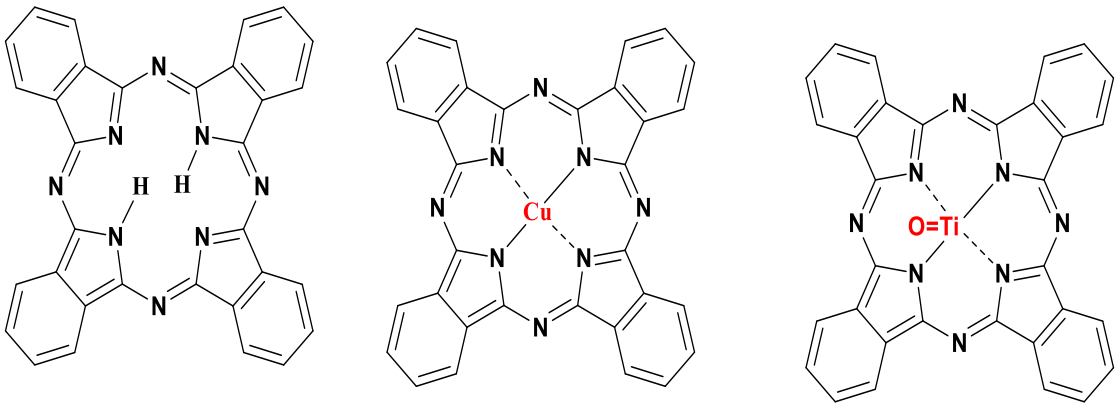


**Figure 1.14.** Constitution of phthalocyanine (1), copper phthalocyanine (2) and oxotitanium (IV) phthalocyanine (3). In the case of oxotitanium (IV) phthalocyanine, the phthalocyanine macrocycle is slightly distorted from planarity.

### 1.5.5. Non-linear Optical Devices Application.

Non-linear optical devices are a subfield focused on the behavior of non-linear media. Research into safeguarding optical sensors and the human eye from laser radiation became important after the introduction of high-intensity light sources with laser mechanisms in the 1960s. There are now several tools and resources available to help with this problem. Organic and organometallic compounds with nonlinear optical characteristics are among the most promising candidates for dampening laser light. Materials in this category include phthalocyanines, fullerenes, organometallic compounds, and porphyrins. Porphyrins and phthalocyanines are particularly valuable due to their non-linear optical characteristics, quick response times, low absorption losses, low dielectric constants, and resilience to heat and environmental conditions [32, 110].

The optical nonlinearity is determined by the characteristics of the core ion. For instance, the nonlinear absorption coefficient of europium phthalocyanine was found to be higher than that of lutetium and terbium complexes. This is because complexes with bigger core ions experienced quicker excitation and a higher population of excited states. By comparing substituted and unsubstituted versions, the effect of peripheral bromine groups on non-linear optical characteristics was determined [32, 111].

### 1.5.6. Biological Applications.

Over the past few years, several Pcs, both free-base and metallated forms, have been studied for their biological applications. Research has focused on the inactivation of microorganisms by introducing structural changes to their skeletons, such as the absence or presence of a metal or the addition of various substituents [95, 96]. Pcs are widely used due to their involvement in the metabolism of living organisms as biological pigments or biochromes [57]. Given their

pharmacological and biological uses including antioxidant, antibacterial, DNA binding/cleavage, and enzyme inhibition, researchers have concentrated on synthesizing water-soluble phthalocyanines [40]. However, the low solubility of Pcs has significantly limited their potential in the biomedical field [48, 112]. Therefore, further studies into molecular docking, enzyme inhibition, and anticancer effects are necessary to fully characterize these drug compounds [83].

It's important to note that while phthalocyanines offer various applications in biological and protein-related research [113], this interaction between phthalocyanines and proteins is complex, due to various factors, including size, charge, and specific chemical modifications. Pcs can be large and negatively charged molecules, and their size and charge of these compounds can affect their ability to enter protein globules or interact with proteins. The electrostatic repulsion between negatively charged pcs and negatively charged regions on proteins may impact their binding or penetration [114].

### 1.5.7. Photodynamic Therapy (PDT) Applications.

PDT is very effective for superficial cancer lesions because of its high precision, low toxicity to healthy cells, and low minimally invasion nature [115, 116]. In PDT, a photosensitizer (PS) sensitive to a specific wavelength range of light, typically between 700 and 800 nanometers, is used to treat cancer without the need for invasive surgery [117, 118]. The success of PDT relies on many factors, including cell culture, the quantity and distribution of photosensitizer, and eventually, photosensitizer itself. Phthalocyanines represent the next generation of safe and effective photosensitizers, distinguished by their interesting chemical structures, widespread absorption spectrum, and widespread utility [119]. The effectiveness of phthalocyanine as a sensitizer may be enhanced by modifying its substituent type and central metal atom [89, 120]. Because of its strong absorption in the red region of the visible spectrum, which may be photoactive, a heavy central atom like indium delivers a high triplet yield [86, 120]. Certain Pcs are excellent photon sources for PDT, with activation wavelengths between 670 and 690 nm and well-defined tissue penetration in target cells. Pcs have several advantageous properties, including high absorption of long-wavelength light, localization within cells, and high triplet yield, allowing them to be used safely at low concentrations [47, 81].

In recent years, researchers have explored the potential of Pcs in developing new cancer treatments with fewer side effects. It is well established that anticancer drugs can bind to DNA either covalently or noncovalently, subsequently cleaving it via nucleotide hydrolysis and DNA oxidation pathways. Phthalocyanines, due to their functional groups' strong DNA-binding abilities, are indispensable in a wide range of pharmacological and biological diagnostic applications [18, 58].

One method of PDT involves the local or systemic application of a light-sensitive photosensitizer to the affected tissue or cell [42]. In the second method, the photosensitizer is then activated by lights of a certain wavelength; if the photosensitizer concentration in the lesion is sufficiently high and the ratio to neighboring normal tissue cells is satisfactory, then the photosensitizer transfers energy to surrounding oxygen, generating cytotoxic reactive oxygen species (ROS) that kill the cancer cell. The targeted destruction of lesions results from a cascade of cellular and molecular events [121-123].

Raab first observed this phenomenon when he noted that visible light rapidly killed paramecia in the presence of oxygen and small quantities of dyes. This process was further explored after Auler and Banzer demonstrated that certain porphyrins, such as hematoporphyrin, had a greater affinity for malignant tissues than normal tissues. [124]. As shown in **Figure 1.15**

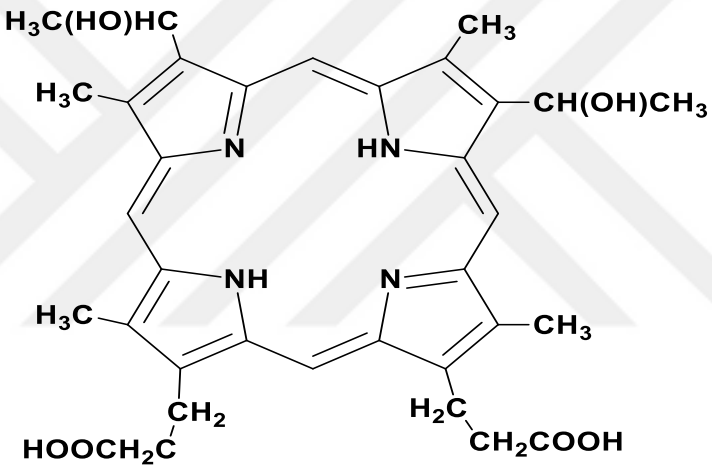


**Figure 1.15.** Structure of hematoporphyrin.

In photodynamic treatment, the photosensitizer drug is excited by visible or infrared light, which converts molecular oxygen from its triplet ground state to its singlet excited state ($^1O_2$). Singlet oxygen ($^1O_2$) is the most common kind of ROS [100]. According to, the electronic configuration of singlet oxygen is $O_2(^1\Delta g)$, representing its least excited state. Singlet oxygen is often generated by transferring energy from a photosensitizer to triplet molecular oxygen $O_2(^3\Sigma g)$. Direct excitation from $O_2(^3\Sigma g)$ to $O_2(^1\Delta g)$ is forbidden, but energy transfer occurs via photosensitization [125, 126]. As shown in **Figure 1.16**.

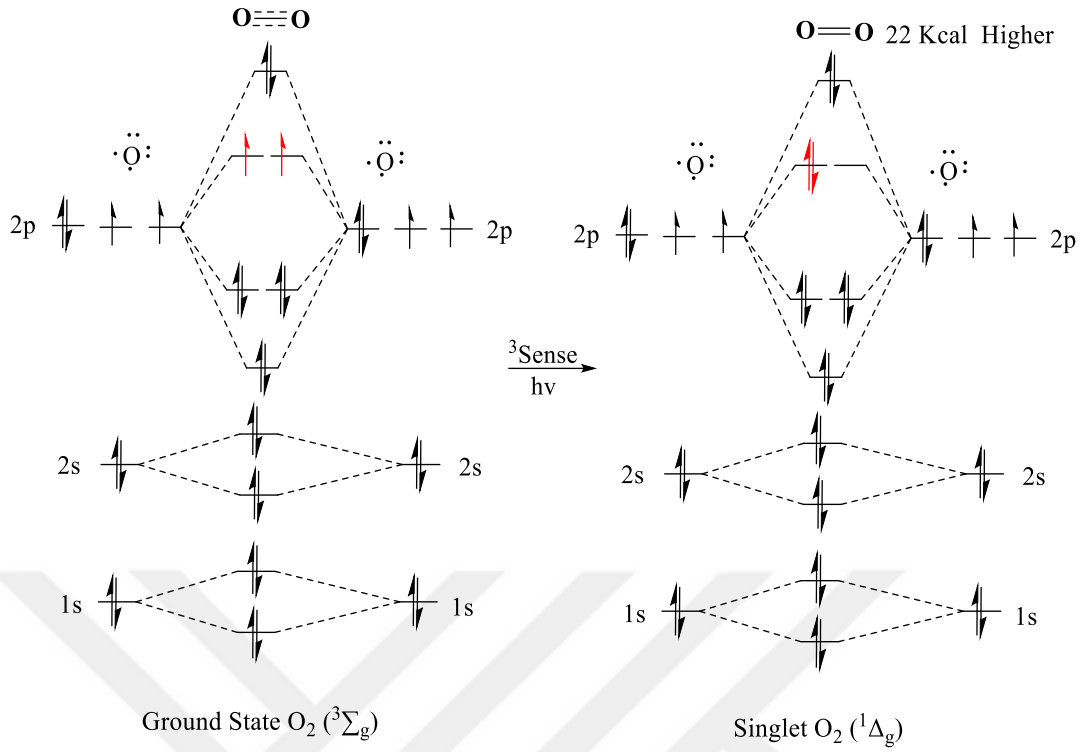


**Figure 1.16.** Singlet oxygen $O_2$ ($^1\Delta g$) and triplet oxygen $O_2$ ($^3\sum g$) electronic configurations.

By absorbing light in its lowest excited singlet ($S_1$) state, a photosensitizer is generated; this photosensitizer is subsequently excited to its lowest excited triplet ($T_1$) state, where it transfers its energy to $O_2$ ($^3\sum_g$) to form $O_2$ ($^1\Delta_g$), as shown in **Figure 1.17**. Applications including photodynamic cancer treatment PDT, photooxidation of hazardous compounds, and photoproduction of critical intermediates for various chemicals benefit from singlet oxygen's ($^1\Delta_g$) potent oxidation capabilities. Extensive research has been conducted on photosensitizers as singlet oxygen producers [125, 127].

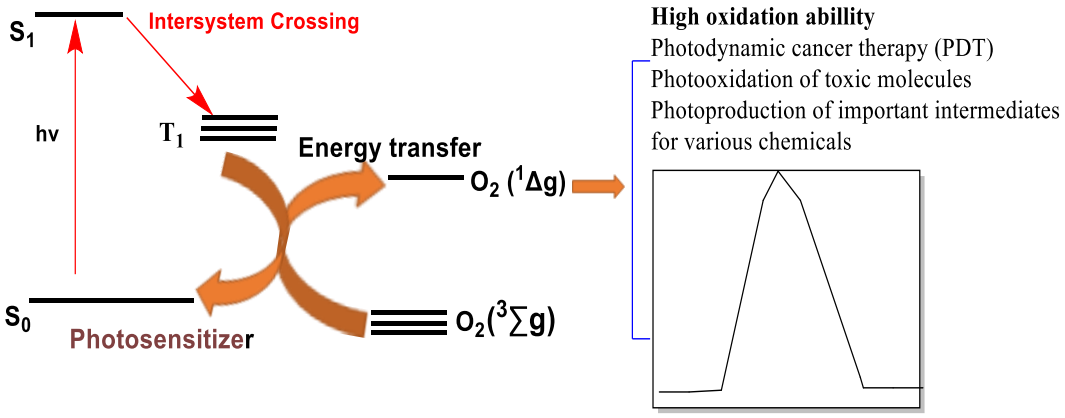


**Figure 1.17.** Mechanism of generation singlet oxygen and it is luminescence.

### 1.5.8. Solar cell Applications.

Since their discovery, phthalocyanines have been extensively used not only as dyes and catalysts but also in cutting-edge technical applications such as the active layers of solar cells, diodes, and transistors [72, 83]. Phthalocyanines are excellent sensitizers for dye-sensitized solar cells (DSSCs). Ragoussi et al. described the synthesis and utilization of several Pc derivatives with 2,6-diphenylphenoxy groups as DSSCs [85]. Pcs are utilized in DSSC because to their excellent absorption spectrum, high thermal stability, and chemical inertness. They also provide a more affordable substitute for standard silicon-based electronics [20, 128]. Throughout the last century, phthalocyanine derivatives' electrochemical, photochemical, and photophysical characteristics have garnered a lot of attention [35], so they have been used as catalysts, semi-conductors, and light-harvesting dyes in solar cells [78]. However, metal-free phthalocyanine-sensitized solar cells have been unable to generate photocurrent because the energy level of their excited singlet state LUMO is lower than the conduction band of $TiO_2$. However, by introducing zinc metalation, the LUMO level of the phthalocyanine was elevated, resulting in an exergonic free energy change, that enabled efficient electron injection. Consequently, the zinc phthalocyanine-sensitized solar cell achieved a power conversion efficiency of 0.57% and a maximum IPCE (incident photon-to-current conversion efficiency) of 4.9% in the near-infrared region [46].

## 1.6. Synthesis of phthalocyanines.

The general synthesis of phthalocyanine involves several key steps. It is essential to specify the type of phthalocyanine desired (metal-free or metal-substituted) [129] [130] and the specific substituents intended for incorporation, as the synthesis may vary accordingly. Below is a general overview of the synthesis of metal phthalocyanine and metal-free phthalocyanines [131]. Phthalocyanines are typically synthesized from phthalonitrile, which serves as the central building block [132]. Phthalonitrile can be synthesized by heating phthalic anhydride in the presence of ammonia or a primary amine. The reaction generally involves nucleophilic substitution to form the nitrile groups [133, 134]. The reaction typically occurs at elevated temperatures and may require a solvent such as dimethyl formamide or dimethylacetamide. The resulting phthalonitrile is a solid compound [135] [136].

### 1.6.1. General Synthesis of Phthalocyanine.

Phthalocyanines are very stable chemical substances that have been synthesized but are not found in nature. Researchers have been intrigued by the 18π electron structure and the stability of these molecules [40, 83]. Additionally, most commercial MPc are synthesized and are available inexpensively from major chemical producers [27, 137].

Most metal-containing Pcs are synthesized by heating phthalic acid, phthalic anhydride, 2-cyanobenzamide, phthalimide, diiminoisoindoline, or phthalonitrile to temperatures over 200 ºC in the presence of the relevant metal or metal salt. These processes can be carried out using either a suitable solvent or the melt itself. Incorporating a metal halide during the melting process often results in a monohalogenated form of Pc. A nitrogen supply, often urea, is necessary for cyclotetramerizations except when using phthalonitrile and diiminoisoindoline. The in situ synthesis and cyclotetramerization of phthalonitrile by the action of copper(I) cyanide (the Rosenmund-von Braun reaction) also utilizes 1,2-dibromobenzene as a precursor to PcCu(II) [138, 139]. As shown in **Figure 1.18**. Pc has been capacity to form coordination compounds with most metal attoms in the periodic table [75].

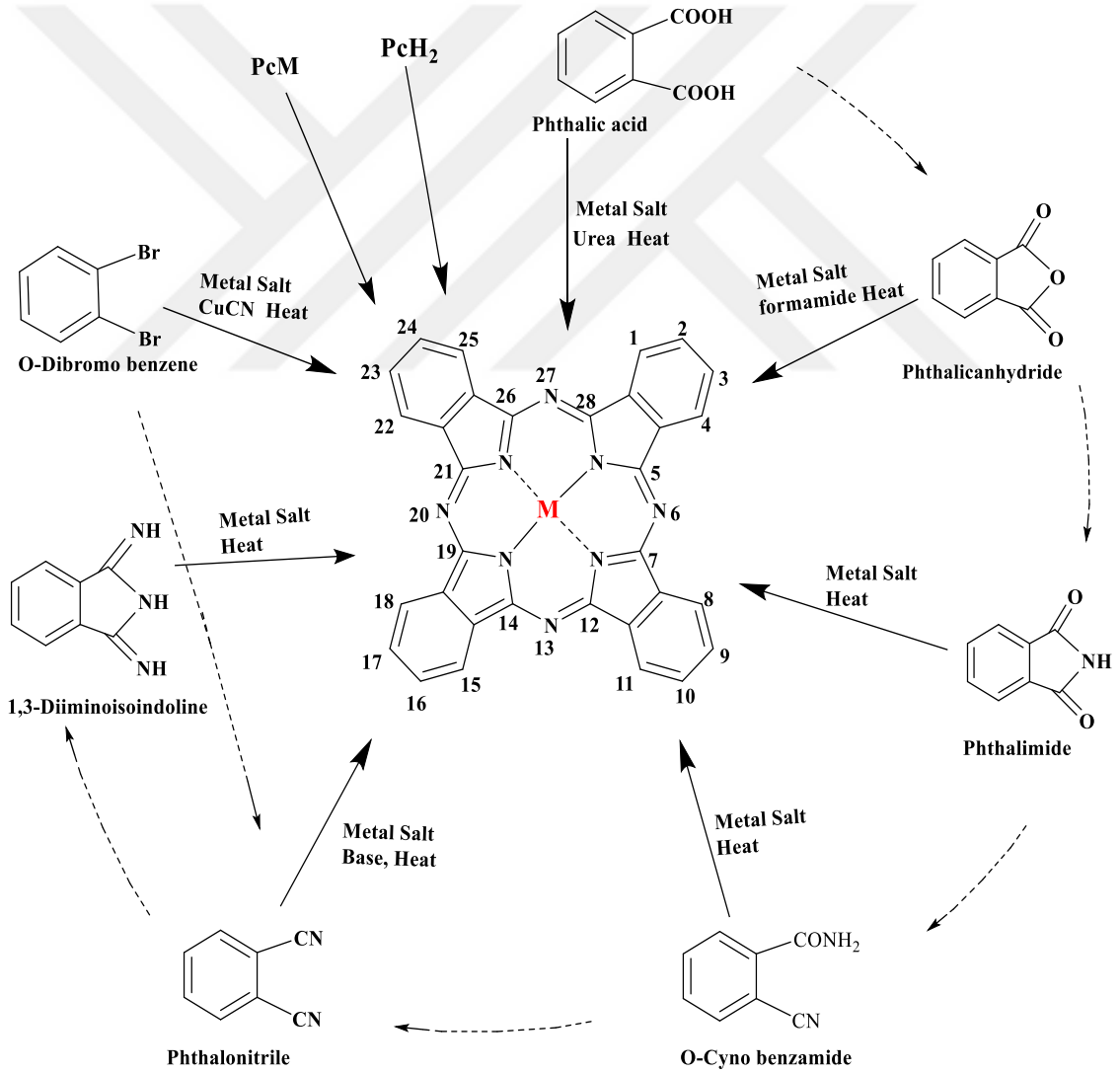


**Figure 1.18.** General principles for metall-phthalocyanine synthesis.

The initial synthesis of a phthalocyanine compound was documented in 1907. It was discovered that subjecting o-cyanobenzamide to high temperatures resulted in the formation of a blue compound as shown in **Figure 1.9**. However, this compound was not fully characterized until twenty-five years later [124].

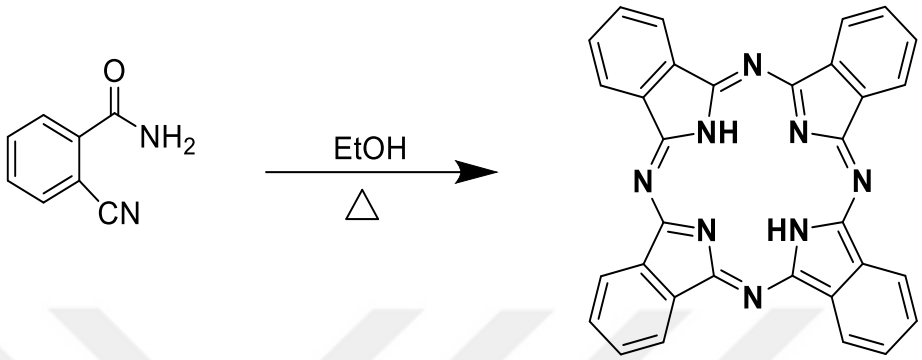


**Figure 1.19.** First metal-free phthalocyanine synthesis.

### 1.6.2. Formation Mechanisms of Phthalocyanines.

The formation mechanism of phthalocyanines is challenging to fully elucidate to understand the nature of phthalocyanine compounds due to the specific reaction conditions, the abundance of initial materials, and the elevated temperatures involved. Various synthesis methods have been employed, and while some of these methods allow for the identification of intermediate products along the known reaction pathway, a complete understanding of the formation mechanism remains largely elusive. Despite all these obstacles, isolatable intermediates obtained from the reaction media provide valuable insights into the creation of the phthalocyanine complex. These intermediate products are depicted as shown in **Figure 1.20.** Notably, intermediates (a) and (b) arise from the reaction of isoindoline with $NiCl_2$ in pentanol [140]. Intermediate (c) is similarly obtained through electrochemical methods [141]. For metal-free phthalocyanines, the reaction progresses through isolated intermediates (d), (e), (f), and (g), which remain unaffected by the absence of metals [142, 143]. However, the general applicability of these intermediates cannot be universally extended to all phthalocyanine complexes [144].

Possible path ways for the formation of metal phthalocyanines during synthesis are shown in **Figure 1.21**.

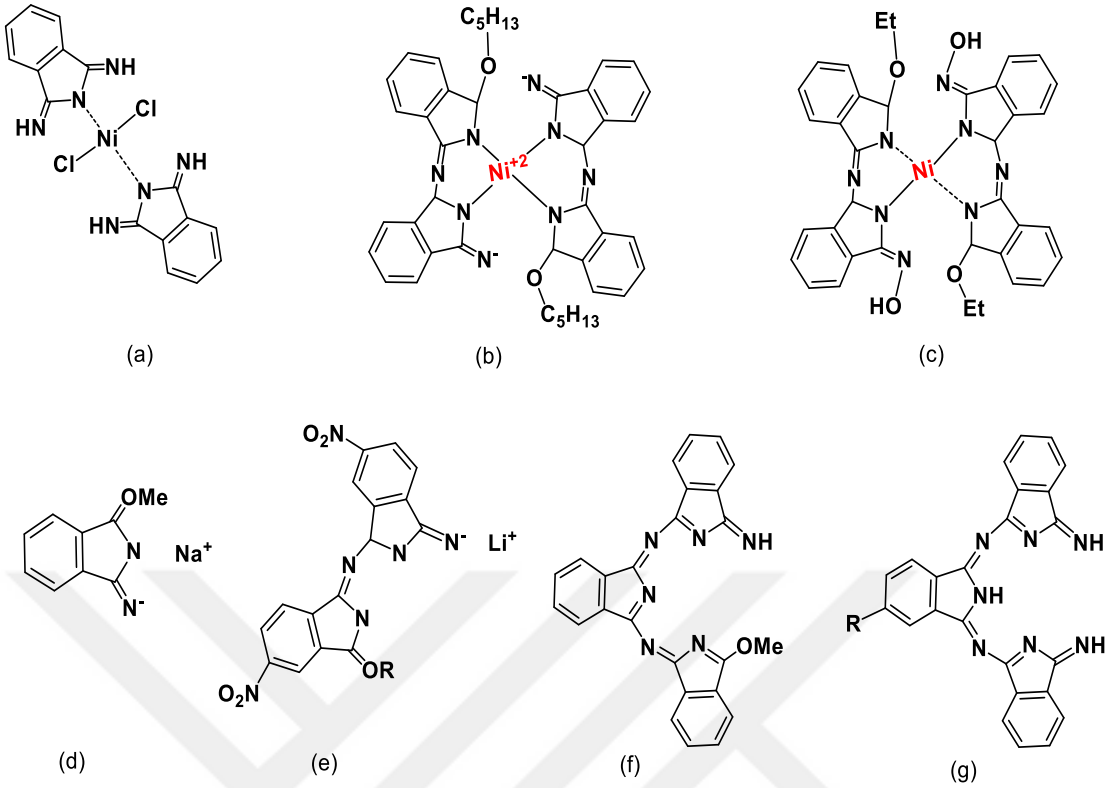


**Figure 1.20.** Isolated intermediates in the synthesis of metal and non-metallic phthalocyanines.

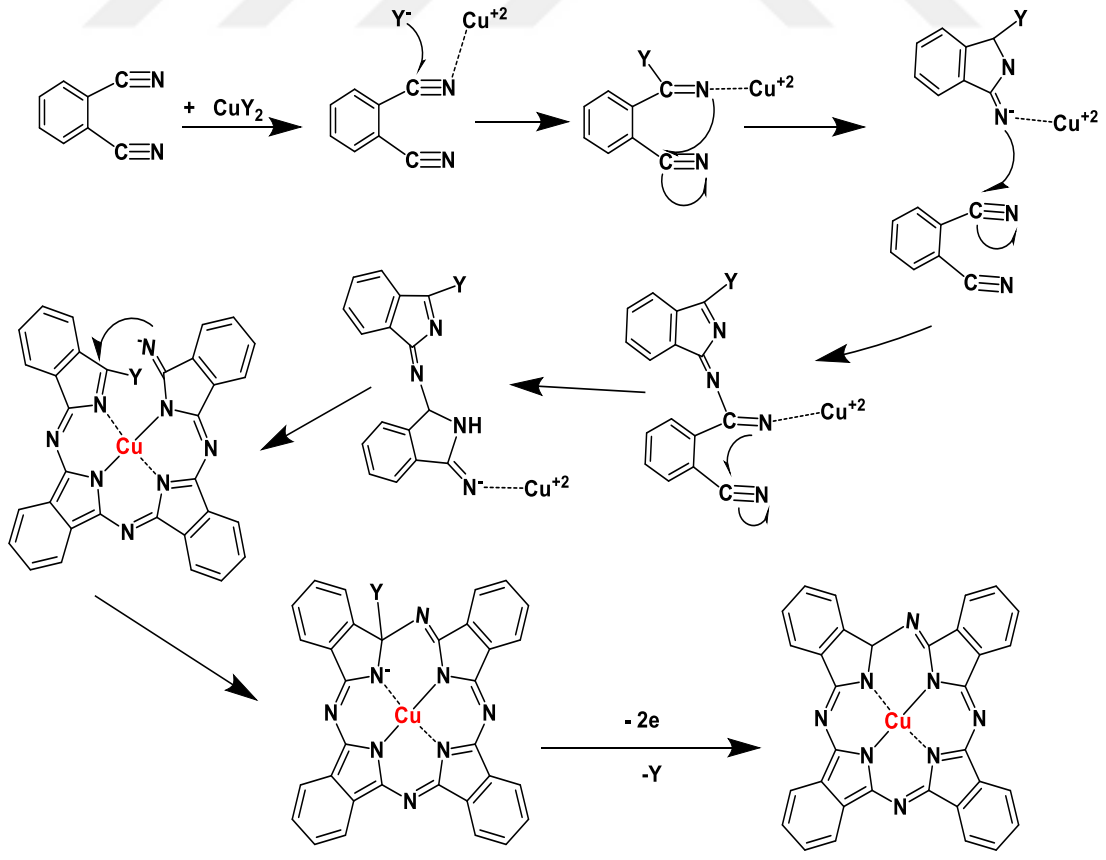


**Figure 1.21.** Possible formation mechanism of metal phthalocyanines.

### 1.6.3. Using Phthalic anhydride.

Synthesizing phthalocyanines using phthalic anhydride as a starting material is a common laboratory method. Phthalic anhydride ($C_8H_4O_3$) is first converted into phthalonitrile ($C_8H_4N_2O_2$), which serves as the key precursor for phthalocyanine synthesis. Phthalic anhydride is heated with urea (used instead of ammonia as a nitrogen source due to its higher stability) in the presence of a suitable catalyst, typically zinc chloride, sodium chloride, or ammonium molybdate. The reaction occurs under elevated temperatures and produces phthalonitrile as a solid product [61, 145]. As shown in **Figure 1.22**.

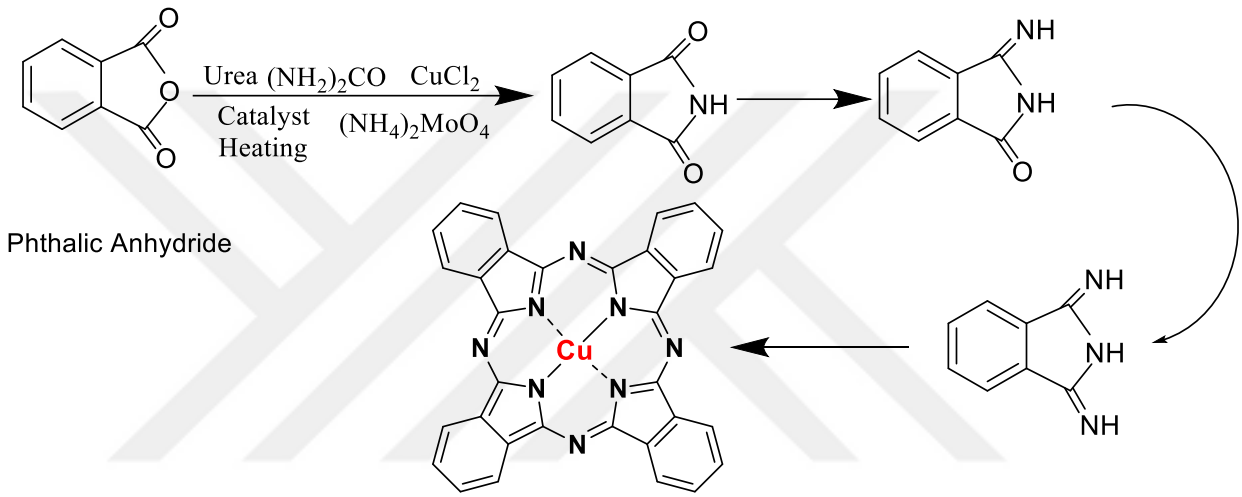


**Figure 1.22.** Syntheses of phthalocyanines using phthalic anhydride.

### 1.6.4. Using Phthalimide

Preparative procedures for obtaining pure phthalocyanine derivatives from phthalimide have been sought after for quite some time. These starting substrates are both more readily available and less costly than phthalonitrile or diiminoisoindoline derivatives [146].

The syntheses MPc often involve cyclotetramerization of phthalic acid analogs such as phthalimide (PI) requiring high temperatures of approximately 200 ºC and prolonged reaction durations of 10-24 h. Despite needing a co-reagent like urea or ammonium chloride, phthalic acid analogue techniques are preferred in the industry because of the lower cost precursor [147].

CuPc can be prepared from Phthalimide using $CuCl_2$, p-toluenesulfonic acid monohydrate, and hexamethyldisilazane (HMDS), these reagents were placed in a glass tube and heated to 100 °C for 1 hour under an argon atmosphere while being agitated. The mixture had cooled when DMF was added. The mixture was then placed in a sealed tube and heated to 150 ºC. A solid dark purple product appears instantaneously. The mixture is then heated for 10 hours before being cooled and

filtered. Methanol was used to clean the solid. DMF produced a higher yield, compared to DMSO [146]. As shown in **Figure 1.23**.

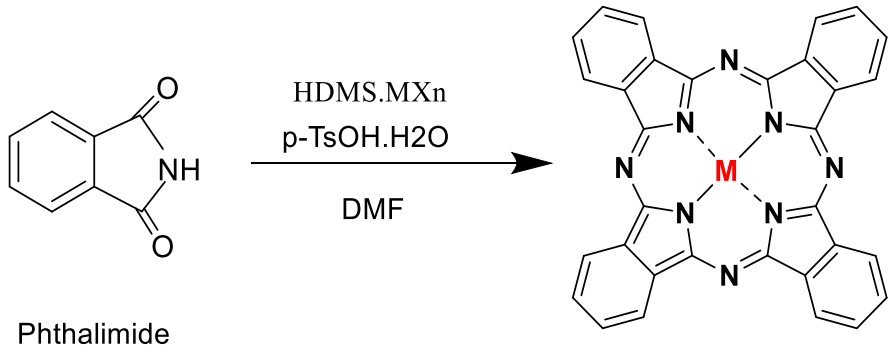


**Figure 1.23.** Syntheses of phthalocyanines by using phthalimide as starting material.

### 1.6.5. Synthesis of Metal Phthalocyanine.

The structural versatility of MPc improves their solubility, as the ring can be customized by substituting functional groups. Changing the metal cations within the MPc's core structure allows for its synthesis of a variety of forms. The phthalocyanine moiety has a large enough central cavity to hold the most metal cations [148]. However, the catalytic characteristics of MPcs vary depending on the metal atom utilized as a coordinated atom in this macrocycle, which is why various metals are used [149]. Metal phthalocyanines are widely used as dyes, photoconductors, solar cells [150], catalysts, nonlinear optical materials, and more [151].

The metal phthalocyanines were prepared by heating a combination of phthalonitrile compounds, with anhydrous metal salt ($CuCl_2$), for 24 hours at 160 ºC in dry n-pentanol in a sealed tube. The green product was precipitated using ethanol and then filtered out once the reaction was complete. The green solid result was washed with hot ethanol, distilled water, and diethyl ether. The product was dried in a vacuum and purified on a basic alumina column using a chloroform-methanol solvent [148]. The presence of Zn(II) and Cu(II) metal ions in the core of the phthalocyanines, as well as the unique chemical groups substituted on the Pc rings, are likely responsible for their observed activity [152] **Figure 1.24**.

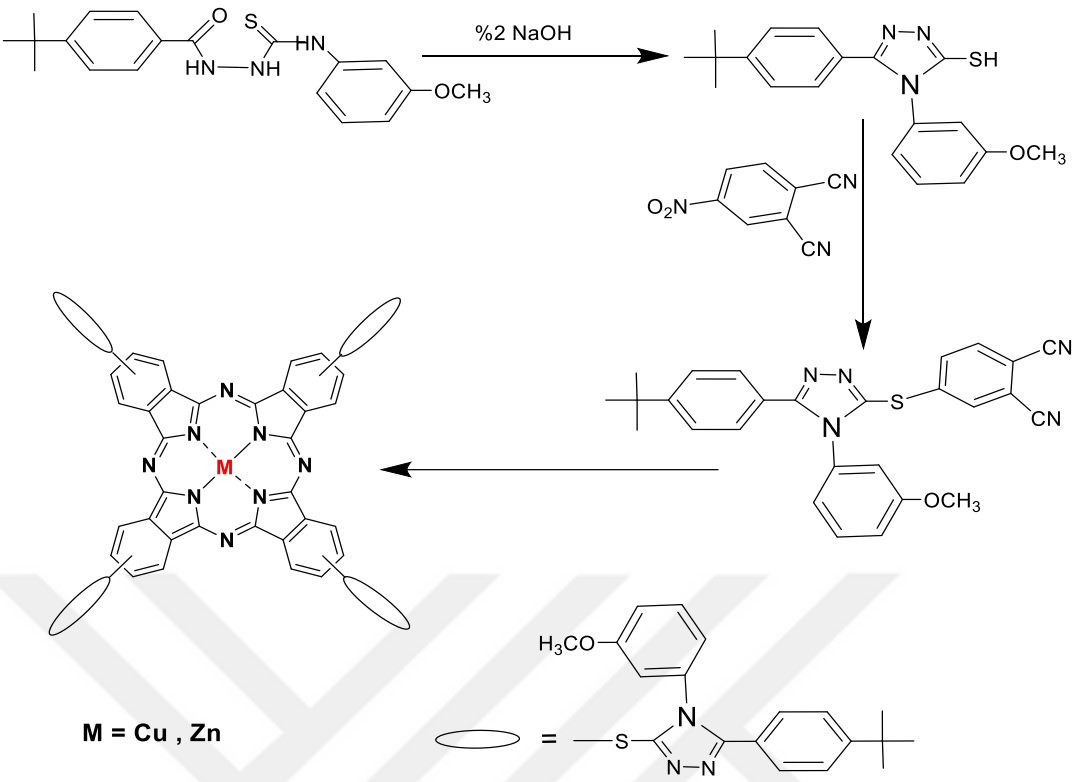


**Figure 1.24.** Syntheses of metal phthalocyanines.

### 1.6.6. Synthesis of Unsymmetrically-substituted phthalocyanine.

Unsymmetrically-substituted phthalocyanines are compounds in which different substituents are attached to the peripheral positions of the phthalocyanine macrocycle. By introducing different substituents at specific positions around the phthalocyanine ring, the properties of the compound can be modified for various applications [128].

The most widely used strategy for the synthesis of monofunctionalized A3B-type Pcs involves the statistical reaction of two different phthalonitrile or diiminoisoindoline precursors A and B in ratios 3:1 equivalents (or a slight excess of A) as shown in **Figure 1.25**. In this approach, compound A contains a chemically inert moiety like tert-butyl or mono- or dioxyether groups, while compound B provides the functional group to be incorporated into the Pc scaffold. This is the general schematic representation of the statistical condensation strategy for preparing unsymmetrically substituted A3B-type phthalocyanines. However, severe aggregation of Pcs is typically seen but this may be avoided by introducing chemically inert bulky groups, these bulky groups not only improve solubility but, also modify the electronic properties (electron-donating or electron-withdrawing characteristic) of the Pcs [153].

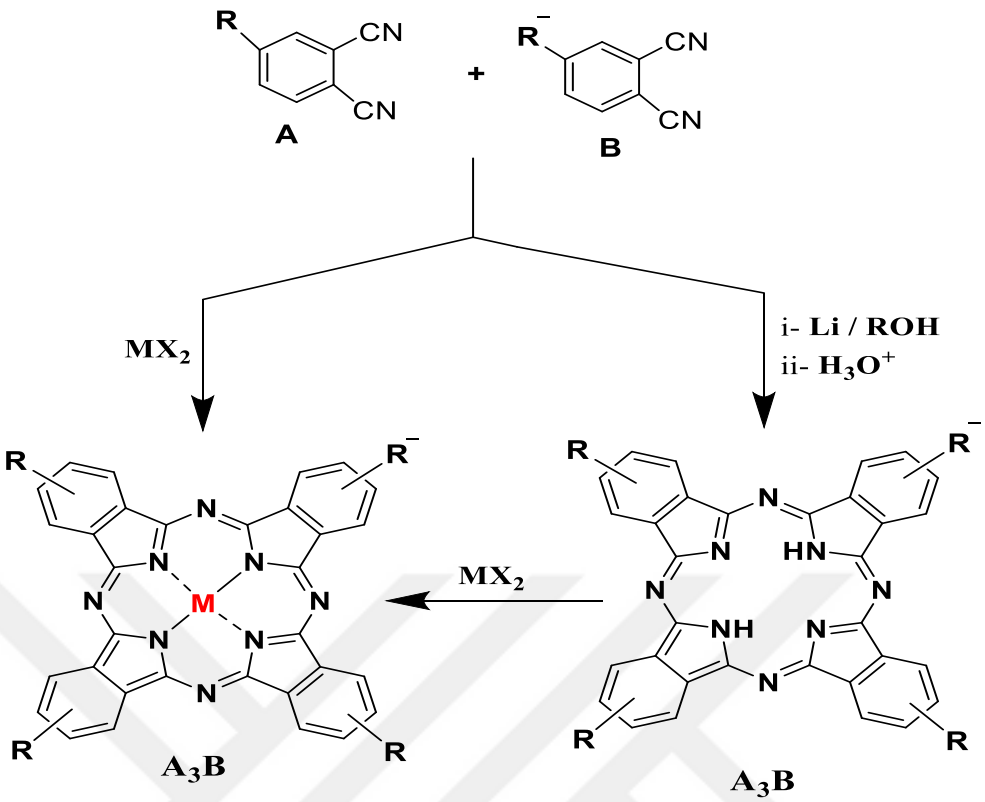


**Figure 1.25.** Syntheses unsymmetrical-substituted phthalocyanine.

In 1997, two separate research groups led by van Lier and Torres reported the successful synthesis of a highly soluble A3B-type zinc(II) Pc, in this context, A denotes substituted tert-butyl isoindolines, and B represents an iodine-containing unit. The first group synthesis of mononitro Pc by combining 4-nitrophthalonitrile and 4-tert-butylphthalonitrile via statistical condensation in the presence of zinc acetate [154]. As shown in **Figure 1.26**.

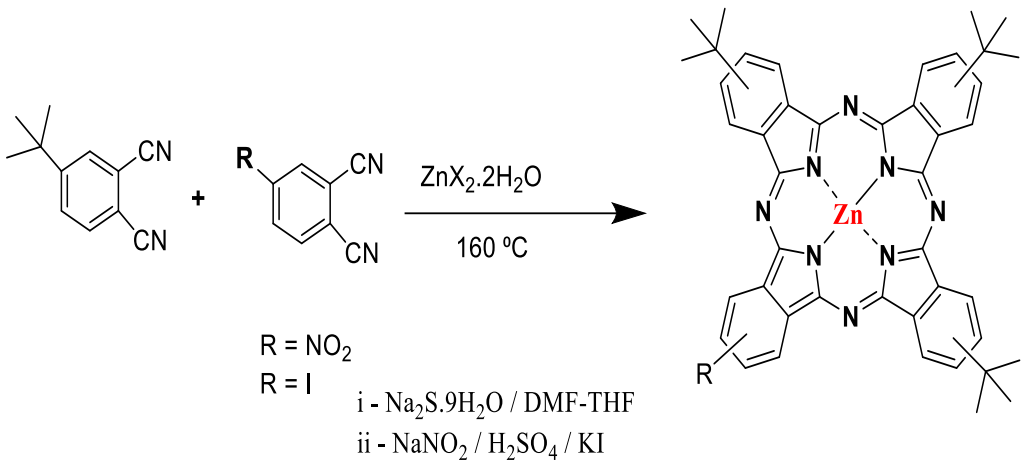


**Figure 1.26.** Methods for preparing monoiodo Pc.

### 1.6.7. Syntheses of Ball-type Phthalocyanines.

Ball-type or face-to-face diphthalocyanines were not previously reported until 2002 [66]. The Zefirov team reported the first successful synthesis of dinuclear ball-type metallo phthalocyanines [153]. These compounds consist of two Pc monomers arrayed and connected by four substituents at the ring's outermost locations. Unlike the parent monomers, the distance between the two Pc monomers in these compounds is highly variable and dependence on the linker components [155]. This variability makes these compounds appealing catalysts for the discovery of novel chemical processes. Two-metal-centered ball-type or cofacial bis-phthalocyanines have garnered significant interest recently owing to their unusual properties [74]. As shown in **Figure 1.27**. Dioxygen reduction catalysis which is particularly important for fuel cell applications, and ball-type cobalt phthalocyanines have shown strong catalytic activity in this regard [66].

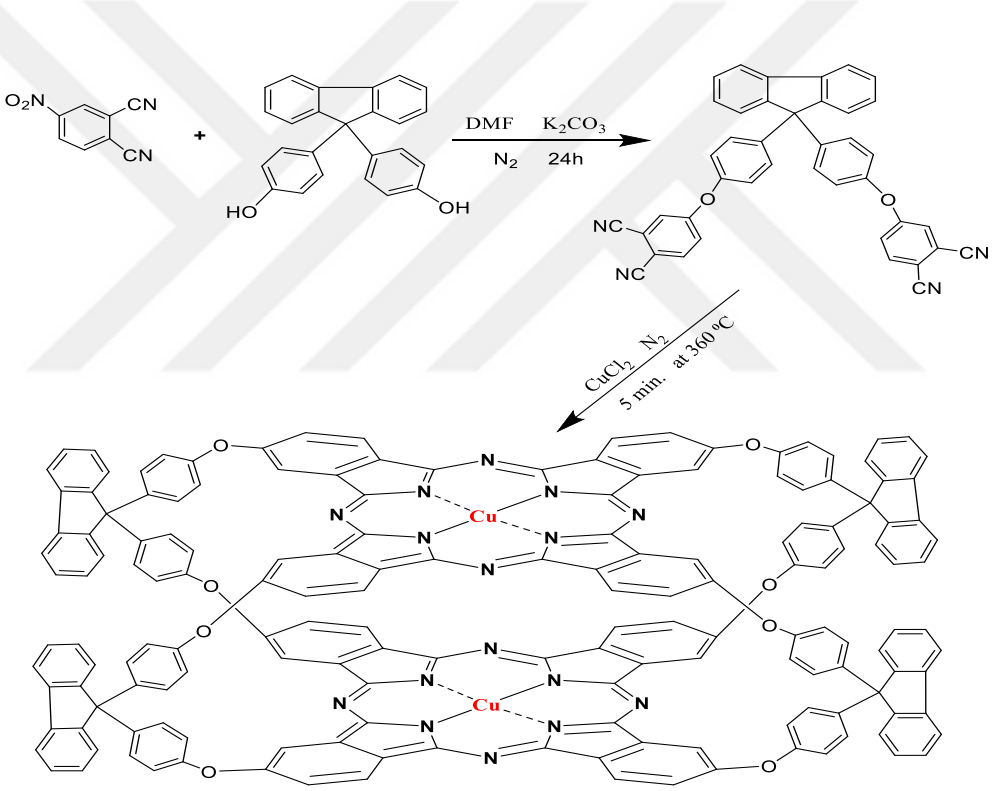


**Figure 1.27.** Syntheses of Ball type Pc.

### 1.6.8. Synthesis of Double Decker Phthalocyanines.

Double-decker phthalocyanines are a class of synthetic compounds consisting of two phthalocyanine rings stacked on top of each other. These compounds have gained significant attention due to their unique electronic, optical, and magnetic properties, making them suitable for various applications, including organic electronics, catalysis, and sensing [156].

The syntheses of mixed porphyrin-phthalocyanine sandwich complexes typically begin with refluxing the porphyrin with excess $M(acac)_3.nH_2O$ in 1,2,4-trichlorobenzene to produce the (porphyrin) M(acac) complex. This is followed by the addition of dilithium phthalocyanine ($Li_2Pc$) and prolonged reflux. Depending on the reaction circumstances, the metal used, and the macrocycle substituents, various stacking structures, including double and triple stacks, may be produced [157].

Novel Co(II), Cu(II), and double decker Lu(III) phthalocyanine have been synthesized, characterized, and reported on for their optical limiting features. The nonlinear absorbance is greatest in the lutetium and copper phthalocyanine complexes, and minimal in the cobalt phthalocyanine compound. Bis(phthalocyaninato) lanthanide complexes can be synthesized through several different methods, all requiring relatively high temperatures and longer reaction durations than monomeric phthalocyanines. To generate heteroleptic bis- and tris(phthalocyanine) compounds in high yields, Pushkarev and colleagues have proposed a novel synthesis process [37]. As shown in **Figure 1.28**.

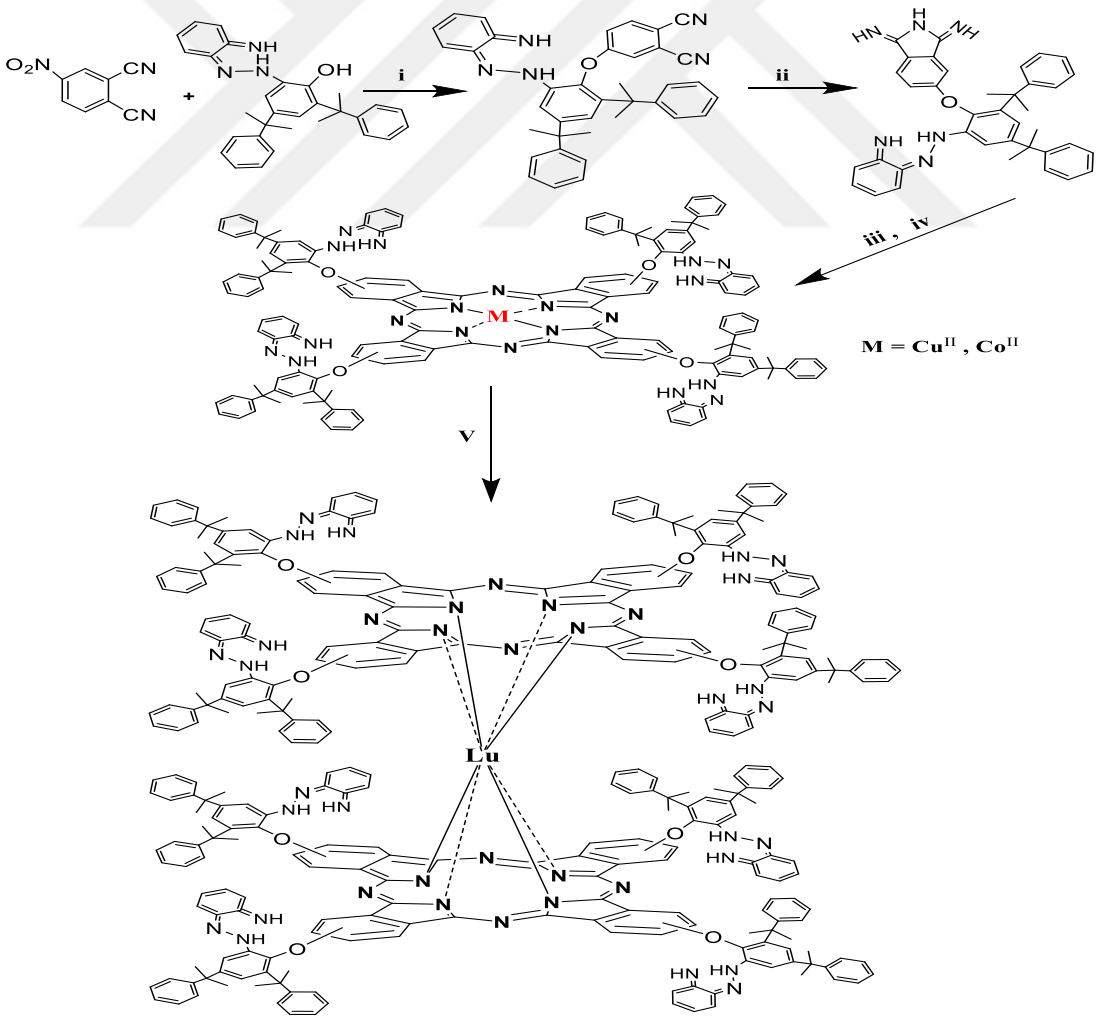


**Figure 1.28.** Syntheses double decker (i) $K_2CO_3$, DMF, Ar; (ii) $NH_3$, $CH_3$ ONa; (iii) $Co(CH3COO)_2{\cdot}4H_2O$, DMF, Ar; (iv) $Cu(CH_3COO)_2{\cdot}2H_2O$, DMF, Ar; (v) $Lu(CH_3COO)_3{\cdot}H_2O$, DBU, octanol, Ar.

### 1.6.9. Synthesis of Triple-decker phthalocyanines.

Triple-decker phthalocyanine refers to a class of coordination compounds consisting of three phthalocyanine units stacked on top of each other. These compounds have attracted interest due to their unique electronic and optical properties. The synthesis of triple-decker phthalocyanines can be challenging and often requires specialized techniques. One common approach involves the stepwise assembly of the phthalocyanine units using metal-mediated coupling reactions [158]. By reacting $Bi_2$ $Se_3$ with 1,2-dicyanobenzene at 220 ºC, triclinic crystals of bismuth(III) triple-decker phthalocyanine, $Bi_2$ $Pc_3$, were produced. The bismuth atoms in $Bi_2Pc_3$ are shifted outward from the center ring toward the phthalocyaninato (2-) rings, making the molecule centrosymmetric. Four N-isoindole atoms link each bismuth(III) ion to the outer Pc ring at an average distance of 2.333 Å̄, and four more link it to the inner Pc ring at a further 2.747 Å̄ [159]. In another experiment, was dissolved the "half-sandwich" phthalocyanine complex EuPc(acac) in n-pentanol and heated it with 1,8-diazabicyclo[5.4.0]undec-7-ene (DBU) for 10 hours at 140 ºC while passing a slow stream of nitrogen through the mixture. The resultant green solution cooled at room temperature, and the solution had volatiles removed under vacuum, leaving behind a stable compound. $CHCl_3$ was used in a chromatographic elution to separate the residue [160].

Metallophthalocyanines containing M(III) are very sensitive to the conditions used during their synthesis, which can significantly affect their chemical composition. Using this process a triple-decker phthalocyanine containing indium(III) has been produced through this method. However, while the InPc complex may be formed by direct interaction of pure indium metal with phthalonitril, the $Bi_2$ $Pc_3$ complex cannot be obtained using this approach due to the difference in the oxidation reaction $M \rightarrow M^{+3} + 3e$ between In and Bi. The crystal structure investigation of $In_2Pc_3$ reveals that the unpaired electron is relatively delocalized across both Pc macrocyclic rings [159]. The excellent thermal and chemical durability of triple-decker molecules makes them ideal for use in the production of organic thin films by vacuum sublimation, spin coating, or Langmuire - Blodgett methods [160]. As shown in **Figure 1.29**.

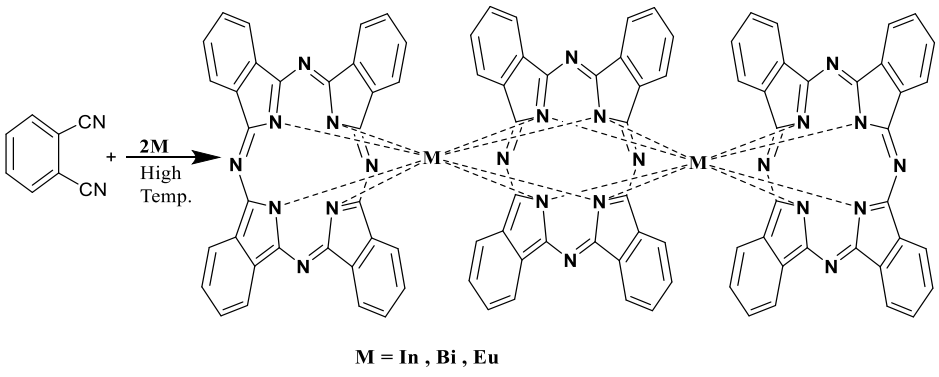


**Figure 1.29.** Syntheses triple decker Pc.

### 1.6.10. Synthesis of Subphthalocyanines.

Subphthalocyanines (SubPc) are relatively new compounds, that have already shown significant promise in materials science, physics, and chemistry. [161] [162]. SubPcs are a class of synthetic macrocyclic compounds derived from phthalocyanines. They share a similar structure to pcs but have an altered central core, leading to unique properties that make them useful in various applications, and are the lowest homologues of phthalocyanines, which are well-known aromatic two-dimensional complexes with peculiar optical and electrical characteristics [163].

These compounds possess a particular macrocyclic ring, arranged by three isoindole subunits bound together by three azabridges. This unique structure results made and gives rise to an aromatic 14 π- electron heteroannulene with specific characteristics, including the ability to accommodate a boron(III) ion within its central binding core [164]. X-ray crystallography has revealed their attractive chemical and physical properties.

In 1972, Meller and Ossko coincidentally discovered SubPcs while attempting to synthesize BPc. The anticipated cyclotetramerization product was not produced by the condensation reaction of phthalonitrile in chloronaphthalene in the presence of boron trichloride at 200°C. Instead, they observed the formation of a purple substance, which subsequent studies confirmed as chloro-SubPc [161, 164]. These compounds are known exclusively as boron derivatives. Nowadays, SubPcs are produced with an excellent yield of up to 90% occasionally by cyclotrimerization of phthalonitrile precursors in the presence of a boron derivative, usually a boron trihalide of the $BX_3$ type [163]. As shown in **Figure 1.30**.

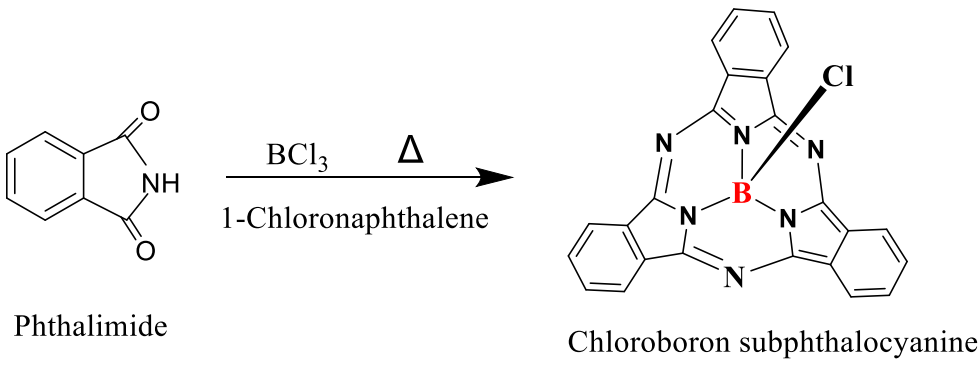


**Figure 1.30**. First SubPc synthesized.

### 1.6.11. Synthesis of Superphthalocyanines.

Superphthalocyanine (SPc) is the only compound known to have five isoindole units, making it a ring-expanded pentapyrrolic congener [165]. In 1964, uranyl SPc, a kind of super phthalocyanine, was synthesized, and in 1975, its structure was validated by x-ray crystallography [124], We have synthesized and extensively described and characterized the first example of an

antiaromatic expanded phthalocyanine, which is a norcorrole of a super-phthalocyanine [166] [162].

The uranyl ion acts as a nucleus in the SPc molecule, allowing four additional phthalonitrile moieties to assemble around it, forming the more common four-subunit uranyl SPc. An unsubstituted SPc with a linear and stiff O=U=O central core was synthesized by condensing $UO_2(OAc)_2$ in DMF with five fumaronitrile molecules at 190 °C for 1 hour. The yield was significantly reduced due to the inclusion of moisture and the use of alternative uranyl salts. Very low yields of alkylated SPcs were also achieved by using substituted phthalonitrile. Additionally, octa-alkylated phthalocyanines can be obtained by reacting the corresponding super-phthalocyanine complexes with either acid (e.g., acetic acid in chlorobenzene), to produce the metal-free complex, or a metal salt (e.g., copper acetate in DMF), generating the metallated complex, due to the inherent instability of SPc's [124, 165]. As shown in **Figure 1.31**..

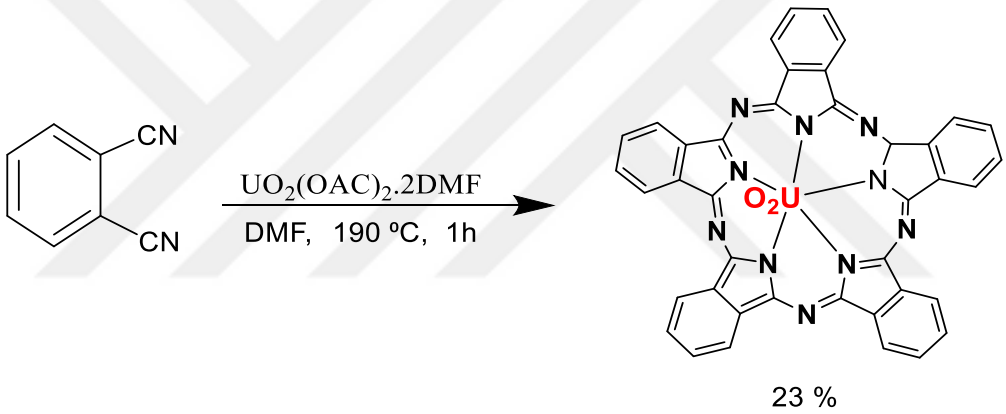


**Figure 1.31**. Superphthalocyanine structure.

### 1.6.12. Synthesize phthalocyanine polymers

There are four categories of phthalocyanine polymers: (1) those where the phenylene rings of neighboring monomers are linked by single bonds similar to biphenyl, (2) variations where monomers are connected through substituents attached to the phenylene ring, (3) a group that has the phenylene rings of the phthalocyanines fused, and (4) polymers where the phthalocyanine molecules are interconnected at the central metallic atom in a stacked arrangement [167, 168]. To prepare polymeric phthalocyanines, metal salts or metals are typically used in cyclatetramerization reactions of bifunctional monomers such as tetracarbonitriles, various oxy-, arylenedioxi-, alkylenedioxy-, and bridged diphthalonitriles, among others [169].

Metal phthalocyanine polymers are of interest due to their high thermostability and potential use as dyes and high-tech materials in industry [170]. They are well-suited for various applications. Moreover, the semiconducting variants of these polymers exhibit higher conductivities compared

to their low molecular weight counterparts. Despite these advantages [169], the use of polymeric phthalocyanines is limited to specific fields due to their inability to dissolve in water and common solvents [169, 171].

The method developed by Hanack and colleagues to generate main-chain-type polymers based on Pcs is particularly appealing as it involves the connection of the metal ions within the core through suitable bivalent bridges. Using this method, the Pc molecules are arranged in a cofacial fashion inside the "shish-kebab" polymer. When suitable groups are attached to the perimeter of the Pc macrocycles, the resulting macromolecules may contain up to 200 macrocyclic units and exhibit relatively good solubility. Pc units in phthalocyaninato-polysiloxane 28 have crown ethers connected to chiral alkyl side chains, inducing helicity in the columnar architecture, making it an exemplary member of this class of rod-like polymers. The Pc rings are stacked closely together (0.34 nm) because the polysiloxane backbone goes right through the middle of them [97, 154, 167]. As shown in **Figure 1.32**.

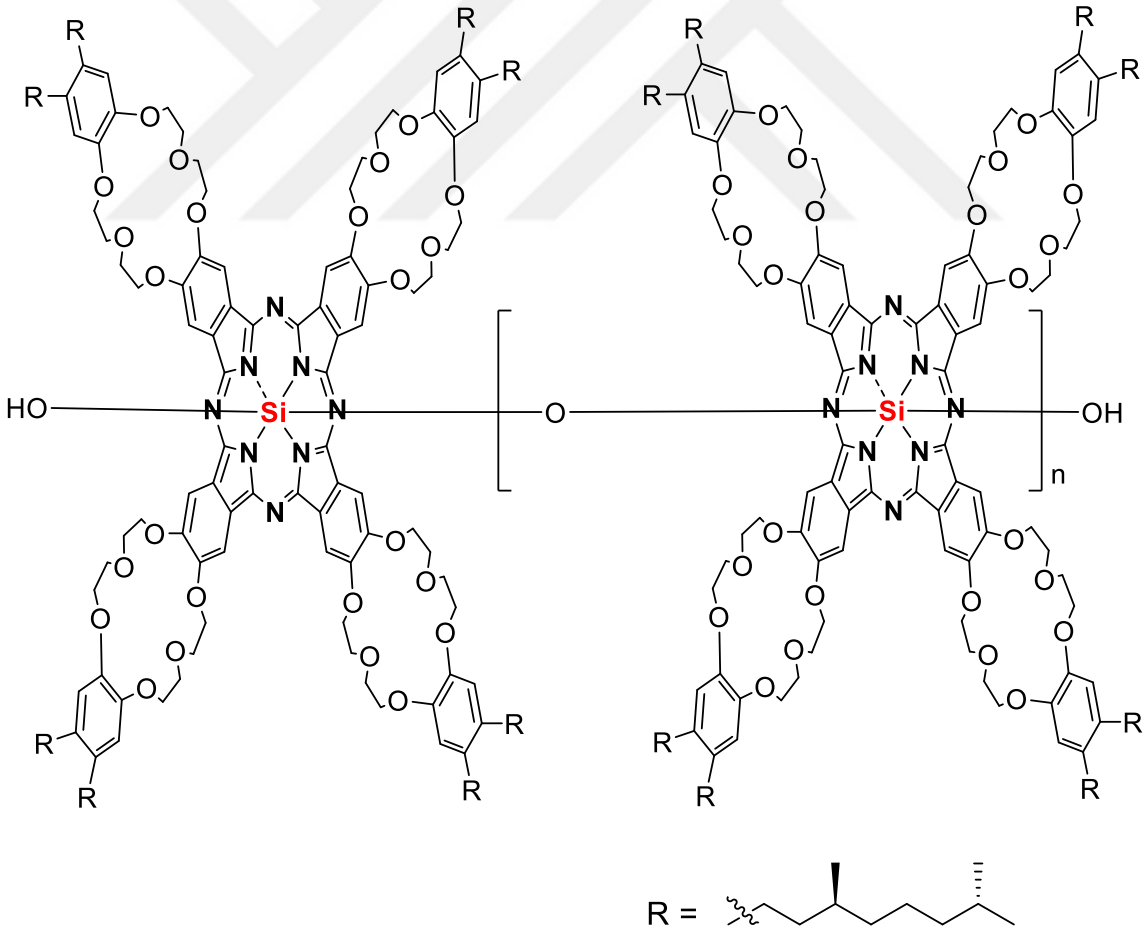


**Figure 1.32.** The Pc polymer is a main-chain polysiloxane.

# 2. MATERIAL AND METHOD

Common glassware and other general laboratory equipment were used during the synthesis, purification, and identification of the synthesized compounds in the laboratory.

The synthesized compounds were analyzed and characterized by using the following instruments.

**IR-Spectroscopy**

Infrared spectra were recorded on a PerkinElmer, Spectrum One FT-IR Spectrophotometer (in the range of 4000-450 $cm^{-1}$) at the (Chemistry Department, Fırat University). Solid substances were ground with spectroscopic grade KBr and pressed into pellets.

**NMR-Spectroscopy**

Nuclear magnetic resonance ($^{1}H$ and $^{13}C$ NMR) spectra were obtained using a Bruker Avance III 400 MHz NMR Spectrometer with deuterated dimethyl sulfoxide (DMSO-$d_6$) as the solvent and tetramethylsilane (TMS) as the internal standard at the (Chemistry Department, Fırat University). Chemical shifts are reported in δ [ppm].

**UV/Visible Spectroscopy**

Electronic spectra obtain by Shimadzu 1900 i UV–Visible spectrophotometers. (Chemistry Department-Fırat University). All spectra were recorded in DMF solution, with the path length of 1 cm.

**Elemental analyses**

Elemental analyses were performed by Leco CHNS 932.

**Thermal analysis**

Thermal characterizations, thermogravimetric analysis, and differential thermal analysis (TG/DTA), of the samples were done by SHIMADZU TGA 50 series thermal analysis instrument with a 20 °C/min scan rate. (Chemistry Department-Fırat University).

**Electrochemical Properties**

Electrochemical properties work done by Gamry Interface 1010 B, in DMF, with glassy carbon electrode as working electrode, Pt electrode as counter electrode tetrabutyl ammonium tetrafluoro borate (TBTFB) as supporting electrolyte using ferrocene/ferrocenium as sudo reference electrode. (Chemistry Department-Firat university).

## 2.1. Materials and Methods

Materials used in this study included Argon (HABAŞ), Ammonia gas ($NH_3$) (HABAŞ), 65% nitric acid (Merck), 98% sulfuric acid (Sigma Aldrich), $NH_3$ (25%) (Merck), anhydrous potassium carbonate (Merck), anhydrous potassium Bromide (Merck), Thionyl chloride (Merck), Copper(II)

acetate (Merck), Nickel(II) acetate (Merck), Cobalt(II) acetate (Merck), Zinc(II) acetate (Merck), Fe(II) acetate, Cr(II) acetate, 2-mercaptobenzothiazole, 8-Hydroxyquinoline, and 4-hydroxyacetamide (Acros Organics), (DMF) (CHEM SOLUTE), dimethyl sulfoxide (DMSO) (Carlo Erba), tetrahydrofuran (THF) acetonitrile (Merck), acetone (Carlo Erba), chloroform (Merck), and Ethanol (Sigma Aldrich).

All reactions were carried out under an argon atmosphere unless otherwise specified. Commercially available chemicals from Merck, Carlo Erba, and Sigma-Aldrich were used, and all solvents were dried according to standard procedures. The starting materials were prepared according to published protocols.

In this study, the experiments were conducted out, in several different steps. The process involved in the synthesis and creation of phthalocyanine compounds, both metal-free and metalated, starts with the synthesis of 4-nitrophthalonitrile. To achieve this, phthalimide is first nitrated to produce 4-nitrophthalimide. Subsequently, 4-nitrophthalimide is converted into 4-nitrophthalamide. Following this step, it is transformed into 4-nitrophthalonitrile using thionyl chloride in dimethylformamide (DMF).

In the next step, 4-nitrophthalonitrile undergoes nucleophilic substitution by reacting with 2-mercaptobenzothiazole, 8-Hydroxyquinoline, and 4-hydroxyacetamide, resulting in the formation of 4-(benzo[d]thiazol-2-ylthio) phthalonitrile, 4-(quinolin-8-yloxy) phthalonitrile, and 2-(4-(3,4-dicyanophenoxy)phenyl) acetamide, respectively. Metalated phthalocyanine complexes were then synthesized by cyclotetramerizing these ligands in the presence of different metals to produce various metal Phthalocyanine compounds. Finally, the synthesized phthalocyanine compounds are subjected to purification.

## 2.2. Synthesis 4-Nitrophthalonitril.

The synthesis of 4-nitrophthalonitrile involves the introduction of a nitro group ($NO_2$) at the 4-position of phthalonitrile. The nitration reactions can be hazardous, and appropriate safety precautions should be taken, including the use of safety equipment and working in a well-ventilated area.

### 2.2.1. Synthesis of 4-Nitrophthalimide.

4-Nitrophthalimide was prepared in a 500 ml three-neck round bottom flask equipped with a magnetic stirrer, a dropping funnel, and a thermometer. The flask was charged 280 ml of concentrated sulfuric acid (95%). Then 80 ml of fuming nitric acid (%96-97) was added dropwise at 0 °C, using an ice bath to cool the mixture. 50 g (339.83 mmol) of phthalimide was gradually added to the mixture over a period of 2 hours, with constant stirring to maintain a uniform

temperature. The reaction mixture was kept at 0-5 °C while phthalimide was being added. After all the phthalimide had been added, the reaction mixture was left in the ice bath to slowly warm to room temperature overnight. As shown in **Figure 2.1**.

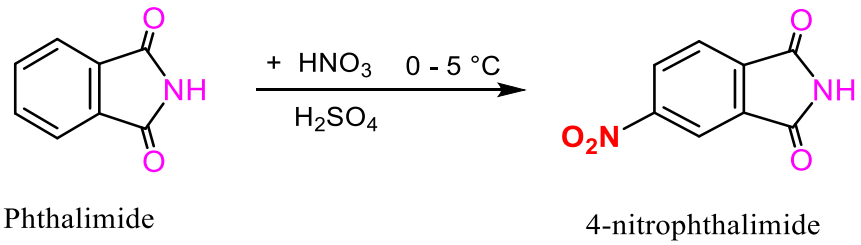


**Figure 2.1.** Syntheses 4-Nitrophthalimide.

The clear, light-yellow solution was added to 500 g of ice to precipitate, and filtered then washed with cold water several times to bring pH to neutral. The obtained white solid dried at room temperature. To purify the product, it was dissolved in hot boiling alcohol (Ethyl alcohol) then allowed to cool to room temperature to crystalize, and then filtered, product 42 g of white 4-nitrophthalimide, with a yield of 64.4%.

### 2.2.2. Synthesis of 4-Nitrophthalamide.

4-Nitrophthalamide was synthesized in a 500 ml three-neck round bottom flask equipped with a magnetic stirrer, and thermometer. 26 g (135.32 mmol) of the 4-nitrophthalimide was added to the flask followed by 250 ml of Ethanol and 20 ml of THF. The temperature was raised to 40 °C, and ammonia gas was bubbled through the reaction mixture and continued for about 15 minutes. The reaction was monitored by FTIR. When the reaction was complete the mixture was cooled to room temperature, filtered, and dried product in air at room temperature. A yield was 28 g, corresponding to 94%, of 4-nitrophthalamide was obtained which has a white color, as shown in **Figure 2.2.**

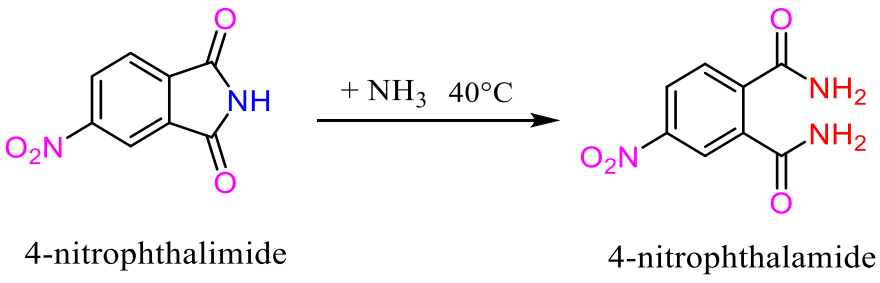


**Figure 2.2**. Synthesize of 4-nitrophthalamide.

### 2.2.3. Synthesis 4-Nitrophthalonitrile.

4-Nitrophthalonitrile was synthesized in a 500 ml three-neck round bottom flask equipped with a magnetic stirrer and thermometer. The flask was charged with 120 ml of dry DMF, and the mixture was cooled to 0 °C using an ice bath. At a temperature below 5 °C, 16 mL of thionyl chloride ($SOCl_2$) was added dropwise using a dropper. After stirring for 10 minutes, 20 g (95.62 mmol) of 4-nitrophthalamide was added for 1 hour, while maintaining the temperature at 0-5 °C, and stirring continued for 1 h. Also, the mixture was stirred for an additional 20 hours at room temperature. After this period, the mixture was poured into 200 mL of ice and stirred for 1 hour to obtain the product. The precipitate was filtered and washed several times with water, and dried, 14.50 g, of 4-nitrophthalonitrile, representing an 87.61 % yield. The product appears white color. As shown in **Figure 2.3**.

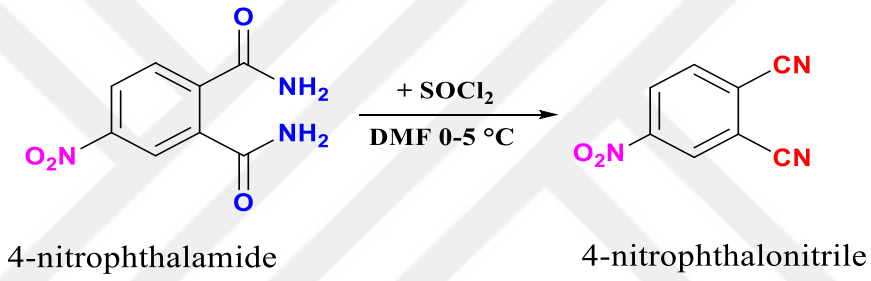


**Figure 2.3.** Synthesized 4-Nitrophthalonitril.

## 2.3. Synthesis of Ligands.

Ligands are often organic molecules that can be synthesized using various organic synthesis techniques. The method synthesis varies widely depending on the specific ligands being prepared and their intended application. The coupling of 4-Nitrophthalonitril with the molecule containing alcohol group was performed in DMF under inert gas (Ar) at temperature 70-90 °C

### 2.3.1. Synthesis 4-(benzothiazol-2-ylthio) phthalonitrile.

In a 100 ml three-necked round bottom flask, 4-nitrophthalonitrile 2.20 g (12.70 mmol) was dissolved in 40 ml DMF under an argon gas. To this solution, 2-mercaptobenzothiazole 2.38 g (14.23 mmol) was added. After stirring for 20 minutes at room temperature, finely powdered anhydrous potassium carbonate 2.5 g (18.08 mmol) was added portion-wise over 1 h at 70-90 °C. The reaction was carried out for an additional 24 h, during which the color of the reaction mixture changed pale yellow to brown. After 24 hours, the homogeneous mixture was precipitated in 200 ml of water and filtered then the product was dried. The final product, 4-(benzothiazol-2-ylthio)

phthalonitrile, was obtained as a light yellow solid with a yield of 3.2 g, corresponding to an 85.79 % yield. As shown in **Figure 2.4**.

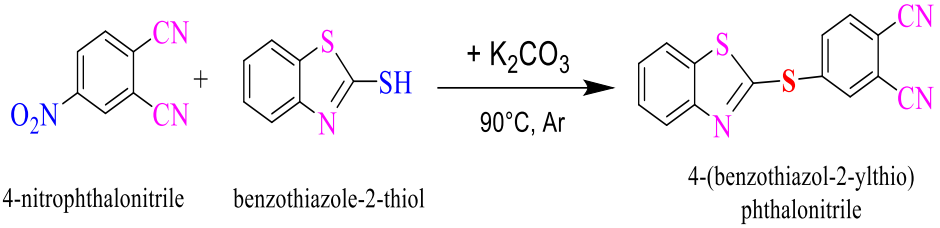


**Figure 2.4.** Synthesized 4-(benzo[d]thiazol-2-ylthio) phthalonitrile.

### 2.3.2. Syntheses of 4-(quinolin-8- yloxy) phthalonitrile

In a 100 mL three-necked round-bottom flask, 3 g (17.32 mmol) of 4-nitrophthalonitrile and 2.5 g (17.22 mmol) of 8-hydroxyquinoline were dissolved in 45 mL of dry DMF under an argon atmosphere. After stirring for 30 minutes, finely powdered anhydrous potassium carbonate $K_2CO_3$ 2.39 g (17.29 mmol) was added in portions over 1 hour period. The reaction mixture was then stirred at 90°C for 24 hours. Then the mixture was added to 500 mL of an ice-water mixture to precipitate the product. The precipitate was filtered, washed with water, and dried at room temperature. The yield of the product was 3.57 g, corresponding to a 76.106 % yield, and a brown color product was obtained. As shown in **Figure 2.5**.

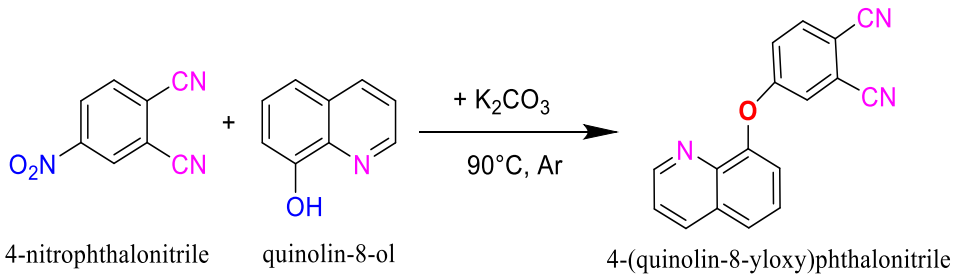


**Figure 2.5.** Synthesized 4-(quinolin-8- yloxy)phthalonitrile.

### 2.3.3. Syntheses of 2-(4-(3,4- dicyanophenoxy)phenyl)acetamide.

In a 100 mL three-necked round-bottom flask, 1 g (5.77 mmol) of 4-nitrophthalonitrile was dissolved in 25 mL of DMF under an argon atmosphere. To this solution, 0.9 g (5.95 mmol) of 2-(4-hydroxyphenyl) acetamide was added. After stirring for 20 minutes, 1.38 g of anhydrous potassium carbonate (9.98 mmol) was added portion-wise over 1 hour time. The reaction mixture was then stirred under argon gas at 90 °C for an additional 24 hours. Then reaction mixture was precipitated in 500 mL of water, followed by filtration, washed with water then dried at room

temperature. The final product obtained was a light-yellow color, 1.4 g, with a yield of 87.5 %. The reaction is shown in **Figure 2.6.**

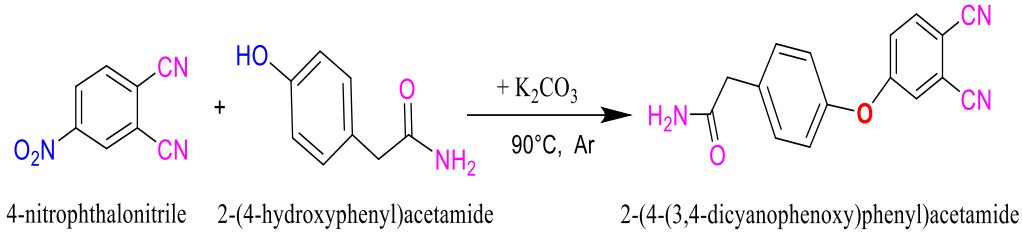


4-nitrophthalonitrile 2-(4-hydroxyphenyl)acetamide 2-(4-(3,4-dicyanophenoxy)phenyl)acetamide

**Figure 2.6.** Synthesized of 2-(4-(3,4- dicyanophenoxy)phenyl)acetamide.

## 2.4. Syntheses of metallated and metal-free phthalocyanine compounds

The phthalocyanine moiety contains a sufficiently large central cavity to accommodate almost all the metal cations. In this study, novel phthalocyanines were synthesized, each incorporating metal cations and functional ligand groups at non-peripheral sites of the phthalocyanine macrocycle. Under high temperature boiling and in an anhydrous solvent in the presence of a catalyst, the phthalonitrile derivative reacted with metal salts, leading to cyclotetramerization to form substituted MPcs. The resulting compounds were purified by solving in solvent generally DMF and precipitating several times.

### 2.4.1. Synthesis of 4-(benzothiazol-2-ylthio) phthalocyaninato metal complexes (A) (M: Cr, Fe, Co, Ni, Cu, Zn).

Within a 2 cm diameter glass tube fitted with an argon inlet, 0.25 g (0.85 mmol) of 4-(benzo[d]thiazol-2-ylthio) phthalonitrile and 0.08 g (0.47, 0.45, 0.45, 0.45, 0.44, 0.43) mmol of metal acetate salts (Cr, Fe, Co, Ni, Cu, Zn) respectively, were added. Then, 3 mL of DMF was added under an argon atmosphere, and the mixture was heated to a stable boiling point of DMF under an argon atmosphere followed by adding 3-4 drops of DBU as a catalyst. The reaction continued for 24 hours. The progress of the reaction was monitored visually checking the color of the solution to turn to green or blue color, when the intensity of color did not increase, the reaction was stopped. Once the reaction was complete, the mixture was cooled down and diluted with 2 mL of ethanol. The resulting solution was then precipitated by adding to 200 mL of water drop by drop while stirring. The precipitate was filtered and washed multiple times with distilled water and ethanol until the eluent became colorless. The solid product, which had a blue-green color, was dried first at room temperature and then at 75 °C in a drying oven. The products obtained were 0.22 g, 0.087 g, 0.221 g, 0.22 g, 0.183 g, and 0.175g, with (66%, 26%, 66%, 66%, 55%, 53%) yields for Cr, Fe, Co, Ni, Cu, and Zn respectively. As shown in **Figure 2.7**. and **Table 2.1.**

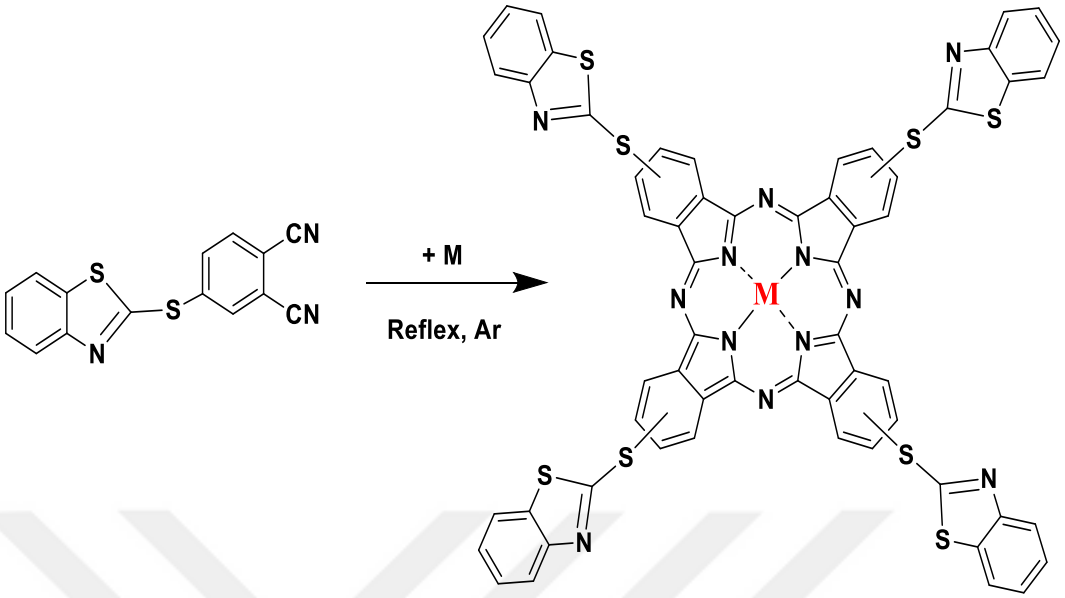


**Figure 2.7.** Synthesized of 2,2',2",2"'(2,9,16,23-tetrayltetrakis(sulfanediyl))tetrakis(benzothiazole) Metal phthalocyanine complexes (A). (M: Cr, Fe, Co, Ni, Cu, and Zn).

### 2.4.2. Syntheses metal free phthalocyanine ($H_2Pc$).

The same procedure was used to synthesize metal-free phthalocyanine, but without adding metal acetate; all other steps remained unchanged. This resulted in 0.246 g of product, with a yield of 74.5%. As shown in **Figure 2.8.**

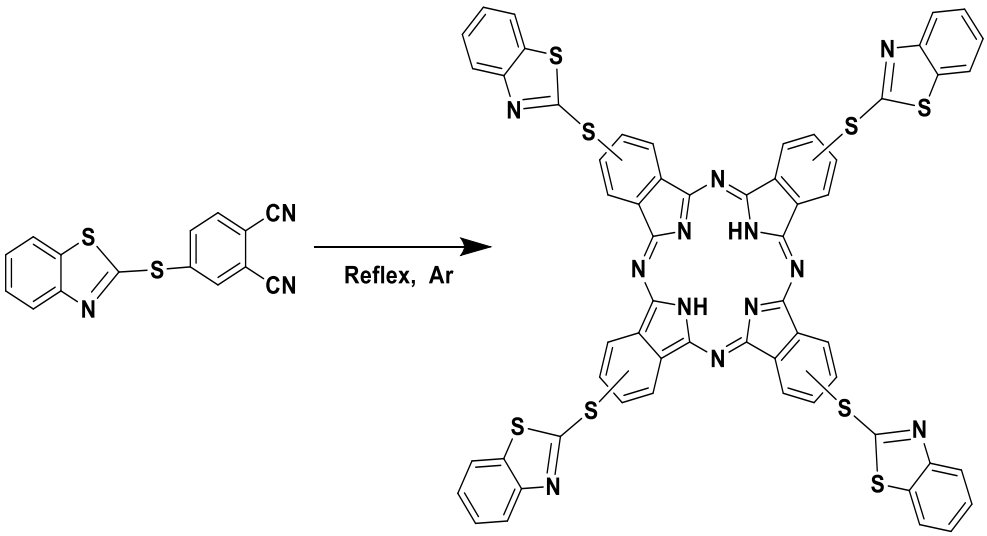


**Figure 2.8.** Synthesized of 2,2',2",2"'-(phthalocyanine-2,9,16,23-tetrayltetrakis(sulfanediyl)) tetrakis (benzo [d] thiazole) (A).

**Table 2.1.** Elemental analysis of the ligand and phthalocyanine complexes, including their molecular formula, molecular weight, and experimental yield (A).

| Name | Molecular Formula | Molecular Weight (g/mol) | Yield % | Elemental Analysis (Theo.) Exp. | | | |
|---|---|---|---|---|---|---|---|
| | | | | %C | %H | %N | %S |
| **A- Ligand** | $C_{15}H_7N_3S_2$ | 293.36 | 79.6% | (61.41)<br>60.97 | (2.41)<br>2.54 | (14.32)<br>14.24 | (21.86)<br>21.38 |
| **A- CrPc** | $Cr[C_{60}H_{28}N_{12}S_8]$ | 1225.44 | 66 % | (58.81)<br>58.55 | (2.30)<br>2.41 | (13.72)<br>14.67 | (20.93)<br>21.46 |
| **A- FePc** | $Fe[C_{60}H_{28}N_{12}S_8]$ | 1229. 29 | 26% | (58.62)<br>58.16 | (2.30)<br>2.34 | (13.67)<br>13.26 | (20.86)<br>20.22 |
| **A- CoPc** | $Co[C_{60}H_{28}N_{12}S_8]$ | 1232.38 | 66% | (58.48)<br>58.93 | (2.29)<br>2.19 | (13.64)<br>14.31 | (20.81)<br>20.46 |
| **A- NiPc** | $Ni[C_{60}H_{28}N_{12}S_8]$ | 1232.14 | 66% | (58.49)<br>58.23 | (2.29)<br>2.40 | (13.64)<br>13.23 | (20.82)<br>20.93 |
| **A- CuPc** | $Cu[C_{60}H_{28}N_{12}S_8]$ | 1236.99 | 55% | (58.26)<br>58.67 | (2.28)<br>2.38 | (13.59)<br>13.95 | (20.73)<br>20.30 |
| **A- ZnPc** | $Zn[C_{60}H_{28}N_{12}S_8]$ | 1238.83 | 53% | (58.17)<br>57.96 | (2.28)<br>2.40 | (13.57)<br>13.16 | (20.70)<br>20.94 |
| **A- $H_2$Pc** | $C_{60}H_{30}N_{12}S_8$ | 1175.46 | 74.5% | (61.31)<br>61.67 | (2.57)<br>2.46 | (14.30)<br>13.92 | (21.82)<br>21.41 |

### 2.4.3. Synthesis of 2,9,16,23-tetrakis(quinolin-8-yloxy) metal phthalocyanine complexes (B). (M: Cr, Fe, Co, Ni, Cu, and Zn).

Within a 2 cm diameter glass tube fitted with argon inlet, 0.25 g (0.92 mmol) of 4-(quinolin-8-yloxy) phthalonitrile and 0.09 g (0.52, 0.51, 0.50, 0.50, 0.49, 0.49 mmol) of metal acetate salts, (Cr, Fe, Co, Ni, Cu, Zn) respectively, were added. Then, 3 mL of DMF and 3-4 drops of DBU were added under an argon atmosphere, and the mixture was heated to boiling of DMF. The reaction was maintained at this temperature for 24 hours. The progress of the reaction was monitored by checking the color of the reaction mixture. Once the reaction was complete, the mixture was cooled down and diluted with 2 mL of ethanol. The resulting solution was then precipitated by adding to 200 mL of water drop by drop while stirring. The precipitate was filtered and washed multiple times with distilled water and then with ethanol until the eluent became colorless. The solid product, which had a blue-green color, was dried first at room temperature and then at 75 °C in a drying oven. The yield of the solid product was as follows: 0.199 g, 0.112 g, 0.23 g, 0.275 g, 0.208 g, and 0.202 g, corresponding to different percentages of metal phthalocyanine (Fe: 38.25%, Co: 21.38%, Ni: 43.67%, Cu: 52.23%, Zn: 39.17%, 37.92%,) respectively of yield, shown in **Figure 2.9.** and **Table 2.2**.

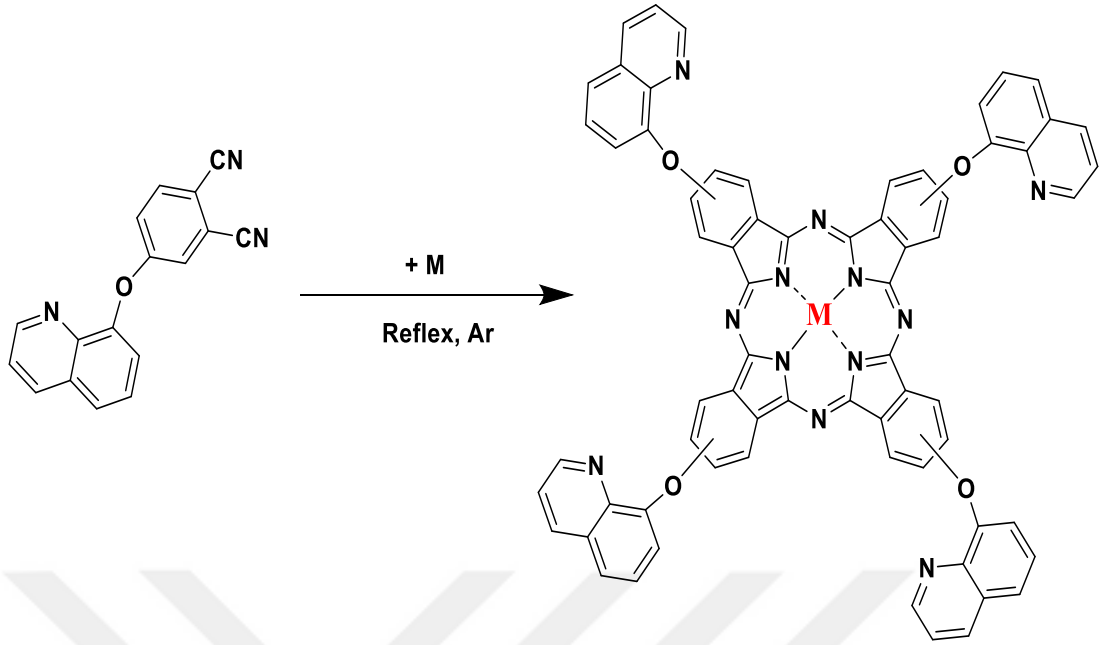


**Figure 2.9.** Synthesized of 2,9,16,23-tetrakis(quinolin-8-yloxy) Metal phthalocyanine complexes (B).

### 2.4.4. Syntheses metal free phthalocyanine ($H_2Pc$).

Using the same procedure as previously to synthesize metal-free phthalocyanine, but without adding metal acetate; all other steps remain unchanged. This results in 0.182 g (0.167 mmol) of product, with a yield of 38.4%, **Figure 2.10.**

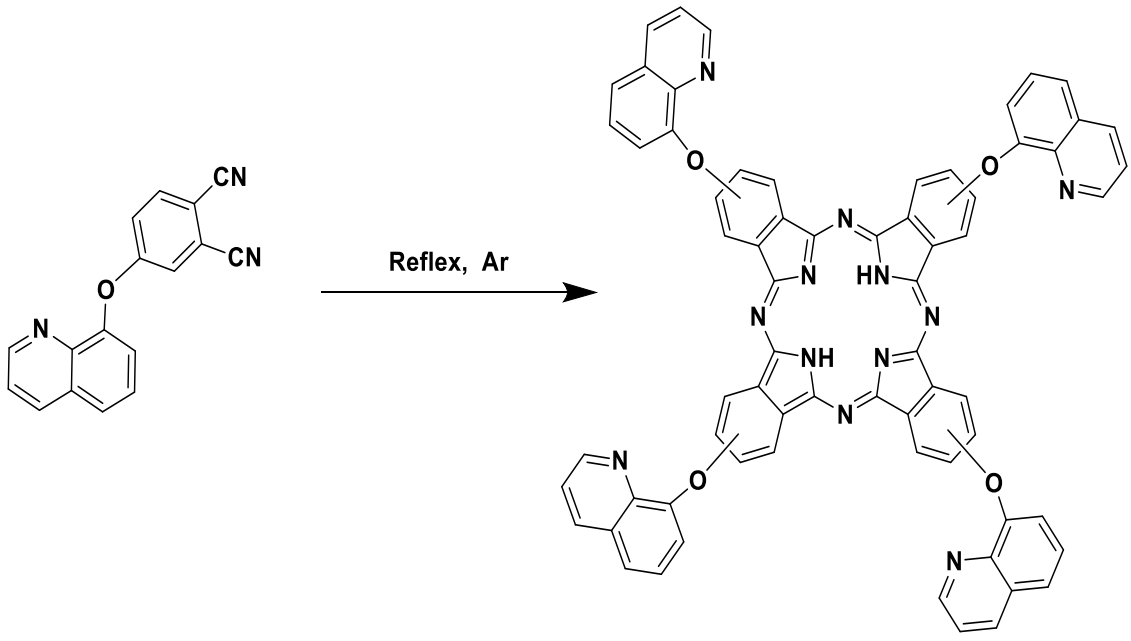


**Figure 2.10**. Synthesized of 2,9,16,23-tetrakis(quinolin-8-yloxy)phthalocyanine (B).

**Table 2.2.** Elemental analysis of the ligand and phthalocyanine complexes, including their molecular formula, molecular weight, and experimental yield (B).

| Compound | Molecular Formula | Molecular Weight (g/mol) | Yield % | Elemental Analysis (Theo.) Exp. | | |
|---|---|---|---|---|---|---|
| | | | | %C | %H | %N |
| **B-Ligand** | $C_{17}H_9N_3O$ | 271.28 | 76.1 % | (75.27)<br>75.63 | (3.34)<br>3.60 | (15.49)<br>15.16 |
| **B-CrPc** | $Cr[C_{68}H_{36}N_{12}O_4]$ | 1137.11 | 38.25 % | (71.83)<br>71.24 | (3.19)<br>3.28 | (14.78)<br>14.93 |
| **B-FePc** | $Fe[C_{68}H_{36}N_{12}O_4]$ | 1140.96 | 21.38 % | (71.58)<br>71.74 | (3.18)<br>3.26 | (14.73)<br>14.39 |
| **B-CoPc** | $Co[C_{68}H_{36}N_{12}O_4]$ | 1144.05 | 43.67 % | (71.39)<br>70.91 | (3.17)<br>3.35 | (14.69)<br>15.02 |
| **B-NiPc** | $Ni[C_{68}H_{36}N_{12}O_4]$ | 1143.81 | 52.23 % | (71.41)<br>71.68 | (3.17)<br>3.25 | (14.70)<br>14.23 |
| **B-CuPc** | $Cu[C_{68}H_{36}N_{12}O_4]$ | 1148.66 | 39.17 % | (71.10)<br>70.59 | (3.16)<br>3.39 | (14.63)<br>14.35 |
| **B-ZnPc** | $Zn[C_{68}H_{36}N_{12}O_4]$ | 1150.50 | 37.92 % | (70.99)<br>70.74 | (3.15)<br>3.31 | (14.61)<br>14.94 |
| **B-$H_2$Pc** | $C_{68}H_{38}N_{12}O4$ | 1087.064 | 38.38 % | (75.13) | (3.52) | (15.46) |

### 2.4.5. Synthesis of 2-(4-(3,4-dicyanophenoxy)phenyl) acetamide phthalocyaninato metal complexes (C). (M: Cr, Fe, Co, Ni, Cu, Zn).

Within a 2 cm diameter glass tube fitted with argon inlet, 0.25 g (0.90 mmol) of 2-(4-(3,4-dicyanophenoxy) phenyl) acetamide and 0.09 g (0.52, 0.51, 0.50, 0.50, 0.49, 0.49) mmol of metal acetate salt [$M(Ac)_2$, where M: Cr, Fe, Co, Ni, Cu, Zn] respectively, then added 3 mL DMF and 3-4 drop DBU under an argon atmosphere and heated to a stable boiling temperature of solvent, reaction continued for 24 hours. Once the reaction was completed, the mixture was cooled down to room temperature and diluted with 10 mL of ethyl alcohol. The resulting solution was precipitated adding drop by drop to 200 mL of water while stirring. The precipitate was filtered and washed multiple times with distilled water and then with ethyl alcohol until the eluent turned from dark brown to colorless. The solid product, which had a blue-green color, was dried first at room temperature and then at 75 °C in a drying oven. The yield of the metal phthalocyanine was as follows: 0.208 g, 0.21 g, 0.201 g, 0.23 g, 0.213 g, 0.202 g, also CrPc (19.80 %), FePc (20 %), CoPc (21.10 %), NiPc (21.9 %), CuPc (20.09 %), ZnPc (19.05 %) respectively, **Figure 2.11.** and **Table 2.3.**

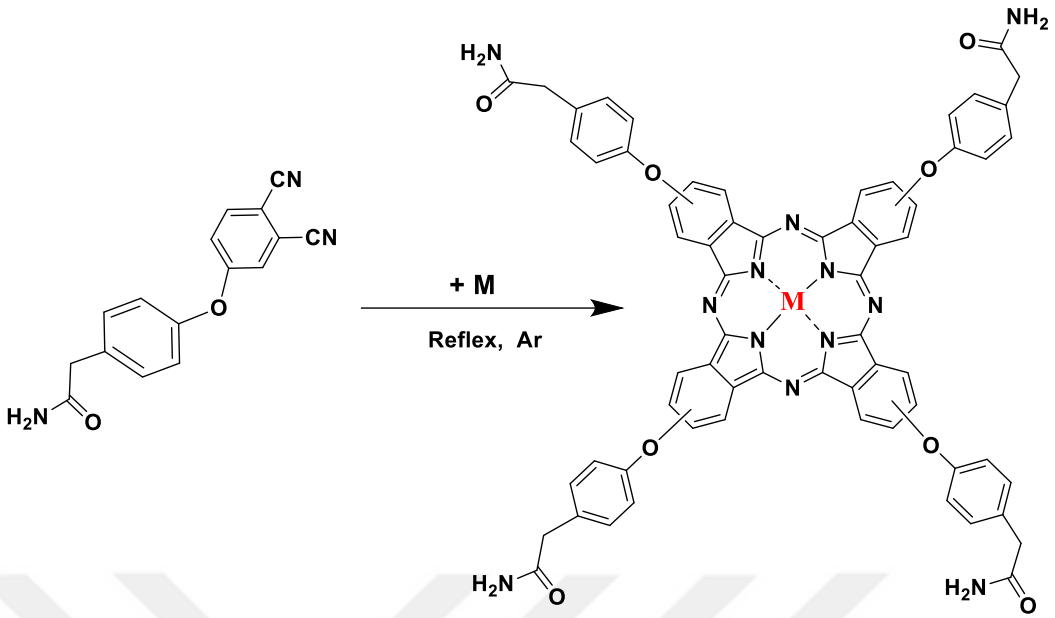


**Figure 2.11**. Synthesized of 2,2',2",2'"((2,9,16,23-tetrayltetrakis(oxy))tetrakis(benzene-4,1-diyl)) tetraacetamide Metal phthalocyanine (C).

### 2.4.6. Syntheses metal free phthalocyanine ($H_2Pc$).

Using the same procedure as previously to synthesize metal-free phthalocyanine, but without adding metal acetate; all other steps remain unchanged. This results in 0.198 g of product, with a yield of 19.8%, **Figure 2.12.**

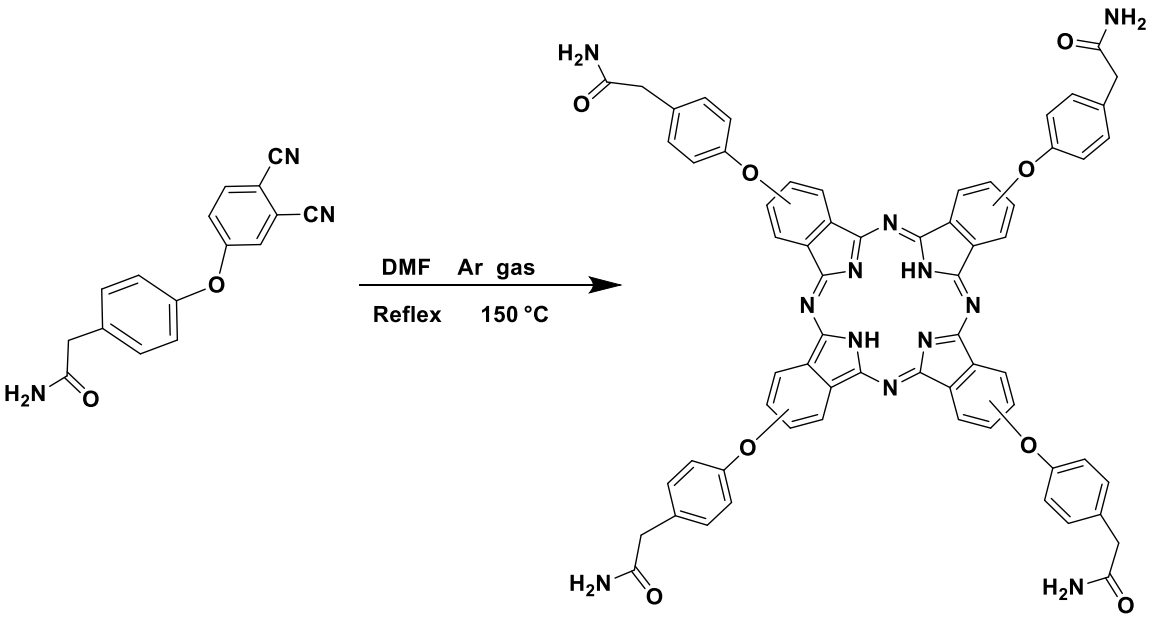


**Figure 2.12.** Synthesized of 2,2',2",2'"-((2,9,16,23-tetrayltetrakis(oxy))tetrakis(benzene-4,1-diyl)) tetraacetamide phthalocyanine (C).

**Table 2.3.** Elemental analysis of the ligand and phthalocyanine complexes, including their molecular formula, molecular weight, and experimental yield (C).

| Name | Molecular Formula | Molecular Weight (g/mol) | Yield % | Elemental Analysis (Theo.) Exp. | | |
|---|---|---|---|---|---|---|
| | | | | %C | %H | %N |
| **C-Ligand** | $C_{16}H_{11}N_3O_2$ | 277.28 | 65% | (69.31)<br>69.01 | (4.00)<br>4.15 | (15.15)<br>14.85 |
| **C-CrPc** | $Cr[C_{64}H_{44}N_{12}O_8]$ | 1161.13 | 19.80% | (66.20)<br>65.72 | (3.82)<br>4.10 | (14.48)<br>14.76 |
| **C-FePc** | $Fe[C_{64}H_{44}N_{12}O_8]$ | 1164.98 | 20% | (65.98)<br>65.54 | (3.81)<br>3.68 | (14.43)<br>14.58 |
| **C-CoPc** | $Co[C_{64}H_{44}N_{12}O_8]$ | 1168.07 | 21.10% | (65.81)<br>66.35 | (3.80)<br>3.91 | (14.39)<br>14.48 |
| **C-NiPc** | $Ni[C_{64}H_{44}N_{12}O_8]$ | 1167.83 | 21.9% | (65.82)<br>66.51 | (3.80)<br>3.67 | (14.39)<br>14.11 |
| **C-CuPc** | $Cu[C_{64}H_{44}N_{12}O_8]$ | 1172.68 | 20.09% | (65.55)<br>65.32 | (3.78)<br>3.96 | (14.33)<br>14.16 |
| **C-ZnPc** | $Zn[C_{64}H_{44}N_{12}O_8]$ | 1174.51 | 19.05% | (65.45)<br>65.66 | (3.78)<br>4.11 | (14.31)<br>14.58 |
| **C-$H_2$Pc** | $C_{64}H_{46}N_{12}O_8$ | 1111.15 | 19.8% | (69.18) | (4.17) | (15.13) |

# 3. RESULTS AND DISCUSSION.

Elemental analysis, Fourier transform infrared (FT-IR) spectroscopy, ultraviolet-visible (UV-Vis) Spectroscopy, and nuclear magnetic resonance (NMR) spectroscopy ($^{1}H$ and $^{13}C$) were used to characterize the produced chemicals. Two regions of the FT-IR spectra are crucial for determining the chemical structures of substances. The first region, known as the functional group area, spans 4000-1400 $cm^{-1}$ and includes significant peaks such as -C=C aromatic, C-H aromatic, and -NH. The second region, known as the fingerprint region, extends from 1440 to 900 $cm^{-1}$. Phthalocyanine compounds are easily recognizable by their distinctive UV-visible spectra, which exhibit a strong band at around 650 nm for metallated phthalocyanine and a double band for metal free phthalocyanine, the latter is responsible for the green to blue hues seen in compounds of this class. Additional bands, also referred to as the B or Soret band, typically overlap with the second band at around 400 nm.

Derivatives Thermogravimetry (DTG) and Thermogravimetry (TG) are techniques used to study the thermal stability, decomposition, and degradation of materials. TG/DTG analysis was performed on each sample using a SHIMADZU TGA 50 series apparatus in the heat flux instrument mode to ascertain the samples' thermal properties. In a dry air environment, samples weighing about 4 mg were heated in (Al pan) aluminum oxide $Al_2O_3$ crucibles at a rate of 10 ºC/min over a temperature range of 20-700 ºC. According to thermogravimetric data was suitable to assess the mass loss caused by the degradation and decomposition of complexes at temperatures up to 220 ºC. [172-174].

In addition, the electrochemical properties of synthesized compounds are studied with techniques like cyclic voltammetry (CV) and square wave voltammetry (SWV), Cyclic voltammetry is a widely used electrochemical technique, that measures the current response of a system concerning an applied potential, particularly emphasizing electron transfer during reaction processes. This technique is instrumental in studying the redox properties of electroactive species in liquid solutions. The procedure involves systematically varying the electrode potential within a specified range at a constant rate while monitoring the resulting current in an electrochemical cell [175]. In this study, CV and SWV measurements of the compounds were performed on a glassy carbon (GC) electrode in DMF using tetrabutylammonium tetrafluoroborate (TBAFB) as a supporting electrolyte. To explore the electrochemical properties of each phthalocyanine molecule, a wider potential range (-2.6 to +1.1 V versus Fc/Fc+) was employed. Relevant data from the literature on similar substances are included for comparison. Phthalocyanine complexes can undergo multiple one-electron reductions and oxidations of the conjugated macrocycle, generating anion and cation radicals, respectively.

## 3.1. 4-Nitrophthalonitrile

Phthalocyanines could be synthesized using traditional processes with various precursors, such as 4-Nitro phthalonitriles. Building on these considerations, our ultimate objective is to achieve the synthesis and characterization of new phthalocyanine. **Figure 3.1**. shows the synthesis of 4-nitrophthalonitrile from phthalimide, in the first step, phthalimide nitrated to form 4-Nitrophthalimide subsequent transformation of 4-nitrophthalimide to 4-nitrophthalamide and finally, 4-nitrophthalonitrile is obtained [134].

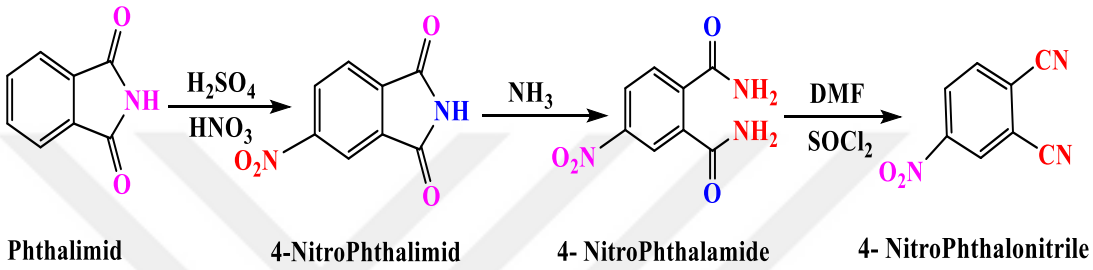


**Figure 3.1.** 4-Nitrophthalonitrile can be synthesized from phthalimide in most cases.

- **IR Spectrum**

We have prepared and employed KBr pellets to analyze the infrared spectrum of 4-nithrophthalimide. The presence of two sharp peaks at 1347 $cm^{-1}$ and 1660 $cm^{-1}$, corresponding to the nitro $NO_2$ group, indicates that the phthalimide compound underwent nitration at position 4, as shown in **Figure 3.2.**

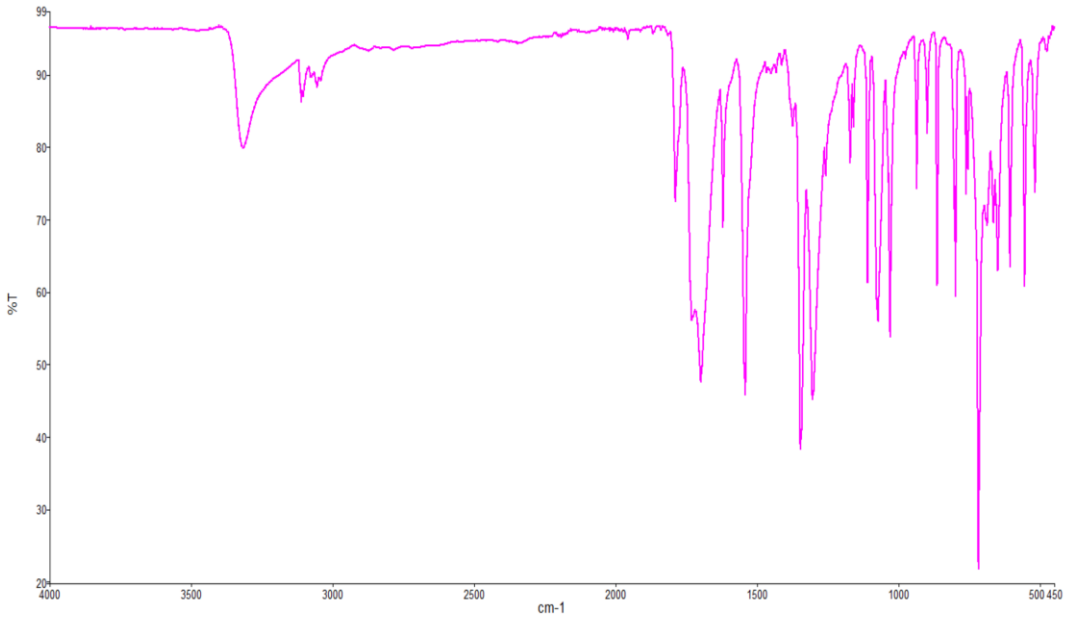


**Figure 3.2**. FT-IR spectrum of 4-Nitrophthalimide.

The IR spectra of 4-nitrophthalamide showed a stretching band at 3427 $cm^{-1}$, indicating the presence of NH groups typical of amides. Additionally, peaks corresponding to amide carbonyl (C=O) bonds were seen at 1660 $cm^{-1}$, as shown in **Figure 3.3.**

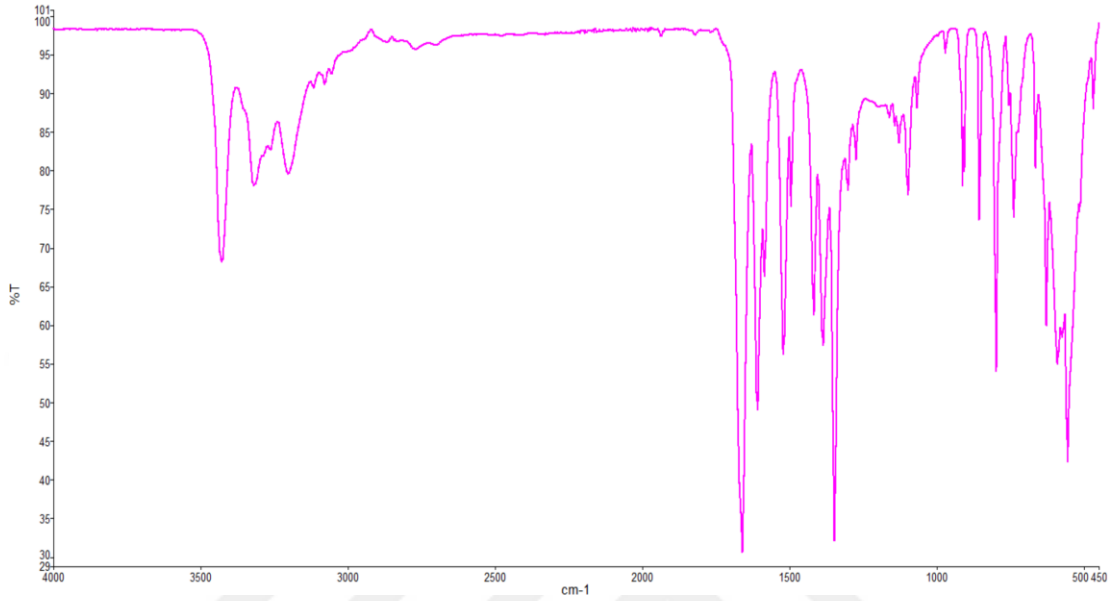


**Figure 3.3**. FT-IR spectrum of 4-NitroPhthalamide.

The presence of the nitrile (-C≡N) signal at 2240 $cm^{-1}$ supports the synthesis of 4-nitrophthalonitrile The IR spectra of 4-nitrophthalonitrile, as seen in **Figure 3.4.** and **Table 3.1**.

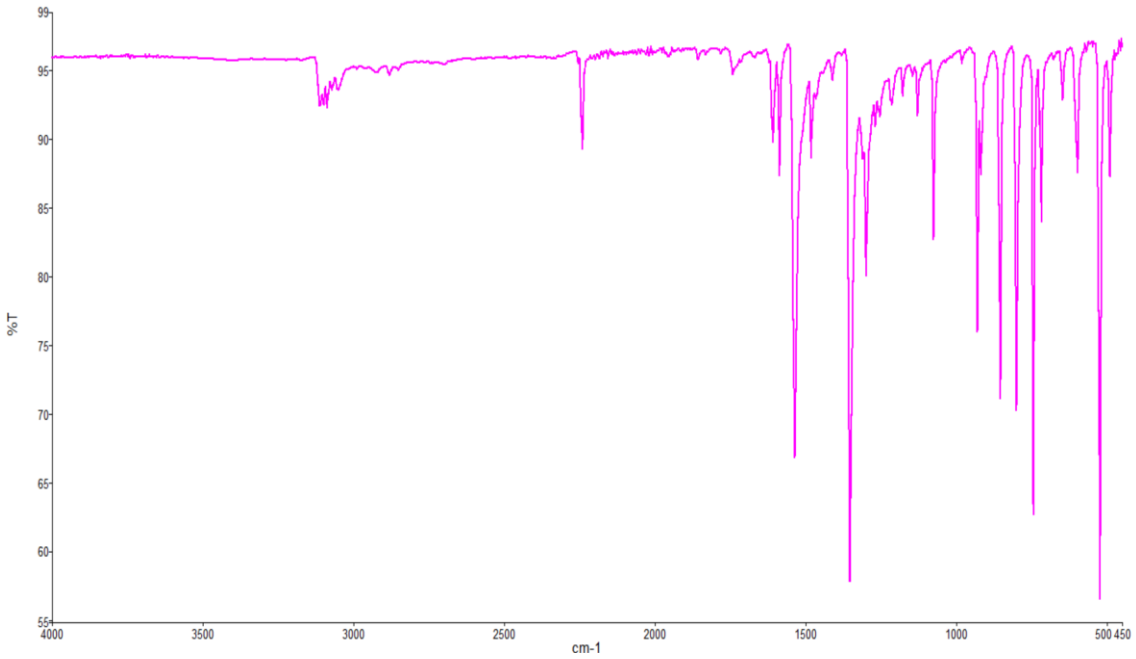


**Figure 3.4**. FT-IR Spectrum of 4- NitroPhthalonitrile.

**Table 3.1.** Important FT-IR spectrum of 4-Nitrophthalonitrile.

| Vibrations ($cm^{-1}$) | Assignment |
|---|---|
| 3082 | Ar-CH |
| 2240 | C≡N |
| 1609 | C=C |
| 1353, 1534 | Aromatic $NO_2$ |

## 3.2. 2-Mercaptobenzothiazole

We utilized 2-mercaptobenzothiazole as the starting material, structure is shown in **Figure 3.5**. The chemical formula is $C_7H_5NS_2$, the molecular weight is 167.24 g/mol and has a white-yellow Color.

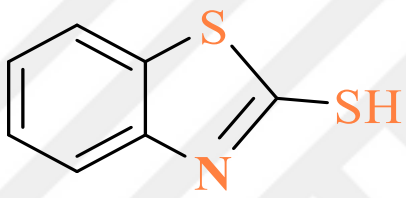


**Figure 3.5**. 2-mercaptobenzothiazole.

FT-IR spectra of 2-mercaptobenzothiazole have distinct peaks that correspond to the various functional groups found in the molecule. This area of the infrared spectrum showed two weak-intensity peaks (C-H aromatic) at 3037 and 2965 $cm^{-1}$. A very weak band was also recognized at 2576 $cm^{-1}$ for the S-H stretching vibration.

The stretching mode of C=C is attributed to the bands seen at 1596, and 1495 $cm^{-1}$. The interaction between the C-N stretching vibrations of the C=N group, when is seen as a strong and weak band at 1244, and 2235 $cm^{-1}$ respectively. The distinct bands seen in a cluster at 1012, 1033, and 1075 $cm^{-1}$ correspond to normal vibrations in the N=C-S groups, **Figure 3.6.** and **Table 3.2.**


**Figure 3.6**. FT-IR Spectrum of benzothiazole-2-thiol.

**Table 3.2.** Important FT-IR spectrum of 2-Mercaptobezotriozole.

| Vibrations ($cm^{-1}$) | Assignment |
|---|---|
| 3037, 2965 | Ar-CH |
| 2244 | C=N |
| 1244 | C-N |
| 1596, 1495 | C=C |
| 1075, 1033 | C-S |
| 2576 | H-S |

## 3.3. 4-(benzothiazol-2-ylthio)phthalonitrile

In a dry, inert environment, the ligand 4-(benzothiazol-2-ylthio)phthalonitrile was synthesized using DMF as a solvent at 90 °C. The chemical formula is $C_{15}H_7N_3S_2$, the molecular weight is 293.36 g/mol and it has a light-yellow Color, **Figure 3.7.**

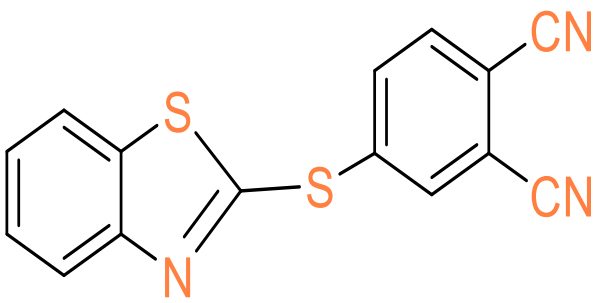


**Figure 3.7.** 4-(benzothiazol-2-ylthio)phthalonitrile.

- **FT-IR Spectrum**

The compound was analysed using FT-IR using a KBr pellet to generate its spectra. As seen in **Figure 3.8** The new ligand is absent two distinct peaks at 1354 $cm^{-1}$ and 1536 $cm^{-1}$, which correspond to the missing of the nitro $NO_2$ group. Other peaks are retained and appear in the graph, as shown in **Table 3.3.**

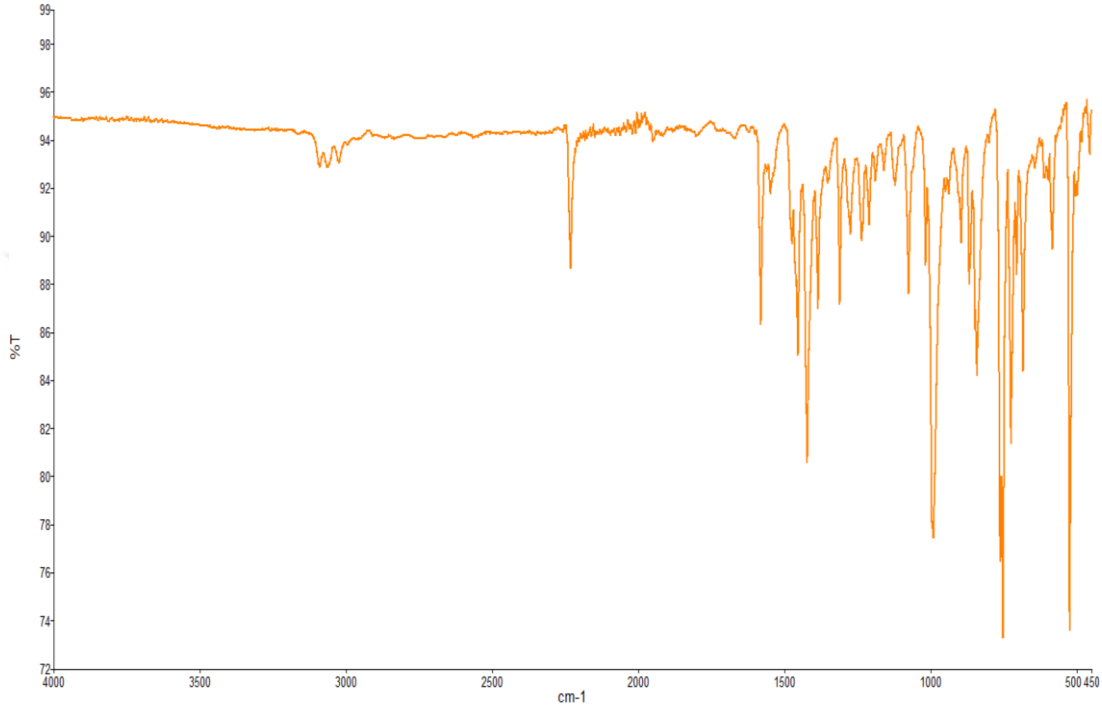


**Figure 3.8**. FT-IR spectrum of 4-(benzothiazol-2-ylthio)phthalonitrile.

**Table 3.3.** Important FT-IR peaks of 4-(benzothiazol-2-ylthio)phthalonitrile.

| **Vibration ($cm^{-1}$)** | **Assignment** |
|---|---|
| 3090-3060, 3023 | C-H Aromatic |
| 1080-1360 | C-N weak |
| 2232 | C≡N |
| 1581, 1454 | C=C |
| 583, 684,724 | C-S |

- **$^1$HNMR Spectrum**

The $^1$HNMR spectrum was recorded in DMSO-d6. The hydrogen atoms of 4-(benzo (d) thiazol-2-yithio), specifically H9, H12, and H3, appeared as doublets at 8.60, 8.30, and 8.20 ppm, respectively. The peaks for hydrogens H1 and H6 were observed as a singlet at 8.12 and 8.03 ppm. While the two hydrogen H7 and H8 were observed as a triplet at 7.56 and 7.53 ppm, respectively. The solvent peak for DMSO-d6 and a water impurity appeared at 2.70 ppm and 1.23 ppm, respectively, as shown in **Figure 3.9**.

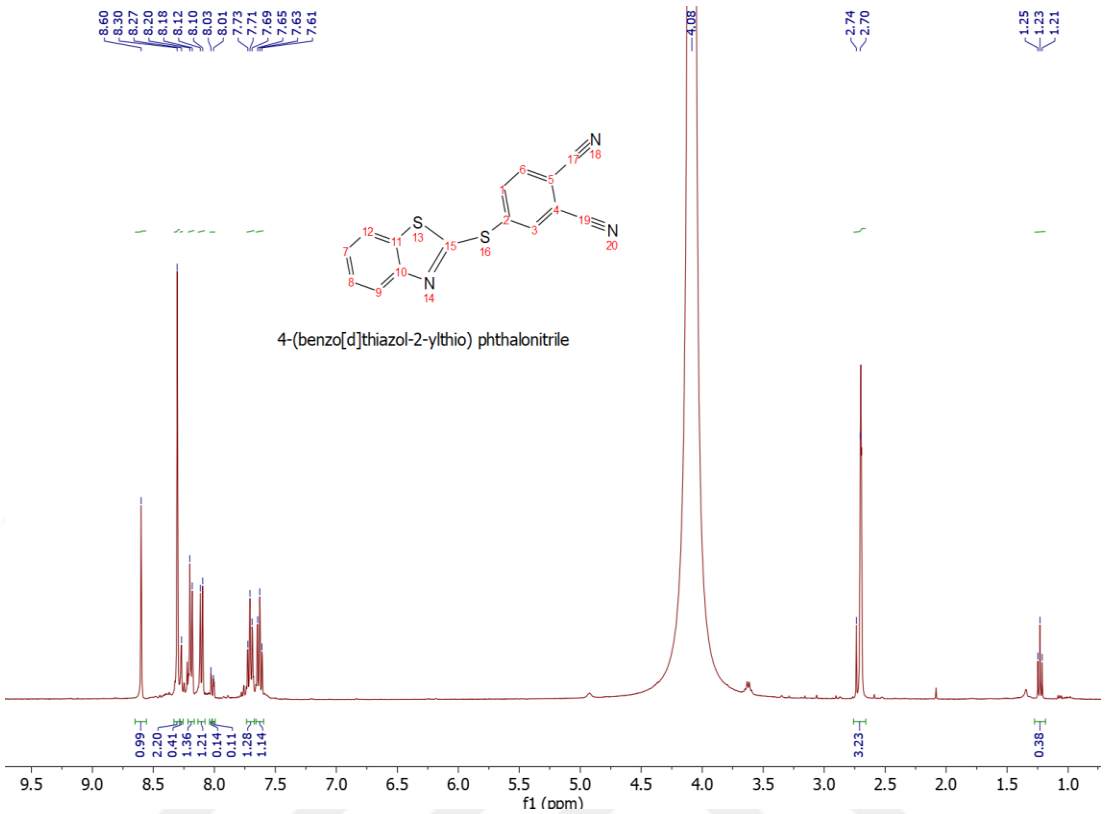


**Figure 3.9.** H-NMR spectrum of 4-(benzothiazol-2-ylthio) phthalonitrile.

## 3.4. 8- Hydroxyquinoline

8-hydroxyquinoline is a colorless solid, its conjugate base is a chelating agent, which is used for the quantitative determination of metal ions. The chemical formula is $C_9H_7NO$, with a molecular weight of 145.16 g/mole, and it has a light brown color shown in **Figure 3.10.**

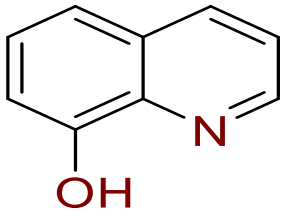


**Figure 3.10.** 8-Hydroxyquinoline (Quinolin-8-ol).

- **FT-IR Spectrum**

The most effective method for determining the functional groups is to analyze the FT-IR spectra. The presence of the OH in the 8-hydroxyquinoline aromatic ring is indicated by a broad band between 3370 -2700 $cm^{-1}$ in the spectrum. Additionally, there is a band around 3047.34 $cm^{-1}$,

and the C=C group vibration in the aromatic ring is responsible for the three peaks at 1470, 1496, and 1432 $cm^{-1}$. The presence of C=N and C-N groups in the aromatic ring is indicated by bands at 1578 $cm^{-1}$ and 1378 $cm^{-1}$ respectively. As shown in **Figure 3.11**. and **Table 3.4.**

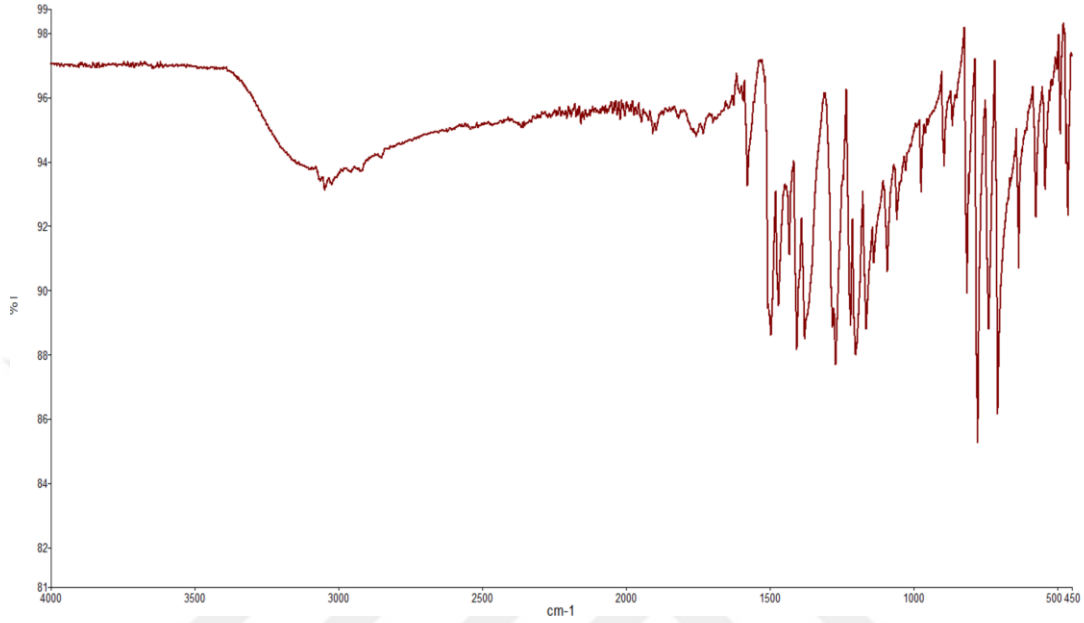


**Figure 3.11**. FT-IR Spectrum of quinolin-8-ol.

**Table 3.4.** Important FT-IR peaks of quinoline-8-ol.

| Vibration ($cm^{-1}$) | Assignment |
|---|---|
| 3047 | C-H Aromatic |
| 1378 | C-N weak |
| 1578 | C=N |
| 1470, 1496, 1432 | C=C |
| 3370 -2700 | H-O wide |

## 3.5. 4-(quinolin-8-yloxy) phthalonitrile.

The ligand was synthesized using 8-hydroxyquinoline and 4-Nitrophthalonitrile in DMF solvent under specific conditions. The final product has the chemical formula $C_{17}H_9N_3O$, with a molecular weight of 271.28 g/mol, and exhibits a dark brown Color. Shown in **Figure 3.12**.

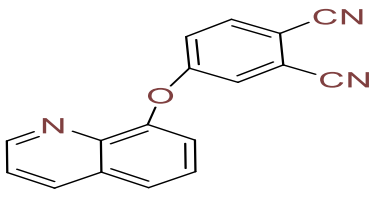


**Figure 3.12**. 4-(quinolin-8-yloxy)phthalonitrile

- **FT-IR Spectrum**

To determine the functional groups most effectively, the FT-IR spectrum was analyzed. The IR spectra of the compound were examined after its production in a KBr tablet. The novel ligand loses the two typical peaks at 1354 $cm^{-1}$ and 1536 $cm^{-1}$, indicating the absence of the nitro $NO_2$ group, however other peaks representing functional groups that were either retained or newly introduced during synthesis may appear. These peaks offer vital information about the structure and composition of the ligand. Shown in **Figure 3.13** and **Table 3.5.**

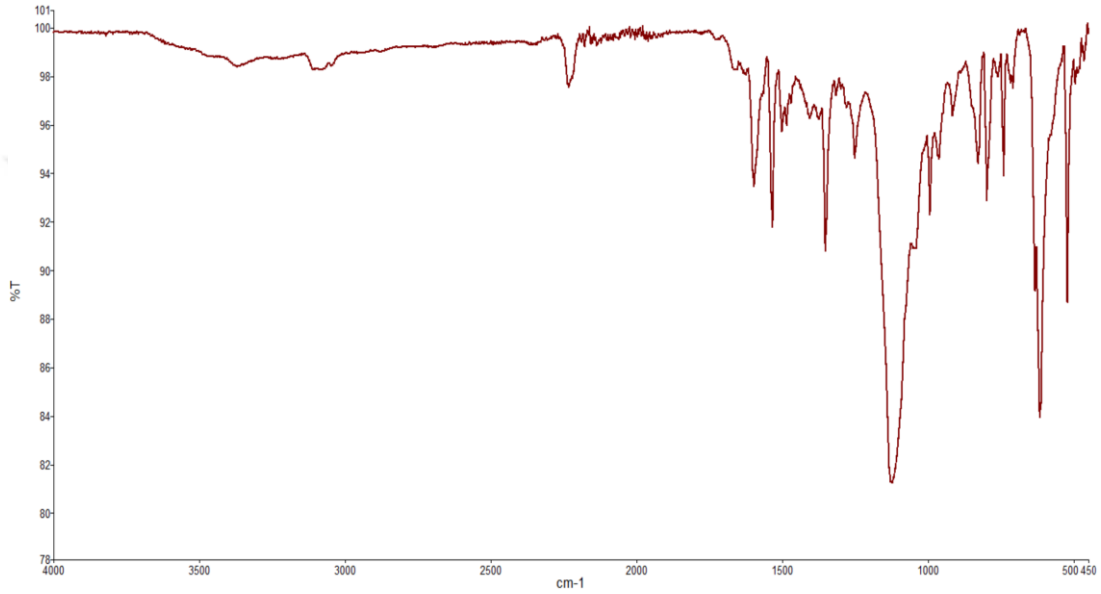


**Figure 3.13**. FT-IR spectrum of 4-(quinolin-8-yloxy)phthalonitrile

**Table 3.5.** Important FT-IR peaks of 4-(quinolin-8-yloxy)phthalonitrile**.**

| **Vibration ($cm^{-1}$)** | **Assignment** |
|---|---|
| 3111-3080, 3047 | C-H Aromatic |
| 1351-1250 | C-N weak |
| 2233 | C≡N |
| 1599, 1534 | C=C |
| 1125 | C-O |

- **$^1$HNMR Spectrum**

The 1HNMR spectrum was recorded in DMSO-d6. The hydrogen atoms of 4-(quinolin-8-yloxy) phthalonitrile, specifically H15, and H17, appeared as singlet at 8.83, and 8.54 ppm, respectively. The peaks for hydrogens H6, H13 and H3 were observed as a doublet at 8.05, 8.00, and 7.76 ppm. The other hydrogens H16, H8, H1, and H9 appeared as a singlet at 7.72, 7.67, 7.29,

and 7.26 ppm respectively. Additionally, The solvent peak for DMSO-d6 and a water impurity appeared at 2.57 ppm and 1.10 ppm, respectively as shown in **Figure 3.14**.

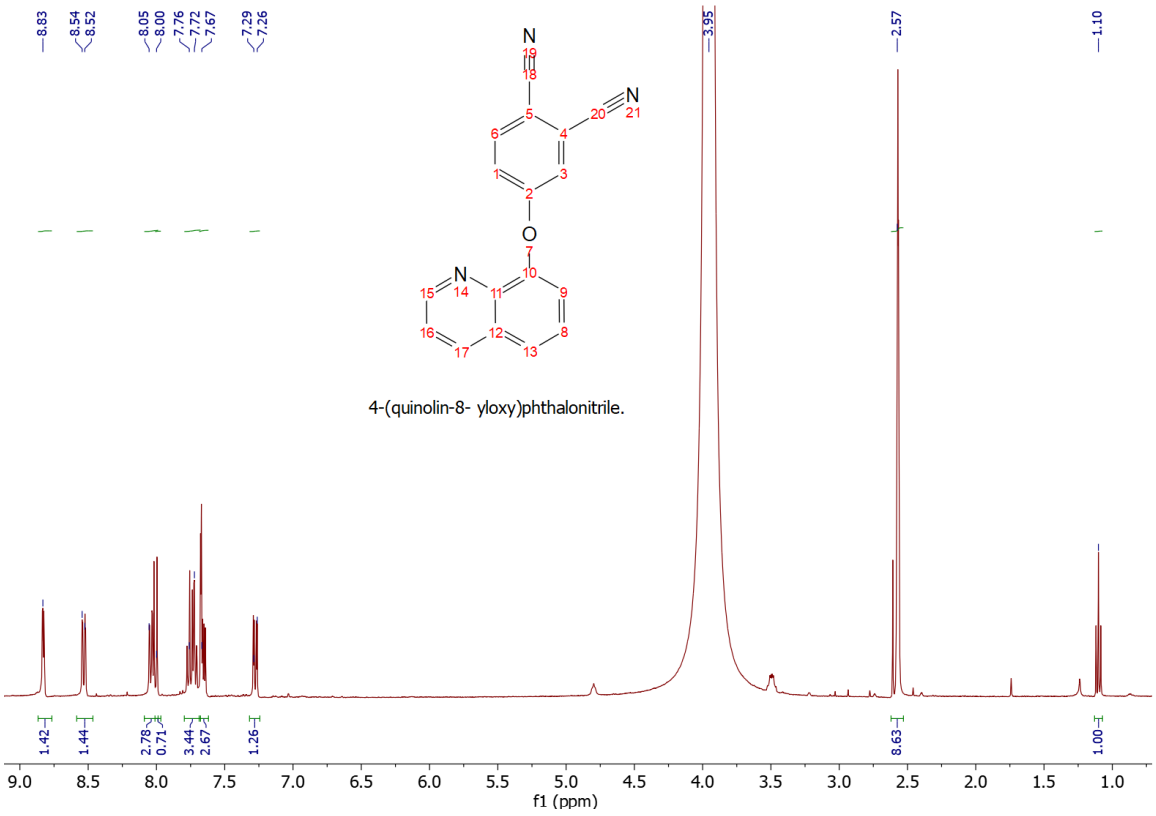


**Figure 3.14.** HNMR of 4-(quinoline-8-yloxy) Phthalonitrile.

## 3.6. 4-Hydroxyacetamitade

4-hydroxyphenyl acetamide has more names like 2-(4-Hydroxyphenyl)acetamide, 4-Hydroxybenzeneacetamide, p-Hydroxyphenylacetamide is finds some use as a plasticizer and as an industrial solvent. The molecular formula of 4-hydroxyphenylacetamitade is $C_8H_9NO_2$ with a molecular weight of 151.16 g/mol, as shown in **Figure 3.15.**

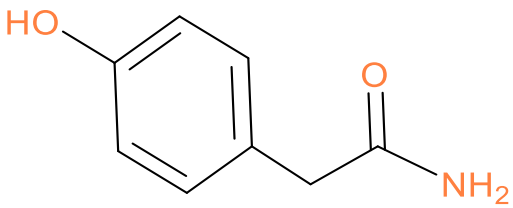


**Figure 3.15**. 2-(4-hydroxyphenyl)acetamide

- **FTIR Spectrum**

A broad, high absorption at 3326 $cm^{-1}$, was attributed to the O-H stretching vibration. A very strong band at 3162 $cm^{-1}$ was seen for the N-H stretching vibrations. The weak band at 3035 $cm^{-1}$ is ascribed to the symmetric stretching vibration of C-H. The heteroaromatic chemical molecule and its derivatives have a close structural relationship with benzene. As a result, they often display several weak bands in the 3100-3000 $cm^{-1}$ range, caused by contractions of the C-H bonds. C-C stretching vibrations in rings typically occur between 1600 and 1400 $cm^{-1}$. A band spanning the range of 1430-1650 $cm^{-1}$ is typical for aromatic compounds, which show strong C-C stretching vibrations at 1443 and 1565 $cm^{-1}$. In this work, the C=C stretching vibrations were found to be particularly prominent in the FTIR spectrum at 1654 $cm^{-1}$.

The stretching vibration of the C-O bond is responsible for the single sharp band as seen often observed between 1690 -1655 $cm^{-1}$, which is the most defining feature of the carbolic group. Typically, the C-O stretching vibrations occur between 1320-1210 $cm^{-1}$. The stretching vibrations of C=O are clearly visible at 1654 $cm^{-1}$, while the C-O stretching vibrations are clearly visible around 1227 $cm^{-1}$. As shown in **Figure 3.16**, and **Table 3.6.**

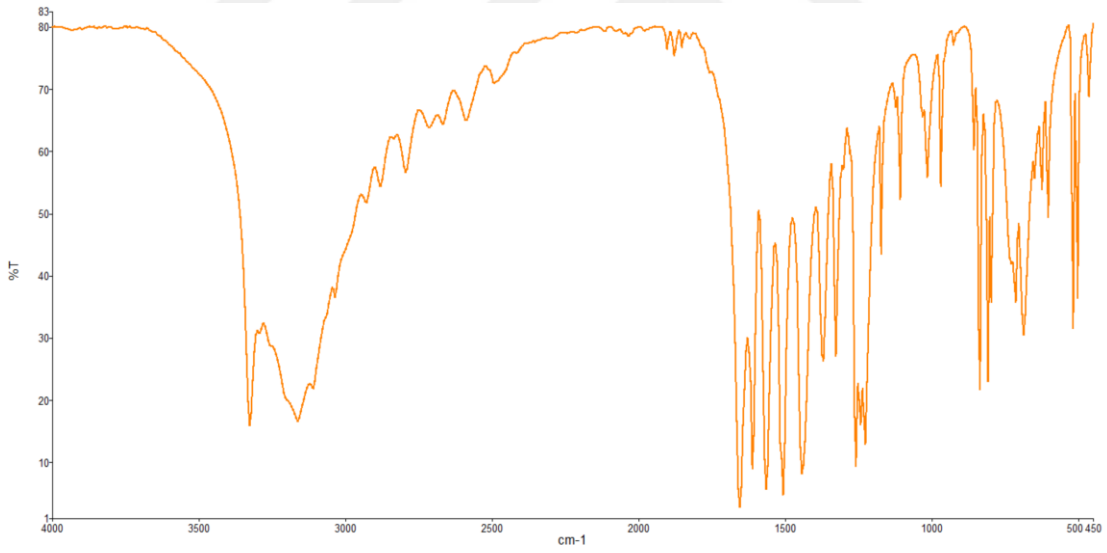


**Figure 3.16**. FT-IR Spectrum of 2-(4-hydroxyphenyl)acetamide.

**Table 3.6.** Important FT-IR peaks of 2-(4-(3,4-dicyanophenoxy) phenyl) acetamide.

| Vibration (cm-1) | Assignment |
|---|---|
| 3326, | C-H Aromatic |
| 3162 | H-N |
| 1654 | C=C |
| 1654 | C=O |
| 1227 | C-O |
| 1611, 1593, 855 | N-H |

## 3.7. 2-(4-(3,4-dicyanophenoxy) phenyl) acetamide.

In a dry, inert environment, the ligand 2-(4-(3,4-dicyanophenoxy) phenyl) acetamide was synthesized using DMF as a solvent at 90 °C. The chemical formula is $C_{16}H_{11}N_3O_2$, the molecular weight is 277.28 g/mol and it has a light-yellow Color. As shown in **Figure 3.17**.

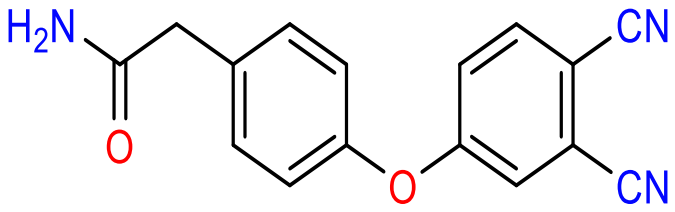


**Figure 3.17**. 2-(4-(3,4-dicyanophenoxy)phenyl)acetamide

- **FTIR Spectrum**

Removal of nitro groups was indicated by the absence of nitro ($NO_2$) peaks at 1354 $cm^{-1}$ and 1536 $cm^{-1}$ and emerging a new peak at 2228 cm belonging to the C≡N group confirms the formation of ligand. The structure and content of the synthesized ligand may be inferred from these peaks. As shown in **Figure 3.18.** and **Table 3.7.**


**Figure 3.18**. FT-IR Spectrum of 2-(4-(3,4-dicyanophenoxy)phenyl)acetamide.

**Table 3.7.** Important FT-IR peaks of 2-(4-(3,4-dicyanophenoxy)phenyl)acetamide.

| Vibration ($cm^{-1}$) | Assignment |
|---|---|
| 3203-3140, 3077 | C-H Aromatic |
| 2228 | C≡N |
| 1557 | C=C |
| 1666 | C=O |
| 1249, 1202 | C-O |
| 1611, 1593, 855 | N-H |

- **$^{1}$HNMR Spectrum**

The 1HNMR spectrum was recorded in DMSO-d6. The hydrogen atoms of 2-(4-(3,4-dicyanophenoxy) phenyl) acetamide, specifically H6, H3, and H1, appeared as doublets at 8.04, 7.93, and 7.82 ppm, respectively. The peaks for hydrogens H13 and H15 were observed as a singlet at 7.55 ppm. The amide hydrogen (H10) appeared at 7.47 ppm, while hydrogens H12 and H16 were observed as a doublet at 7.29 ppm. Additionally, H8 was seen as a doublet at 3.51 ppm. The solvent peak for DMSO-d6 and a water impurity appeared at 2.19 ppm and 1.25 ppm, respectively shown in **Figure 3.19.**

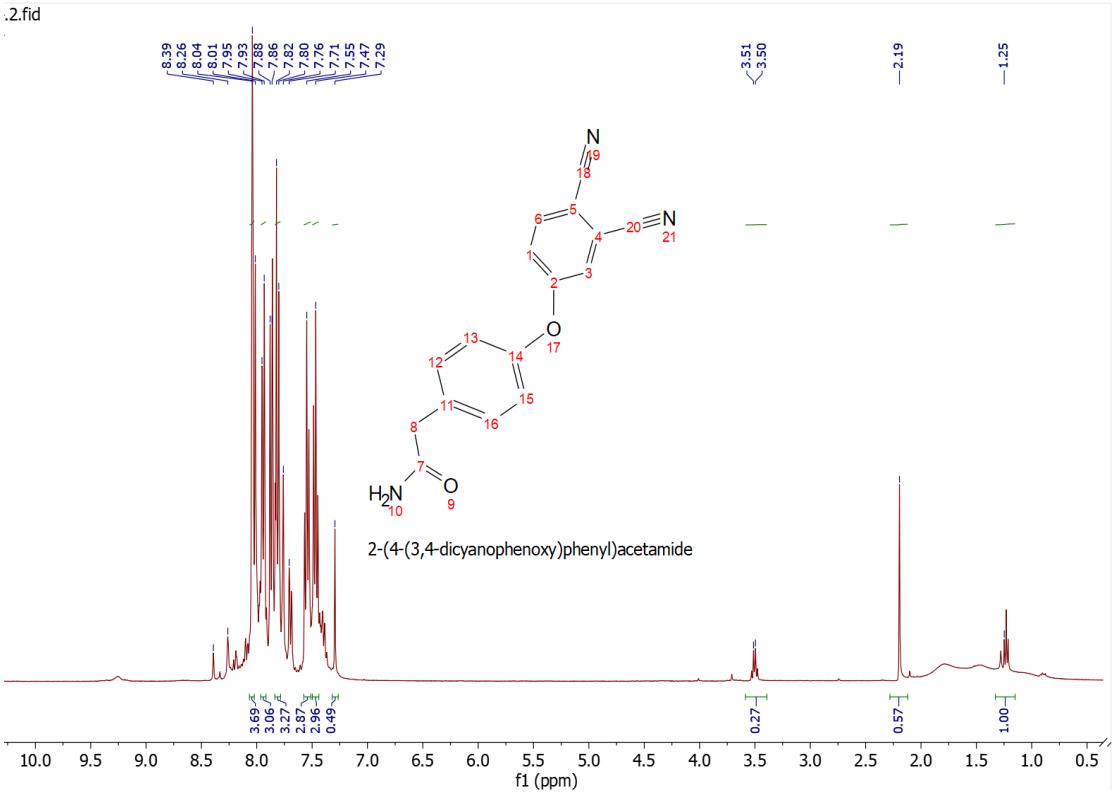


**Figure 3.19.** H-NMR spectrum of 2-(4-(3,4-dicyanophenoxy)phenyl)acetamide.

### 3.8. 2,2',2'',2'''(2,9,16,23-tetrayltetrakis(sulfanediyl))tetrakis(benzothiazole) Chromium phthalocyanine

The chromium phthalocyanine (CrPc) was prepared by reacting 4-(benzothiazol-2-ylthio) phthalonitrile with chromium (II) acetate under an argon atmosphere in DMF. The presence of Cr(II) salt in this condition caused the cyclotetramerization of four phthalonitrile ligands to form green-colored CrPc, a characteristic property of phthalocyanines. As shown in **Figure 3.20.**

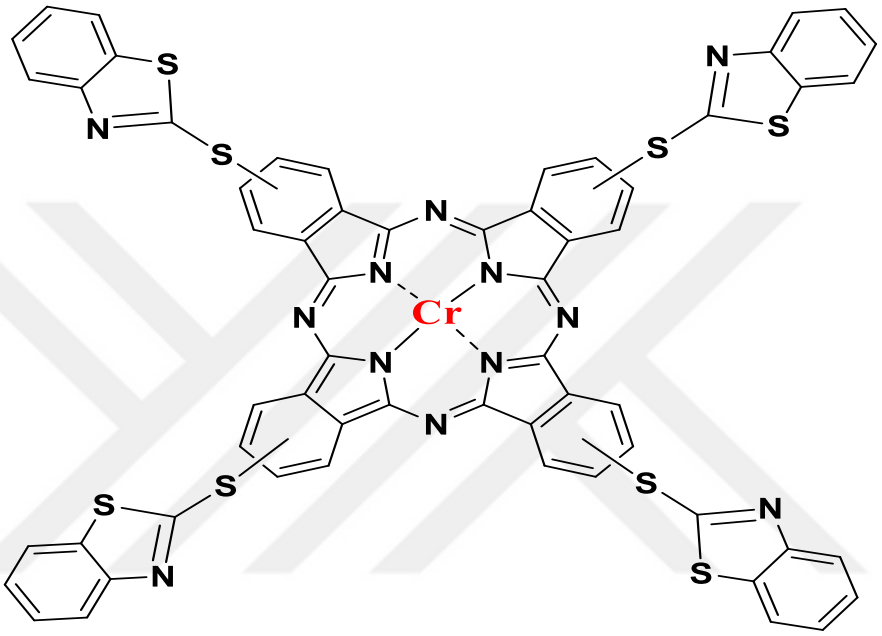


**Figure 3.20.** 2,2',2",2"'(2,9,16,23-tetrayltetrakis(sulfanediyl))tetrakis(benzo[d]thiazole) Chrome phthalocyanine

- **FT-IR Spectrum**

The KBr pellet in IR spectra showed the loss of the C≡N peak at 2232 $cm^{-1}$, indicating the completion of the reaction. Notable peaks include a weak peak at 2923 $cm^{-1}$ corresponding to aromatic C-H stretching, a peak at 1649 $cm^{-1}$ for C=C macrocycle ring deformation, and peaks at 1457 and 1425 $cm^{-1}$ for C=N stretching. Additionally, a peak at 1185 $cm^{-1}$ corresponds to C-N stretching, while peaks at 1042 $cm^{-1}$ and 756 $cm^{-1}$ correspond to C-C and C-S bonds, respectively, shown in **Figure 3.21.**

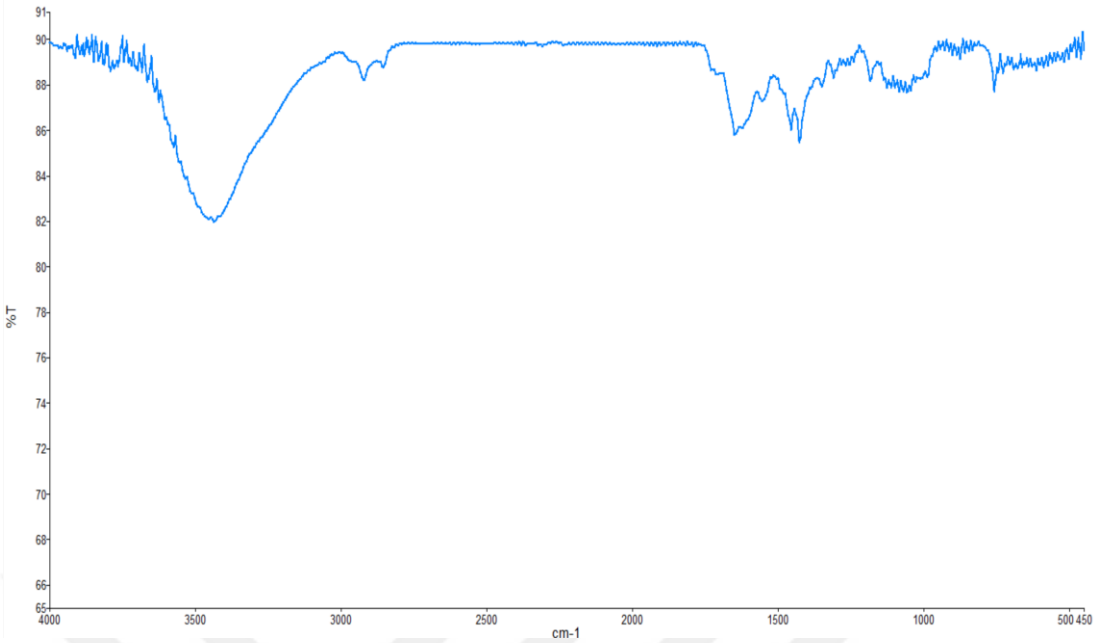


**Figure 3.21.** FT-IR spectrum of Cr(II)phthalocyanine.

- **UV–visible spectrum**

MPcs in DMF have strong absorptions between 600 -700 nm in the Q band area according to their UV-vis spectra. The π-π* transition from the HOMO to the LUMO of the phthalocyanine ring defines the Q band absorptions of the compounds. The transitions from the deeper π levels to the LUMO caused the B band absorptions of the compounds to be seen in the UV area between 300–400 nm. The CrPc compound in DMF has two absorptions in the Q band area at 683, and 615 nm (shoulder) on the Soret band at 440 nm as shoulder in the UV–vis spectrum, **Figure 3.22**.

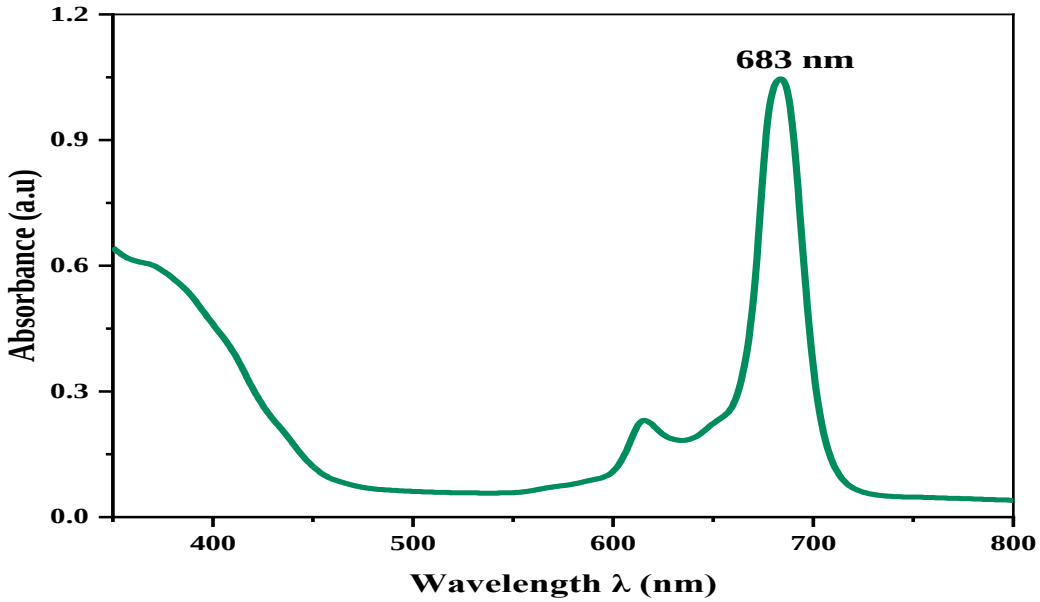


**Figure 3.22.** UV-visible spectrum of Cr(II)phthalocyanine

- **Thermal analysis**

The TG and DTG analyses of the CrPc complex demonstrated thermal stability up to 250 °C, starting of thermogram less than 100 caused by experimental error, resulting in a weight loss of approximately 4%. The complex then undergoes a three-step decomposition process: First exothermic decomposition occurs between 270-420 °C, with a 15% weight loss. Following that, a second exothermic decomposition happened, taking place at 425-520 °C, with a 30% weight loss. Finally, a third decomposition occurs between 520-680 °C, leading to a 22% weight loss. The total weight loss is 71%, and the TG thermograms reveal that CrPc decomposes without displaying a melting point, leaving about 26% of residue, as shown in **Figure 3.23.**

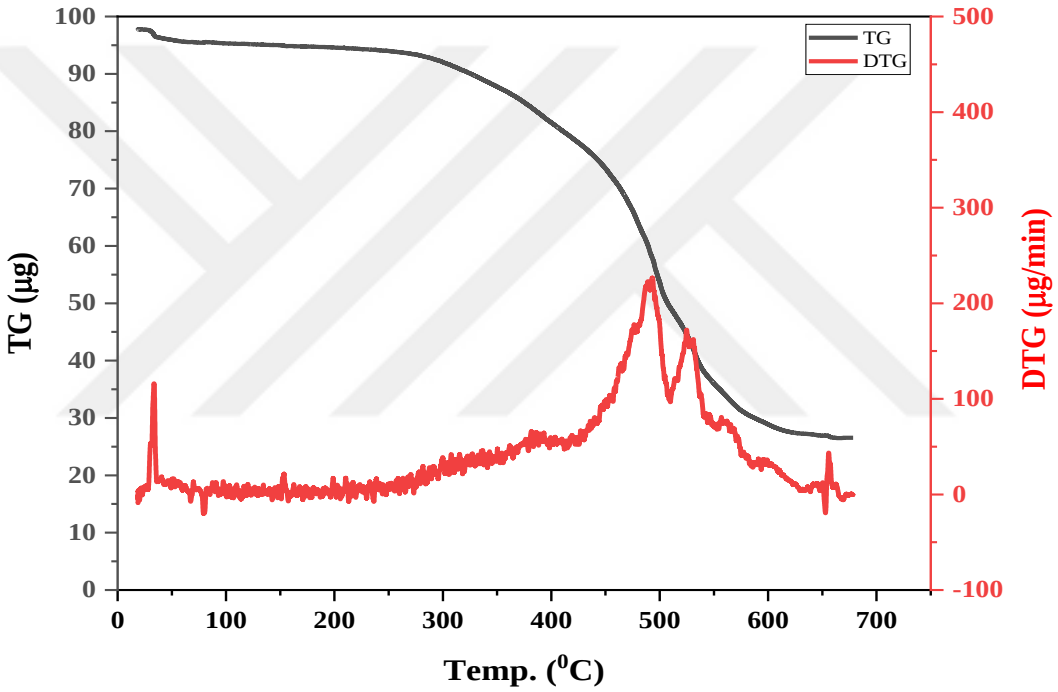


**Figure 3.23.** TG and DTG of Cr(II)phthalocyanine

- **Electrochemical Properties**.

The electrochemical analysis of CrPc was conducted using cyclic voltammetry (CV) and square wave voltammetry (SWV), in DMF with tetra butyl ammonium tetrafluoroborate (TBAFB) as the supporting electrolyte. The Fc/Fc+ pair, ferrocene, and ferrocenium ion served as a sudo reference electrode. Potentials were measured relative to Fc/Fc+ in non-aqueous solutions. Due to the limited solubility of CrPc, the intensity of the CV voltammogram was great. On the other hand, the SW voltammogram has better results than CV. Multiple reduction and oxidation reactions observed occur across the macrocycle's moiety of CrPc seen in **Figure 3.24** and **Figure 3.25**. The SW voltammogram of CrPc reveals four reduction waves at -1.28, -1.52 -1.83, and -2.14 volts,

representing $R_1$, $R_2$, $R_3$, and $R_4$, respectively, with only one oxidation wave ($O_1$) at 0.83 volts. It also has a redox wave of Chromium(II/III) metal (Mr) at -1.04 V.

In phthalocyanine rings, the redox behaviour is associated with the removal of electrons from the HOMO, whereas the LUMO may accept up to four more electrons. The electrochemical molecule bandgap is equal to the difference in energy between these oxidation and reduction processes. These redox reactions often exhibited quasi reversible behaviour in terms of peak separations and peak potential variations with scan rate.

There are four redox processes indicated as $R_1$, $R_2$, $R_3$, and $R_4$ on the CV and SWV attributed to Cr(II)Pc-2/Cr(II)Pc-3, Cr(II)Pc-3/Cr(II)Pc-4, Cr(II)Pc-4/Cr(II)Pc-5, and Cr(II)Pc-5/Cr(II) Pc-6 respectively. $O_1$, and $O_2$ are corresponding to the oxidation process of CrPc, specifically Cr(II)Pc-2/Cr(III)Pc-1, and Cr(III)Pc-1/Cr(III)Pc0 respectively. Additionally, there metal-based redoxes process refers to Cr(II)Pc-2/Cr(I)Pc-2 because the $Cr^{2+}$ ion redoxes are active in phthalocyanine complexes [176].

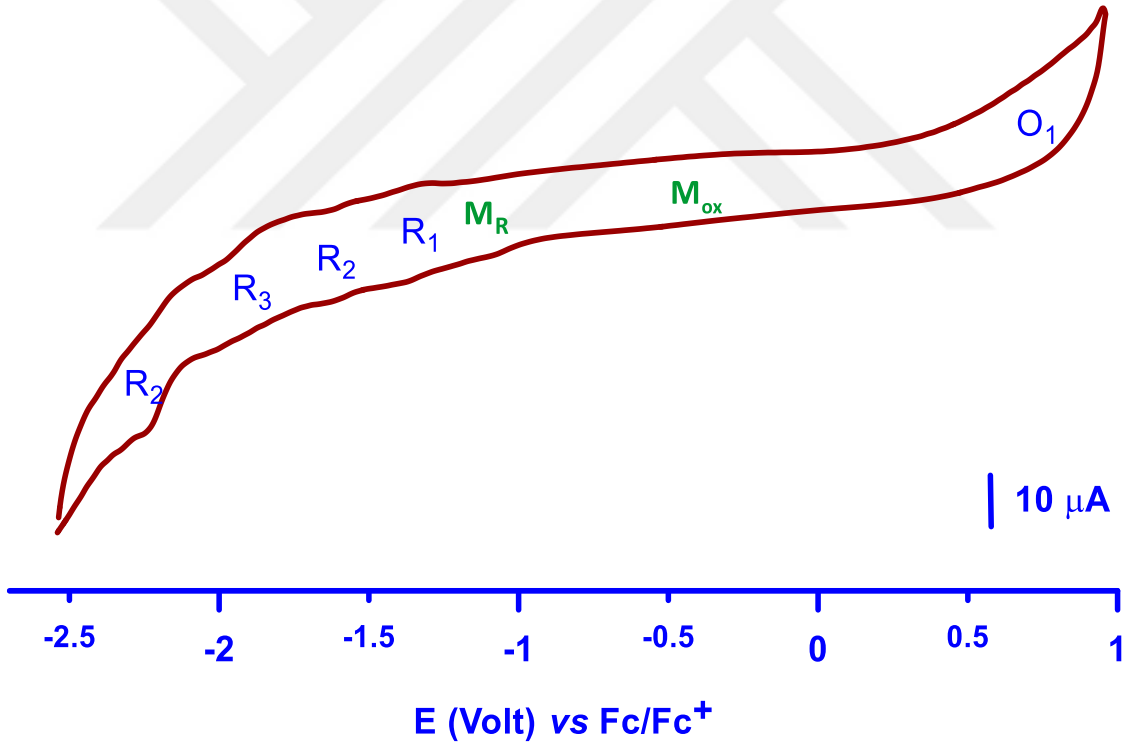


**Figure 3.24.** Cyclic voltammogram of Cr(II)phthalocyanine.

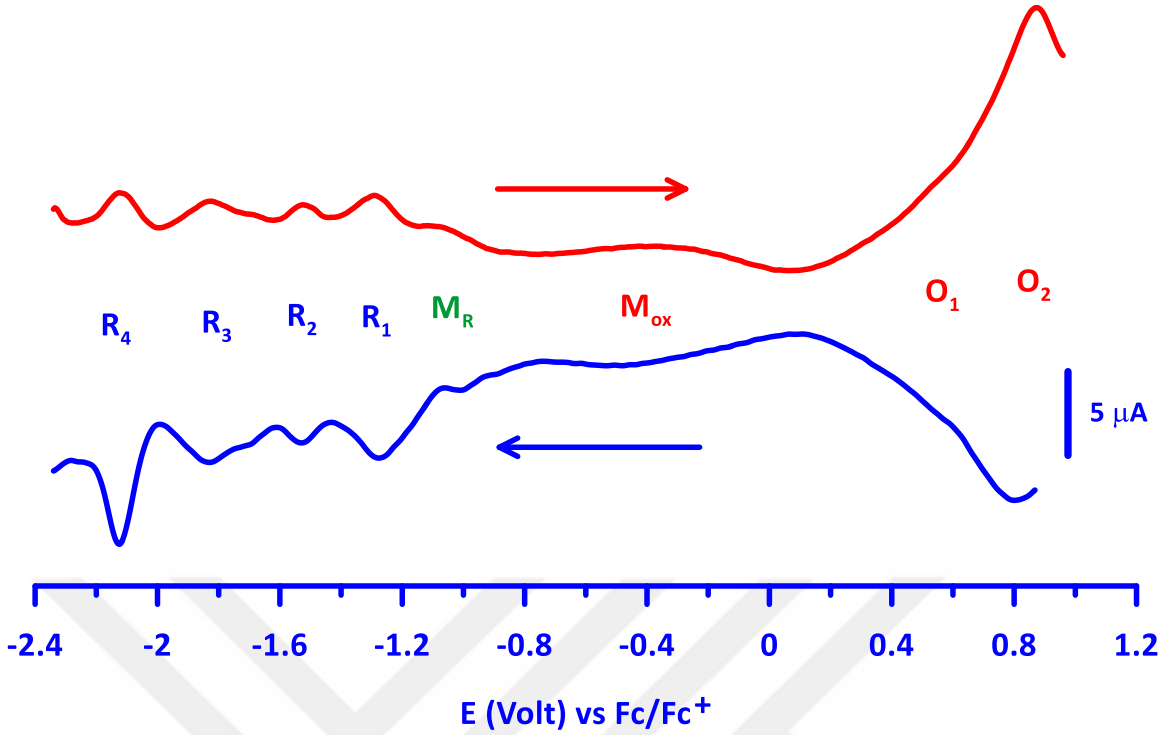


**Figure 3.25.** Square wave voltammogram of Cr(II)phthalocyanine.

### 3.9. 2,2',2'',2'''(2,9,16,23-tetrayltetrakis(sulfanediyl))tetrakis(benzo[d]thiazole) Iron phthalocyanine.

The Iron phthalocyanine FePc was prepared from 4-(benzo[d]thiazol-2-ylthio) phthalonitrile with Fe(II)acetate under an argon atmosphere in DMF. The presence of Fe(II) helps cyclotetramerization of four phthalonitrile ligands to form green-colored FePc, **Figure 3.26.**

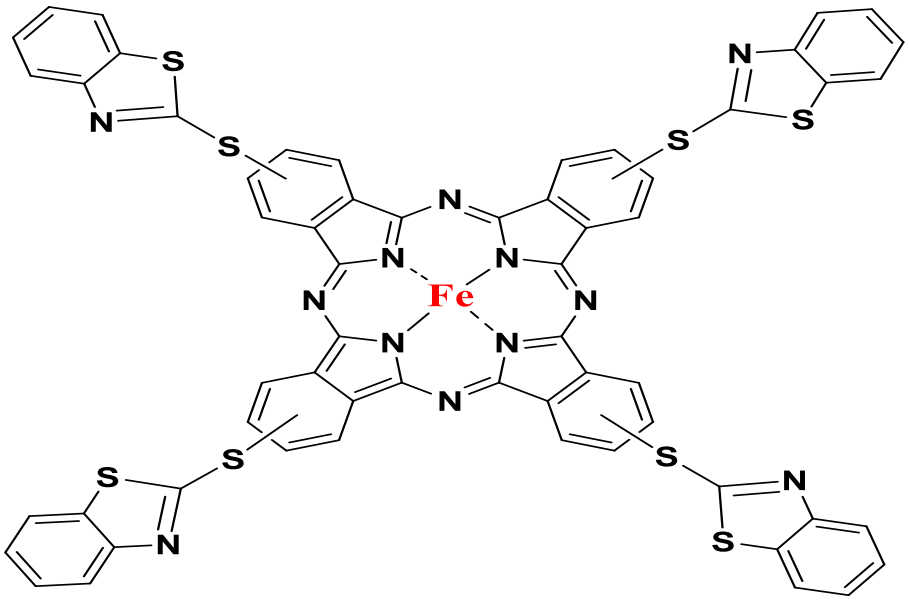


**Figure 3.26.** 2,2',2",2'"(2,9,16,23-tetrayltetrakis(sulfanediyl))tetrakis(benzo[d]thiazole) Iron phthalocyanine.

- **FT-IR Spectrum**

The KBr pellet in IR spectra showed no C≡N peak at 2232 $cm^{-1}$ indicating the reaction completion. Two peaks at 2978 and 2926 $cm^{-1}$ indicate aromatic C-H stretching, while one at 1632 $cm^{-1}$ indicates C=C macrocycle ring stretching. Three peaks at 1516, 1452, and 1424 $cm^{-1}$ indicate C=N stretching. Other peaks at 1315 $cm^{-1}$ and 1140 $cm^{-1}$ relate to the stretching of carbon atoms C-N. In addition, the C-S bond peaks at 756 and 725 $cm^{-1}$, and the C-C bond's peak at 1050 $cm^{-1}$ is also visible. as shown in **Figure 3.27.**

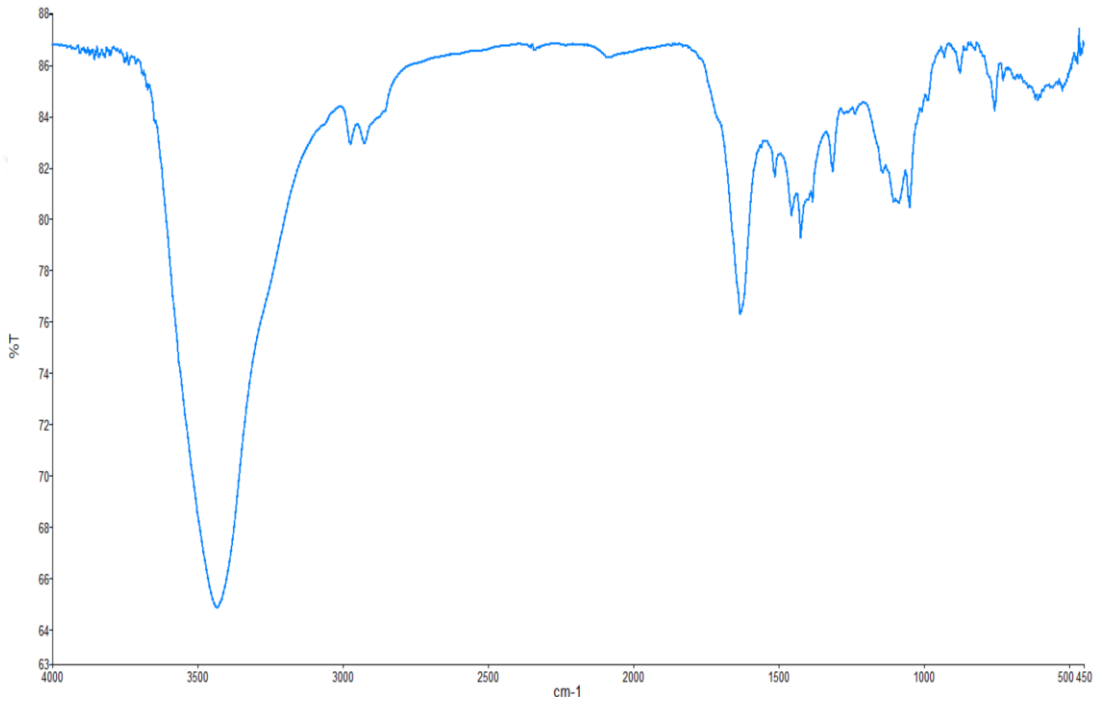


**Figure 3.27.** FT-IR spectrum of Fe(II)phthalocyanine.

- **UV–visible spectrum**

MPcs in DMF had normal absorptions between 600 and 700 nm in the Q band area according to their UV-vis spectra. The π-π* transition from the HOMO to the LUMO of the phthalocyanine ring defines the Q band absorptions of the compounds. The transitions from the deeper π levels to the LUMO caused the B band absorptions of the compounds to be seen in the UV area around 300–400 nm. FePc compound in DMF has two absorptions in the Q band area at 683, and 614 nm and the Soret band at 370 nm on the UV–vis spectrum as shown in **Figure 3.28.**

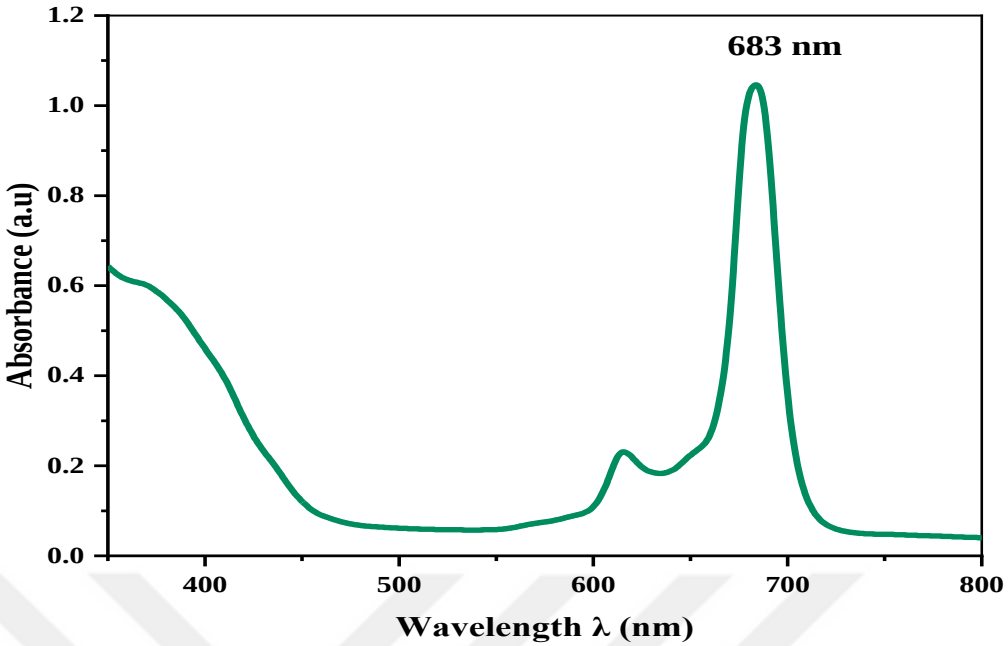


**Figure 3.28.** UV-visible spectrum of Fe(II)phthalocyanine.

- **Thermal analysis**

The TG and DTG analyses of the FePc complex demonstrated thermal stability up to 200 °C, iron phthalocyanine complex undergoes a one-step decomposition process, an exothermic decomposition occurs between 200-400 °C with a 50% weight loss, then there was no weight loss observed up to 700 °C. The total weight loss is 64%, and the TG thermograms reveal that FePc decomposes without displaying a melting point, leaving about 36 % residue, **Figure 3.29.**

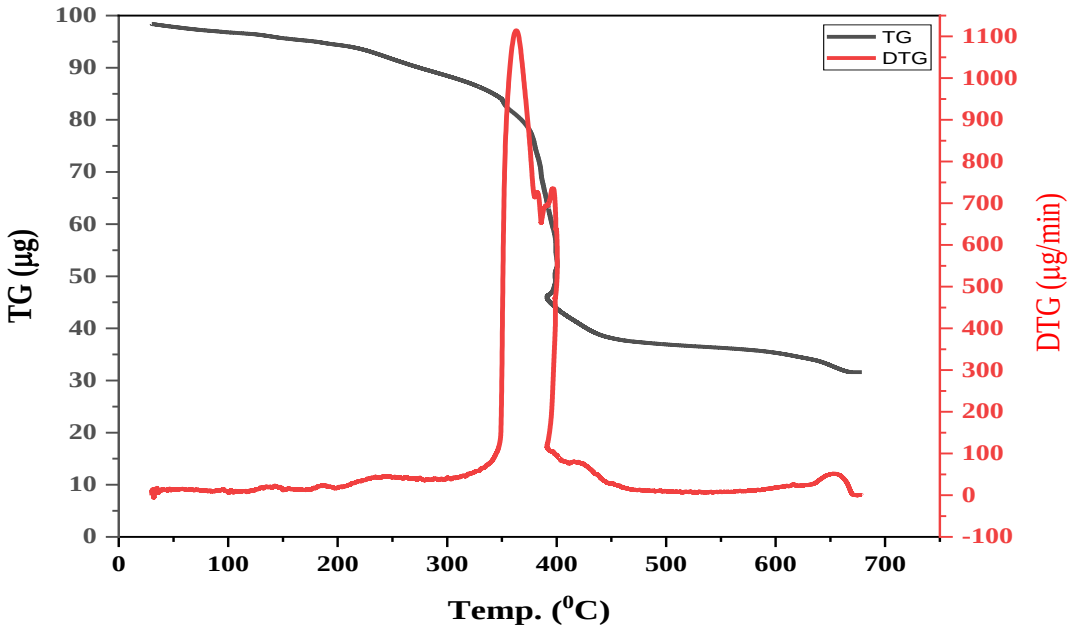


**Figure 3.29**. TG and DTG of Fe(II)phthalocyanine.

- **Electrochemical Properties**.

FePc reveals four reduction waves at -0.86, -1.61, -2.20, and -2.39 volts, along with two oxidation waves at 0.28, and 0.59 volts, representing $R_1$, $R_2$, $R_3$, $R_4$, and $O_1$, $O_2$, respectively. Also, have oxidation reduction on metal Mr and Mo at -0.56 and -0.07 Vs respectively. All of these redox reactions labeled $R_{1-4}$ originate in macrocycle rings. In phthalocyanine rings, the redox behavior is associated with the removal of electrons from the HOMO, whereas the LUMO may accept up to four more electrons **Figure 3.30,** and **Figure 3.31.**

The redox processes $R_1$, $R_2$, $R_3$, and $R_4$ are assigned to Fe(II)Pc-2/Fe(II)Pc-3, Fe(II)Pc-3/Fe(II)Pc-4, Fe(II)Pc-4/Fe(II) Pc-5, and Fe(II)Pc-5/Fe(II)Pc-6, respectively. $O_1$ and $O_2$ correspond to the two FePc oxidation processes, which are Fe(II)Pc-2/Fe(III)Pc-1 and Fe(II)Pc-1/Fe(III)Pc0, respectively. Furthermore, as the $Fe^{2+}$ and $Fe^{3+}$ ions are redox and oxidize active in phthalocyanine complexes, the metal-based Mr and Mo process refers to Fe(II)Pc-2/Fe(I)Pc-2 and Fe(II)Pc-2/Fe(III)Pc-2 respectively.

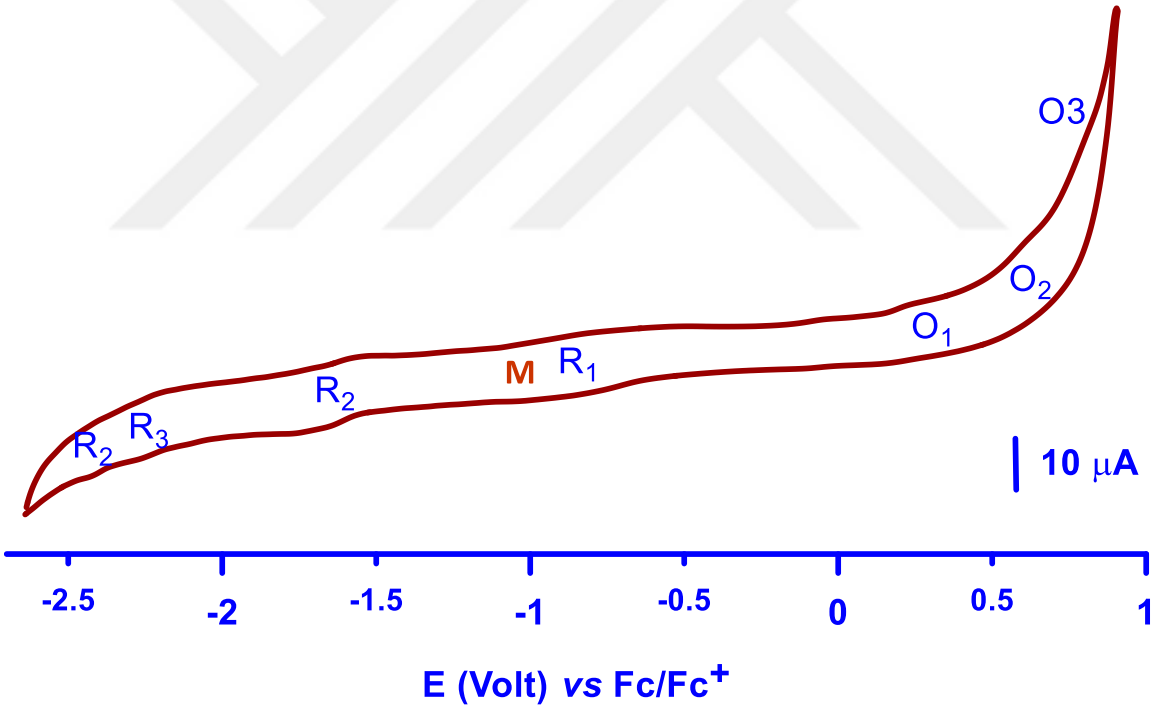


**Figure 3.30.** Cyclic voltammogram of Fe(II)phthalocyanine.

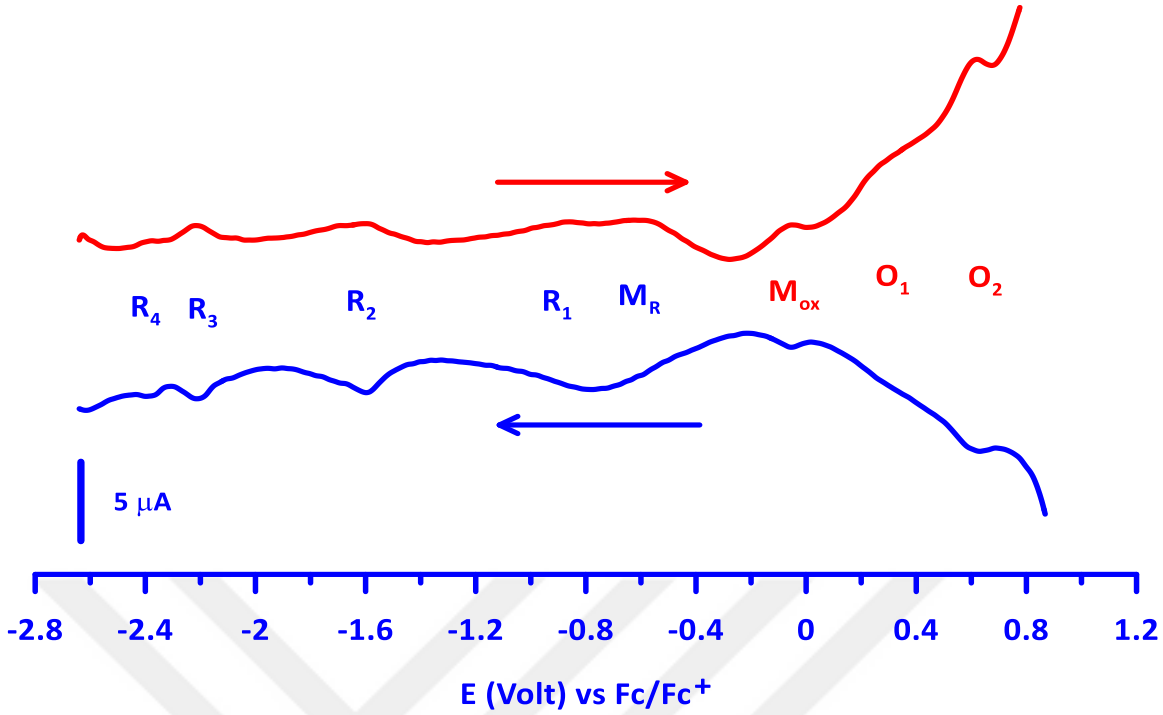


**Figure 3.31.** Square wave voltammogram of Fe(II)phthalocyanine.

### 3.10. 2,2',2'',2'''(2,9,16,23-tetrayltetrakis(sulfanediyl))tetrakis(benzo[d]thiazole) Cobalt phthalocyanine.

The Cobalt phthalocyanine CoPc was prepared from 4-(benzothiazol-2-ylthio) phthalonitrile with Co(II)acetate under an argon atmosphere in DMF. The presence of Co(II) salt in this condition caused the cyclotetramerization of four phthalonitrile ligands to form green-colored CoPc, **Figure 3.32.**

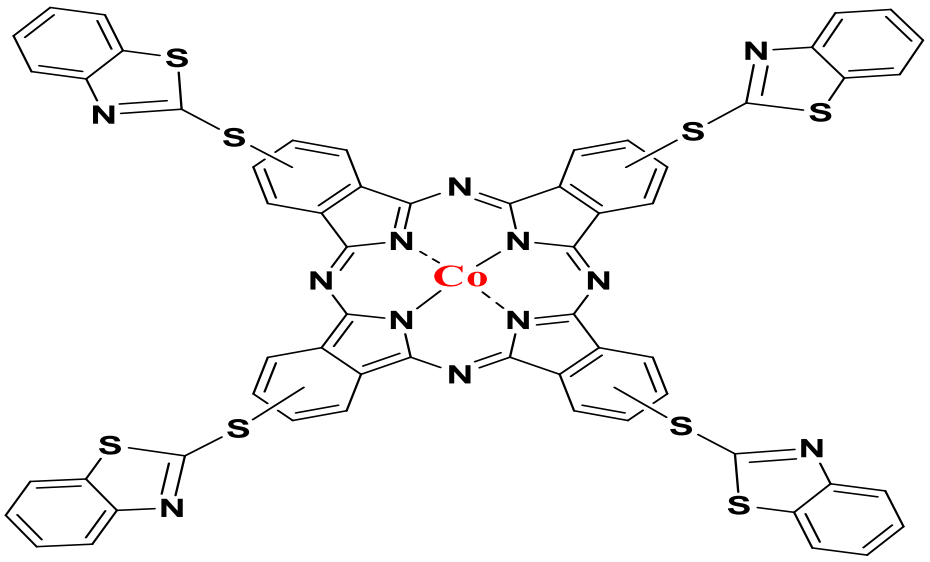


**Figure 3.32.** 2,2',2",2'"(2,9,16,23-tetrayltetrakis(sulfanediyl))tetrakis(benzothiazole) Cobalt phthalocyanine.

- **FT-IR Spectrum**

The FT-IR spectrum recorded using KBr pellet, showed the disappearance of the C≡N peak at 2232 $cm^{-1}$. Aromatic C-H stretching appeared as two weak peaks at 2978 and 2926 $cm^{-1}$, while C=C macrocycle ring stretching at 1640 and 1605 $cm^{-1}$. Three distinct peaks at 1521, 1455, and 1424 $cm^{-1}$ were attributed to C=N stretching. The stretching of carbon atoms' C-N bonds was associated with the other peaks at 1311 $cm^{-1}$. The peaks at 754 and 725 $cm^{-1}$ correspond to the C-S bonds, and the peaks at 1101 and 1049 $cm^{-1}$ were assigned to the C-C bond, and are all clearly visible. As shown in **Figure 3.33.**

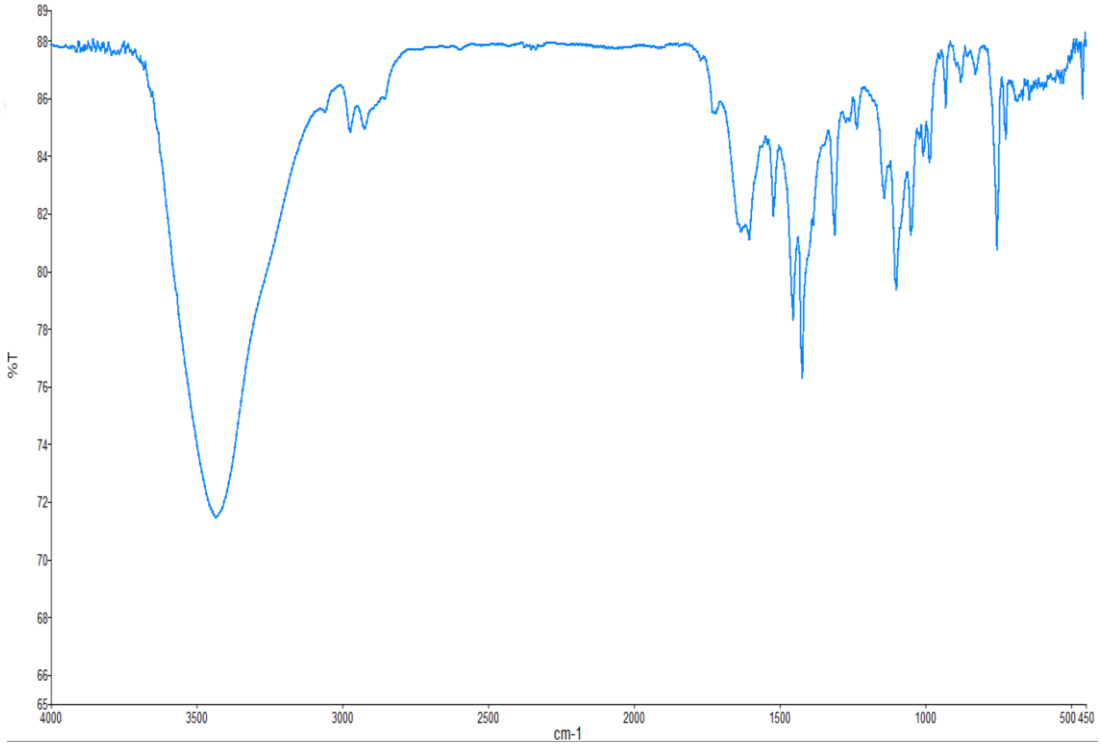


**Figure 3.33.** FT-IR spectrum of Co(II)phthalocyanine.

- **UV–visible spectrum**

MPcs in DMF had normal absorptions between 600 and 700 nm in the Q band area according to their UV-vis spectra. The π-π* transition from the HOMO to the LUMO of the phthalocyanine ring defines the Q band absorptions of the compounds. The transitions from the deeper π levels to the LUMO caused the B band absorptions of the compounds to be seen in the UV area between 300–400 nm. CoPc compound in DMF has two absorptions in the Q band area at 668, and 606 nm a weak shoulder on the UV–vis spectrum. As shown in **Figure 3.34.**

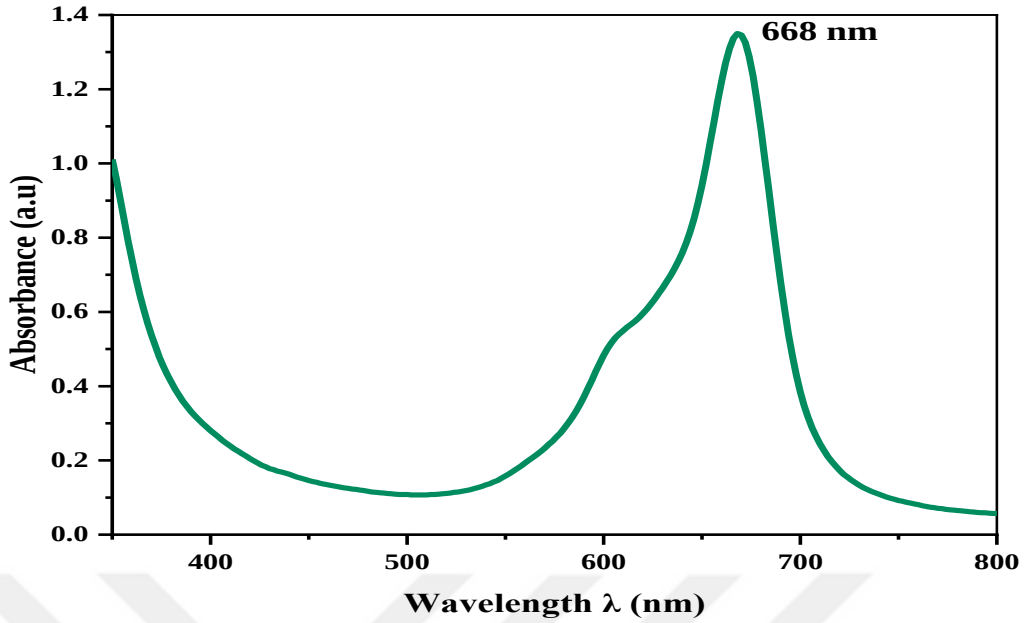


**Figure 3.34.** UV-visible spectrum of Co(II)phthalocyanine.

- **Thermal analysis**

The TG and DTG curves show that CoPc is thermal stabile up to 250 °C, with a minor weight loss of 3% attributed to the loss of adsorbed surface water. The decomposition happened in two stages: The first stage occurred around 250-380 °C, with a weight loss of about 18%. The second thermal event corresponds to the decomposition of the complex starting from 380-575 °C, with about 65% weight loss. The total weight loss was 86 %, leaving approximately 14% residue [177]. As shown in **Figure 3.35.**

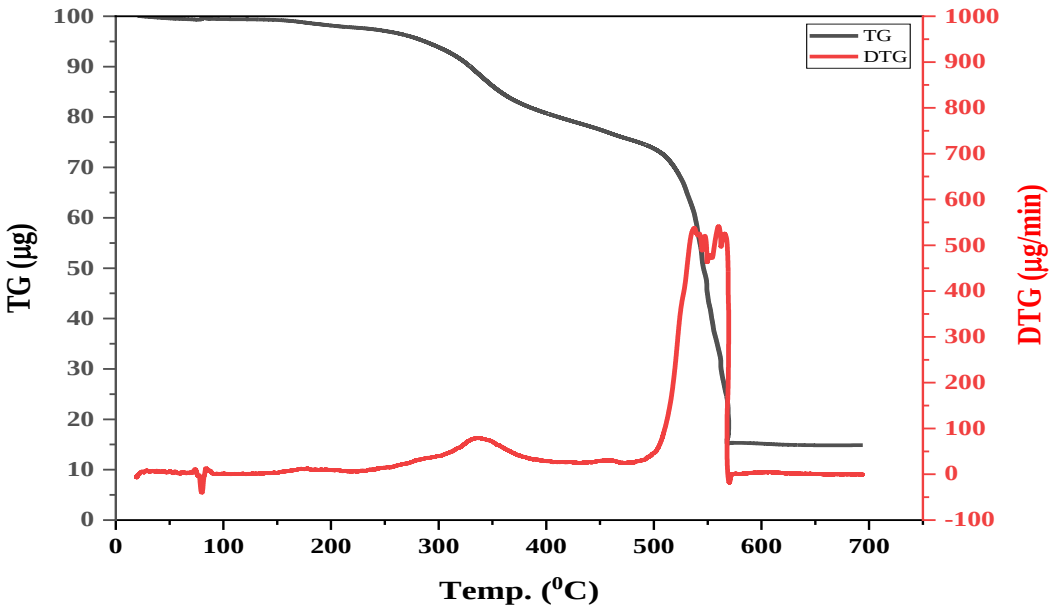


**Figure 3.35**. TG and DTG of Co(II)phthalocyanine.

- **Electrochemical Properties.**

The electrochemical analysis of CoPc was conducted using CV and SWV in DMF with TBAFB as the supporting electrolyte. The Fc/Fc+ pair served as a sudo reference electrode. Potentials were measured relative to Fc/Fc+ in non-aqueous solutions. Due to the limited solubility of CoPc, the CV voltammogram was not able to effectively demonstrate the redox processes. On the other hand, the experiment performed using the SW voltammogram, provided a better result than CV. There for all the electrochemical data given here is taken from the SW Voltammogram average of anodic and cathodic redox potentials.

There are four waves that represent the reductions of CoPc, labeled $R_1$, $R_2$, $R_3$, and $R_4$, with -1.25, -1.61, -2.18, and -2.36 V respectively. There were, two oxidations' waves, labeled $O_1$ and $O_2$, at 0.48 and 0.68 V, which is phthalocyanine ring based oxidation, in addition, cobalt based redox waves were also observed labeled with Mr and Mo at -0.77 and 0.16 V respectively. An important part of the redox activity is the removal of electrons from the HOMO of the phthalocyanine ring, which could accommodate up to four additional electrons in the LUMO. MPcs typically have a potential difference of 1.5 V between the initial reduction and oxidation, while CoPc has a value of 1.2 V. As shown in **Figure 3.36** and **Figure 3.37.**

However, there are four redox processes $R_1$, $R_2$, $R_3$, and $R_4$ attributed to Co(II) Pc-2/Co(II) Pc-3, Co(II) Pc-3/Co(II) Pc-4, Co(II) Pc-4/Co(II) Pc-5, and Co(II) Pc-5/Co(II) Pc-6 respectively. Nonetheless, $O_1$, and $O_2$ are corresponding to the two oxidation processes of CoPc, specifically Co(II) Pc-2/Co(III) Pc-1, and Co(III)Pc-1/Co(III)Pc0 respectively. Additionally, there are metal-based redox processes referred to as Co(II)Pc-2/Co(I)Pc-2, and Co(II)Pc-2/Co(III)Pc-2, labelled Mr and Mo respectively.

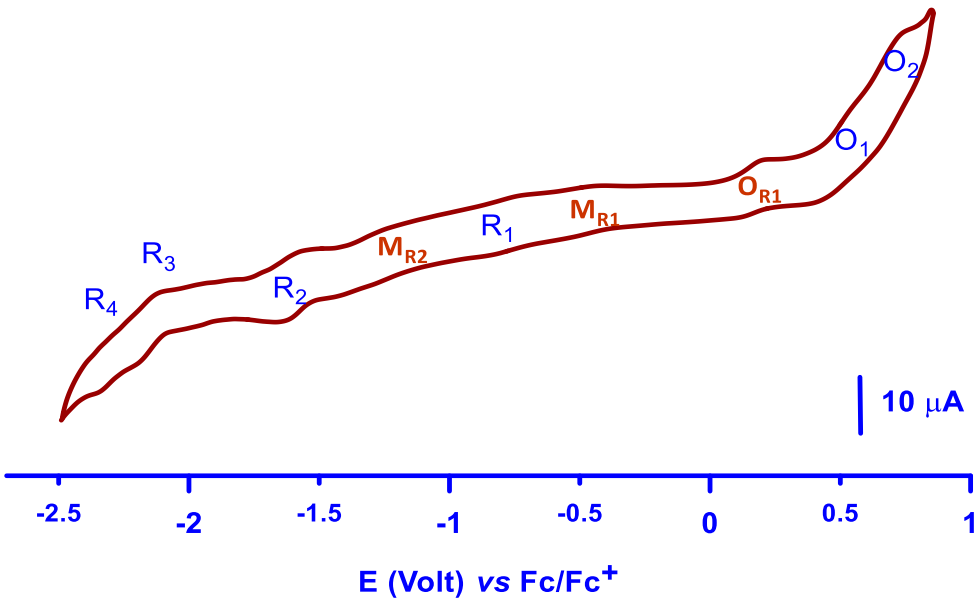


**Figure 3.36.** Cyclic voltammogram of Co(II)phthalocyanine.

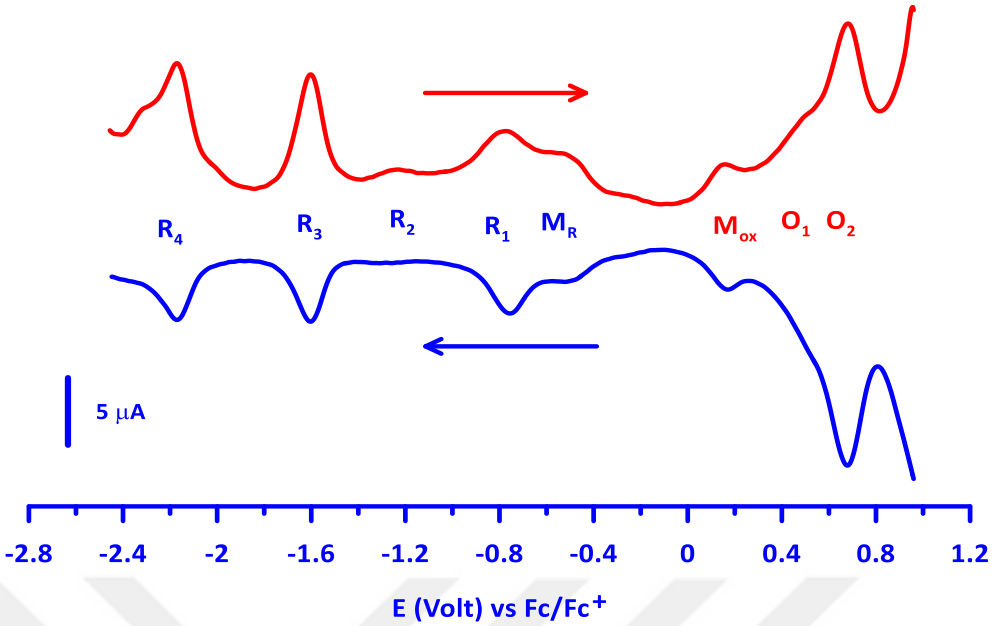


**Figure 3.37.** Square wave voltammogram of Co(II)phthalocyanine.

## 3.11. 2,2',2'',2'''(2,9,16,23-tetrayltetrakis(sulfanediyl))tetrakis(benzo[d]thiazole) Nickel phthalocyanine

The Nickel phthalocyanine NiPc was prepared from 4-(benzothiazol-2-ylthio) phthalonitrile with Ni(II)acetate under an argon atmosphere in DMF. The presence of Ni(II) salt in this condition cyclotetramerization of four phthalonitrile ligands afforded the green-colored NiPc, shown in **Figure 3.38.**

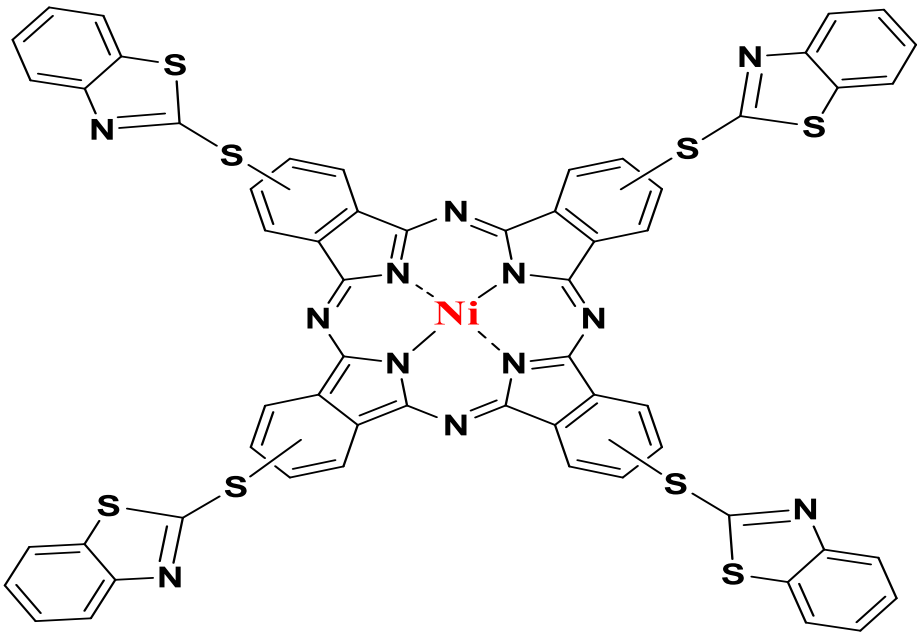


**Figure 3.38**. 2,2',2",2'"(2,9,16,23-tetrayltetrakis(sulfanediyl))tetrakis(benzothiazole) Nickel phthalocyanine.

- **FT-IR Spectrum**

The KBr pellet in IR spectra showed that the C≡N peak disappeared at 2232 $cm^{-1}$ indicating no starting material is present. Three weak peaks at 3060, 2976, and 2928 $cm^{-1}$ indicate aromatic C-H stretching, while a peak at 1603 $cm^{-1}$ indicates C=C macrocycle ring stretching, and three peaks at 1532, 1455, and 1424 $cm^{-1}$ were attributed to C=N stretching. Other peaks at 1311 $cm^{-1}$ and 1236 $cm^{-1}$ correspond to the stretching of carbon atoms C-N. In addition, the C-S bond's peaks at 753 and 725 $cm^{-1}$, and the C-C bond's peaks at 1098 $cm^{-1}$ and 1049 $cm^{-1}$ are also visible. as shown in **Figure 3.39.**

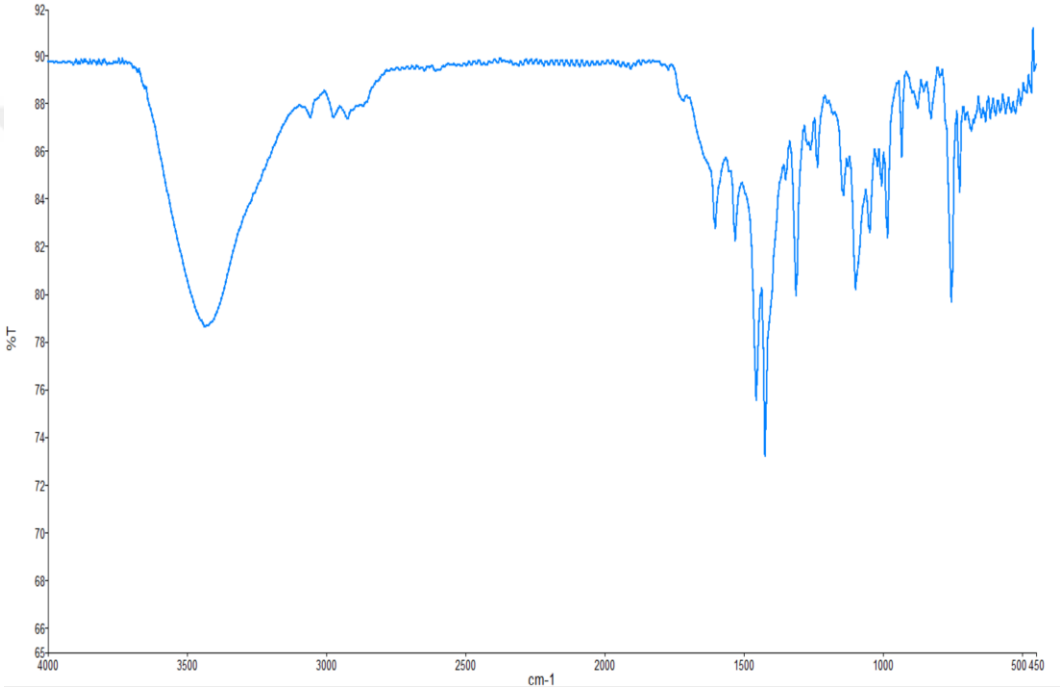


**Figure 3.39.** FT-IR spectrum of Ni(II)phthalocyanine.

- **UV–visible spectrum**

The Q band absorptions between 600 -700 nm in their UV–vis spectra were observed in the UV-visible spectra of the nickel phthalocyanine complex in DMF. The compounds' Q band absorptions reflect the π-π* transition from the phthalocyanine ring's HOMO to LUMO. The compounds' B band absorptions were found between 300-400 nm in the UV area, resulting from transitions from deeper π levels to the LUMO. In DMF, the NiPc compound had three absorption peaks at 611 and 675 nm (Q band), and Soret (B) band at 450 nm, also has absorption at 845 nm in the UV–visible, as shown in **Figure 3.40** indicating strong aggregation in DMF**.**

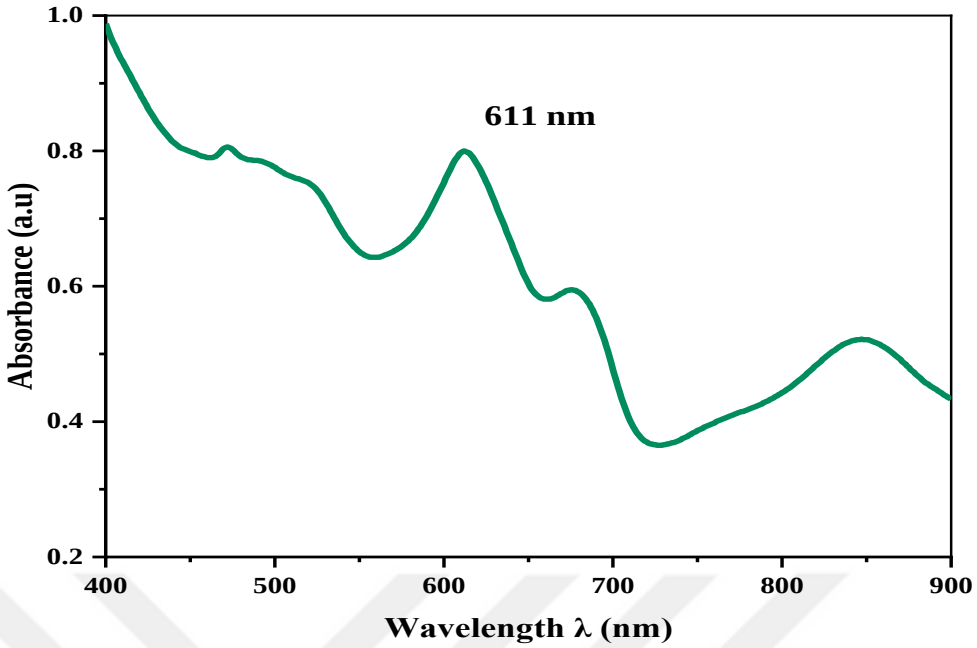


**Figure 3.40.** UV-visible spectrum of Ni(II)phthalocyanine.

- **Thermal analysis**

The TG and DTG curves show that NiPc is thermal stabile up to 270 °C, with a minor weight loss of 3% attributed to the loss of adsorbed surface water. The decomposition happened in three stages: The first stage occurred around 300-480 °C, with a weight loss of about 27%. The second thermal event corresponds to the decomposition of the complex starting from 480-540 °C, with about 8% weight loss, also third stage starting from 540-600 °C, with about 32% weight loss. The total weight loss was 70%, leaving approximately 30% residue. As shown in **Figure 3.41.**

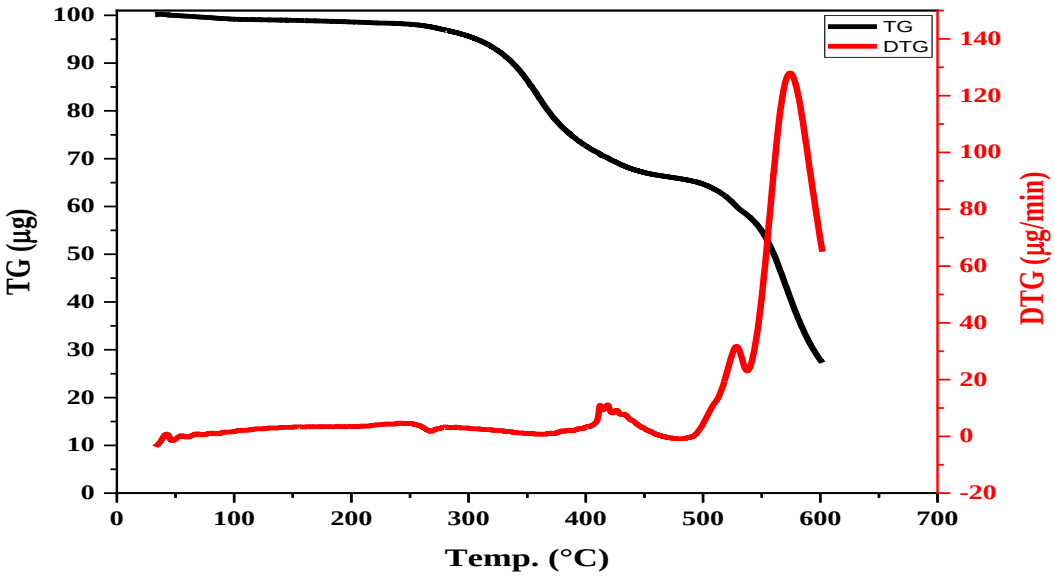


**Figure 3.41.** TG and DTG of Ni(II)phthalocyanine.

- **Electrochemical Properties**

The electrochemical analysis of NiPc was conducted using CV and SWV in DMF with TBAFB as the supporting electrolyte. Potentials were measured relative to Fc/Fc+ in non-aqueous solutions. Due to the limited solubility of NiPc, the CV and SW voltammograms were not able to effectively demonstrate the redox processes.

There are four waves that repairs represent the reductions of NiPc, labeled $R_1$, $R_2$, $R_3$, and $R_4$, at -1.18, -1.59, -1.94, and -2.37 V respectively, with two oxidations' waves, labeled $O_1$ and $O_2$, were observed at 0.38 and 0.70 V, representing the oxidation potentials of NiPc respectively. Due to the presence of redox-inactive Ni(II) metal in the phthalocyanine complex, all the redox processes originate from phthalocyanine macrocycle rings, as shown in **Figure 3.42** and **Figure 3.43**. The four redox processes $R_1$, $R_2$, $R_3$, and $R_4$ are identified as follows: Ni(II)Pc-2/Ni(II)Pc-3, Ni(II)Pc-3/Ni(II)Pc-4, Ni(II)Pc-4/Ni(II)Pc-5, and Ni(II)Pc-5/Ni(II)Pc-6 respectively. In addition, $O_1$ and $O_2$ correspond to the two NiPc oxidation processes, which are Ni(II)Pc-2/Ni(II)Pc-1 and Ni(II)Pc-1/Ni(II)Pc0, respectively. Because $Ni^{2+}$ is not redox active in phthalocyanine, therefore there is no metal-based redox waves in voltammograms.

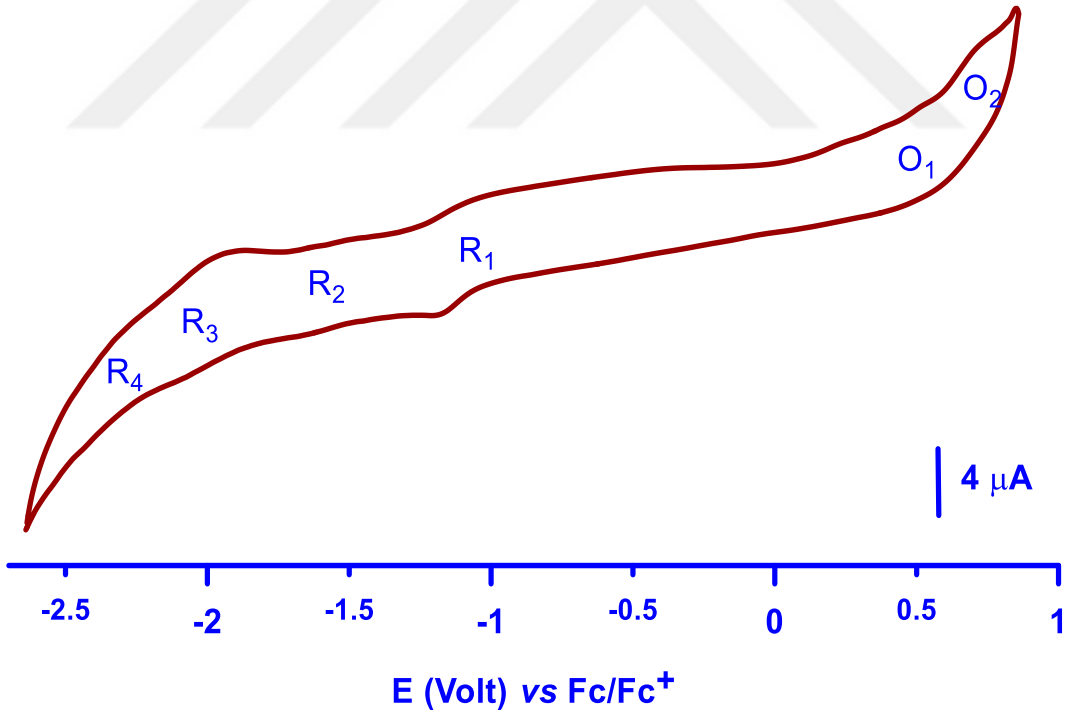


**Figure 3.42.** Cyclic voltammogram of Ni(II)phthalocyanine.

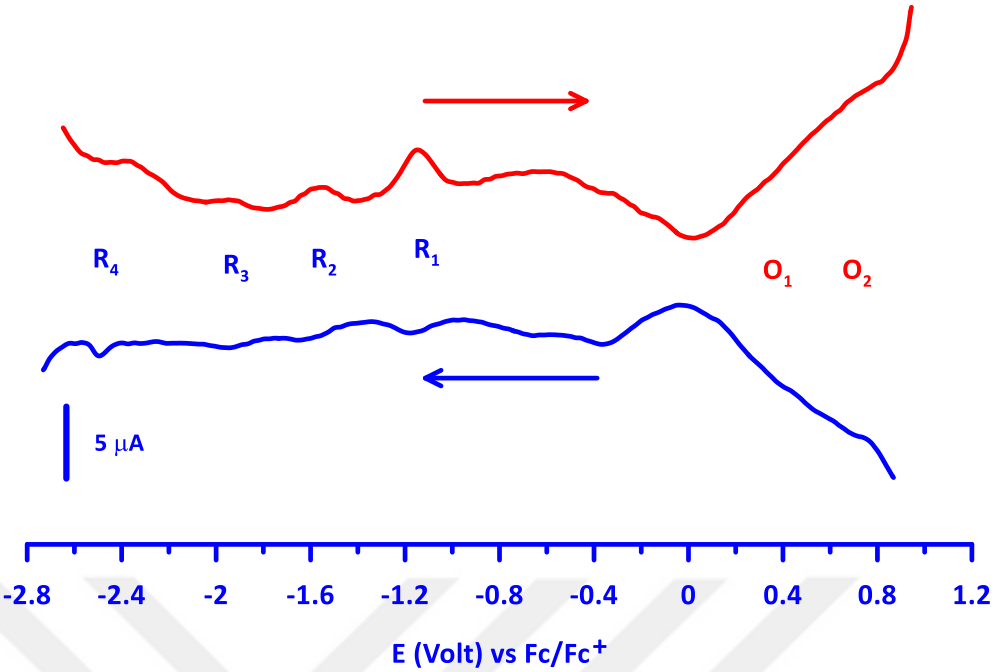


**Figure 3.43.** Square wave voltammogram of Ni(II)phthalocyanine.

## 3.12. 2,2',2'',2'''(2,9,16,23-tetrayltetrakis(sulfanediyl))tetrakis(benzo[d]thiazole) Copper phthalocyanine

The Copper phthalocyanine CuPc was prepared from 4-(benzothiazol-2-ylthio) phthalonitrile with Cu(II)acetate under an argon atmosphere in DMF. Cu(II) induced the cyclotetramerization of four phthalonitrile ligands, resulting in the formation of green-colored CuPc, phthalocyanines complex, shown in **Figure 3.44.**

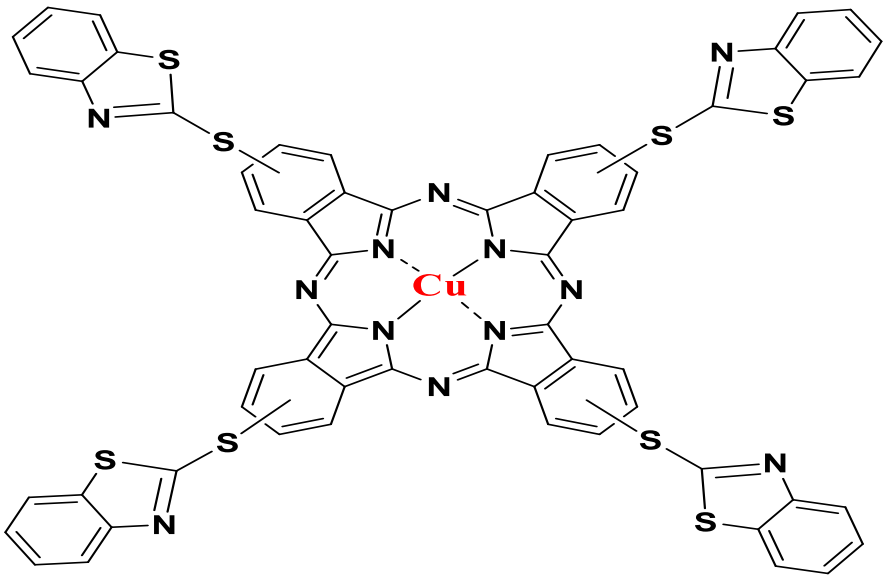


**Figure 3.44**. 2,2',2",2"'(2,9,16,23-tetrayltetrakis(sulfanediyl))tetrakis(benzothiazole) Copper phthalocyanine.

- **FT-IR Spectrum**

The FT-IR spectrum, recorded using a KBr pellet, showed the disappearance of the C≡N peak at 2232 $cm^{-1}$. There are distinct peaks at 2978 and 2920 $cm^{-1}$ for aromatic C-H stretching, while a peak at 1699 $cm^{-1}$ for C=C macrocycle ring deformation. Peaks at 1454 and 1424 $cm^{-1}$ were associated with C=N stretching. The peaks at 1275 $cm^{-1}$, 1188 $cm^{-1}$, and 1137 $cm^{-1}$ are corresponding to C-N starching. The C-C bond was indicated by a peak at 1049 $cm^{-1}$, and peaks at 755 and 727 $cm^{-1}$ correspond to the C-S bond, shown in **Figure 3.45.**

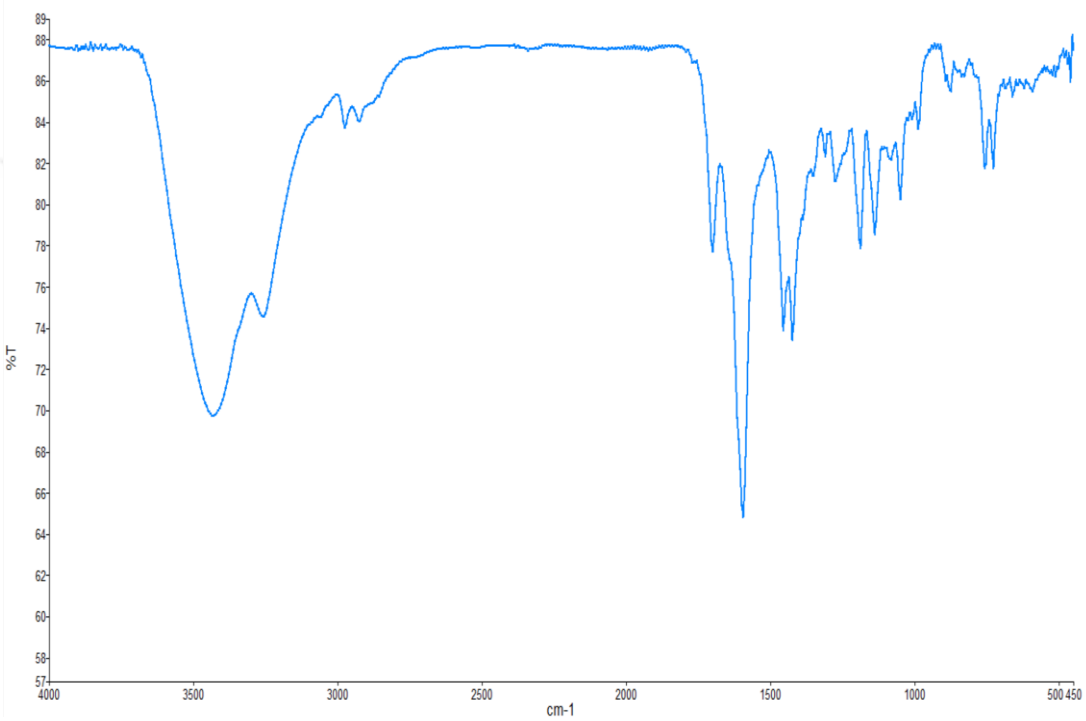


**Figure 3.45**. FT-IR spectrum of Cu(II)phthalocyanine.

- **UV–visible spectrum**

MPcs Q band absorptions bands observed between 600 -700 nm in their UV–vis spectra. The compounds' Q band absorptions reflect the π-π* transition from the phthalocyanine ring's HOMO to LUMO. The compounds' B band absorptions were found between 300-400 nm in the UV area, resulting from transitions from deeper π levels to the LUMO. In DMF, the CuPc compound had absorptions at 610 and 681 nm, in UV-visible spectra, **Figure 3.46.**

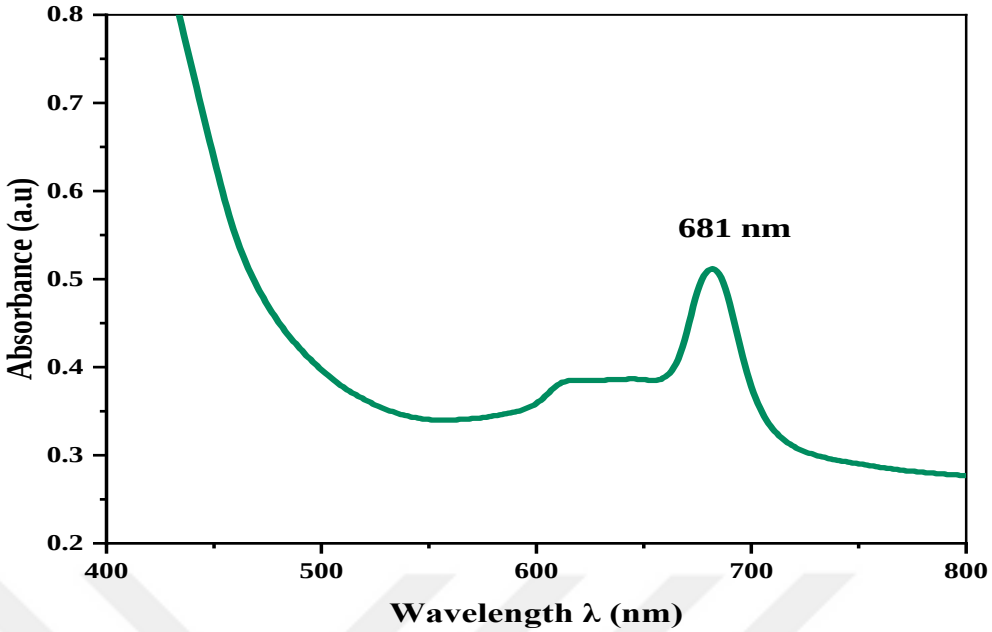


**Figure 3.46.** UV-visible spectrum of Cu(II)phthalocyanine.

- **Thermal analysis**

According to the TG/DTG curves, the CuPc complex remained thermally stable up to 220 °C, with a 2% weight loss likely due to the loss of absorbed water from the surface of the complex. The first stage of decomposition occurs between 220-340 °C with a weight loss of about 15%. The second exothermic decomposition occurs at temperatures ranging from 350 to 440 °C, resulting in a weight loss of 40 %. Without melting, resulting in a 65% total mass loss up to 700 °C, **Figure 3.47.**

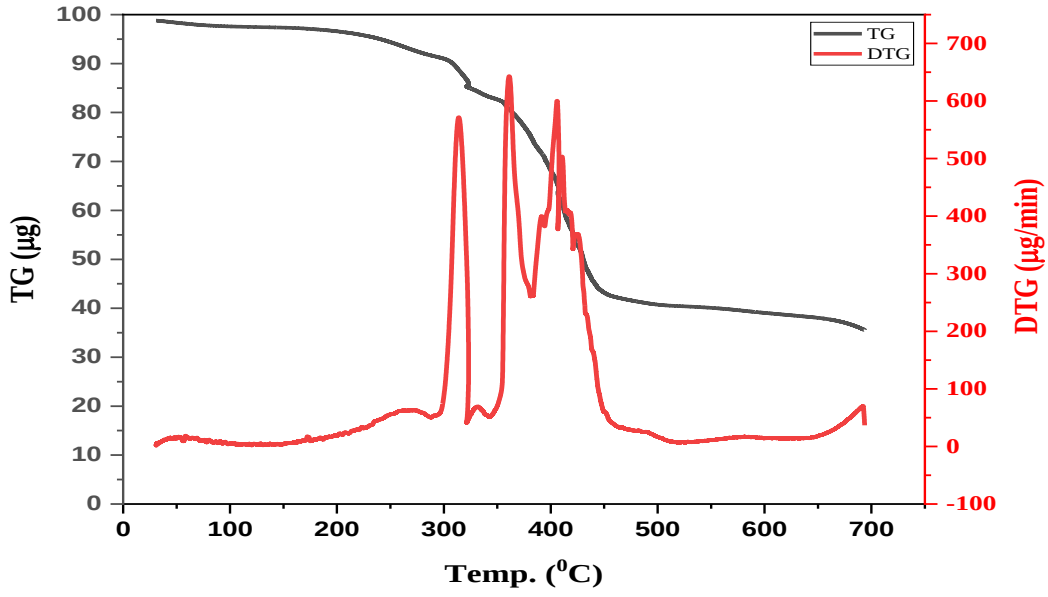


**Figure 3.47.** TG and DTG of Cu(II)phthalocyanine.

- **Electrochemical Properties**

The electrochemical analysis of CuPc was conducted using CV and SWV in DMF with TBAFB as the supporting electrolyte. Due to the limited solubility of CuPc, the CV voltammogram was not able to effectively demonstrate the redox processes. The experiment was performed using SW voltammetry, which provides better results than CV for the redox processes of CuPc, therefore all the electrochemical data were obtained from SW voltammogram.

The CuPc complex exhibited four reduction peaks, labeled $R_1$, $R_2$, $R_3$, and $R_4$, at potentials of -1.61, -1.86, -2.06, and -2.32 V, respectively. Additionally, two oxidation waves $O_1$ and $O_2$ were observed at 0.04 and 0.66 V, respectively. Also, it has redox potential attributed to Cu metal (Mr) at -1.22 V, **Figure 3.48.** and **Figure 3.49.**

The redox processes $R_1$, $R_2$, $R_3$, and $R_4$ ascribed to Cu(II)Pc-2/Cu(II)Pc-3, Cu(II)Pc-3/Cu(II)Pc-4, Cu(II)Pc-4/Cu(II)Pc-5, and Cu(II)Pc-5/Cu(II)Pc-6, respectively. On the other hand, $O_1$ and $O_2$ correspond to oxidation of the cupper phthalocyanine complex oxidation processes that is Cu(II)Pc-2/Cu(II)Pc-1 and Cu(II)Pc-1/Cu(II)Pc0, respectively. There is also a metal-based redox process known as Cu(II)Pc-2/Cu(I)Pc-2, which observed at -1.22 V

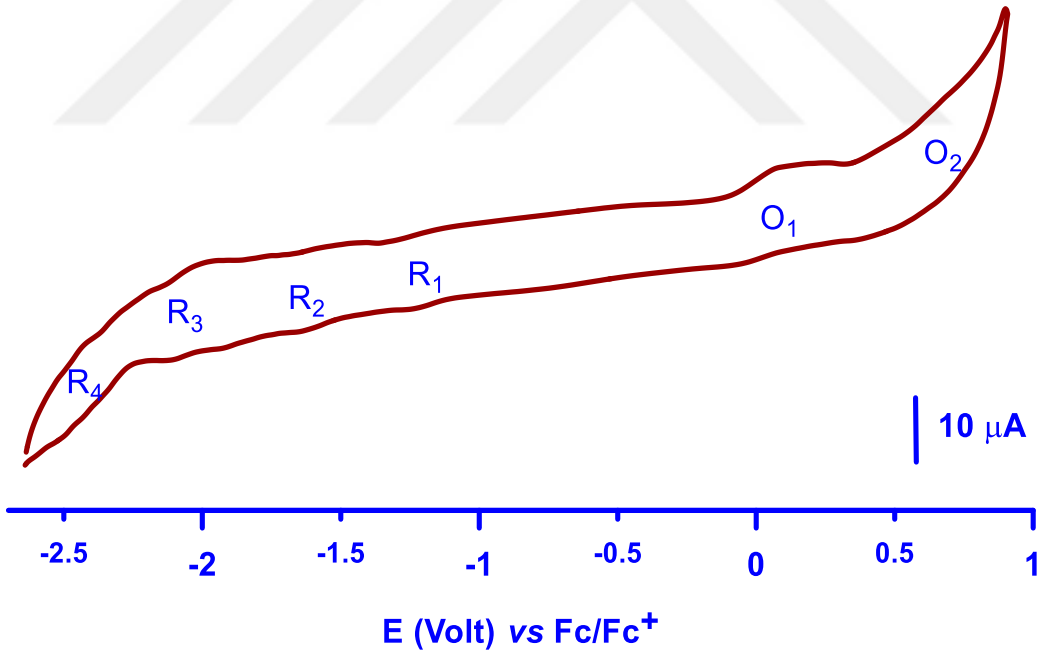


**Figure 3.48.** Cyclic voltammogram of Cu(II)phthalocyanine.

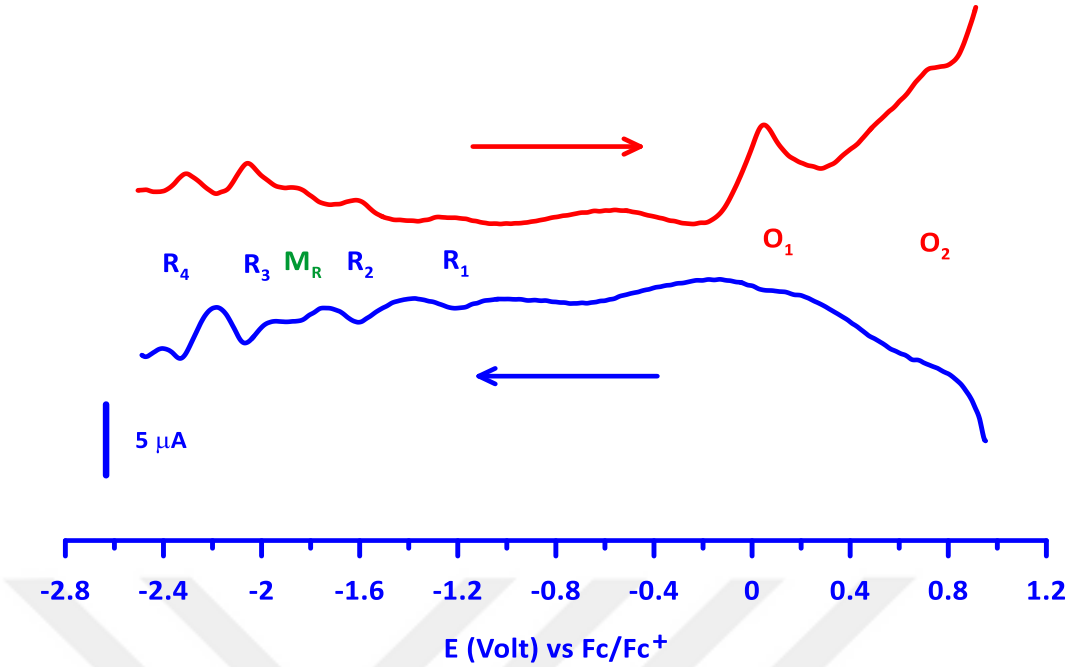


**Figure 3.49.** Square wave voltammogram of Cu(II)phthalocyanine.

## 3.13. 2,2',2'',2'''(2,9,16,23-tetrayltetrakis(sulfanediyl))tetrakis(benzothiazole) Zinc phthalocyanine.

Zinc phthalocyanine (ZnPc) was prepared from 4-(benzothiazol-2-ylthio) phthalonitrile with Zinc(II)acetate under argon atmosphere in DMF. Template effect of Zn(II) ion help to cyclotetramerization of four phthalonitrile ligands, resulting in the formation of green-colored ZnPc, **Figure 3.50.**

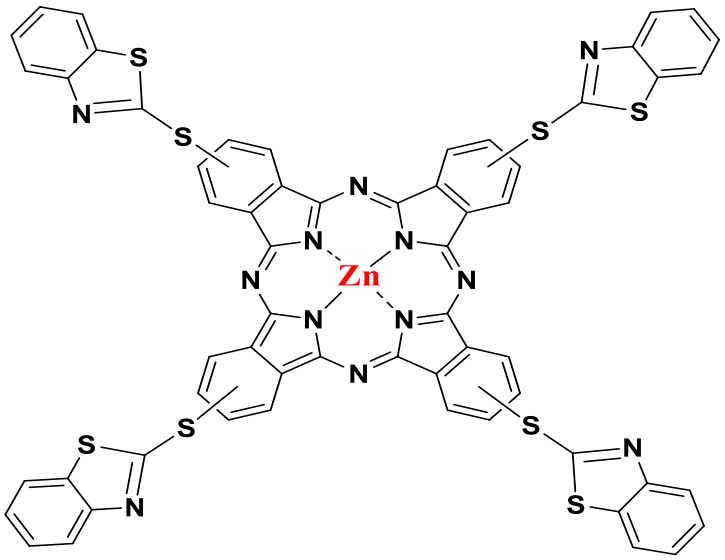


**Figure 3.50**. 2,2',2",2"'(2,9,16,23-tetrayltetrakis(sulfanediyl))tetrakis(benzo[d]thiazole) Zinc phthalocyanine.

- **FT-IR Spectrum**

The FT-IR spectrum, obtained from the KBr pellet, shows the disappearance of the C≡N peak at 2232 $cm^{-1}$. Aromatic C-H stretching appears as two peaks at 2970 and 2923 $cm^{-1}$. The C=C macrocycle ring stretching is observed at 1643 $cm^{-1}$, while C=N stretching is represented by three peaks at 1554, 1456, and 1425 $cm^{-1}$. The C-N stretching related to peaks at 1381 $cm^{-1}$ and 1309 $cm^{-1}$. The peaks at 756 $cm^{-1}$, correspond to the C-S bond, and the peaks at 1096 and 1047 $cm^{-1}$ correspond to the C-C bond, all are visible in **Figure 3.51.**

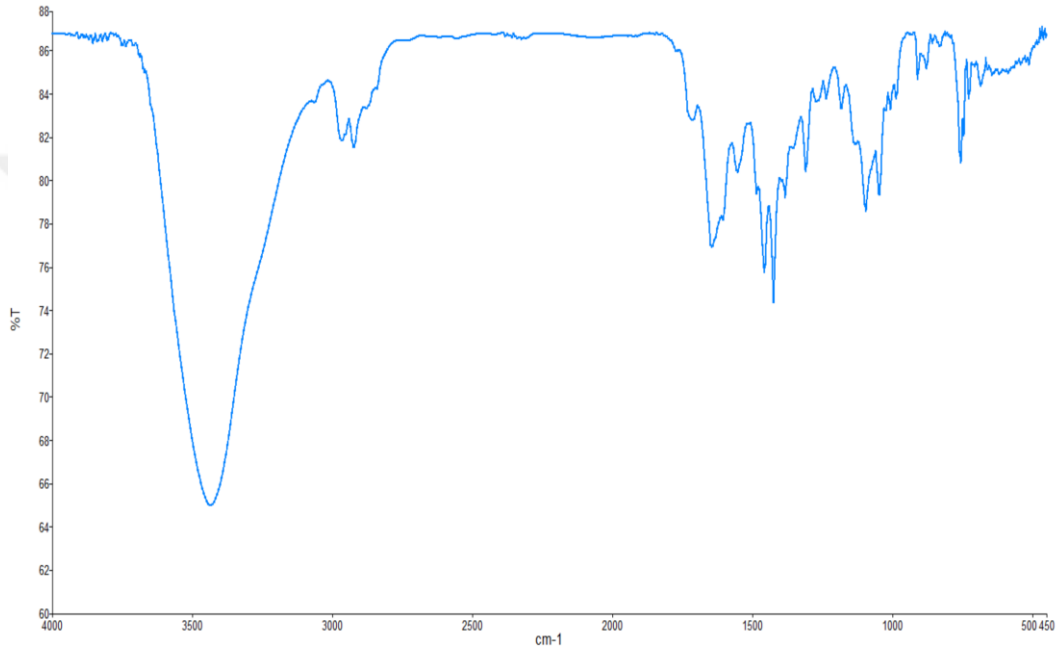


**Figure 3.51**. FT-IR spectrum of Zn(II)phthalocyanine.

- **UV–visible spectrum**

In DMF solution, MPcs' UV–vis spectra display Q band absorptions between 600-700 nm which reflects the absorptions of the π-π* transition from HOMO to LUMO of the phthalocyanine ring. Soret or B-band absorptions were found in the UV range between 365 nm, resulting from transitions from deeper π levels to the LUMO. Q-band of the ZnPc complex in DMF shows absorptions at 684, shown in **Figure 3.52.**

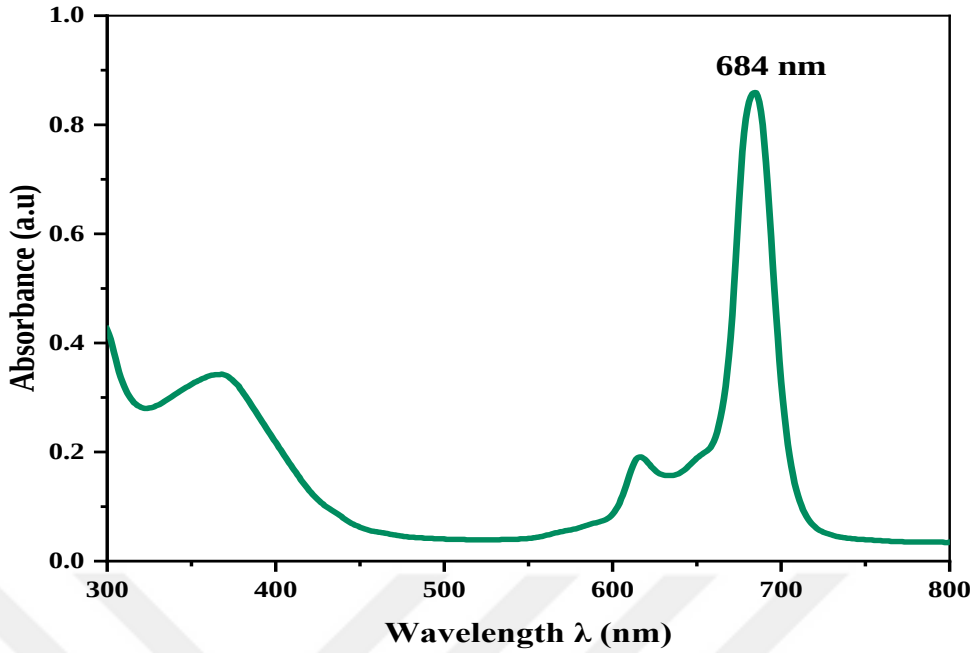


**Figure 3.52.** UV-visible spectrum of Zn(II)phthalocyanine.

- **Thermal analysis**

According to the TG/DTG curves, the ZnPc complex remained thermally stable up to 250 °C, with a 7% weight loss likely due to the loss of absorbed water from the surface of the complex. The first stage of decomposition occurs between 250-450 °C with a weight loss of about 22%. The second exothermic decomposition occurs at temperatures ranging from 450 to 490 °C, resulting in a weight loss of 5 %. Last stage decomposition from 490- 610 °C, weight loss around 40% Without melting, resulting in a 74% total mass reduced, also 26% remained. As shown in **Figure 3.53.**

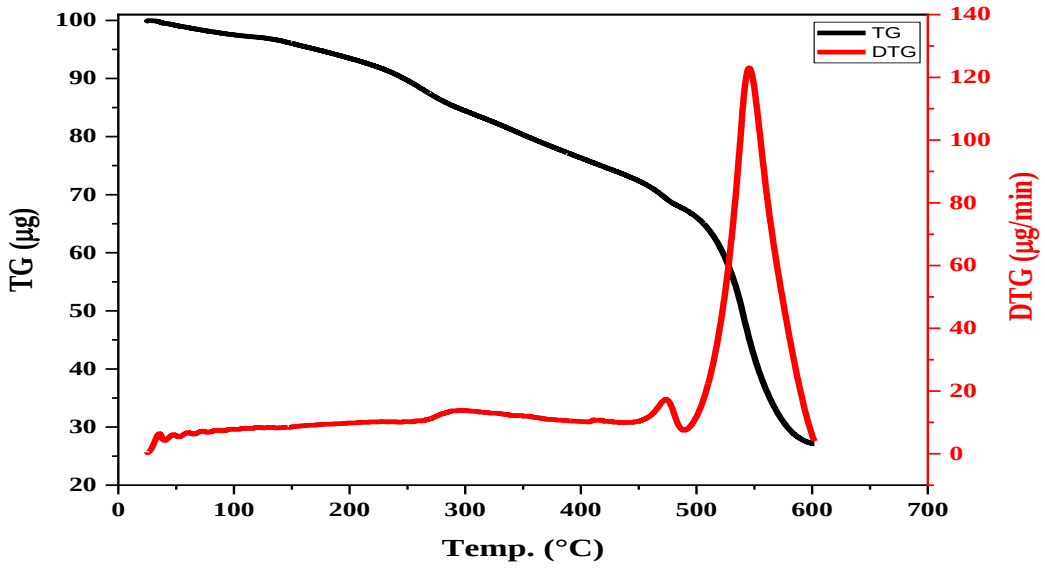


**Figure 3.53.** TG and DTG of Zn(II)phthalocyanine.

- **Electrochemical Properties**.

The electrochemical properties of the ZnPc complex were analyzed using CV in DMF, with TBAFB as the supporting electrolyte. The CV revealed six (oxidation and reduction) redox processes labeling $O_1$ = 0.44 V, $O_2$ = 0.72 V, $R_1$ = -1.09 V, $R_2$ = -1.35 V, $R_3$ = -2.02 V, and $R_4$ = -2.48 V. The complex exhibits characteristic electrochemical behavior of phthalocyanine base, the first reduction and first oxidation processes are phthalocyanine ring. The separation between these processes ($O_1$-$R_1$ = 1.65 V) corresponds to the complex's HOMO-LUMO gap, **Figure 3.54,** and **Figure 3.55.**

However, There are four redox processes $R_1$, $R_2$, $R_3$, and $R_4$ attributed to Zn(II)Pc-2/Zn(II) Pc-3, Zn(II)Pc-3/Zn(II)Pc-4, Zn(II) Pc-4/Zn(II)Pc-5, and Zn(II)Pc-5/Zn(II)Pc-6 respectively. $O_1$, and $O_2$ are corresponding to the two oxidation processes of Zn(II) Pc-2/Zn(II) Pc-1, and Zn(II) Pc-1/Zn(II) Pc0 respectively.

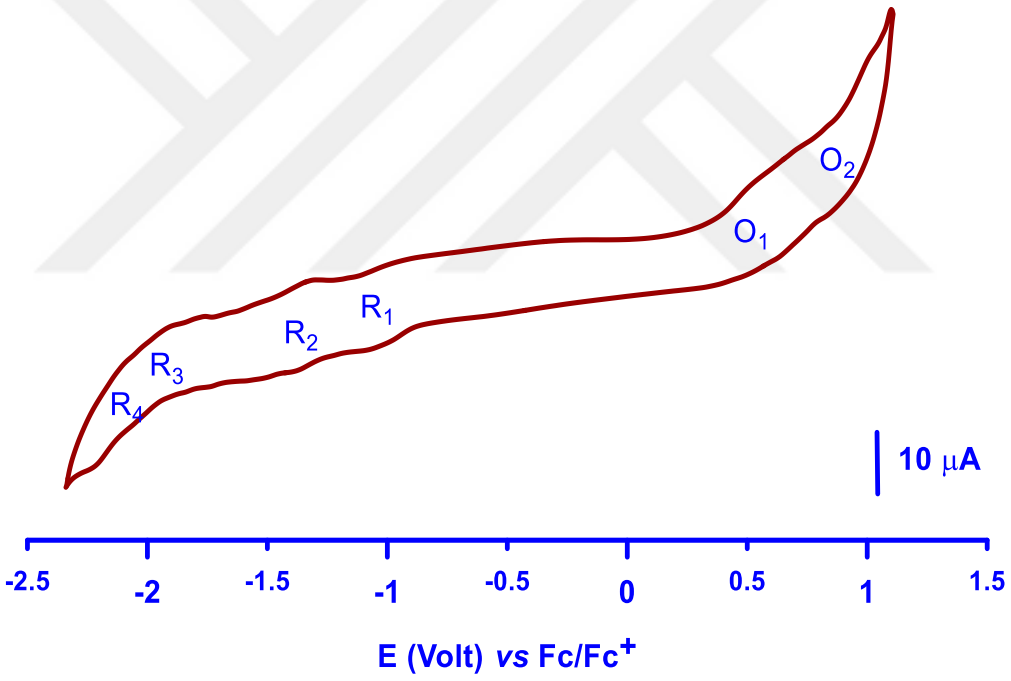


**Figure 3.54.** Cyclic voltammogram of Zn(II)phthalocyanine.

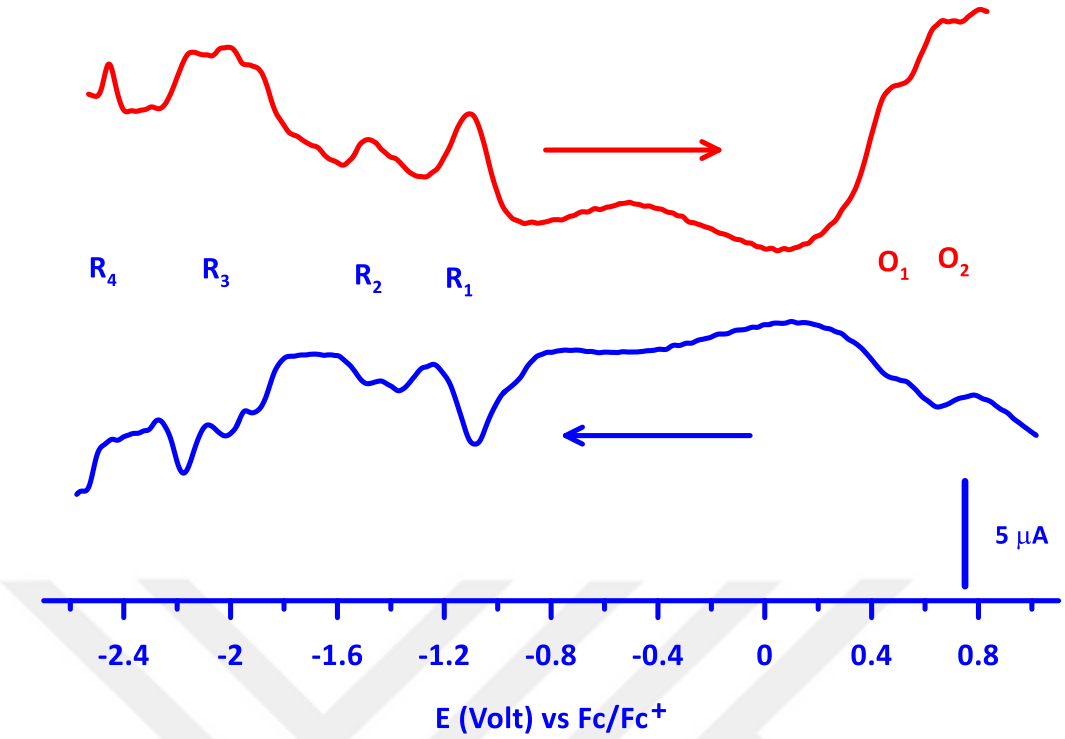


**Figure 3.55.** Square wave voltammogram of zinc(II)phthalocyanine.

## 3.14. 2,2',2'',2'''-(2,9,16,23-tetrayltetrakis(sulfanediyl))tetrakis (benzothiazole) phthalocyanine

The metal-free phthalocyanine $H_2Pc$ was prepared from 4-(benzothiazol-2-ylthio) phthalonitrile under an argon atmosphere in DMF. The $H_2Pc$ complex was obtained free of starting materials, as a green-colored $H_2Pc$ solid, **Figure 3.56.**

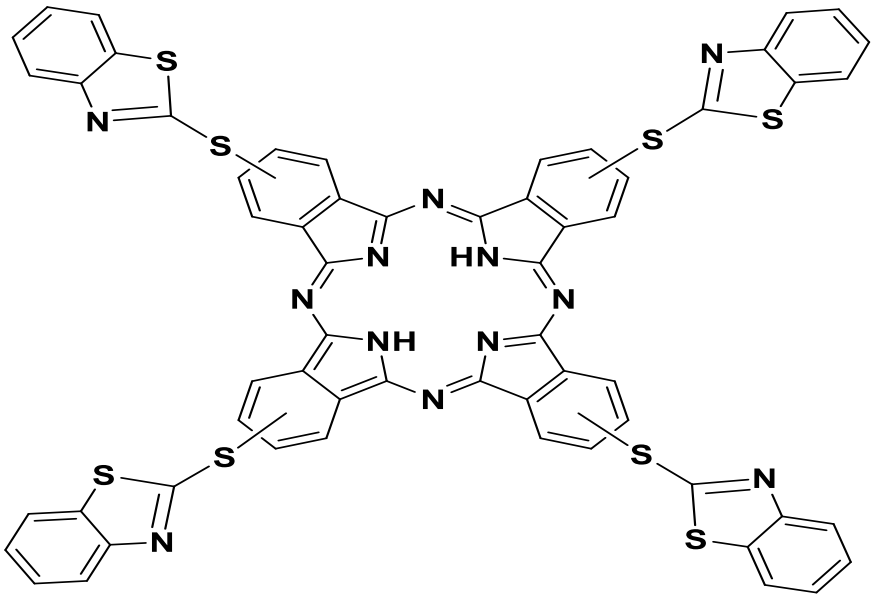

**Figure 3.56.** 2,2',2",2'"-( -2,9,16,23-tetrayltetrakis(sulfanediyl))tetrakis (benzothiazole) phthalocyanine.

- **FT-IR Spectrum**

Based on the KBr pellet sample, the FT-IR spectrum confirmed that the C≡N peak disappeared at 2232 $cm^{-1}$. Two peaks at 2973 and 2926 $cm^{-1}$ indicate aromatic C-H stretching, while a weak peak at 1632 $cm^{-1}$ indicates C=C macrocycle ring stretching, and C=N stretching by a peak at 1424 $cm^{-1}$. Other peaks at 1124 $cm^{-1}$ and 873 $cm^{-1}$ relate to the C-N and H-N bonds respectively. In addition to, the C-S bond peak appears at 713 $cm^{-1}$, and the C-C bond peak is visible at 1050 $cm^{-1}$, **Figure 3.57.**

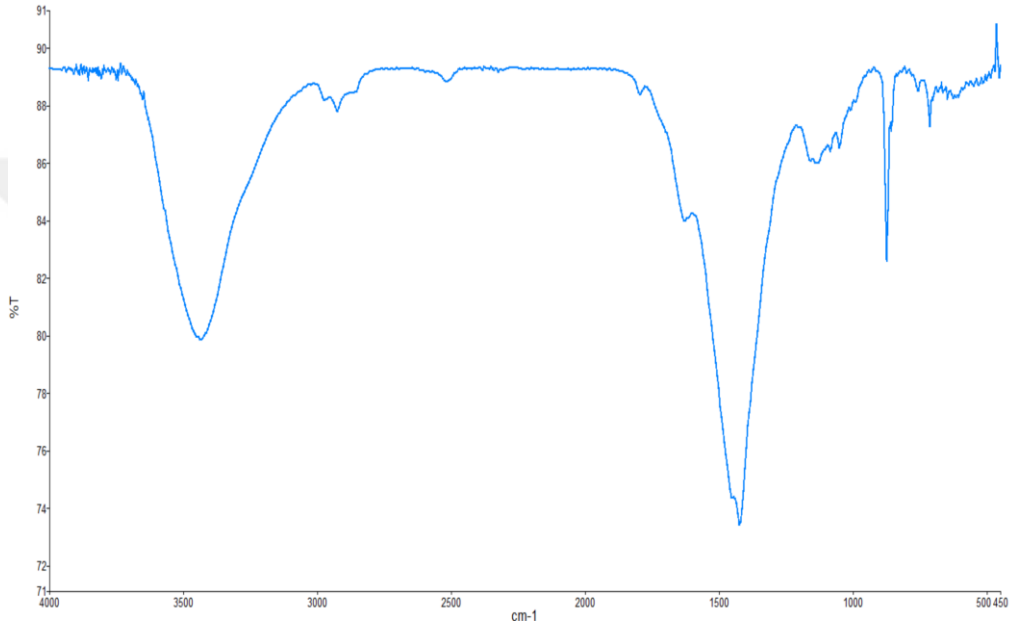


**Figure 3.57**. FT-IR spectrum of free metal phthalocyanine.

- **UV–visible spectrum**

In DMF, Pc compounds UV–vis spectra display Q band absorptions between 600-700 nm. Compounds Q band absorptions reflect the π-π* transition from HOMO to LUMO of the phthalocyanine ring. B-band absorptions of compounds were found in the UV range between 300-400 nm, resulting from transitions from deeper π levels to the LUMO. A Q-band UV–vis spectrum of the $H_2Pc$ complex in DMF shows strong absorption at 629 nm and so small shoulder at 687 nm. As shown in **Figure 3.58**. Unmetalated phthalocyanine has a characteristic double band at 600-700 nm, in this spectrum we see strong absorption at 629 nm and a relatively weak band at 687 nm caused by the stacking of the phthalocyanine compounds forming strong aggregate in solution. Therefore we can not see the general unmetalated phthalocyanine spectra.

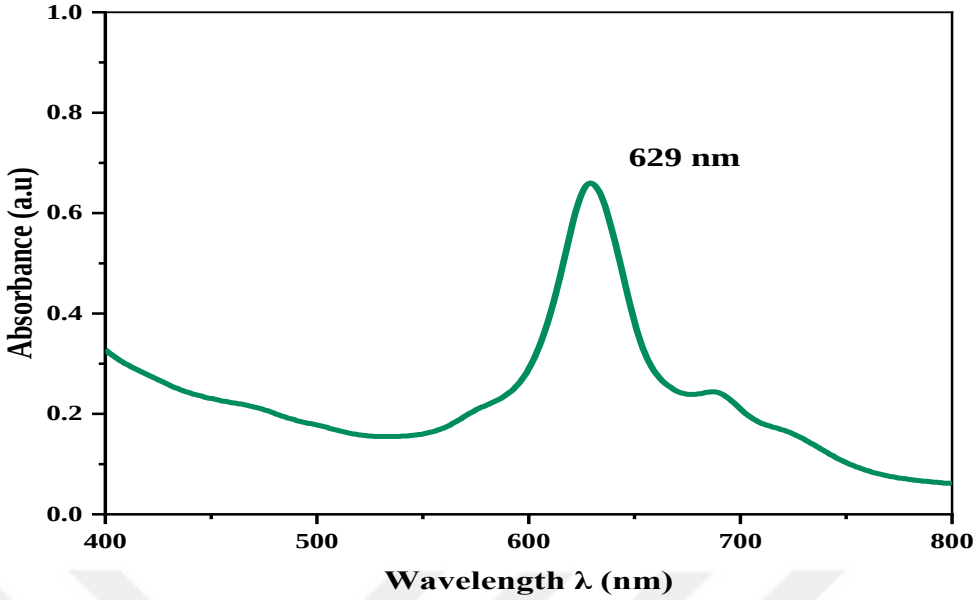


**Figure 3.58.** UV-visible spectrum of unmetallic phthalocyanine.

- **Thermal analysis.**

Based on the TG and DTG curves of $H_2P$ indicates thermal stability up to 250 °C, with a mass loss of 2%. Beyond this temperature, three distinct phases of mass loss were observed. The first phase, involving low thermal decomposition, occurs between 250-370 °C, with an approximate weight loss of 7%. The second phase, characterized by exothermic decomposition occurs between 380 and 550 °C, also resulting 8% weight loss. The third phase of degradation, occurs between 580 -720 °C, with a 30% weight loss. The thermogram analysis suggests that $H_2Pc$ decomposed without showing a melting point, resulting in a 45% mass loss up to 700 °C. The residue after decomposition accounts for approximately 53%, as shown in **Figure 3.59.**

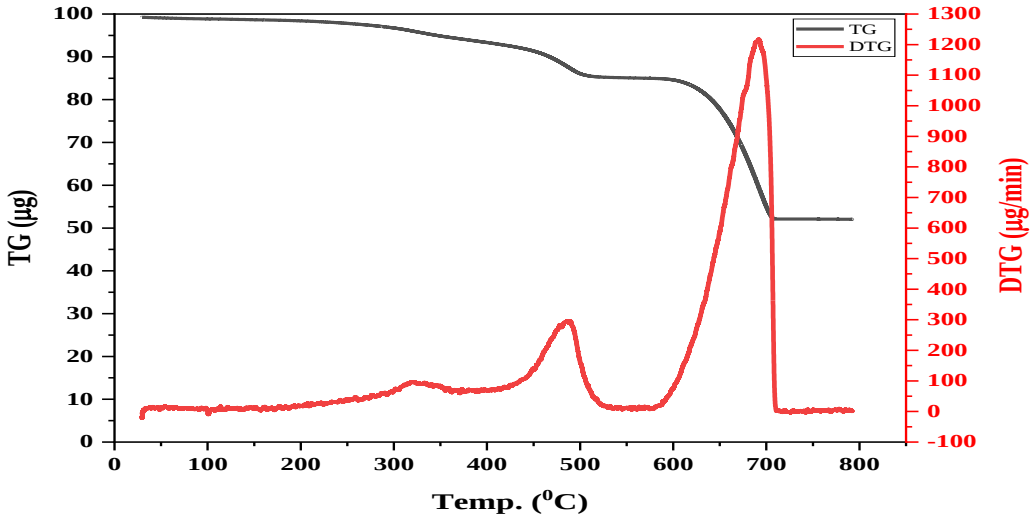


**Figure 3.59.** TG and DTG of free metal phthalocyanine.

- **Electrochemical Properties.**

The electrochemical analysis of $H_2Pc$ was conducted using CV in **Figure 3.60** and SWV **Figure 3.61** in DMF with TBAFB as the supporting electrolyte. Potentials were measured relative to Fc/Fc+ in non-aqueous solutions. Due to the limited solubility of $H_2Pc$, the CV voltammogram was not able to effectively demonstrate the redox processes. Therefore, the experiment was performed using the SW voltammogram, since it provides better results than CV for the redox processes.

There are four electrochemical waves that represent the reductions of $H_2Pc$, labeled $R_1$, $R_2$, $R_3$, and $R_4$, at -1.22, -1.68, -2.02, and -2.19 V respectively, with two oxidations waves, labeled $O_1$ and $O_2$, were observed at 0.33 and 0.76 V, respectively. All of these redox waves originate from phthalocyanine macrocyclic ring. An important part of the redox activity is the removal of two electrons from the HOMO of the phthalocyanine ring, which could accommodate up to four additional electrons in the LUMO.

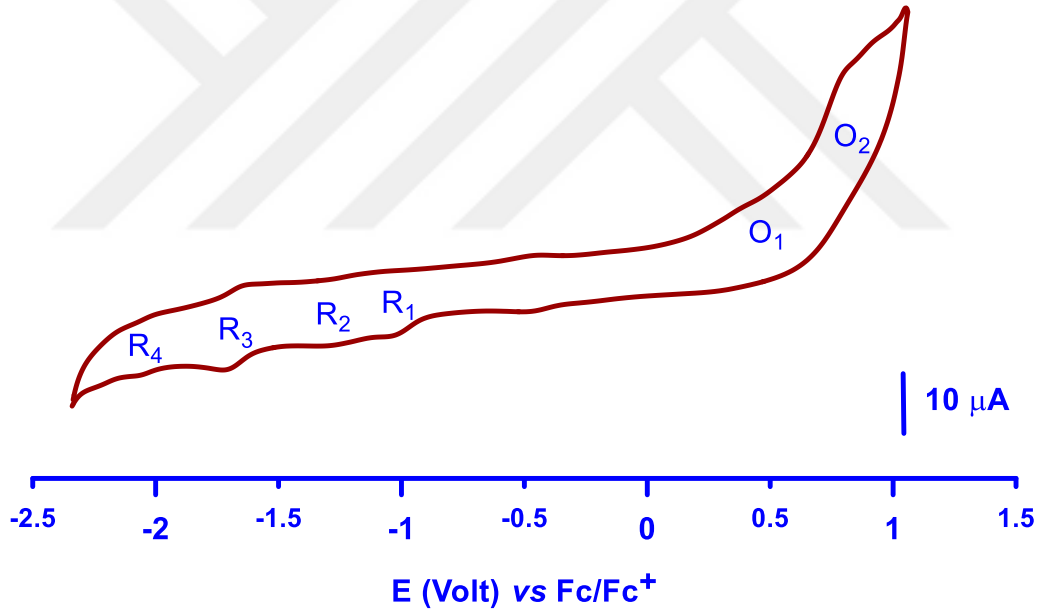


**Figure 3.60.** Cyclic voltammogram of unmutilated phthalocyanine.

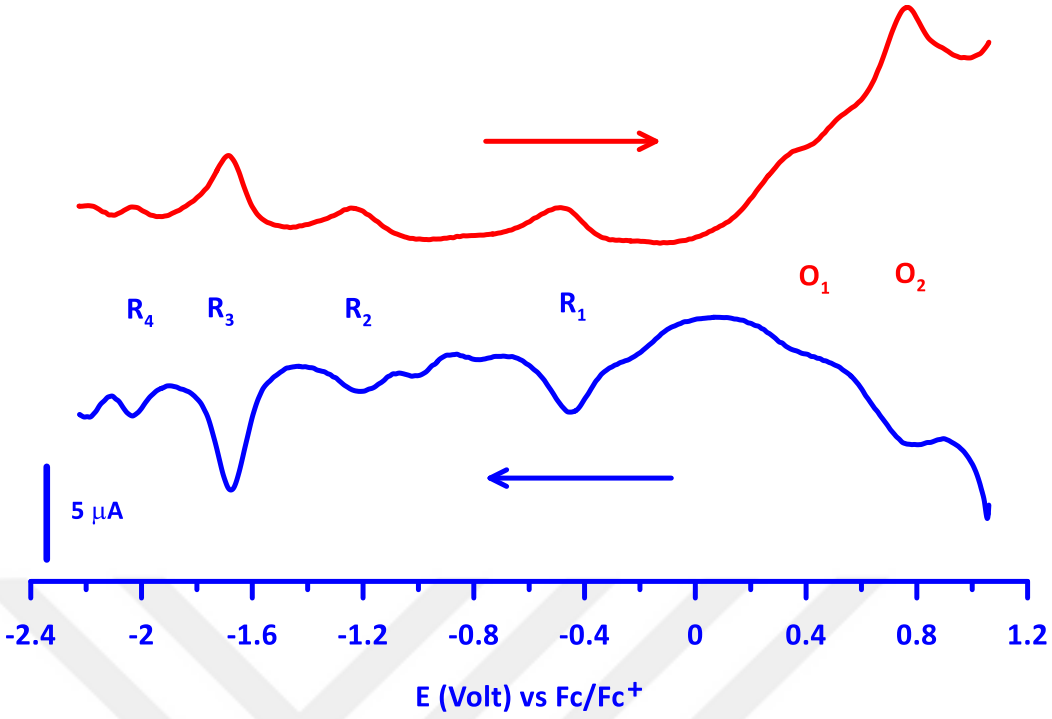


**Figure 3.61.** Square wave voltammogram of un-metalated phthalocyanine.

## 3.15. 2,9,16,23-tetrakis(quinolin-8-yloxy) Chrome phthalocyanine.

Chrome phthalocyanine CrPc was synthesized from 4-(quinolin-8-yloxy) phthalonitrile and Chrome(II)acetate under an argon atmosphere in DMF. The CrPc complex, which is green in color and possesses the characteristic properties of phthalocyanines, is shown in **Figure 3.62.**

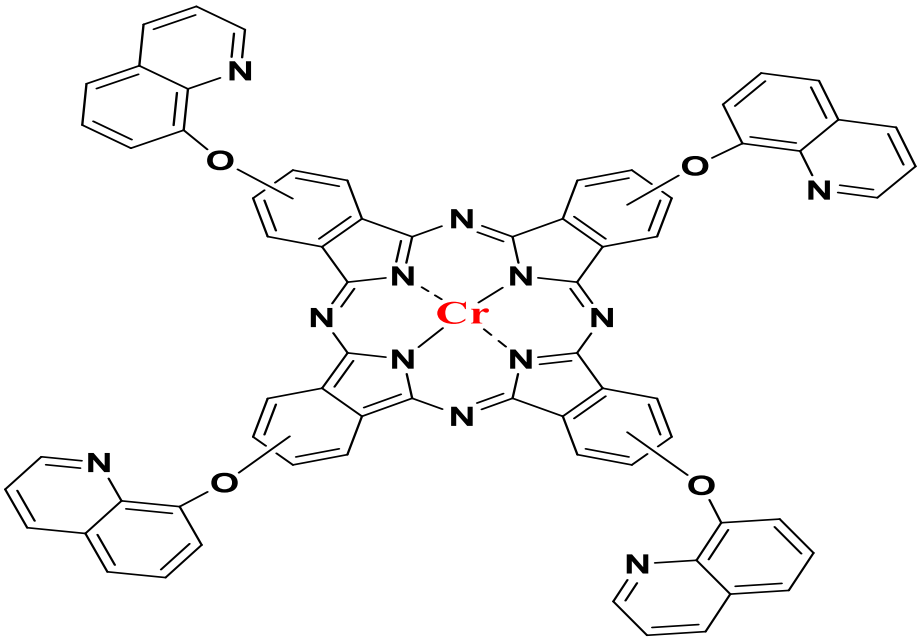


**Figure 3.62.** 2,9,16,23-tetrakis(quinolin-8-yloxy) Chrome phthalocyanine.

- **FT-IR Spectrum**

The FT-IR spectrum showed that the C≡N stretching mode at 2233 $cm^{-1}$ was absent. A weak peak at 2921 $cm^{-1}$ was observed for the C-H bond. The bands at 1640 $cm^{-1}$ and 1499 $cm^{-1}$ corresponded to the aromatic C=C stretching vibration and the C=N stretching vibration, respectively. A peak at 747 $cm^{-1}$ was identified for the substituted benzene ring. Aromatic C-H bending vibrations were found at 1466 $cm^{-1}$ and 1247 $cm^{-1}$. While the band at 788 $cm^{-1}$ was attributed to C-C macrocycle ring distortion. Typical C-O stretching vibrations of the complex were detected at 1111 and 1087 $cm^{-1}$, **Figure 3.63.**

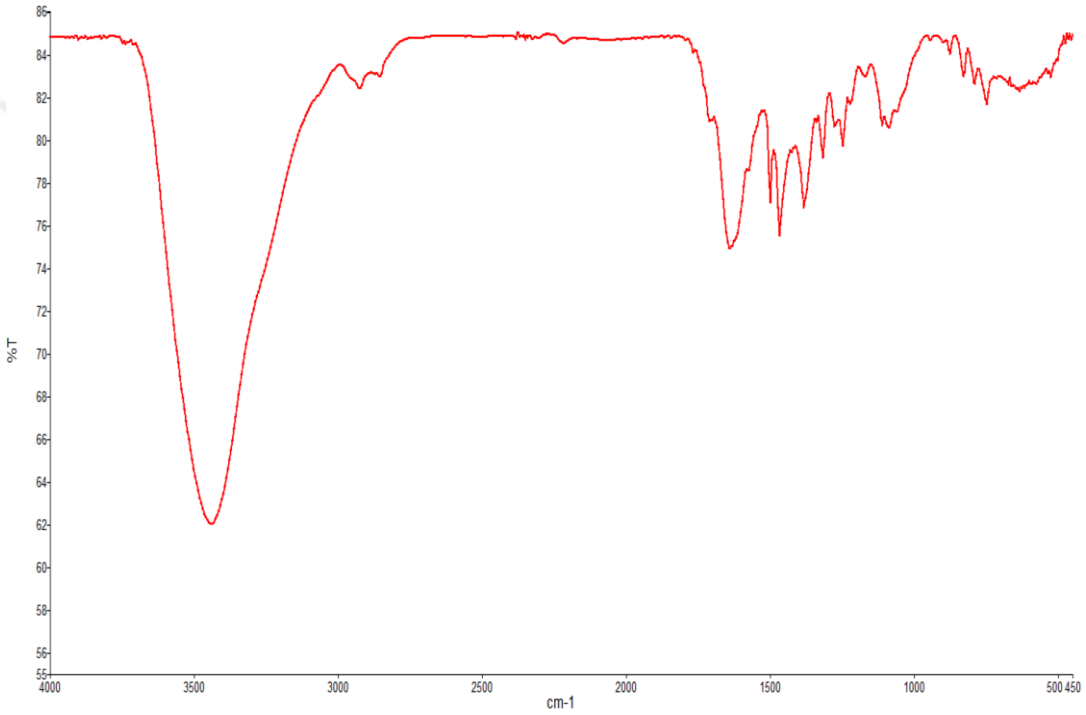


**Figure 3.63.** FT-IR spectrum of Cr(II)phthalocyanine.

- **UV–visible spectrum**

The UV-visible spectra of MPcs (CrPc) in DMF showed different absorption bands in the Q band area, which were located at 612 (shoulder) and 680 nm, as shown in **Figure 3.64**. The Q-band was ascribed to a transition from the orbital HOMO to the LUMO of the phthalocyanine ring, which was characterized by a $\pi \rightarrow \pi^*$ transition.

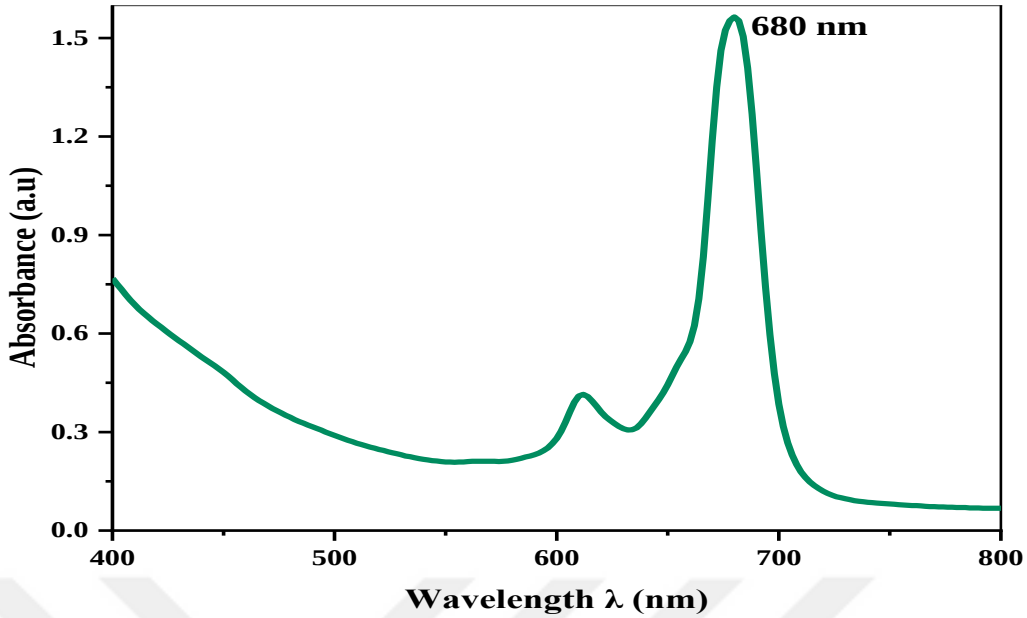


**Figure 3.64.** UV-visible spectrum of Cr(II)phthalocyanine.

- **Thermal analysis**

The TG and DTG analysis of CrPc shows three stages of mass loss. The first phases occurred between 20 to 130 °C involved approximately 4% weight loss, likely due to losing surface adsorbed water. The second stage (200–330 °C) involved a weight loss of about 11%, corresponding to the decomposition of the complex. Also, a weight loss of 64% was observed between (340-490 °C) which may be attributed to the decomposition remaining of the complex. The total weight loss of mass was 87 %, with 18% of the residue remaining, **Figure 3.65**.

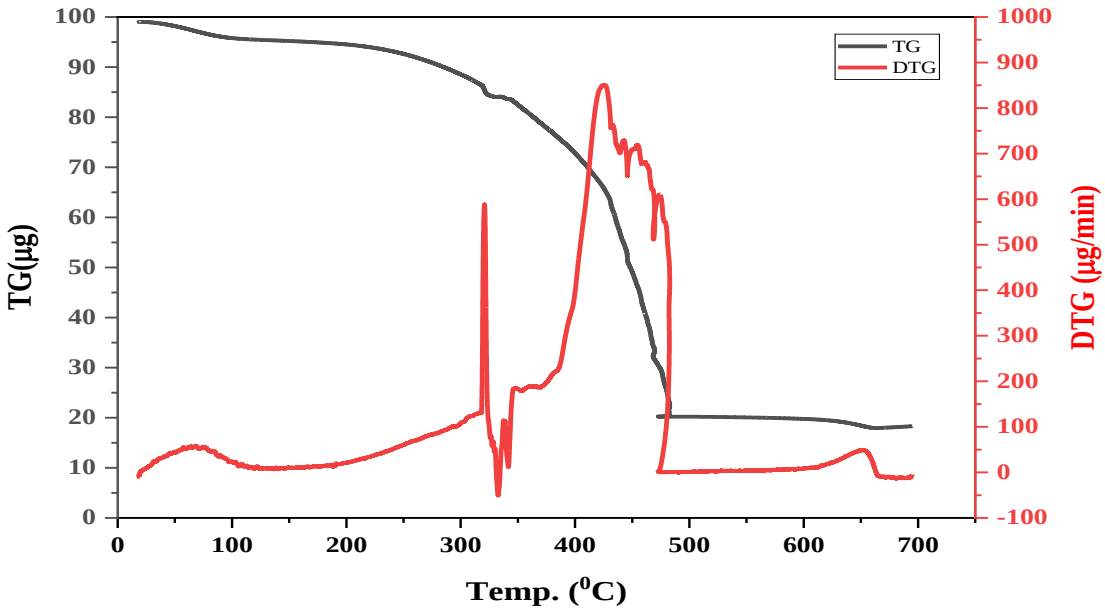


**Figure 3.65**. TG and DTG of Cr(II)phthalocyanine.

- **Electrochemical Properties**.

The electrochemical analysis of CrPc was conducted using CV and SWV in DMF with TBAFB as the supporting electrolyte. Potentials were measured relative to Fc/Fc+ in non-aqueous solutions. Due to the limited solubility of CrPc, the CV voltammogram was not able to effectively demonstrate the redox processes, on the other hand, the SW voltammogram, provided better results, therefore all the data were obtained from SW voltammogram.

There are four waves that repairs represent the reductions of CrPc, labeled $R_1$, $R_2$, $R_3$, and $R_4$, at -1.29, -1.66, -1.86, and -2.26 V respectively, and two oxidations' waves, labeled $O_1$ and $O_2$ were observed at 0.44 and 0.82 V, respectively. Also has redox waves of chromium metal Mr at -0.66 V. An important part of the redox activity is the removal of electrons from the HOMO of the phthalocyanine ring, which could accommodate up to four additional electrons in the LUMO. As shown in **Figure 3.66,** and **Figure 3.67.**

There are four redox processes $R_1$, $R_2$, $R_3$, and $R_4$ attributed to Cr(II)Pc-2/Cr(II)Pc-3, Cr(II)Pc-3/Cr(II)Pc-4, Cr(II)Pc-4/Cr(II)Pc-5, and Cr(II)Pc-5/Cr(II)Pc-6 respectively. Nonetheless, $O_1$, and $O_2$ are corresponding to the two oxidation processes of CrPc, specifically Cr(II) Pc-2/Cr(III) Pc-1, and Cr(II) Pc-1/Cr(III) Pc0 respectively. Additionally, their metal-based reduction process refers to Cr(II)Pc-2/Cr(I)Pc-2 because the $Cr^{2+}$ ion redox active in phthalocyanine complexes.

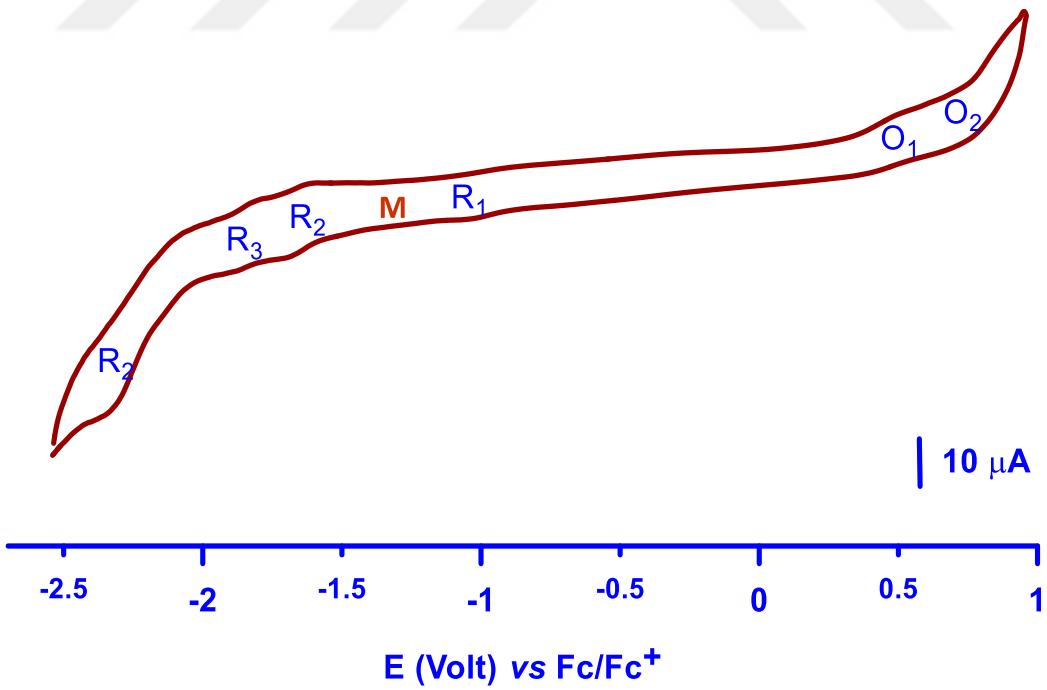


**Figure 3.66.** Cyclic voltammogram of Cr(II)phthalocyanine.

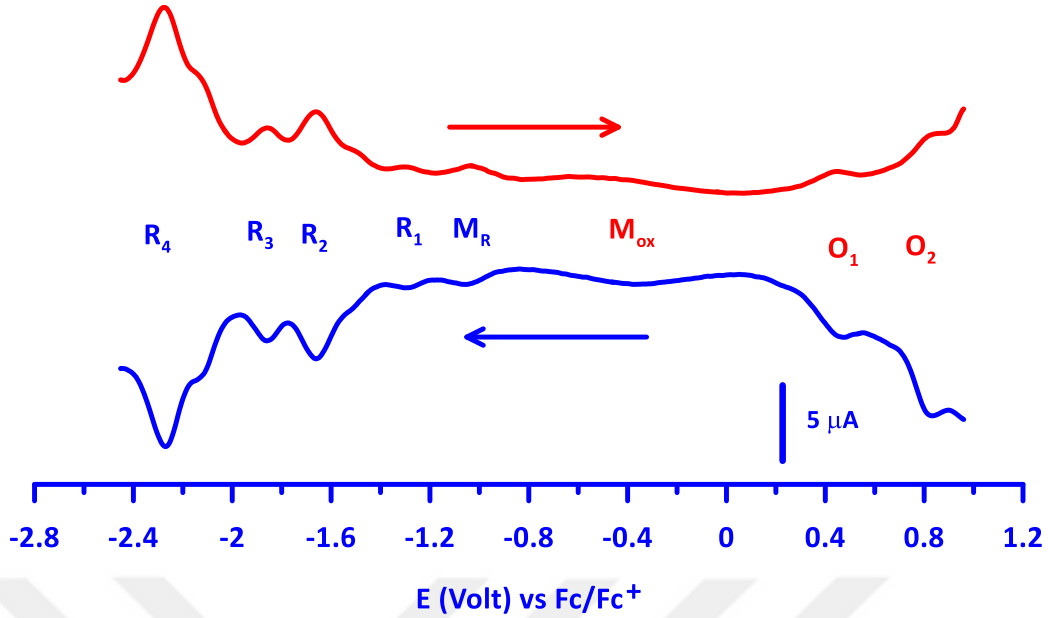


**Figure 3.67.** Square wave voltammogram of Cr(II)phthalocyanine.

### 3.16. 2,9,16,23-tetrakis(quinolin-8-yloxy) Iron phthalocyanine.

The Iron phthalocyanine FePc was synthesized from 4-(quinolin-8-yloxy) phthalonitrile with Fe(II)acetate under an argon atmosphere in DMF. The FePc complex, characterized by its green color and possessing the properties of phthalocyanines, was obtained by the through the cyclotetramerization of four phthalonitrile ligands with a Fe(II), shown in **Figure 3.68.**

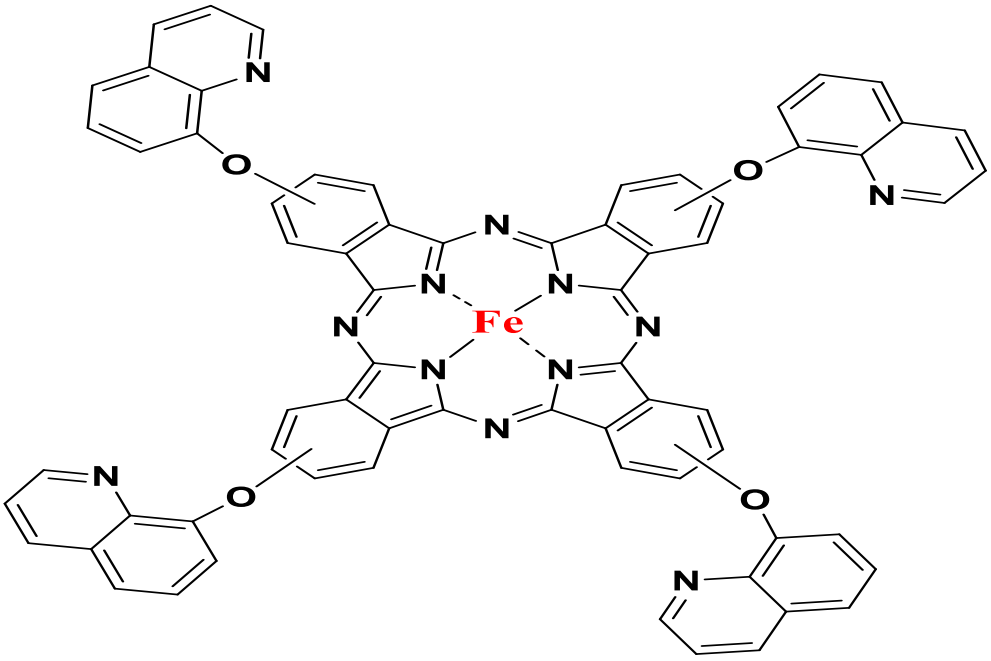


**Figure 3.68.** 2,9,16,23-tetrakis(quinolin-8-yloxy) Iron phthalocyanine.

- **FT-IR Spectrum**

The experimental results did not show a C≡N stretching mode at 2233 $cm^{-1}$. The weak peaks at 3060 $cm^{-1}$ and 2926 $cm^{-1}$ were detected for the C-H bond. The bands seen at 1615 $cm^{-1}$ and 1499 $cm^{-1}$ were identified as the aromatic C=C stretching vibration and the C=N stretching vibration, respectively. An absorption peak at 751 $cm^{-1}$ was observed for the substituted benzene ring, indicating a C-C macrocycle ring. The aromatic C-H bending vibrations were detected at 1466 and 1248 $cm^{-1}$. While the characteristic C-O stretching vibration structure was seen at 1085 $cm^{-1}$, **Figure 3.69.**

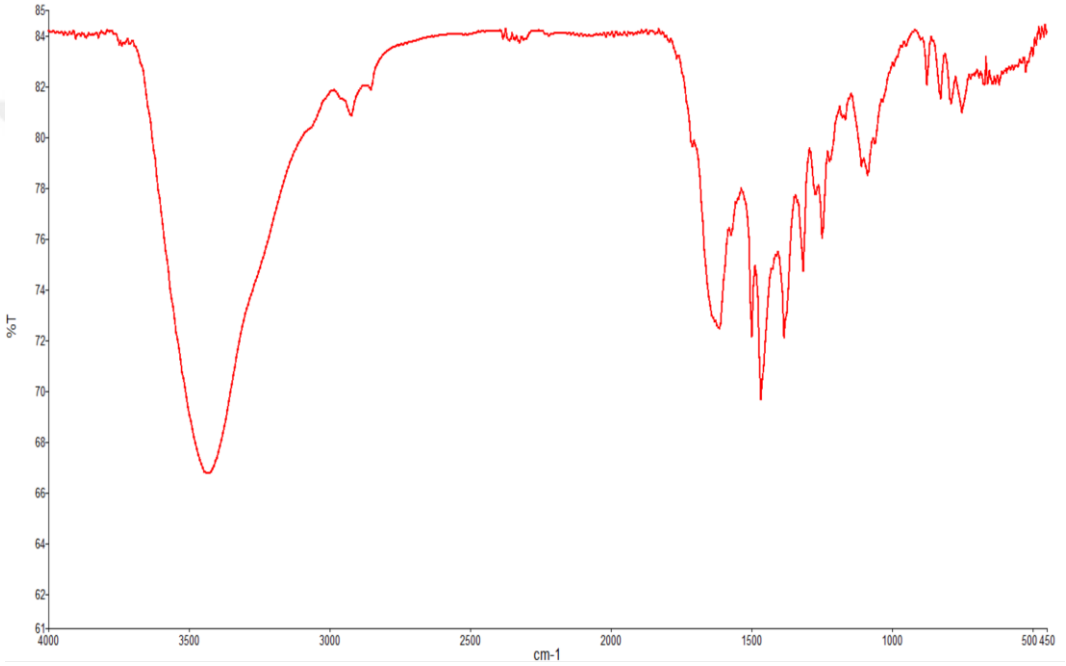


**Figure 3.69.** FT-IR spectrum of Fe(II)phthalocyanine.

- **UV–visible spectrum**

The UV-visible spectra of FePc in DMF showed an absorption band in the Q band region, which was located at 660 nm, as shown in **Figure 3.70**. The Q-band was ascribed to a transition from the HOMO to the LUMO orbital of the phthalocyanine ring.

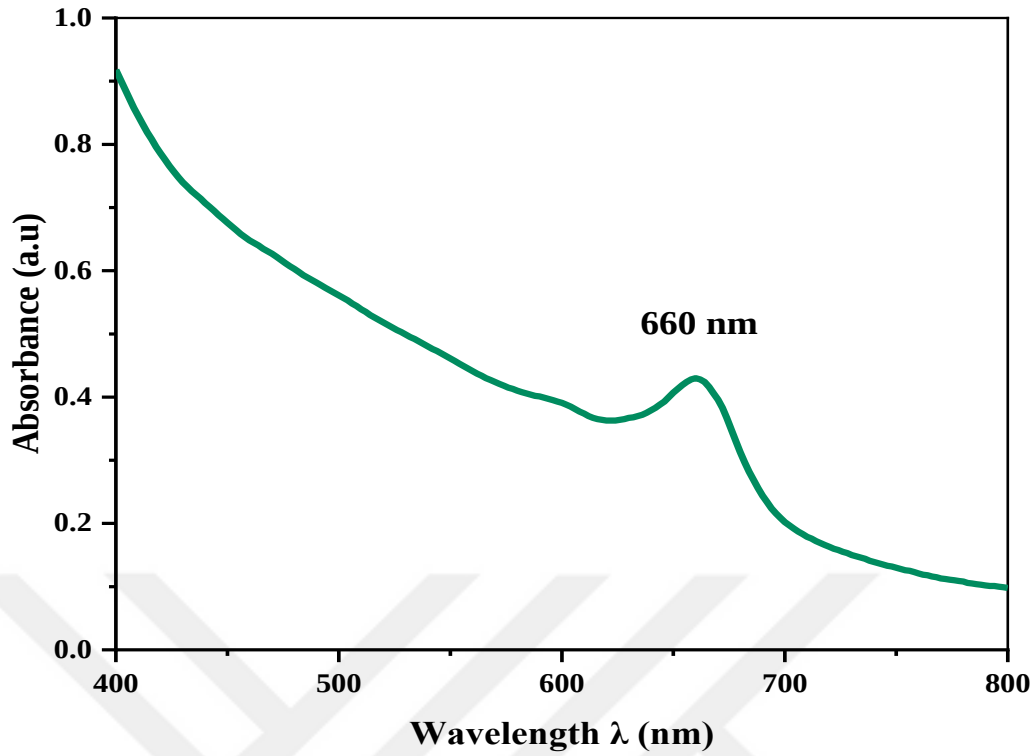


**Figure 3.70.** UV-visible spectrum of Fe(II)phthalocyanine.

- **Thermal analysis**

Based on the TG and DTG analysis, indicated that FePc was thermally stable up to 270 °C, most probably due to the loss of absorbed water, with a weight loss of approximately 12%. Beyond this temperature, there have been two distinct stages of mass loss were observed. The first stage, characterized by low thermal evaporation, occurred between 275-350 °C, with 73% weight loss. The second stage involved exothermic decomposition between 350-460 °C resulting in a 12% weight loss. The thermogram shows that FePc decomposed without showing a melting point, and the total mass loss is 95% with 5% of the residue remaining, shown in **Figure 3.71.**

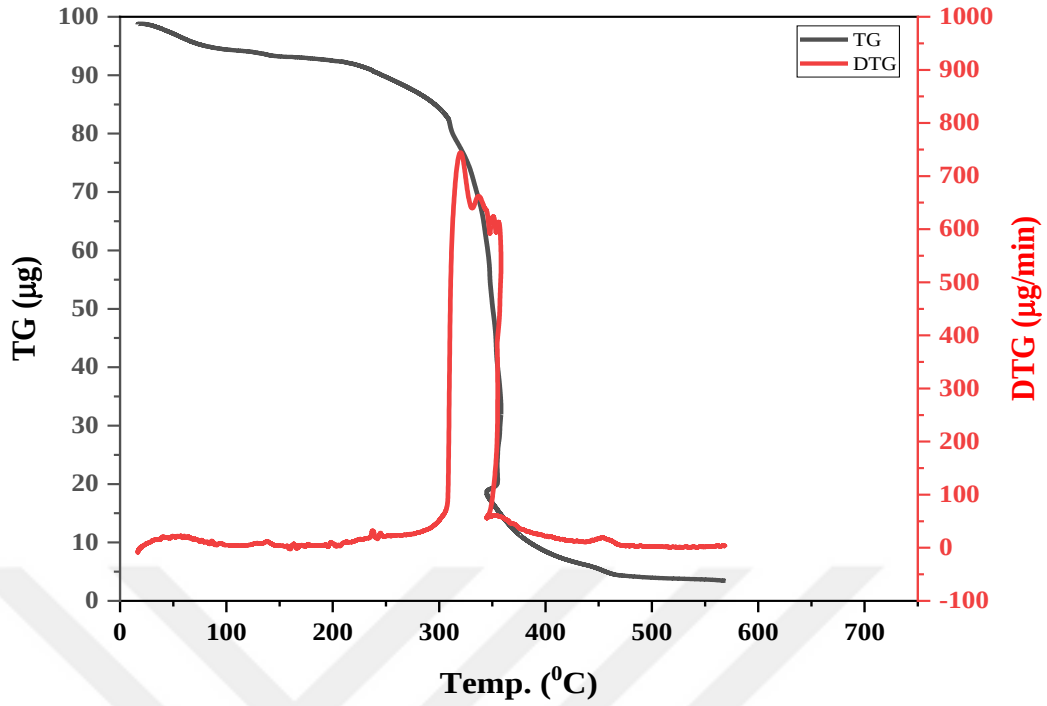


**Figure 3.71.** TG and DTG of Fe(II)phthalocyanine.

- **Electrochemical Properties**.

Electrochemical analysis of FePc was performed using a glassy carbon (GC) electrode in DMF with TBAFB as the supporting electrolyte by CV and SWV techniques and potentials were recorded relative to the ferrocene/ferrocenium couple (Fc/Fc+), which served as a pseudo reference electrode. The CV voltammogram could not adequately reveal redox processes due to the poor solubility of FePc.

The electrochemical voltammogram of FePc has four reduction peaks, namely $R_1$, $R_2$, $R_3$, and $R_4$ occurring at potentials of -1.09, -1.60, -1.94, and -2.52, respectively, and one oxidation $O_1$=0.78 V. Also has oxidation-reduction on metal Mr and Mo at -0.61 and 0.39 V respectively. All of these redox processes originate from phthalocyanine macrocycle rings and iron metal. The redox behavior of the phthalocyanine ring involves the removal of electrons from its HOMO, while up to four more electrons may be added to its LUMO of the phthalocyanine ring CV and SW voltammograms shown in **Figure 3.72,** and **Figure 3.73.**

The redox processes $R_1$, $R_2$, $R_3$, and $R_4$ are assigned to Fe(II)Pc-2/Fe(II)Pc-3, Fe(II)Pc-3/Fe(II)Pc-4, Fe(II)Pc-4/Fe(II)Pc-5, and Fe(II)Pc-5/Fe(II)Pc-6, respectively. However, $O_1$ and $O_2$ correspond to the two FePc oxidation processes, which are Fe(II)Pc-2/Fe(III)Pc-1 and Fe(II)Pc-1/Fe(III) Pc0, respectively. Furthermore, the metal-based Mr and Mo process identified as Fe(II)Pc-2/Fe(I)Pc-2 and Fe(II)Pc-2/Fe(III)Pc-2 respectively.

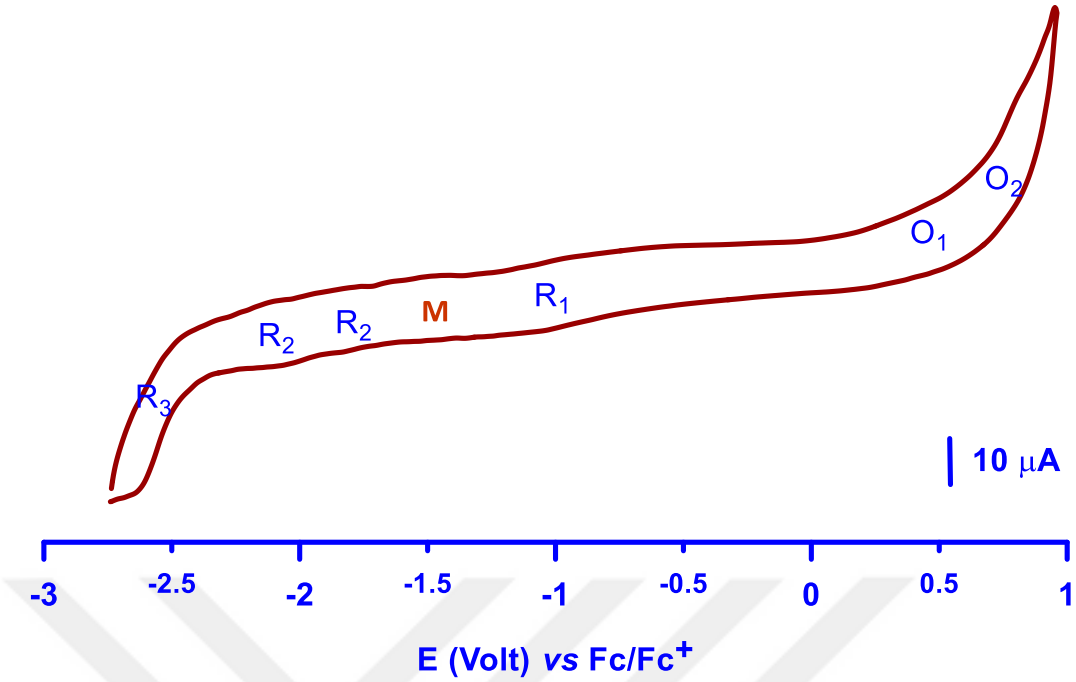


**Figure 3.72.** Cyclic voltammogram of Iron(II)phthalocyanine.

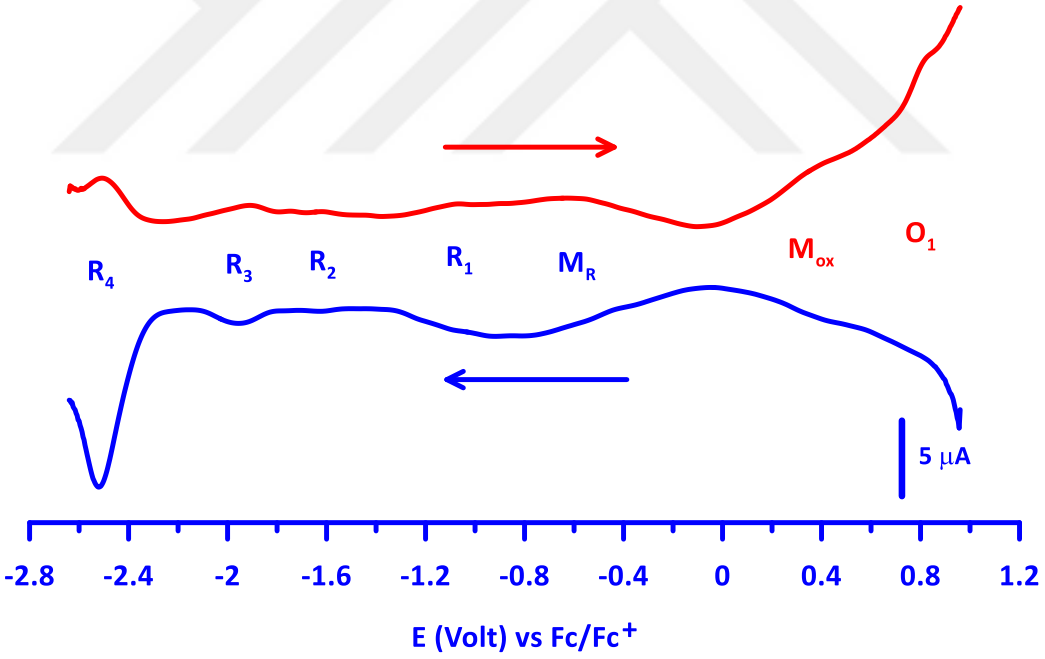


**Figure 3.73.** Square wave voltammogram of Iron(II)phthalocyanine.

### 3.17. 2,9,16,23-tetrakis(quinolin-8-yloxy) Cobalt phthalocyanine.

Cobalt phthalocyanine CoPc was synthesized from 4-(quinolin-8-yloxy) phthalonitrile with Cobalt(II)acetate under argon atmosphere in DMF. FT-IR spectra reveal that the CoPc complex did not contain any starting materials, the molecule structure of CoPc is shown in **Figure 3.74.**

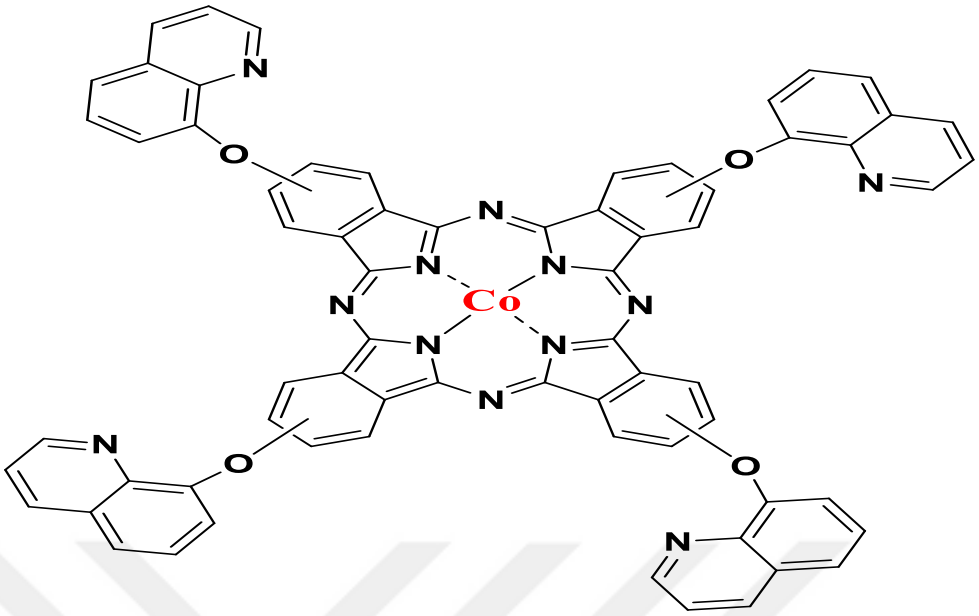


**Figure 3.74**. 2,9,16,23-tetrakis(quinolin-8-yloxy) Cobalt phthalocyanine.

- **FT-IR Spectrum**

The FT-IR spectrum showed no C≡N stretching mode at 2233 $cm^{-1}$. Weak peaks at 3058 and 2926 $cm^{-1}$ were detected in the experimental C-H bond. Bands seen at 1611 $cm^{-1}$ and 1500 $cm^{-1}$ were identified as the aromatic C=C stretching vibration and the C=N stretching vibration, respectively. A peak at 756 $cm^{-1}$ was observed for the substituted benzene ring, attributed to C-C macrocycle ring distortion. Aromatic C-H bending vibrations were found at 1457 and 1247 $cm^{-1}$. While the characteristic C-O stretching vibration was detected at 1094 $cm^{-1}$. FT-IR spectra are given in **Figure 3.75.**

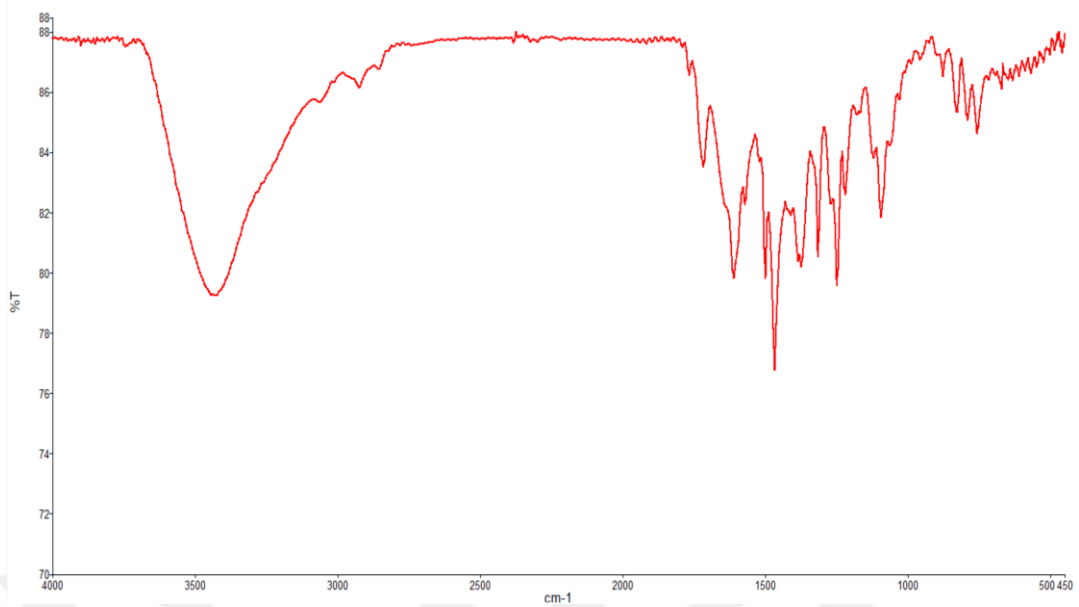


**Figure 3.75.** FT-IR spectrum of Co(II)phthalocyanine.

- **UV–visible spectrum**

The UV-visible spectra of CoPc in DMF showed distinct absorption bands in the Q band region, which were located at 604 (shoulder) and 668 nm, as shown in **Figure 3.76.** The Q-band was ascribed to a transition from the HOMO to the LUMO of the phthalocyanine ring, which was characterized by a transition from π to π*.

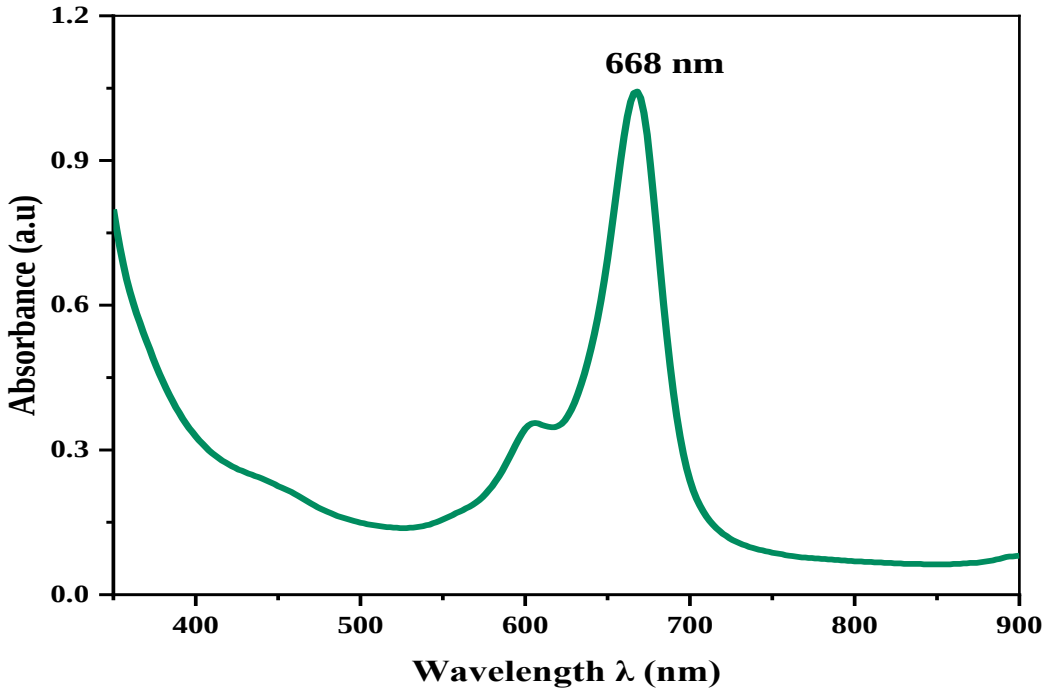


**Figure 3.76.** UV-visible spectrum of Co(II)phthalocyanine.

- **Thermal analysis**

Based on the TG and DTG curves, CoPc demonstrated thermal stability up to 230 °C, with a 5% weight loss, likely due to the loss of absorbed surface water from the complex. Although, two distinct phases of mass loss were observed. The first stage involved exothermic decomposition between 270-500 °C, resulting in a 78% weight loss, and the second stage of degradation occurred between 600-770 °C, involving a 4% weight loss. Thermogram analysis indicated that CoPc decomposed without showing a melting point, the total mass loss was 87% with 13% of the residue remaining, as shown in **Figure 3.77.**

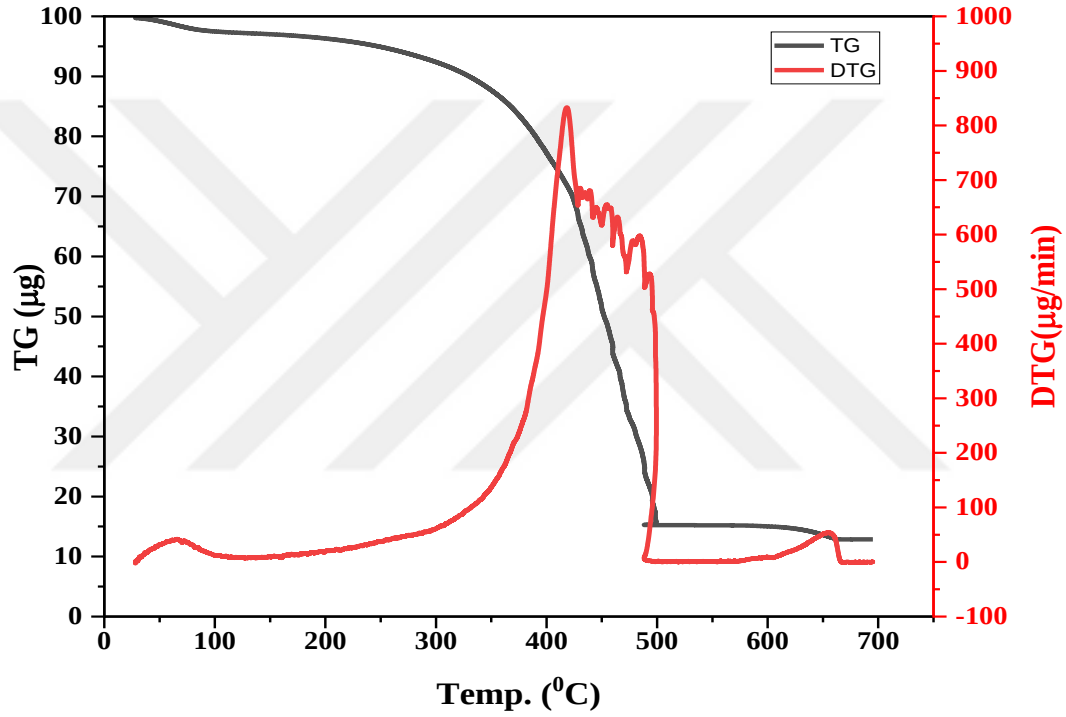


**Figure 3.77**. TG and DTG of Co(II)phthalocyanine.

- **Electrochemical Properties**.

Electrochemical analysis of CoPc was performed using a GC electrode in DMF with TBAFB as the supporting electrolyte. CV and SWV were techniques used, and potentials were recorded in non-aqueous solutions relative to the ferrocene/ferrocenium couple (Fc/Fc+), which served as a pseudo reference electrode.

The CoPc molecule may undergo many cycles of oxidation and reduction of phthalocyanine macrocycle moiety. The electrochemical voltammogram of CoPc has four reduction peaks, namely $R_1$, $R_2$, $R_3$, and $R_4$, occurring at potentials of -1.13, -1.40, -1.83, and -2.57 V, respectively. Additionally, there are two oxidations $O_1$ = 0.04 V and $O_2$ = 0.51 V. Also has oxidation reduction on metal Mr and Mo at -0.92 and 0.08 Vs respectively. The redox behavior of the phthalocyanine

ring involves the removal of two electrons from its HOMO, while up to four more electrons may be added to its LUMO of the ring, **Figure 3.78,** and **Figure 3.79.**

There are four redox processes $R_1$, $R_2$, $R_3$, and $R_4$ attributed to Co(II)Pc-2/Co(II)Pc-3, Co(II)Pc-3/Co(II)Pc-4, Co(II)Pc-4/Co(II)Pc-5, and Co(II)Pc-5/Co(II)Pc-6 respectively. Nonetheless, $O_1$ and $O_2$ are corresponding to the two oxidation processes of CoPc, specifically Co(II) Pc-2/Co(III)Pc-1, and Co(II)Pc-1/Co(III)Pc0 respectively. Additionally, there is a metal-based redox process that refers to Co(II)Pc-2/Co(I)Pc-2, and Co(II)Pc-2/Co(III)Pc-2, Mr, and Mo respectively.

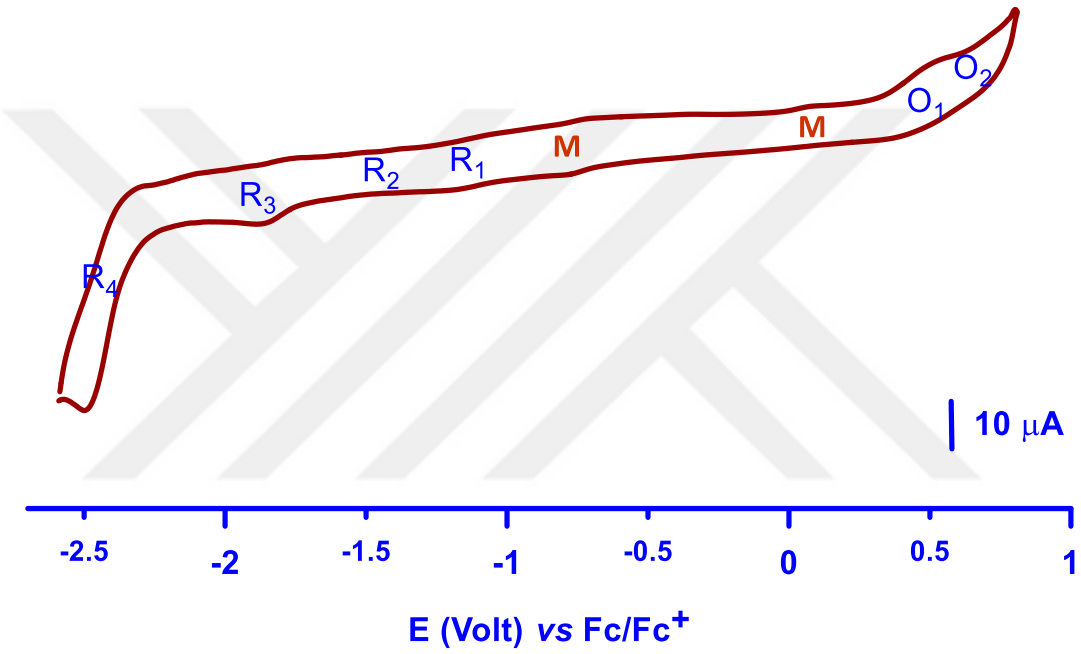


**Figure 3.78.** Cyclic voltammogram of Co(II)phthalocyanine.

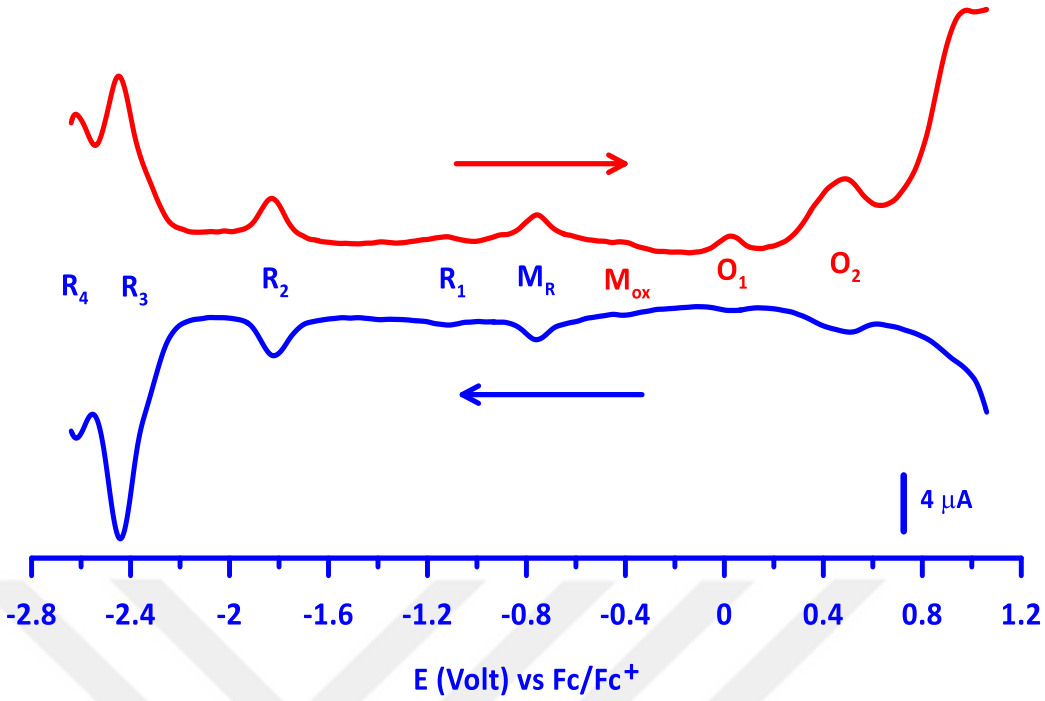


**Figure 3.79.** Square wave voltammogram of Co(II)phthalocyanine.

## 3.18. 2,9,16,23-tetrakis(quinolin-8-yloxy) Nickel phthalocyanine.

The Nickel phthalocyanine NiPc was prepared from 4-(quinolin-8-yloxy) phthalonitrile with Nickel(II)acetate under an argon atmosphere in DMF. The addition of Ni(II) salt triggered the cyclotetramerization of four phthalonitrile ligands, resulting in green NiPc, a phthalocyanine complex shown in **Figure 3.80.**

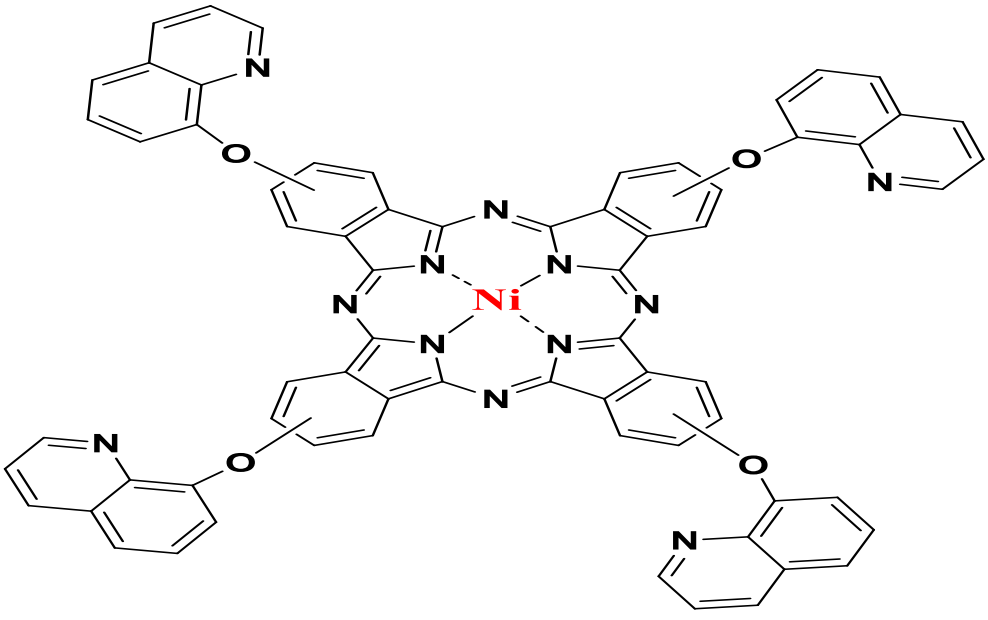


**Figure 3.80.** 2,9,16,23-tetrakis(quinolin-8-yloxy) Nickel phthalocyanine.

- **FT-IR Spectrum**

The experimental results did not show a C≡N stretching mode at 2233 $cm^{-1}$. Weak peaks at 3063 $cm^{-1}$ and 2926 $cm^{-1}$ were detected for the C-H bond. The bands seen at 1611 $cm^{-1}$ and 1498 $cm^{-1}$ were recognized as the aromatic C=C stretching vibration and the C=N stretching vibration, respectively. An absorption peak at 753 $cm^{-1}$ was observed for the substituted benzene ring, attributed to C-C macrocycle ring deformation. The aromatic C-H bending vibrations were detected at 1466 and 1248 $cm^{-1}$, while the characteristic C-O stretching vibration of the structure was seen at 1093 $cm^{-1}$. FT-IR spectra of CoPc are given in **Figure 3.81.**

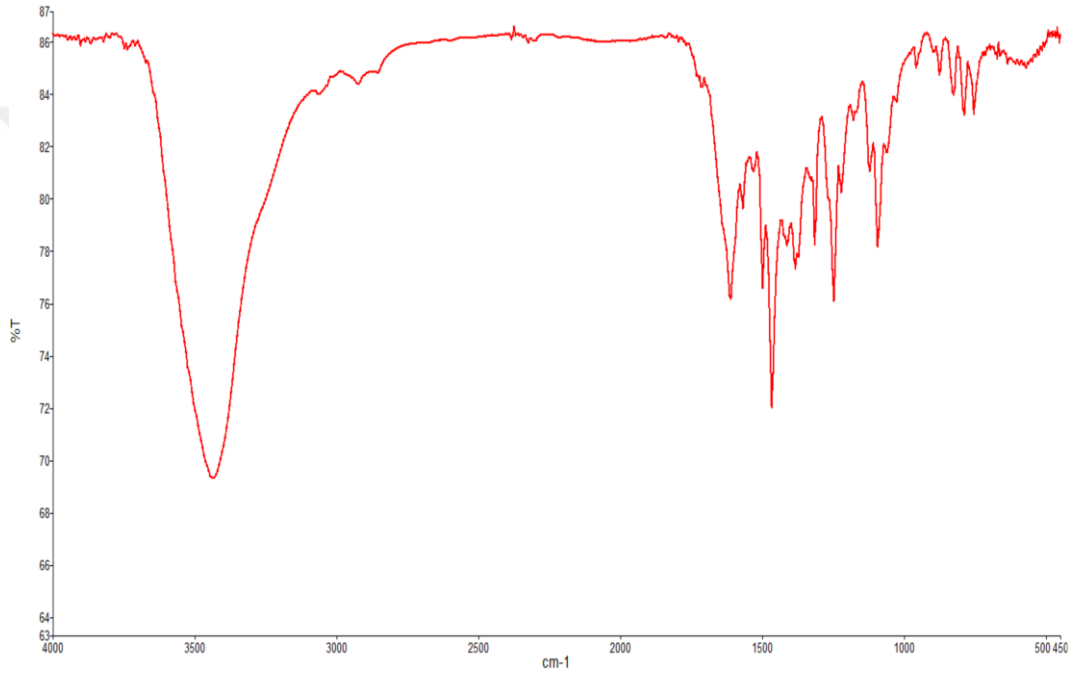


**Figure 3.81**. FT-IR spectrum of Ni(II)phthalocyanine.

- **UV–visible spectrum**

According to, the UV-vis spectra of MPcs in DMF showed the usual absorptions in the Q band region, at 680 and 610 nm (shoulder). The π-π* transition from the HOMO to the LUMO of the Pc ring is attributed to the Q band. As a result of transitions from deeper π levels to the LUMO, the compound B band absorptions were detected in the UV area at 340 nm as a shoulder, shown in Figure **3.82.**

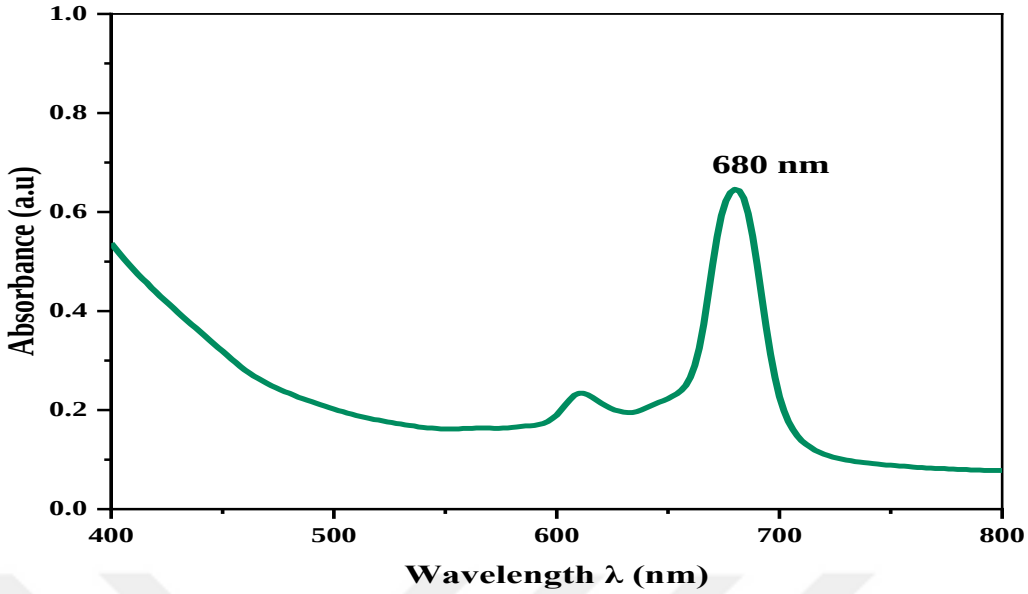


**Figure 3.82.** UV-visible spectrum of Ni(II)phthalocyanine.

- **Thermal analysis**

TG and DTG analyses of NiPc exhibit thermal stability up to 250 °C with a 7% loss of absorbed surface water. The mass loss occurs in one distinct stage, with decomposition occurring between 260-500 °C, causing a 93% mass loss. Then a 7% weight loss up to 500 °C. These results show some anomalies that 100% weight loss at 500 °C is not normal, even if all the organic material is decomposed to $CO_2$ and water, there must be inorganic residue like NiO at the end. In addition, it is impossible for any organic compound pyrolyzed completely at this temperature, which led us to speculate that, during the heating process small explosion of samples caused such results. TG and DTA thermograms are shown in **Figure 3.83.**

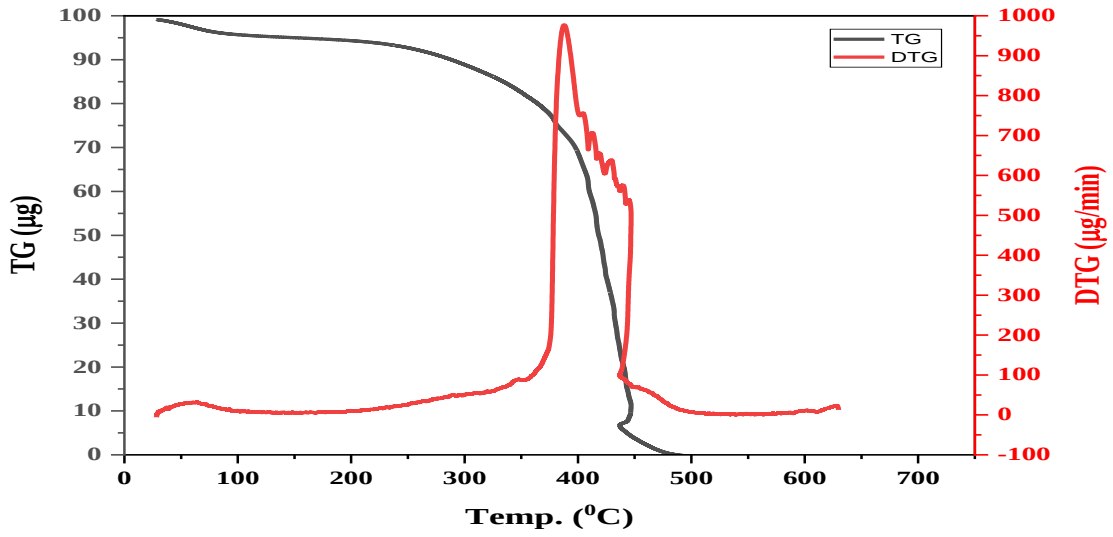


**Figure 3.83**. TG and DTG of Ni(II)phthalocyanine.

- **Electrochemical Properties**.

Electrochemical analysis of NiPc was performed using a GC electrode in DMF with TBAFB as the supporting electrolyte. CV and SWV techniques were used, and potentials were recorded in non-aqueous solutions relative to the ferrocene/ferrocenium couple (Fc/Fc+), which served as a pseudo reference electrode.

As can be seen in **Figure 3.84,** and **Figure 3.85,** the NiPc macrocycle moiety is capable of undergoing many different reduction and oxidation steps. The SW voltammogram reveals four reduction waves that are $R_1$, $R_2$, $R_3$, and $R_4$ at -1.10, -1.54, -1.74, and -2.34 Vs, and two oxidation waves $O_1$ = 0.07 V and $O_2$ = 0.64 V. All of these redox waves belong to phthalocyanine macrocycle rings because of redox inactive Ni(II) metal in the center of the complex. These four redox processes $R_1$, $R_2$, $R_3$, and $R_4$ can be identified as follows: Ni(II)Pc-2/Ni(II)Pc-3, Ni(II)Pc-3/Ni(II)Pc-4, Ni(II)Pc-4/Ni(II)Pc-5, and Ni(II)Pc-5/Ni(II)Pc-6 respectively. Also, $O_1$ and $O_2$ correspond to the two oxidation processes, which are Ni(II)Pc-2/Ni(II)Pc-1 and Ni(II)Pc-1/Ni(II)Pc0, respectively.

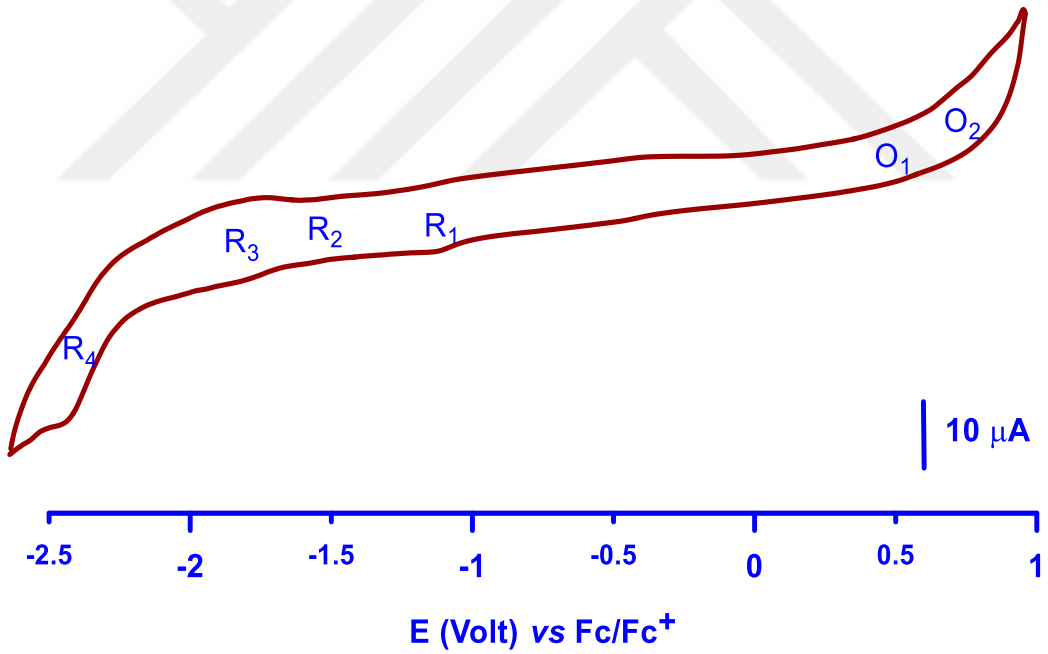


**Figure 3.84.** Cyclic voltammogram of Ni(II)phthalocyanine.

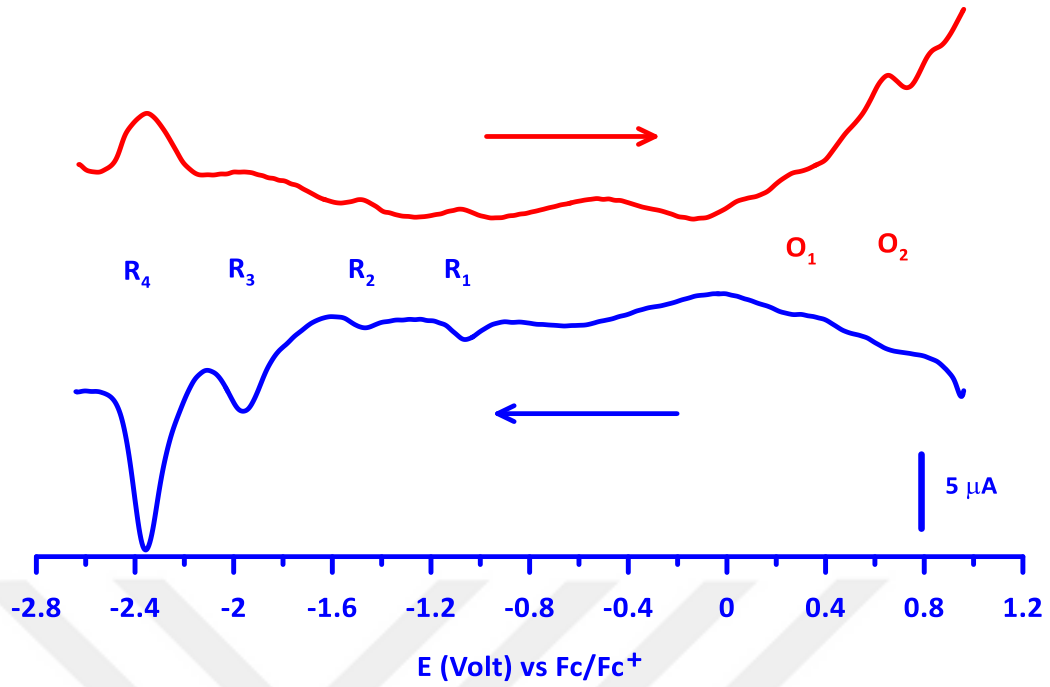


**Figure 3.85.** Square wave voltammogram of Ni(II)phthalocyanine.

## 3.19. 2,9,16,23-tetrakis(quinolin-8-yloxy) Copper phthalocyanine.

The Copper phthalocyanine CuPc was synthesized from 4-(quinolin-8-yloxy) phthalonitrile with Copper(II)acetate under an argon atmosphere in DMF. The addition of Cu(II) salt triggered the cyclotetramerization of four phthalonitrile ligands acting as a template, forming green CuPc, that the molecular structure is given in **Figure 3.86.**

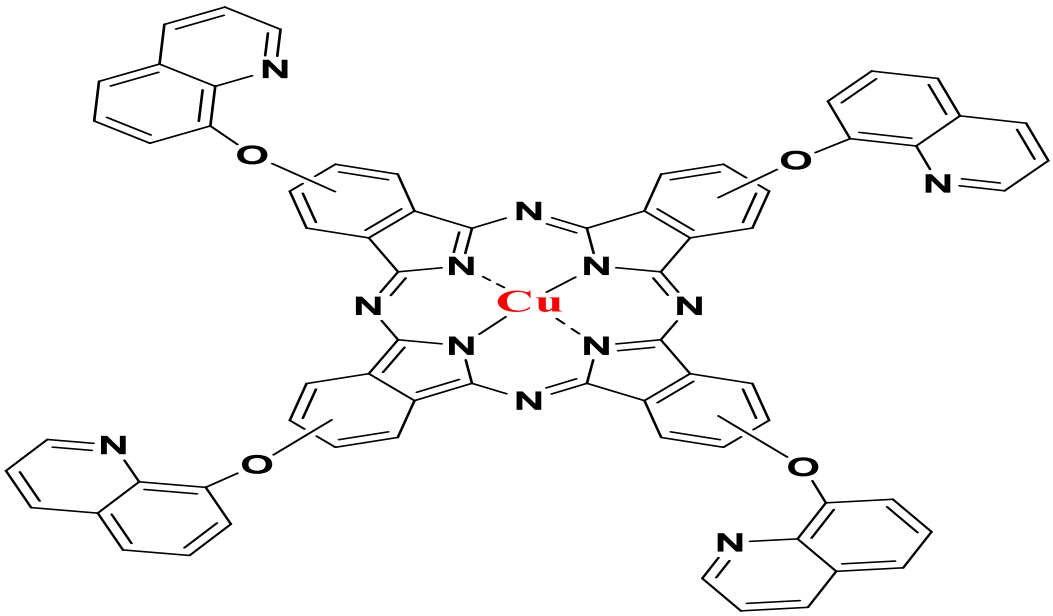


**Figure 3.86.** 2,9,16,23-tetrakis(quinolin-8-yloxy) Cupper phthalocyanine.

- **FT-IR Spectrum**

The FT-IR spectrum showed no C≡N stretching mode at 2233 $cm^{-1}$. Weak peaks at 3055 $cm^{-1}$ and 2926 $cm^{-1}$ were detected for the C-H bond. Bands at 1597 $cm^{-1}$ and 1499 $cm^{-1}$ were identified as the aromatic C=C stretching vibration and the C=N stretching vibration, respectively. An absorption peak with a peak at 713 $cm^{-1}$ was observed for the (C-C) bond in the substituted benzene ring. The C-H aromatic bending vibrations were detected at 1466 and 1250 $cm^{-1}$. While the characteristic C-O stretching vibration of the structure was seen at 1091 $cm^{-1}$, The FT-IR spectra of CuPc were given in **Figure 3.87.**


**Figure 3.87.** FT-IR spectrum of Cu(II)phthalocyanine.

- **UV–visible spectrum**

The UV-vis spectra of CuPc in DMF showed the usual absorptions in the Q band region at 680 nm and 610 nm as a shoulder. The π-π* transition from the HOMO to the LUMO of the CuPc ring at 680 nm is attributed to the Q band of the CuPc complex. As a result of transitions from deeper π levels to the LUMO, the compound B band absorptions were detected at 420 nm as shoulder in the UV-visible spectra of CuPc. UV-visible spectra of CuPc are shown in **Figure 3.88.**

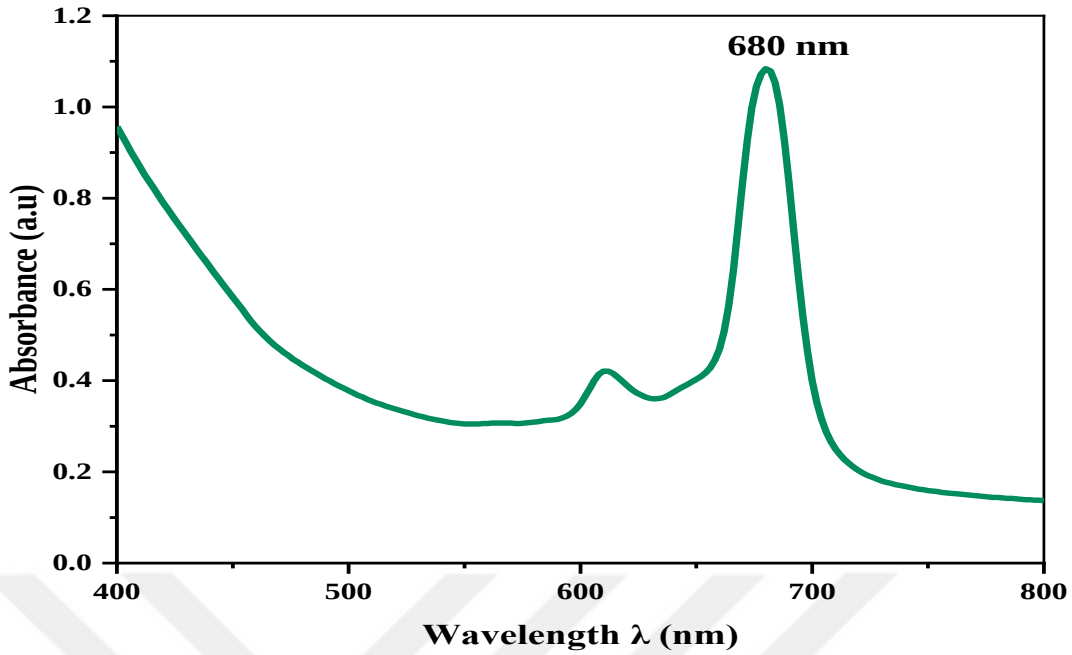


**Figure 3.88.** UV-visible spectrum of Cu(II)phthalocyanine.

- **Thermal analysis**

TG and DTG studies of the CuPc complex are thermally stable up to 250 °C, with a 5% weight loss, likely due to the loss of surface adsorbed water. The mass loss occurred in two distinct stages. Initially, there is a decomposition between 300-410 °C, resulting in a 53% mass reduction. The second stage involves decomposition between 600-680 °C, causing a 10% mass loss, with the total mass loss leading to 68%. The Thermogram of CuPc is shown in **Figure 3.89.**

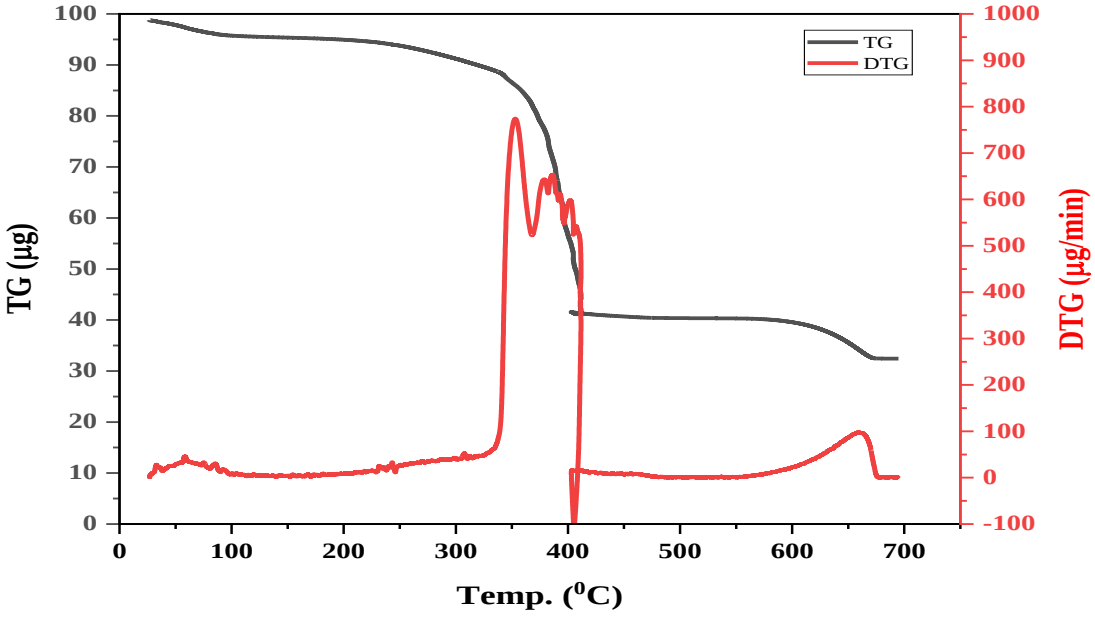


**Figure 3.89.** TG and DTG of Cu(II)phthalocyanine.

- **Electrochemical Properties**.

Electrochemical analysis of CuPc was performed using a glassy carbon (GC) electrode in DMF with TBAFB as the supporting electrolyte. CV and SWV were techniques used, and potentials were recorded in non-aqueous solutions relative to the ferrocene/ferrocenium couple (Fc/Fc+), which served as a pseudo reference electrode.

As can be seen in **Figure 3.90,** and **Figure 3.91**, the CuPc macrocycle moiety is capable of undergoing a number of different reduction and oxidation steps. The electrochemical voltammogram of CuPc reveals that $R_1$, $R_2$, $R_3$, and $R_4$ are each represented by four reduction waves at -1.06, -1.47, -1.95, and -2.37 Vs, and together with two oxidations waves represented as $O_1$ and $O_2$ at 0.23 and 0.66 Vs. When removing one electron from the HOMO, phthalocyanine rings show oxidative activity, on the other hand, when an electron is added to the LUMO of phthalocyanine molecule up to four more electrons, it shows reduction waves in the voltammogram.

The redox processes $R_1$, $R_2$, $R_3$, and $R_4$ ascribed to Cu(II)Pc-2/Cu(II)Pc-3, Cu(II)Pc-3/Cu(II)Pc-4, Cu(II)Pc-4/Cu(II)Pc-5, and Cu(II)Pc-5/Cu(II)Pc-6, respectively. On the other hand, $O_1$ and $O_2$ correspond to CuPc two oxidation processes: Cu(II) Pc-2/Cu(II)Pc-1 and Cu(II)Pc-1/Cu(II)Pc0, respectively.

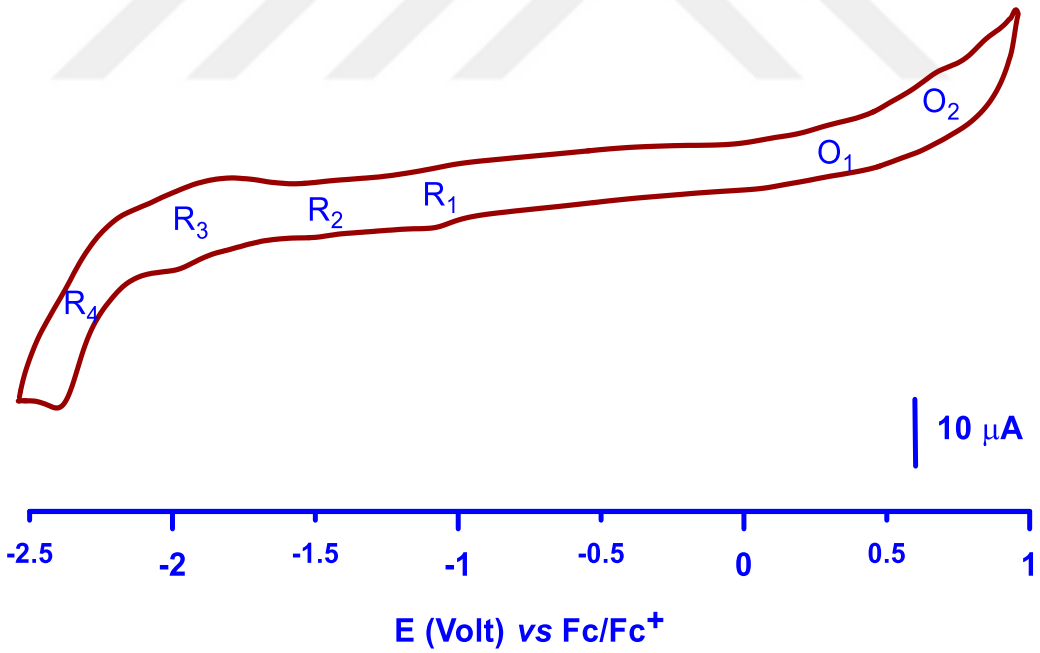


**Figure 3.90.** Cyclic voltammogram of Cu(II)phthalocyanine.

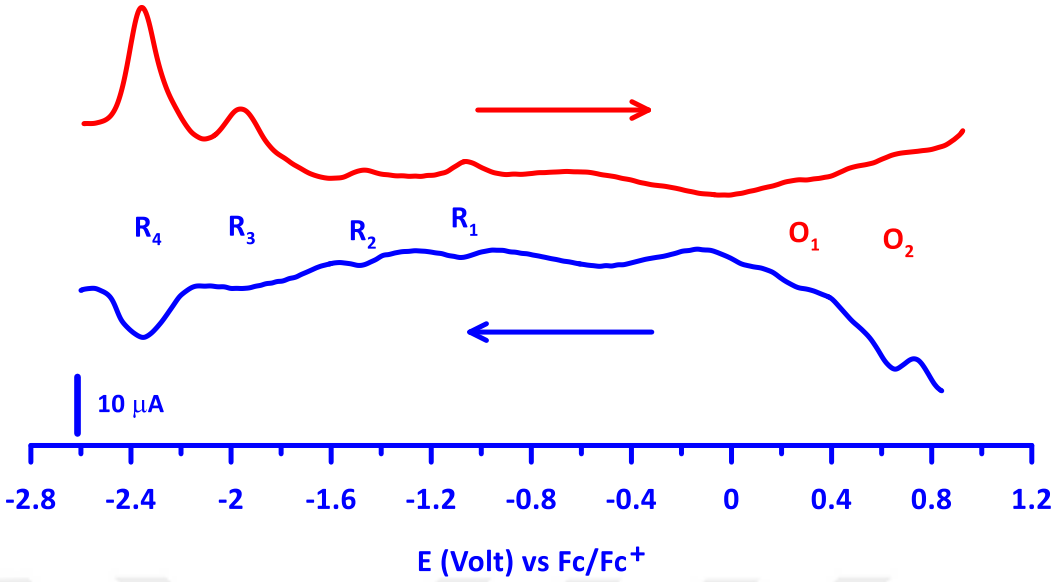


**Figure 3.91.** Square wave voltammogram of Cu(II)phthalocyanine.

## 3.20. 2,9,16,23-tetrakis(quinolin-8-yloxy) Zinc phthalocyanine.

Zinc phthalocyanine ZnPc was synthesized from 4-(quinolin-8-yloxy) phthalonitrile with Zinc(II)acetate under an argon atmosphere in DMF. The addition of Zn(II) salt triggered the cyclotetramerization of four phthalonitrile ligands, resulting in the formation of ZnPc, shown in **Figure 3.92.**

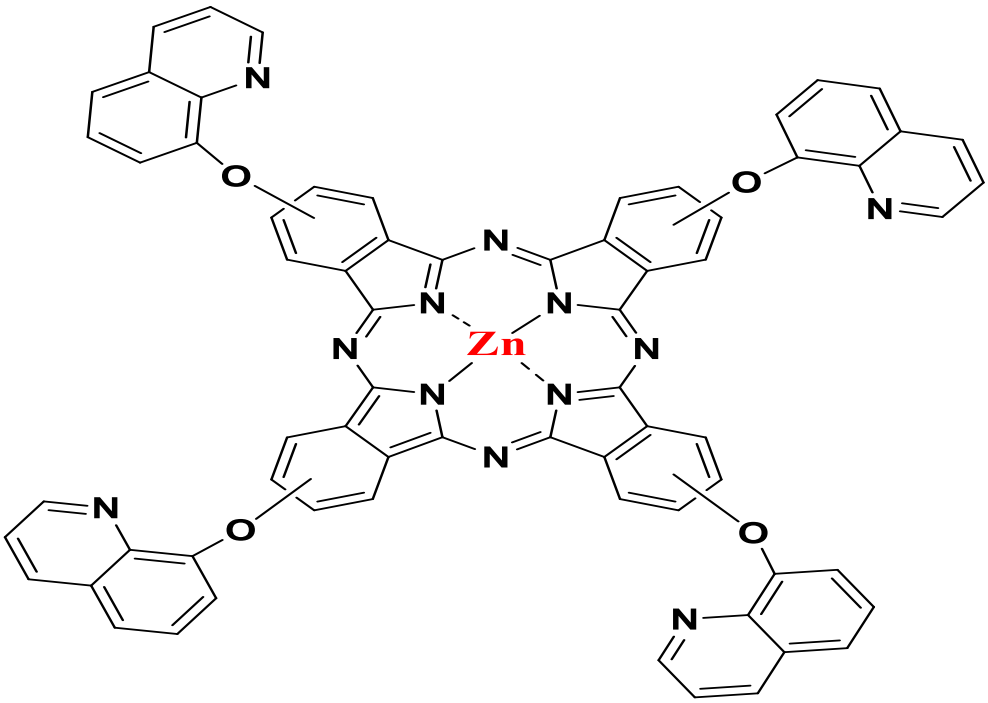


**Figure 3.92.** 2,9,16,23-tetrakis(quinolin-8-yloxy) Zinc phthalocyanine.

- **FT-IR Spectrum**

The FT-IR spectrum analysis did not show a C≡N stretching mode at 2233 $cm^{-1}$, which means all the phthalonitrile was converted to phthalocyanine. Weak peaks of the C-H bond were observed at 3063 and 2926 $cm^{-1}$. Bands at 1610 $cm^{-1}$ and 1499 $cm^{-1}$ corresponded to the aromatic C=C stretching vibration and the C=N stretching vibration, respectively. An absorption peak at 761 $cm^{-1}$, indicating deformation of the C-C macrocycle ring, was noted for the substituted benzene ring. Aromatic C-H bending vibrations were detected at 1467 and 1247 $cm^{-1}$. While the C-O stretching vibration characteristic of the complex was identified at 1089 $cm^{-1}$. FT-IR spectra of ZnPc are shown in **Figure 3.93.**


**Figure 3.93**. FT-IR spectrum of Zn(II)phthalocyanine.

- **UV–visible spectrum**

The UV-vis spectra of ZnPc in DMF showed the usual absorptions in the Q band region at 683 nm and 612 nm as a shoulder. The π-π* transition from the HOMO to the LUMO of the ZnPc ring at 683 nm is attributed to the Q band of the ZnPc complex. As a result of transitions from deeper π levels to the LUMO, the compound B band absorptions were detected at 354 nm as shoulder in the UV-visible spectra of ZnPc. Are shown in **Figure 3.94**.

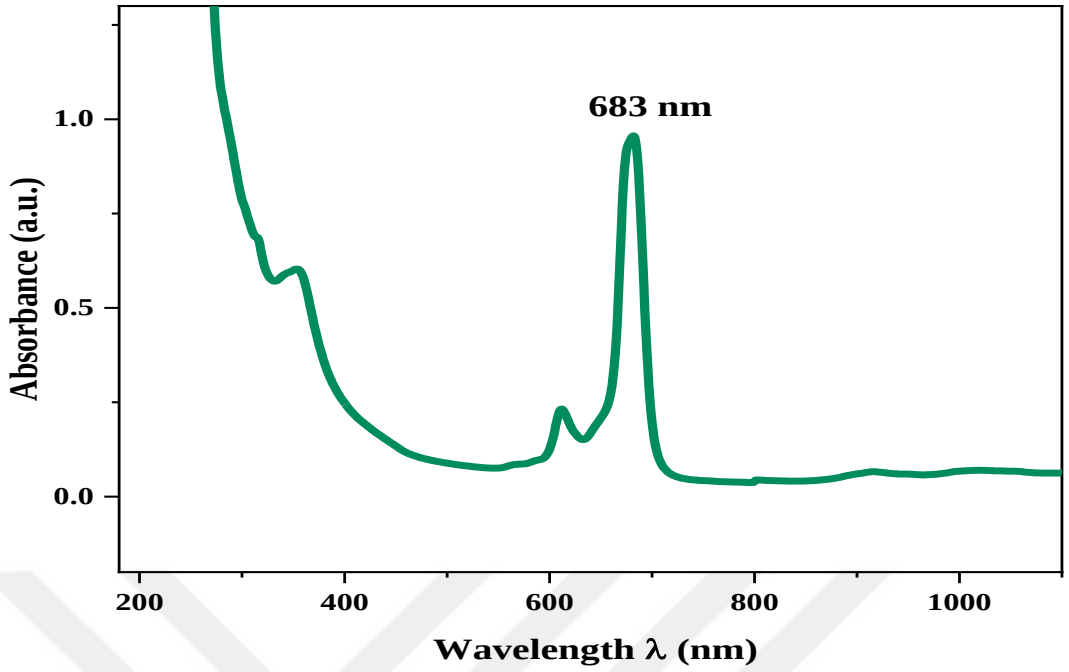


**Figure 3.94.** UV-visible spectrum of Zn(II)phthalocyanine.

- **Thermal analysis**

TG and DTG analyses of ZnPc exhibit thermal stability up to 220 °C with a 7% loss of absorbed surface water. The mass loss occurs in two distinct stages, with decomposition occurring between 220-475 °C, causing a 31% mass loss. Then a 46% weight loss between 475-610 °C. These results show total reducing as 84%, with a 16% remained, that are shown in **Figure 3.95.**

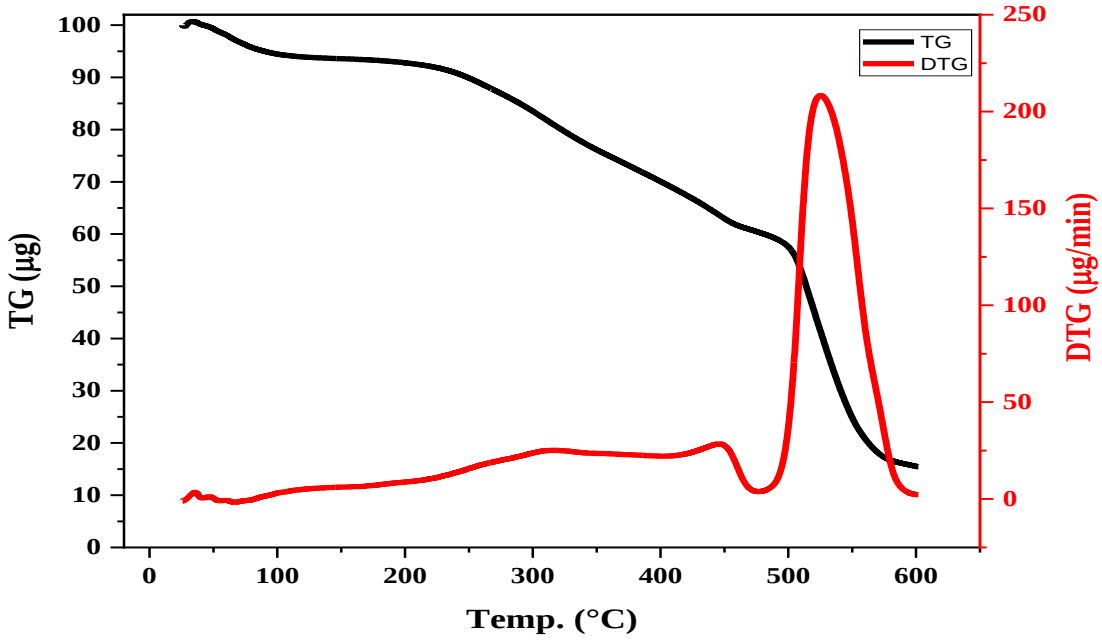


**Figure 3.95.** TG and DTG of Zn(II)phthalocyanine.

- **Electrochemical Properties**.

Electrochemical analysis of ZnPc was performed using a glassy carbon (GC) electrode in DMF with TBAFB as the supporting electrolyte. CV and SWV were techniques used, and potentials were recorded in non-aqueous solutions relative to the ferrocene/ferrocenium couple (Fc/Fc+), which served as a pseudo reference electrode.

As can be seen in **Figure 3.96,** and **Figure 3.97.** the ZnPc macrocycle moiety is capable of undergoing a number of reduction and oxidation steps. The voltammogram of ZnPc reveals four reduction waves represented with $R_1$, $R_2$, $R_3$, and $R_4$ at -1.32, -1.54, -1.69, and -2.29 Vs, and two oxidations waves $O_1$, and $O_2$ at 0.37, and 0.79 V. Because of redox inactive Zn metal in the center of phthalocyanine complex all these redox waves has belonged to phthalocyanine macrocycle rings

These four redox processes $R_1$, $R_2$, $R_3$, and $R_4$ attributed to Zn(II)Pc-2/Zn(II)Pc-3, Zn(II)Pc-3/Zn(II)Pc-4, Zn(II)Pc-4/Zn(II)Pc-5, and Zn(II)Pc-5/Zn(II)Pc-6 respectively and $O_1$, and $O_2$ are corresponding to the two oxidation process of Zn(II)Pc-2/Zn(II)Pc-1, and Zn(II)Pc-1/Zn(II)Pc0 respectively.

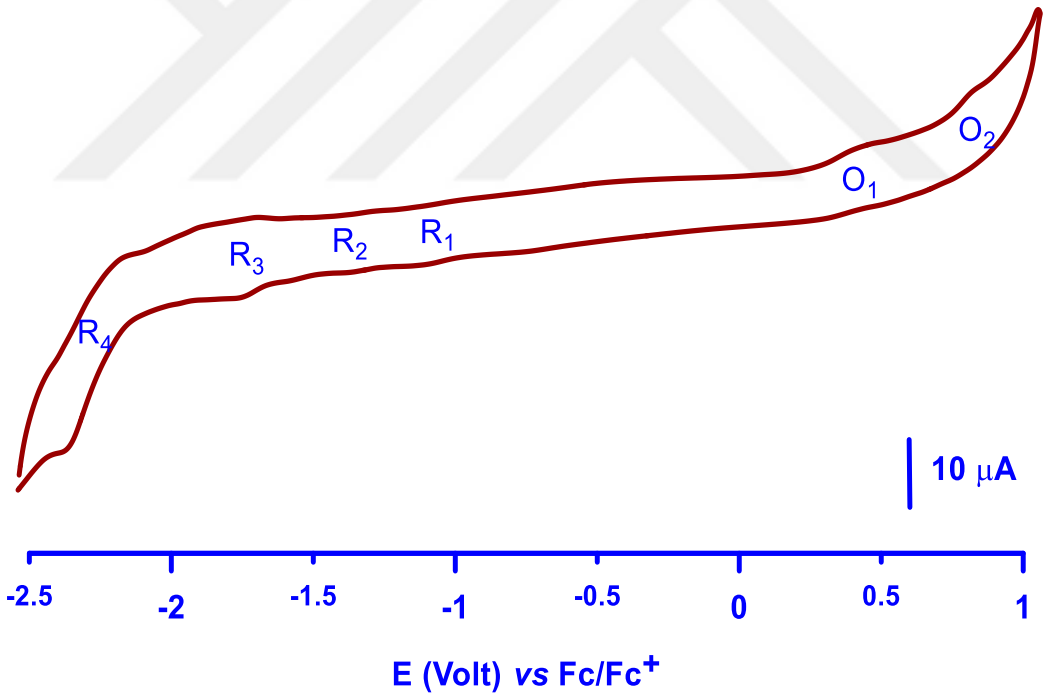


**Figure 3.96.** Cyclic voltammogram of Zinc(II)phthalocyanine.

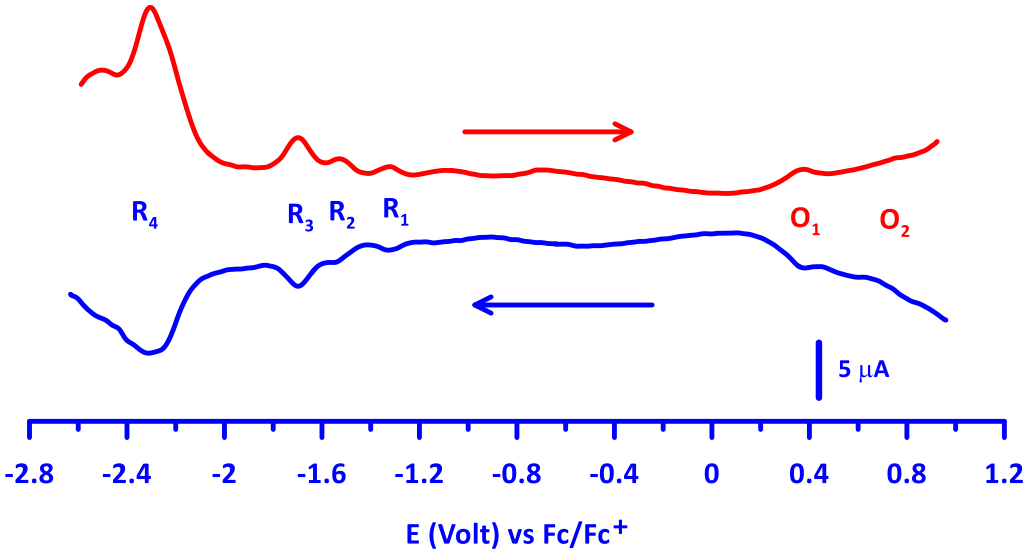


**Figure 3.97.** Square Wave Voltammogram of ZnPc

## 3.21. 2,2',2'',2'''((2,9,16,23-tetrayltetrakis(oxy))tetrakis(benzene-4,1-diyl)) tetraacetamide Chrome phthalocyanine.

The Chrome phthalocyanine, CrPc, was synthesized from 2-(4-(3,4-dicyanophenoxy) phenyl) acetamide with Chrom(II)acetate under an argon atmosphere in DMF. The CrPc complex was formed by cyclotetramerizing four phthalonitrile ligands with Cr(II), **Figure 3.98.**

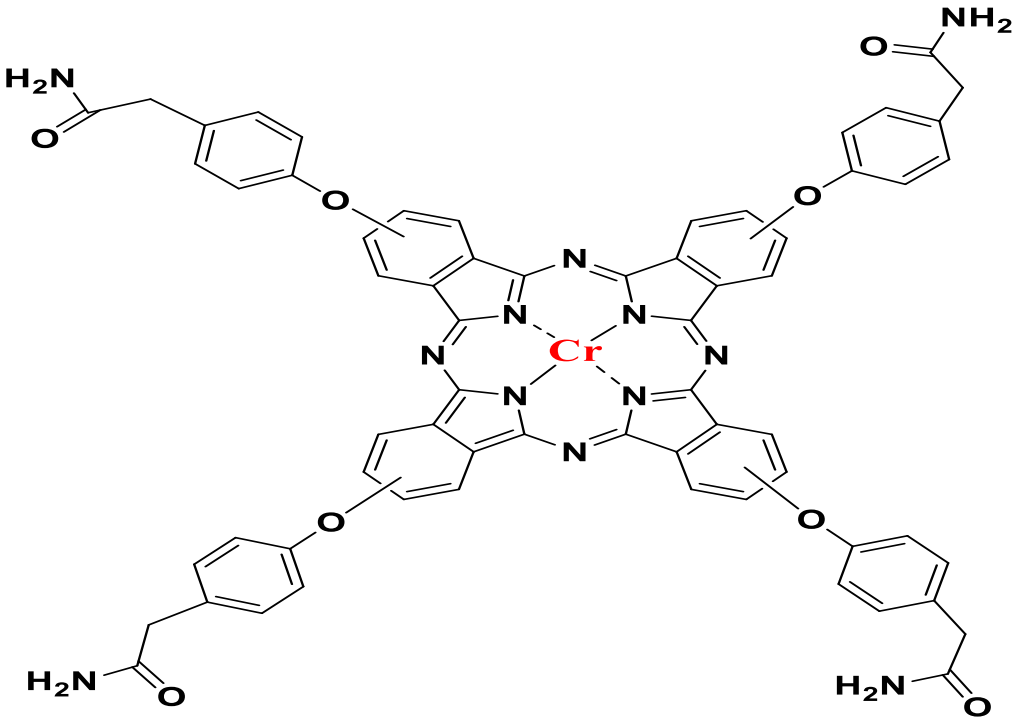


**Figure 3.98.** 2,2',2",2'"((2,9,16,23-tetrayltetrakis(oxy))tetrakis(benzene-4,1-diyl)) tetraacetamide Chrome phthalocyanine.

- **FT-IR Spectrum**

The FT-IR spectrum did not exhibit the C≡N stretching mode at 2233 $cm^{-1}$ but did show C-H stretching peaks at 3066 and 2970 $cm^{-1}$. The bands at 1606 $cm^{-1}$ and 1505 $cm^{-1}$ were identified as aromatic C=C stretching vibrations and C=N stretching vibrations, respectively. The aromatic C-H bending vibrations were identified at 1468 and 1224 $cm^{-1}$. The band at 751$cm^{-1}$ was identified due to C-C macrocycle ring deformation. The characteristic C-O stretching vibration of the structure was detected at a wavenumber of 1094 $cm^{-1}$, **Figure 3.99.**

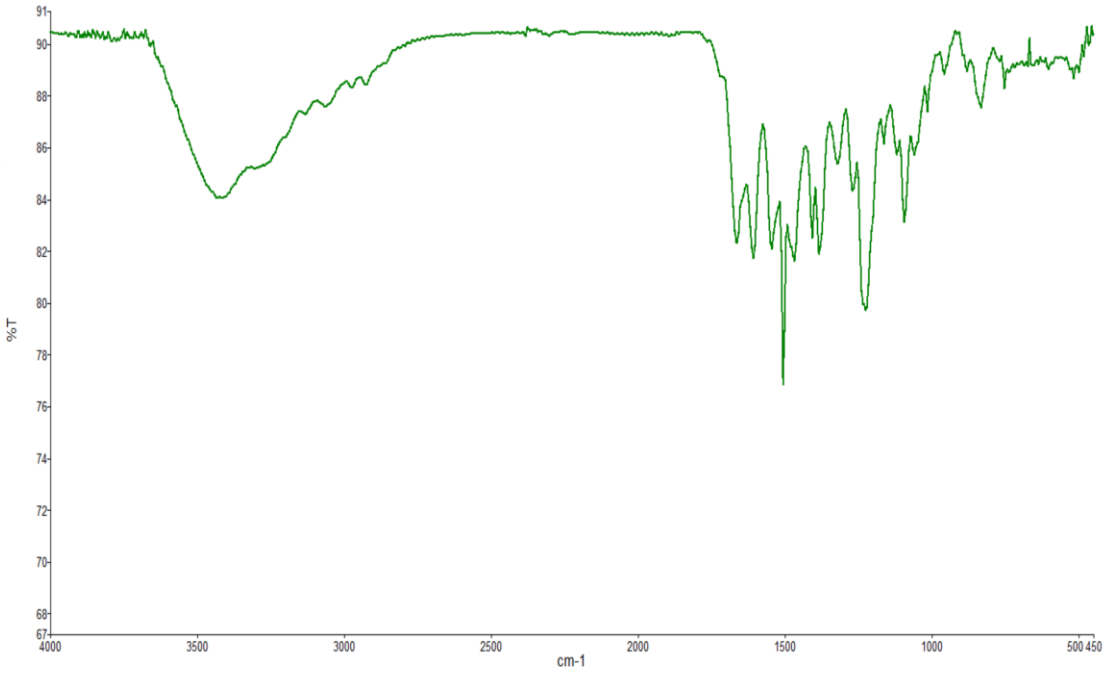


**Figure 3.99**. FT-IR spectrum of Cr(II)phthalocyanine.

- **UV–visible spectrum**

The UV-visible spectra of CrPc in DMF showed the usual absorptions in the Q band region, at 680 nm. This absorption is caused by π-π* transition from the HOMO to the LUMO of the chromium phthalocyanine complex. Transitions from deeper π levels to the LUMO, than HOMO of phthalocyanine compounds called Soret or B band absorptions were not detected in the UV region, because of the high absorption of light in this region. UV-visible spectra of CrPc are shown in **Figure 3.100.**

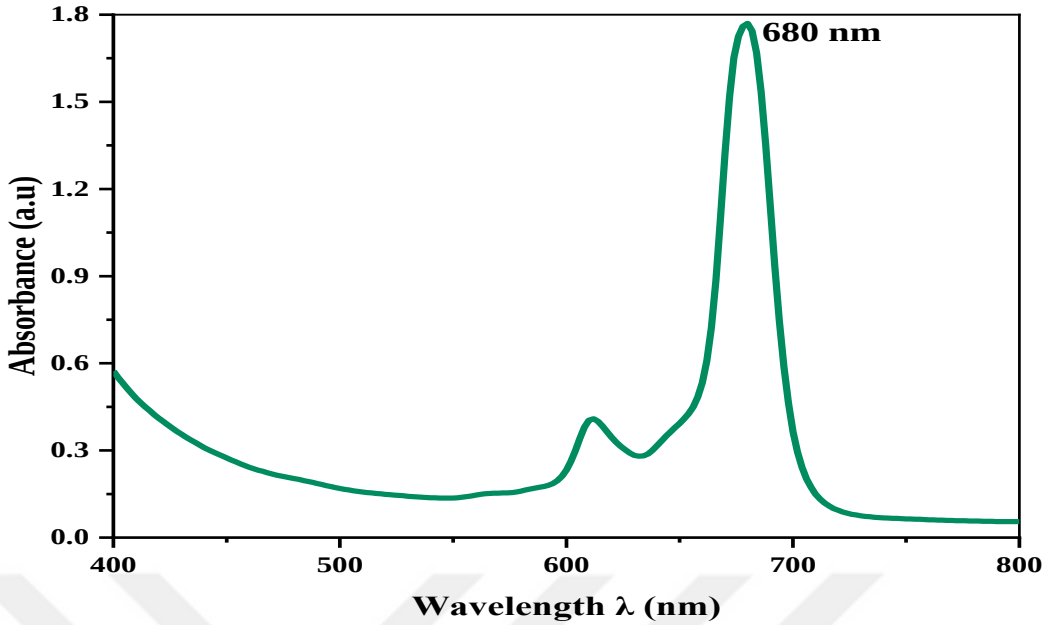


**Figure 3.100.** UV-visible spectrum of Cr(II)phthalocyanine.

- **Thermal analysis.**

According to TG and DTG studies, the CrPc complex shows thermal stability up to 250 °C, while it shows 7% weight loss, due to absorbed water. The mass loss happens in two discrete stages. The initial step comprises decomposition between 270-450 °C, resulting in a 41% mass loss. While the second stage occurs between 470 and 700 °C with a 9% mass loss. Overall, thermogravimetric analysis revealed that CrPc decomposes without a melting point, resulting in a total mass loss of 57%. The Thermogram of CrPc is shown in **Figure 3.101.**

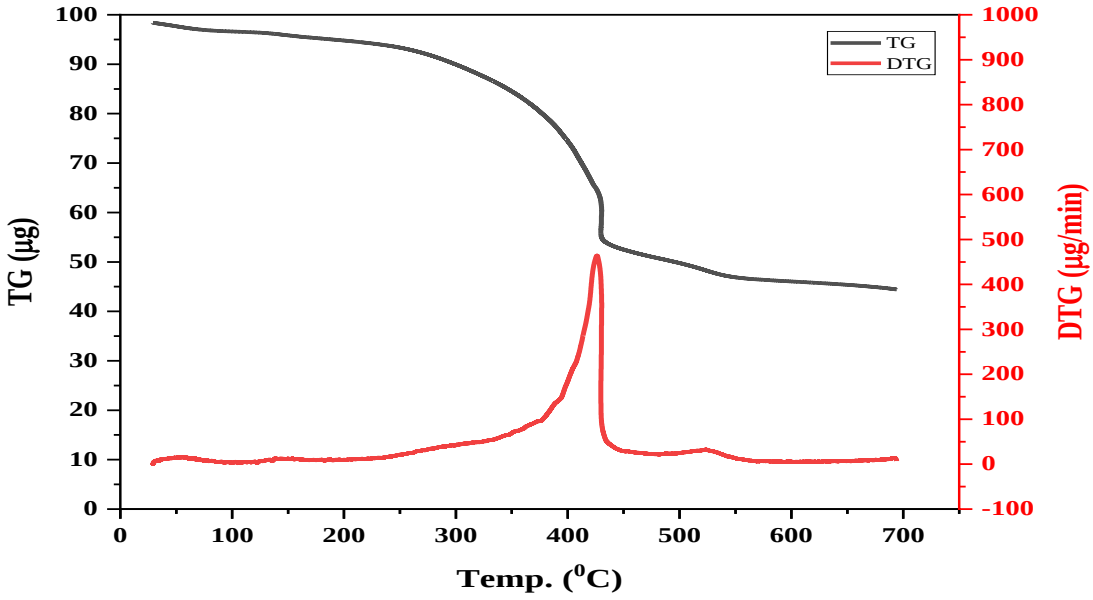


**Figure 3.101.** TG and DTG of Cr(II)phthalocyanine.

- **Electrochemical Properties**.

An electrochemical experiment of CrPc was performed using a GC electrode in DMF with TBAFB as the supporting electrolyte and CV and SWV techniques were used, potentials were recorded in non-aqueous solutions relative to the ferrocene/ferrocenium couple (Fc/Fc+).

The CrPc macrocycle moiety is capable of reduction and oxidation processes. The electrochemical voltammogram of CrPc demonstrated four reduction waves that were $R_1$, $R_2$, $R_3$, and $R_4$ at -1.17, -1.60, -1.86, and -2.22 V, as well as two oxidation waves $O_1$ and $O_2$ at 0.21, and 0.57 Vs respectively, it can be seen the oxidation and reduction waves of chromium metal Mr at -1.05 V, shown in **Figure 3.102**, and **Figure 3.103.**

There are four redox processes $R_1$, $R_2$, $R_3$, and $R_4$ attributed to Cr(II)Pc-2/Cr(II)Pc-3, Cr(II)Pc-3/Cr(II)Pc-4, Cr(II)Pc-4/Cr(II)Pc-5, and Cr(II)Pc-5/Cr(II)Pc-6 respectively. $O_1$, and $O_2$ are corresponding to the two oxidation processes of CrPc, specifically Cr(II)Pc-2/Cr(III)Pc-1, and Cr(II)Pc-1/Cr(III)Pc0 respectively. Additionally, there are metal-based redoxes process referred to as Cr(II)Pc-2/Cr(I)Pc-2 labeled as Mr.

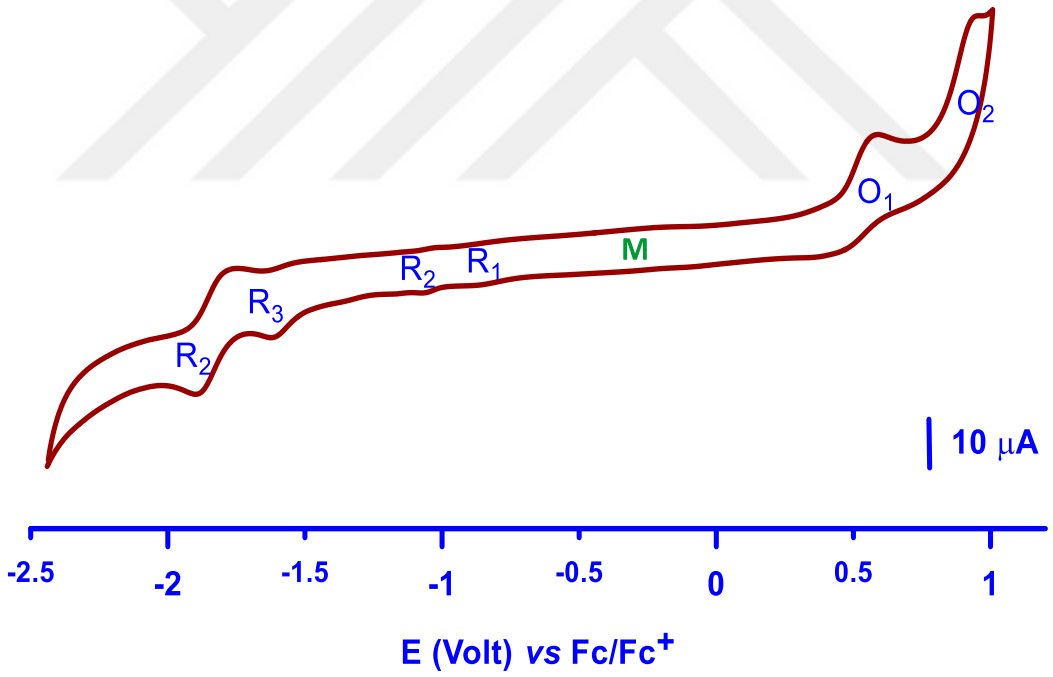


**Figure 3.102.** Cyclic voltammogram of Cr(II)phthalocyanine.

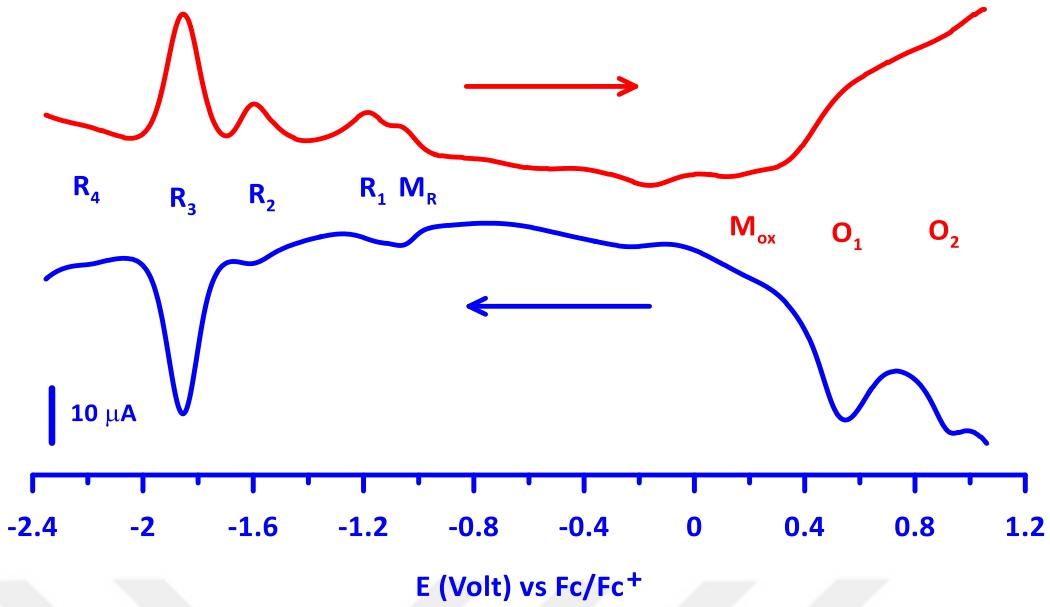


**Figure 3.103.** Square wave voltammogram of Cr(II)phthalocyanine.

## 3.22. 2,2',2'',2'''((2,9,16,23-tetrayltetrakis(oxy))tetrakis(benzene-4,1-diyl)) tetraacetamide Iron phthalocyanine.

The Iron phthalocyanine FePc was synthesized from 2-(4-(3,4-dicyanophenoxy) phenyl) acetamide with Iron(II)acetate under an argon atmosphere in DMF, The FePc complex, was formed by cyclo-tetramerizing four phthalonitrile ligands with Fe(II), which was obtained as green solid, the molecule formula is given in **Figure 3.104.**

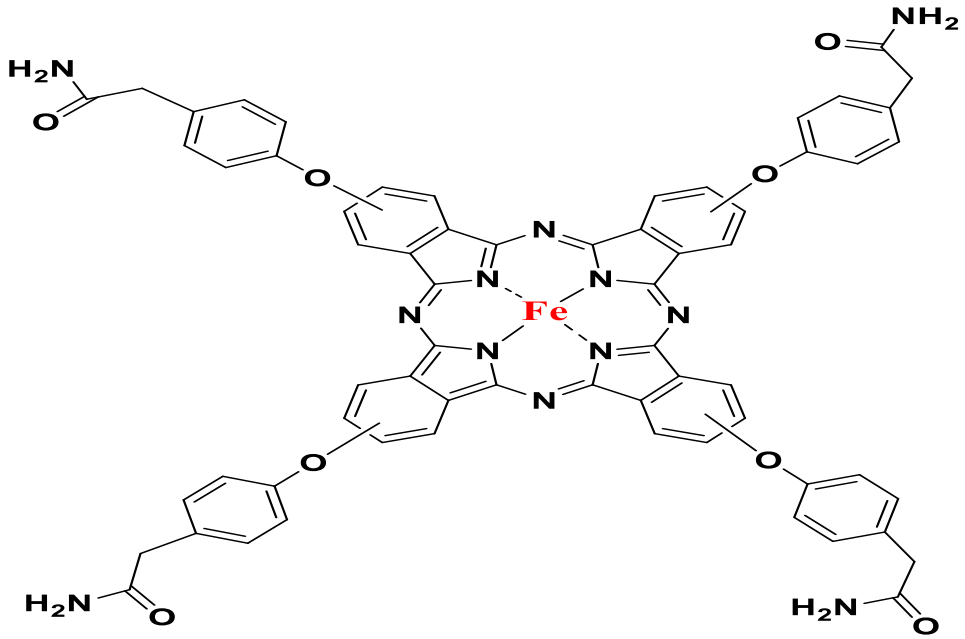


**Figure 3.104.** 2,2',2",2'"((2,9,16,23-tetrayltetrakis(oxy))tetrakis(benzene-4,1-diyl)) tetraacetamide Iron phthalocyanine.

- **FT-IR Spectrum**

The FT-IR spectrum did not exhibit the C≡N stretching mode at 2233 $cm^{-1}$, but it did show a weak C-H stretching peak at 2976 $cm^{-1}$. The bands at 1609 $cm^{-1}$ and 1505 $cm^{-1}$ were attributed to aromatic C=C stretching vibrations and C=N stretching vibrations respectively. The aromatic C-H bending vibrations were identified at 1468 and 1231 $cm^{-1}$. The band at 746 $cm^{-1}$ was identified as C-C macrocycle ring deformation, and the characteristic C-O stretching vibration of the structure was detected at a wavenumber of 1087 $cm^{-1}$. FT-IR spectra are given in **Figure 3.105.**

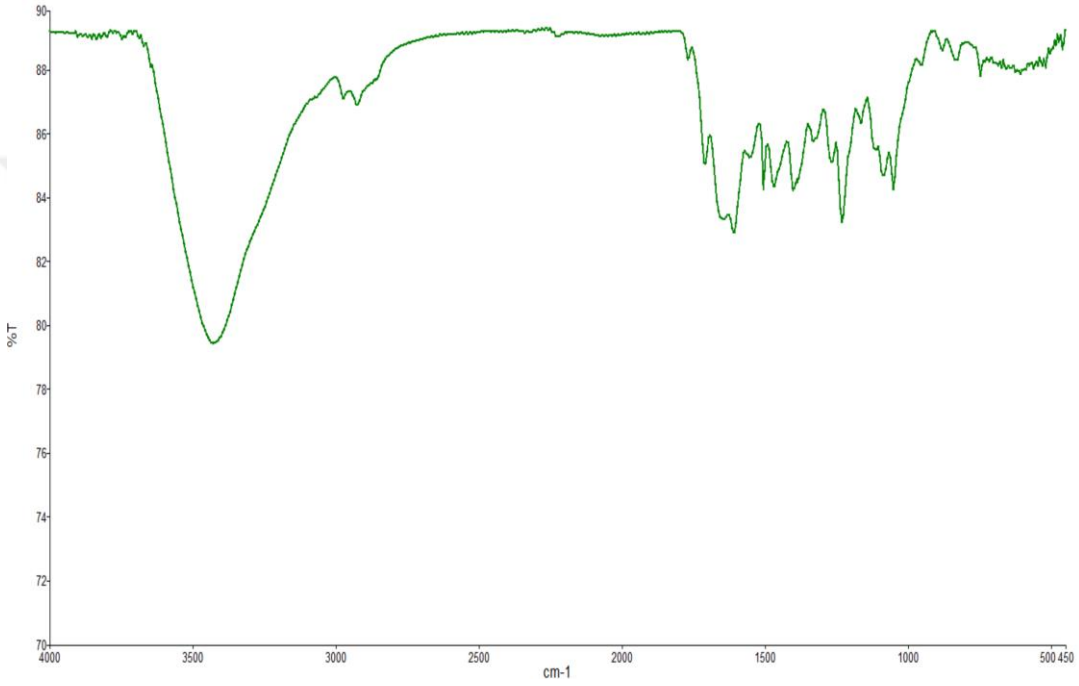


**Figure 3.105.** FT-IR spectrum of Fe(II)phthalocyanine.

- **UV–visible spectrum**

The UV–vis spectra of MPcs dissolved in DMF exhibited characteristic absorption band in the Q band region at 684 nm, strong absorption at 642 nm is due to strong aggregation of phthalocyanine molecules in DMF. The Q band absorptions of the compounds correspond to the π-π* transition between the HOMO and LUMO of the phthalocyanine ring. The compounds exhibited B band are not clearly visible in the UV range 300-450 nm that the result of transitions from the lower π energy levels to the LUMO. The UV–vis spectrum of the FePc complex in DMF exhibits three absorptions at 642 nm, and shoulder at 684 nm, as well as at 810 nm, as shown in **Figure 3.106.**

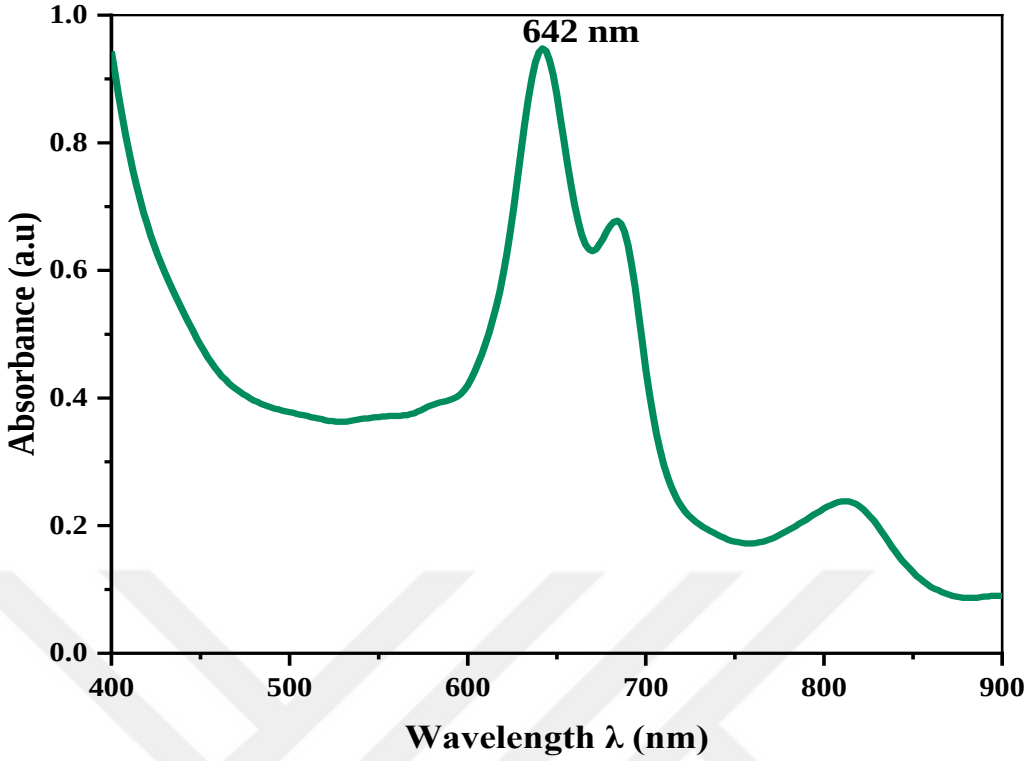


**Figure 3.106.** UV-visible spectrum of Fe(II)phthalocyanine.

- **Thermal analysis**

TG and DTG analysis indicate that FePc is thermally stable up to 220 °C, but the thermogram shows loss of surface absorbed water from the FePc complex of about 8%. The mass loss occurs in two discrete phases. The first step involves decomposition from 230 to 450 °C resulting 46% mass loss. While the second step starts from 450 to 540 °C, with a loss of 29%. Overall, the thermogravimetric analysis revealed that FePc decomposes without melting, resulting in a total mass loss of 86% with 17% of the residue, shown in **Figure 3.107.**

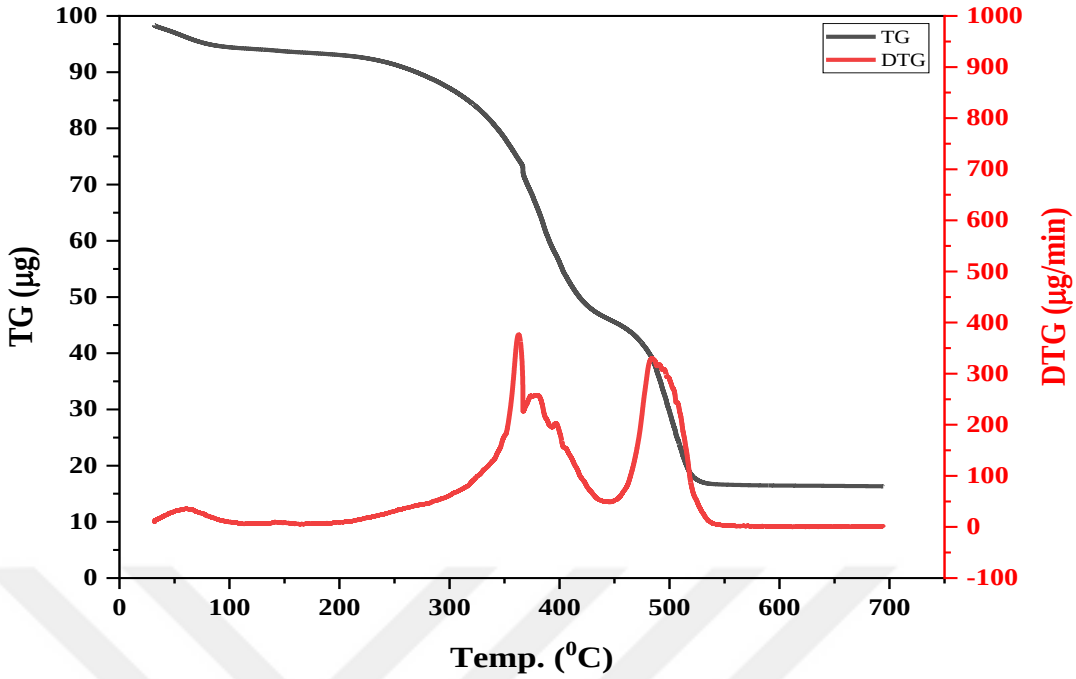


**Figure 3.107.** TG and DTG of Fe(II)phthalocyanine.

- **Electrochemical Properties**.

Electrochemical analysis of FePc was performed on a GC electrode as a working electrode in DMF with TBAFB as the supporting electrolyte, and CV and SWV techniques were used. Potentials were recorded in non-aqueous solutions relative to the ferrocene/ferrocenium couple (Fc/Fc+), which served as a pseudo reference electrode.

The FePc macrocycle moiety is capable of a variety of reduction and oxidation processes. The voltammogram of FePc demonstrates four reduction waves that are labelled as $R_1$, $R_2$, $R_3$, and $R_4$ at -1.11, -1.34, -1.69, and -2.15 Vs, as well as two oxidation waves $O_1$ and $O_2$ at 0.12, and 0.37 Vs, also has redox waves of iron metal Mr at -0.68 V, as shown in **Figure 3.108,** and **Figure 3.109.**

The redox processes $R_1$, $R_2$, $R_3$, and $R_4$ are assigned to Fe(II)Pc-2/Fe(II)Pc-3, Fe(II)Pc-3/Fe(II)Pc-4, Fe(II)Pc-4/Fe(II)Pc-5, and Fe(II)Pc-5/Fe(II)Pc-6, respectively. All these reduction processes are quasi-reversible reactions. $O_1$ and $O_2$ correspond to the two FePc oxidation processes of the phthalocyanine ring, which are Fe(II)Pc-2/Fe(III)Pc-1 and Fe(II)Pc-1/Fe(III)Pc0, respectively. Furthermore, as the $Fe^{2+}$ ions are redox active in phthalocyanine complexes, the metal-based oxidation process $Mo_x$ refers to Fe(II)Pc-2/Fe(III)Pc-2.

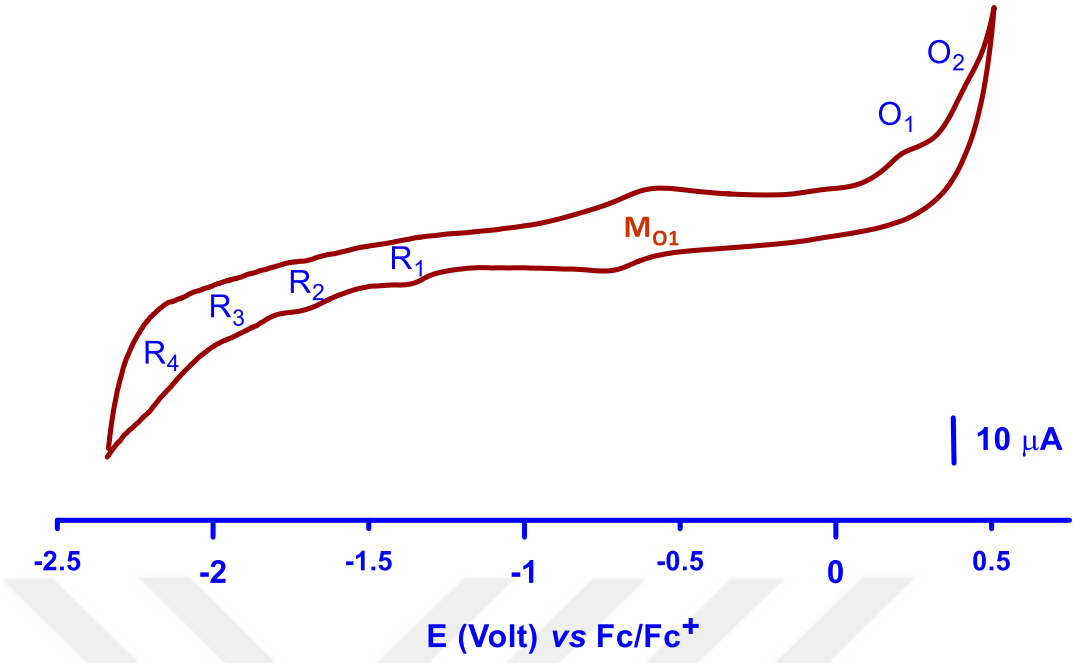


**Figure 3.108.** Cyclic voltammogram of Fe(II)phthalocyanine.

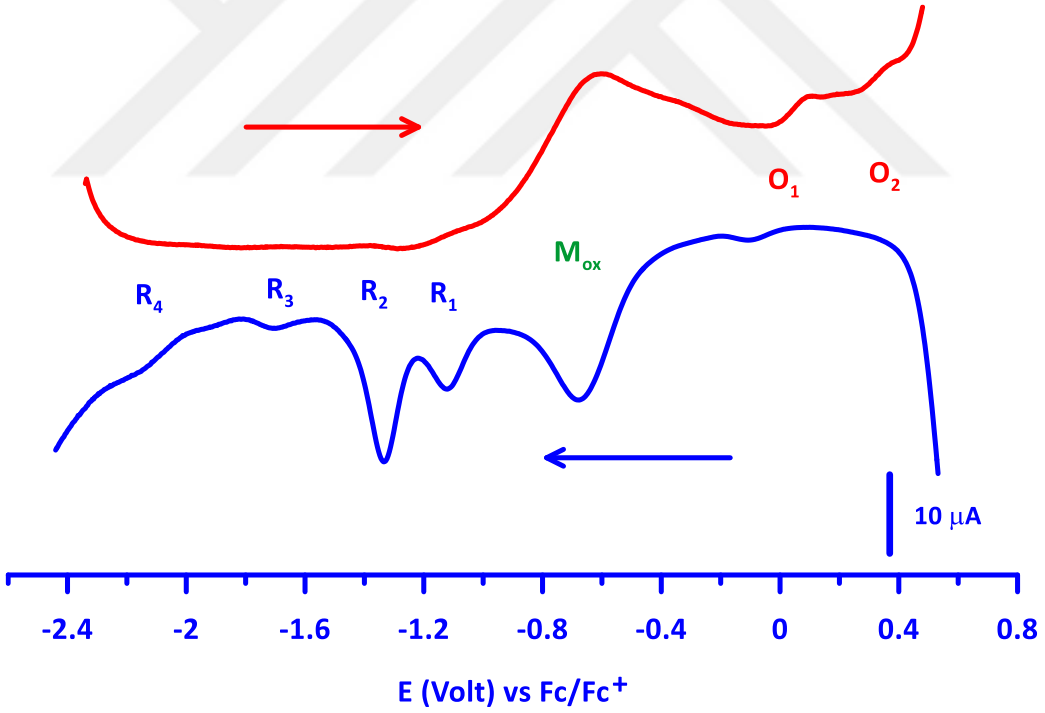


**Figure 3.109.** Square wave voltammogram of Fe(II)phthalocyanine.

### 3.23. 2,2',2'',2'''((2,9,16,23-tetrayltetrakis(oxy))tetrakis(benzene-4,1-diyl)) tetraacetamide Cobalt phthalocyanine.

The Cobalt phthalocyanine CoPc was synthesized from 2-(4-(3,4-dicyanophenoxy) phenyl) acetamide and Cobalt(II)acetate under an argon atmosphere in DMF. The green CoPc complex was

produced by cyclotetramerizing four phthalonitrile ligands with Co(II). The molecule structure of CoPc is shown in **Figure 3.110.**

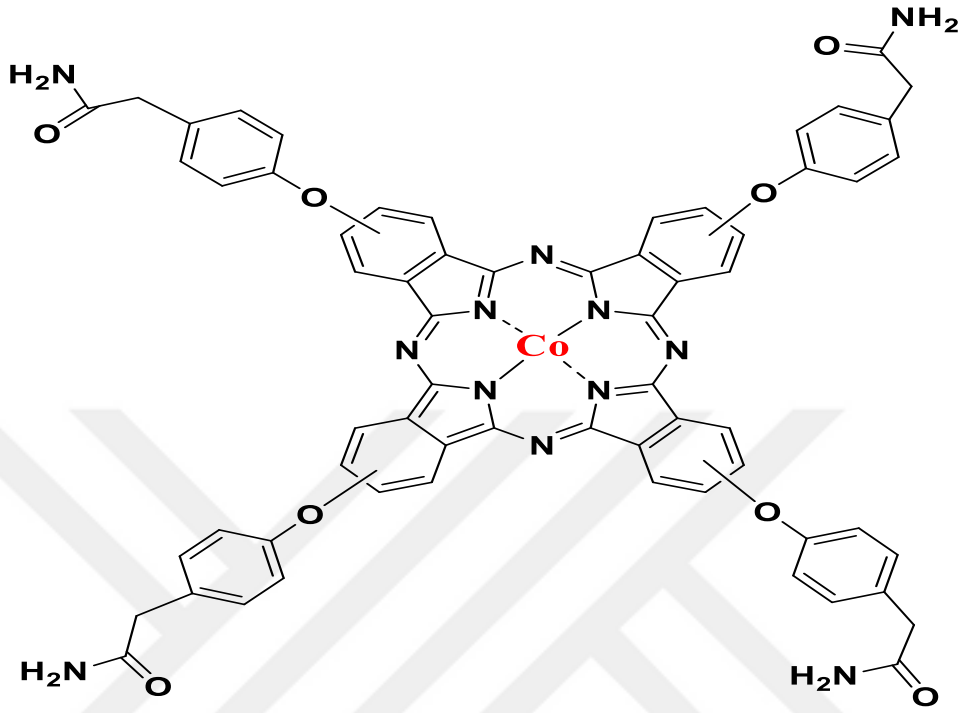


**Figure 3.110.** 2,2',2",2'"((2,9,16,23-tetrayltetrakis(oxy))tetrakis(benzene-4,1-diyl)) tetraacetamide Cobalt phthalocyanine.

- **FT-IR Spectrum**

The FT-IR spectra did not show the C≡N stretching mode at 2233 $cm^{-1}$. However, weak peaks corresponding to the C-H bond were observed peaks at 2976 and 2923 $cm^{-1}$. The bands at 1607 $cm^{-1}$ and 1505 $cm^{-1}$ were assigned aromatic C=C stretching vibrations and C=N stretching vibrations, respectively. Aromatic C-H bending vibrations were identified at 1407 and 1224 $cm^{-1}$. The band at 743 $cm^{-1}$ was attributed to C-C macrocycle ring deformation. The unique C-O stretching vibration of the structure was detected at 1090 $cm^{-1}$. FT-IR spectra of CoPc is given in **Figure 3.111.**

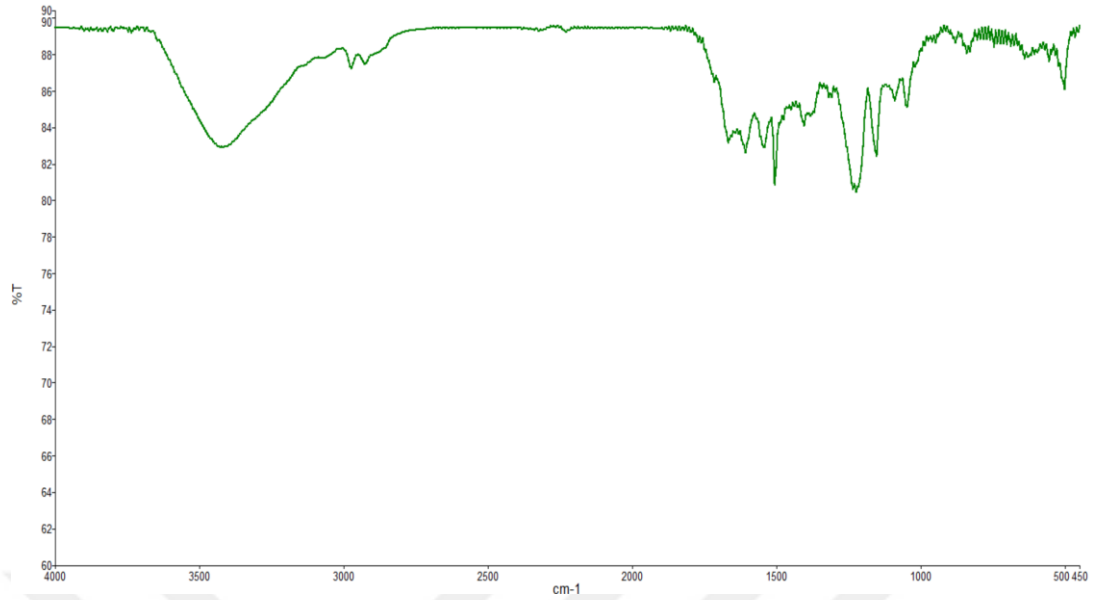


**Figure 3.111**. FT-IR spectrum of Co(II)phthalocyanine.

- **UV–visible spectrum**

The UV–vis spectra of CoPc dissolved in DMF exhibited characteristic absorptions in the Q band region, at 668 nm with a shoulder at 604 nm. The Q band absorptions of the compounds correspond to the π-π* transition occurring between the HOMO and LUMO of the phthalocyanine ring. The compounds exhibited B absorptions band at 450 nm in the UV range which resulted in transitions from the lower π energy levels to the LUMO. The UV–vis spectrum of the CoPc complex in DMF is shown in **Figure 3.112.**

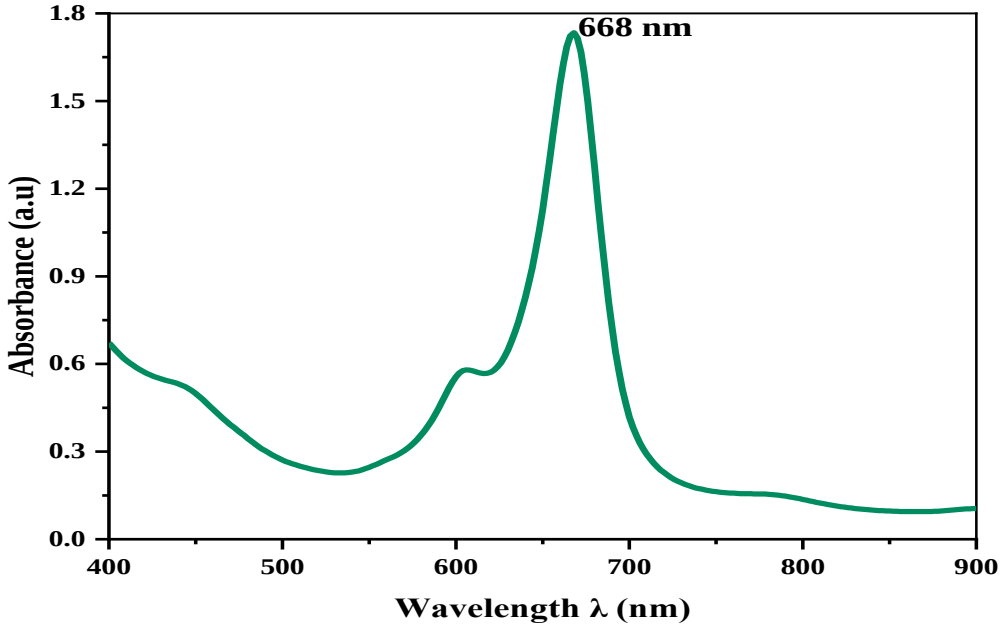


**Figure 3.112.** UV-visible spectrum of Co(II)phthalocyanine.

- **Thermal analysis**

TG and DTG assays indicate that CoPc is thermally stable up to 260 °C. Thermograms also show that CoPc adsorb water up to 5% at room temperature. The mass loss takes place in two discrete stages. The first stage occurs in between 270-500 °C, resulting with 53% mass and the second stage decomposition occurs in between 500-560 °C, resulting in a 5% mass loss. In addition, thermogram data also revealed that CoPc decomposes without melting, resulting in a total mass loss of 68%, with approximately 32% of residue left. The thermogram of CoPc is given in **Figure 3.113.**

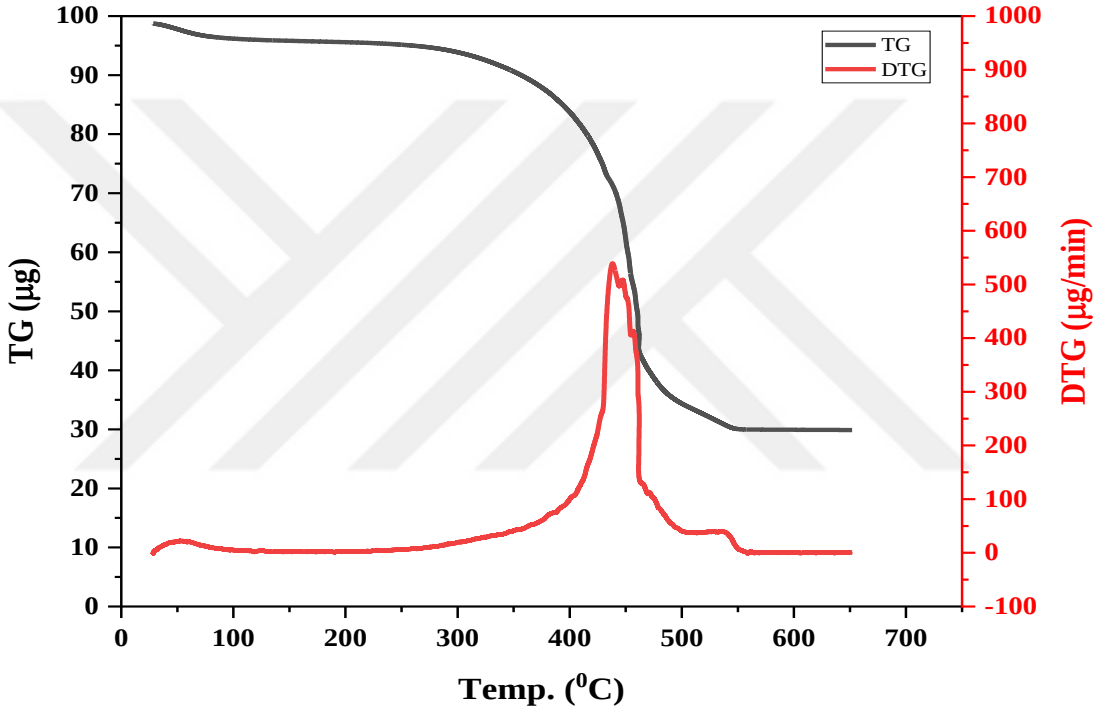


**Figure 3.113.** TG and DTG of Co(II)phthalocyanine.

- **Electrochemical Properties**.

Electrochemical analysis of CoPc was performed using a GC as a working electrode in DMF with TBAFB as the supporting electrolyte. CV and SWV were techniques used, and potentials were recorded in non-aqueous solutions relative to the ferrocene/ferrocenium couple (Fc/Fc+), which served as a pseudo reference electrode. SW voltammogram, which more accurately shows the individual redox reactions, therefore all the data were obtained from SW voltammogram.

The CoPc complex is capable of a variety of reduction and oxidation processes. The electrochemical voltammogram for CoPc shows four reduction waves that are $R_1$, $R_2$, $R_3$, and $R_4$ at -0.93, -1.15, -1.42, and -1.88 V, as well as two oxidation waves $O_1$ and $O_2$ at 0.00, and 0.40 Vs,

belong to phthalocyanine ring. It has also has oxidation and reduction on cobalt metal labelled as Mo at -0.21 and Mr at -0.65 V, as shown in **Figure 3.114,** and **Figure 3.115.**

The four redox processes $R_1$, $R_2$, $R_3$, and $R_4$ attributed to Co(II)Pc-2/Co(II)Pc-3, Co(II)Pc-3/Co(II)Pc-4, Co(II)Pc-4/Co(II)Pc-5, and Co(II)Pc-5/Co(II)Pc-6 respectively. Nonetheless, $O_1$, and $O_2$ are corresponding to the two oxidation processes of CoPc, specifically Co(III)Pc-2/Co(III)Pc-1, and Co(III)Pc-1/Co(III) Pc0 respectively. Additionally, there are metal-based redox processes refers to Mr and Mo Co(II)Pc-2/Co(I)Pc-2, and Co(II)Pc-2/Co(III)Pc-2.

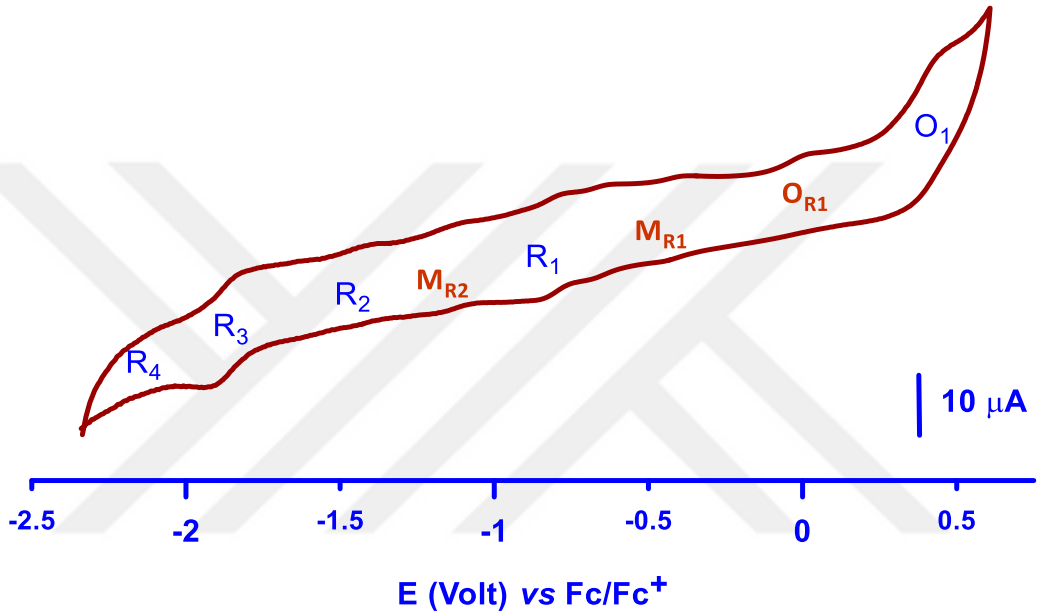


**Figure 3.114.** Cyclic voltammogram of Co(II)phthalocyanine.

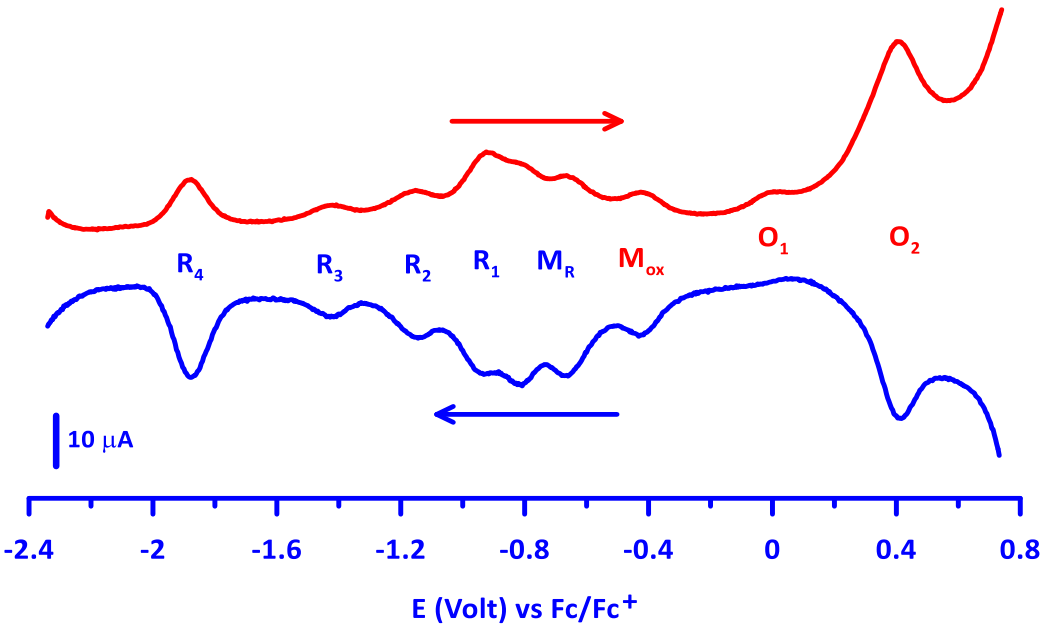


**Figure 3.115.** Square wave voltammogram of Co(II)phthalocyanine.

### 3.24. 2,2',2'',2'''((2,9,16,23-tetrayltetrakis(oxy))tetrakis(benzene-4,1-diyl)) tetraacetamide Nickel phthalocyanine.

The Nickel phthalocyanine NiPc was synthesized from 2-(4-(3,4-dicyanophenoxy) phenyl) acetamide with Nickel(II)acetate under argon atmosphere in DMF. The obtained green NiPc complex was synthesized by cyclotetramerization of four phthalonitrile ligands with Ni(II). The molecule structure of NiPc is shown in **Figure 3.116.**

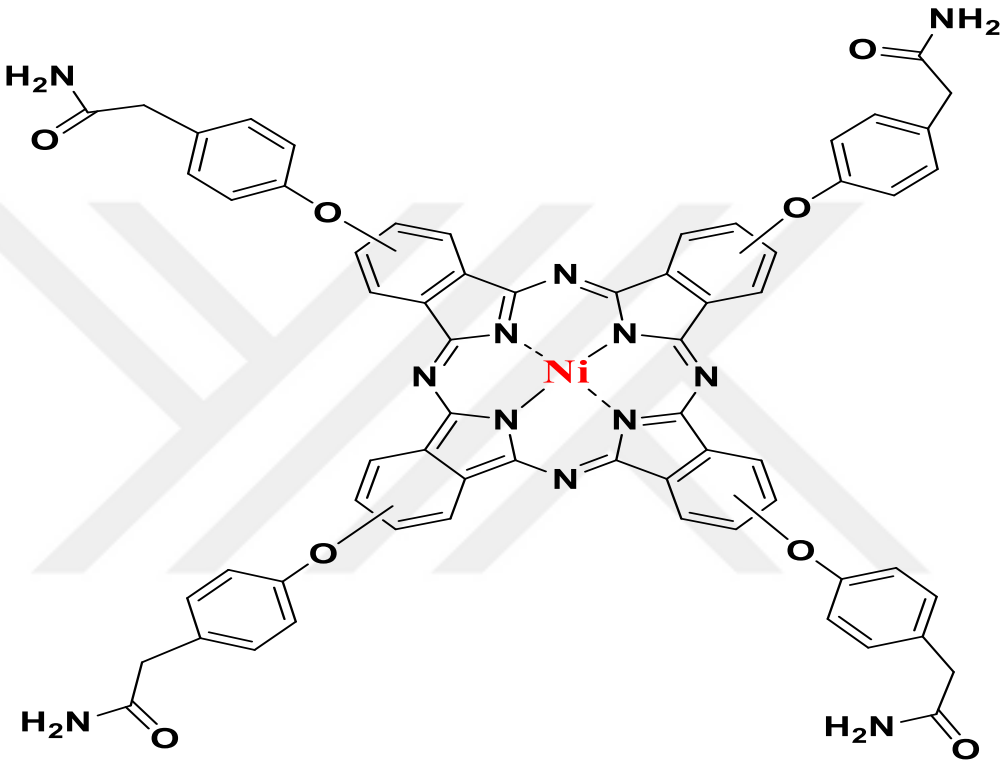


**Figure 3.116**. 2,2',2",2'"((2,9,16,23-tetrayltetrakis(oxy))tetrakis(benzene-4,1-diyl)) tetraacetamide Nickel phthalocyanine.

- **FT-IR Spectrum**

The absence of C≡N stretching mode at 2233 $cm^{-1}$ confirms the formation of a phthalocyanine complex. The C-H bond produced weak peaks at 2976 and 2923 $cm^{-1}$. The bands observed at 1608 cm-$^{1}$ and 1505 $cm^{-1}$ were attributed to aromatic C=C stretching vibrations and C=N stretching vibrations, respectively. Aromatic C-H bending vibrations were identified at 1408 and 1236 $cm^{-1}$. The band at 751 $cm^{-1}$ was assigned to C-C macrocycle ring deformation. The C-O stretching vibration of the title structure was observed at 1092 $cm^{-1}$. FT-IR spectra of NiPc is shown in **Figure 3.117.**

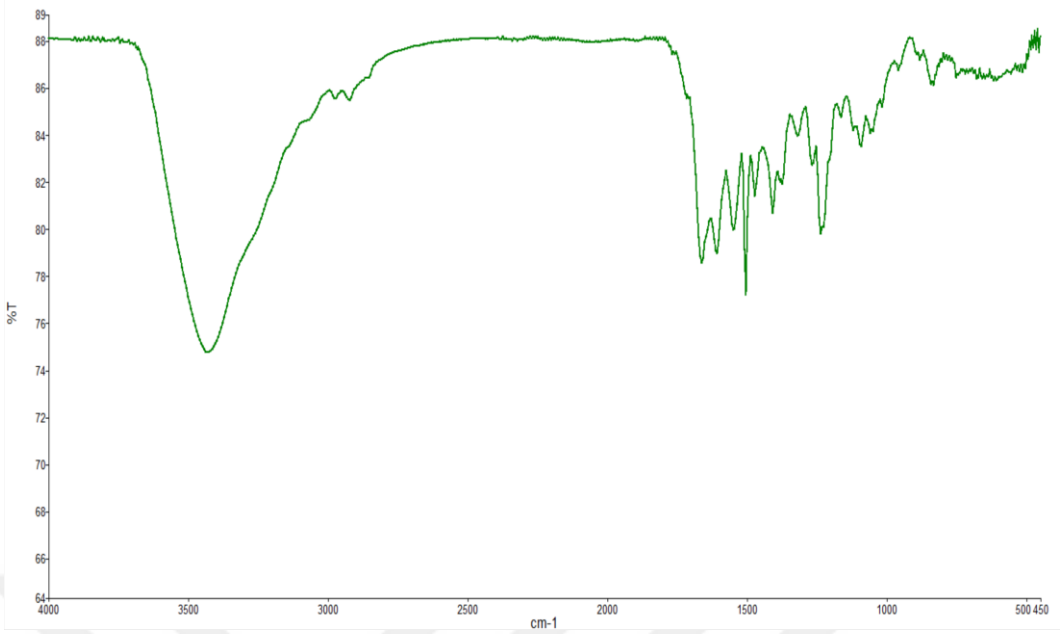


**Figure 3.117**. FT-IR spectrum of Ni(II)phthalocyanine.

- **UV–visible spectrum**

The UV–vis spectra of NiPc dissolved in DMF exhibited characteristic absorptions in the Q band region, at 674 nm and 624 nm as a shoulder. The Q band absorptions of the compounds correspond to the π-π* transition occurring between the HOMO and LUMO of the phthalocyanine ring. The compounds exhibited B band absorptions in the UV range at 450 nm as a result of transitions from the lower π energy levels to the LUMO, shown in **Figure 3.118.**

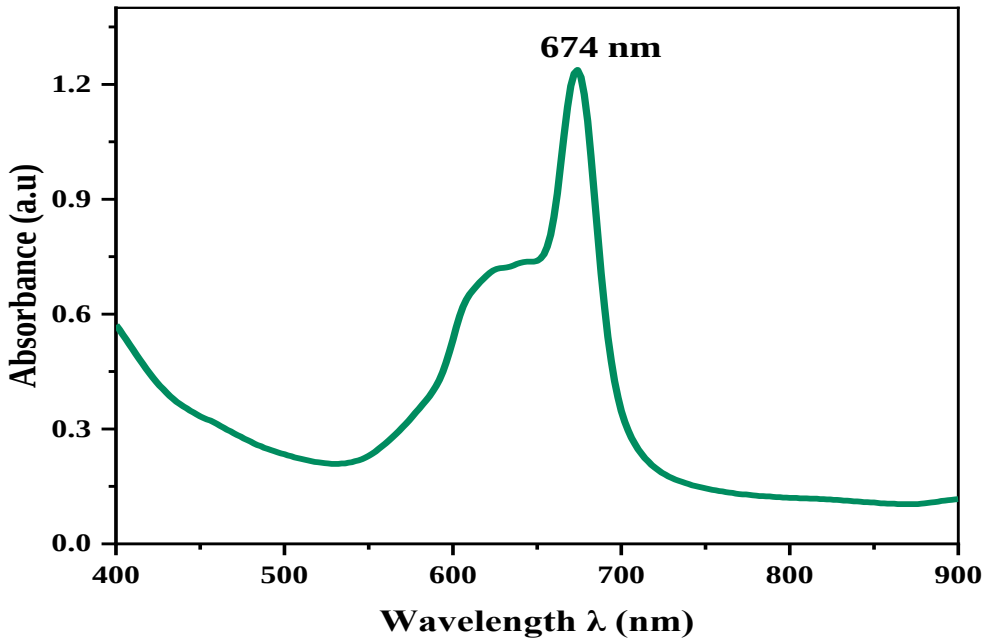


**Figure 3.118.** UV-visible spectrum of Ni(II)phthalocyanine.

- **Thermal analysis**

According to DTG studies, NiPc is thermally stable up to 300 °C, with a 20% weight loss most probably due to the loss of absorbed water from the surface of the complex. Thermogram shows that NiPc has more adsorption than other phthalocyanine complexes with the same ligand. Loss of water starts from room temperature to 300 °C. The mass loss occurs in two distinct stages. The first stage occurring between 300-440 °C, involves decomposing in a 60% mass loss. The second stage, between 450-540 °C, involves further decomposition, leading to a 20% mass loss with no residue, which means the second decomposition reaction is explosive leading to the removal of the sample pan during the heating stage. This is an experimental error we were not able to repeat the experiment due to time constraints, The Thermogram of NiPc is shown in **Figure 3.119.**

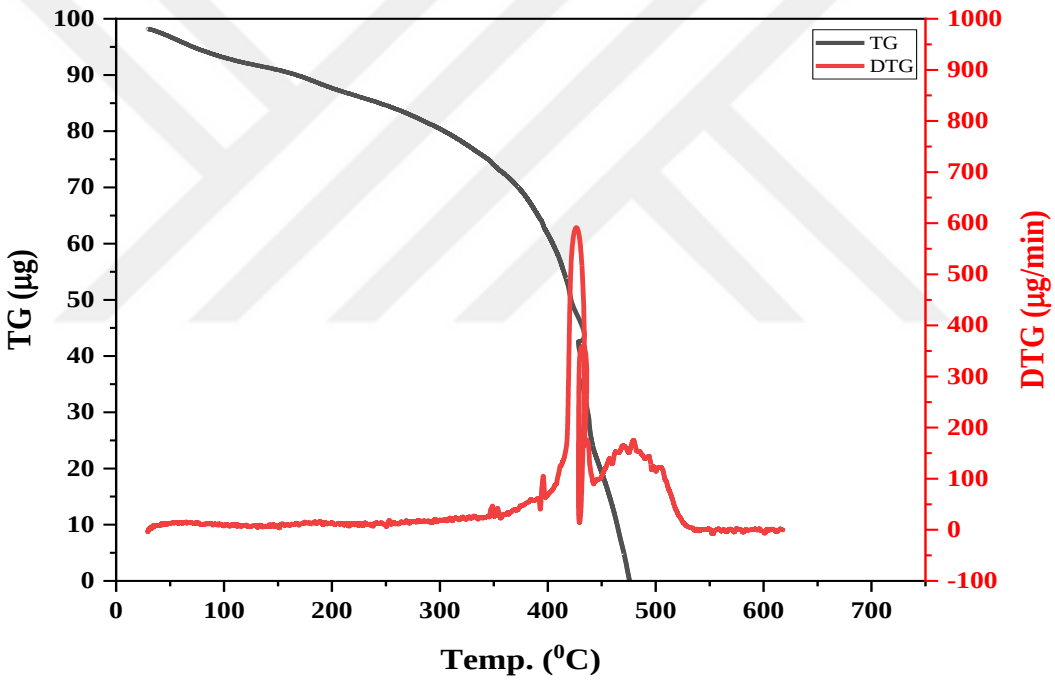


**Figure 3.119.** TG and DTG of Ni(II)phthalocyanine.

- **Electrochemical Properties**.

Electrochemical analysis of NiPc was performed using a GC electrode in DMF with TBAFB as the supporting electrolyte. CV and SWV were techniques used, and potentials were recorded in non-aqueous solutions relative to the ferrocene/ferrocenium couple (Fc/Fc+), which served as a pseudo reference electrode. The CV voltammogram could not adequately reveal redox processes due to the poor solubility of NiPc. Therefore, the experiment was redone using the SW voltammogram, which more accurately shows the individual redox reactions.

The NiPc is capable of a variety of reduction and oxidation processes. The electrochemical voltammogram of NiPc exhibits four reduction waves that are $R_1$, $R_2$, $R_3$, and $R_4$ at -1.16, -1.59, -1.80, and -2.40 V, as well as two oxidation waves $O_1$ and $O_2$ at 0.31, and 0.64 Vs respectively, shown in **Figure 3.120,** and **Figure 3.121.** The initial phase of all of these redox reactions in macrocycle rings because of redox-inactive Ni(II) metal.

There are four redox processes namely as $R_1$, $R_2$, $R_3$, and $R_4$ attributed to Ni(II)Pc-2/Ni(II)Pc-3, Ni(II)Pc-3/Ni(II)Pc-4, Ni(II)Pc-4/Ni(II)Pc-5, and Ni(II)Pc-5/Ni(II)Pc-6 respectively. $O_1$, and $O_2$ are corresponding to the two oxidation processes of NiPc, specifically Ni(II)Pc-2/Ni(II)Pc-1, and Ni(II)Pc-1/Ni(II)Pc0 respectively.

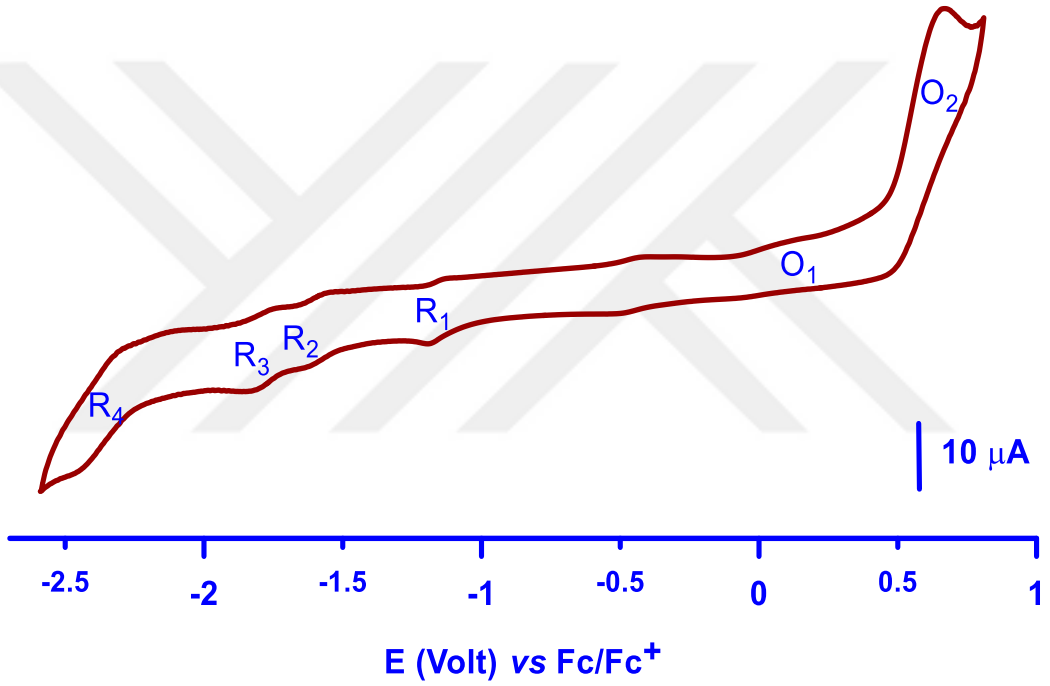


**Figure 3.120.** Cyclic voltammogram of Ni(II)phthalocyanine.

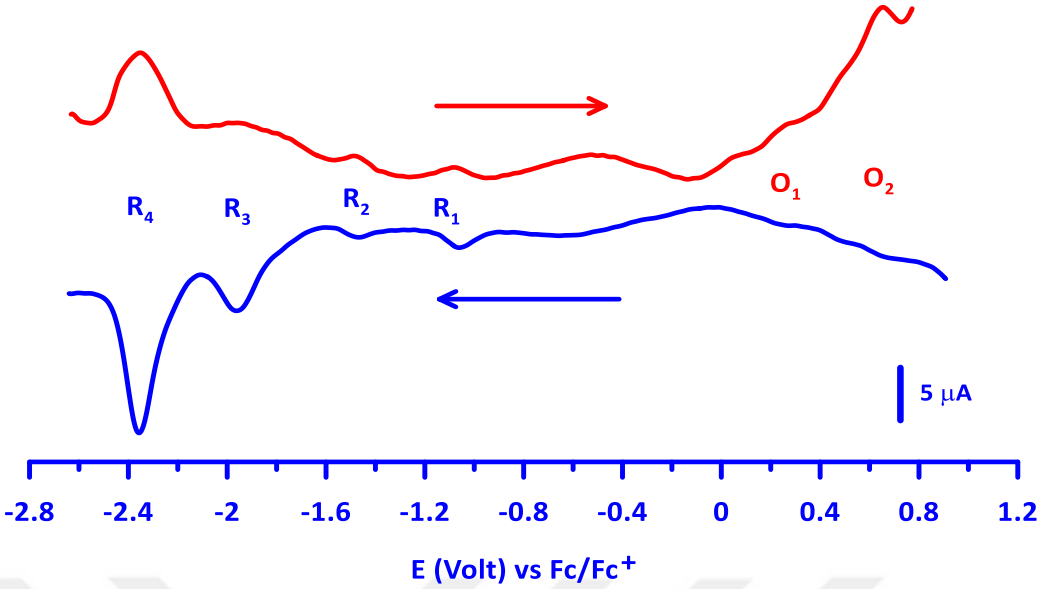


**Figure 3.121.** Square wave voltammogram of Ni(II)phthalocyanine.

## 3.25. 2,2',2'',2'''((2,9,16,23-tetrayltetrakis(oxy))tetrakis(benzene-4,1-diyl)) tetraacetamide Copper phthalocyanine.

The Copper phthalocyanine CuPc was synthesized from 2-(4-(3,4-dicyanophenoxy) phenyl) acetamide with Copper(II)acetate under argon atmosphere in DMF. The green CuPc complex, exhibiting typical phthalocyanine characteristics, was synthesized by cyclotetramerization of four phthalonitrile ligands with Cu(II), the molecule structure of CuPc is shown in **Figure 3.122.**

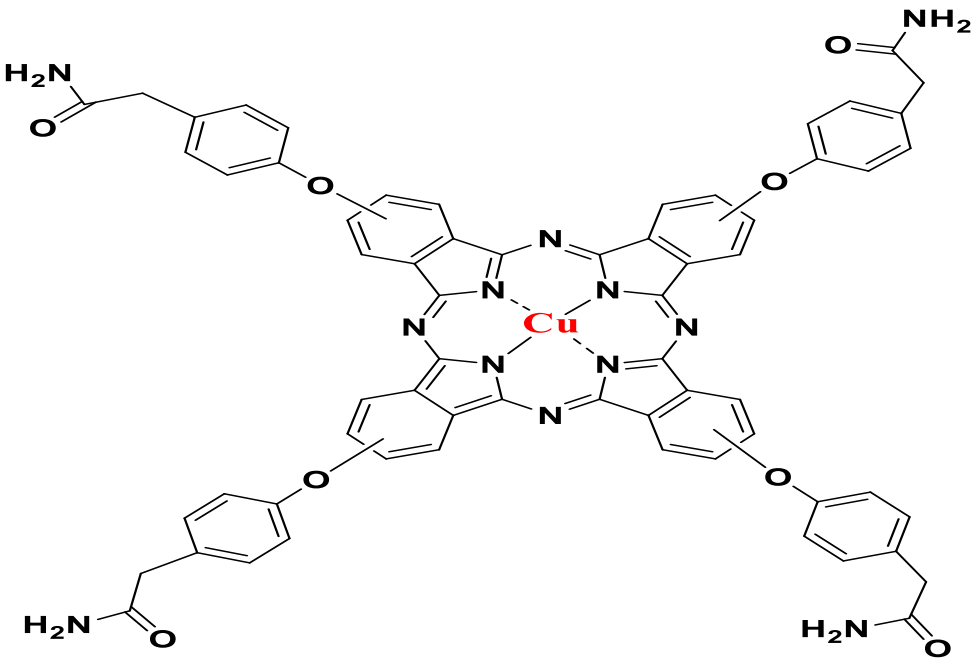


**Figure 3.122.** 2,2',2",2'"((2,9,16,23-tetrayltetrakis(oxy))tetrakis(benzene-4,1-diyl)) tetraacetamide Copper phthalocyanine.

- **FT-IR Spectrum**

FT-IR spectra of CuPc are given in **Figure 3.123,** and have a weak C≡N stretching peak at 2233 $cm^{-1}$ due to impurities left in the CuPc. The C-H bond showed weak peaks at 2976 and 2928 $cm^{-1}$. The bands observed at 1598 $cm^{-1}$ and 1505 $cm^{-1}$ were attributed to aromatic C=C stretching vibrations and C=N stretching vibrations, respectively. Aromatic C-H bending vibrations were identified at 1474 and 1230 $cm^{-1}$. The band at 749 $cm^{-1}$ was assigned to C-C macrocycle ring deformation. Additionally, the unique C-O stretching vibration of the complex was observed at 1093 $cm^{-1}$.

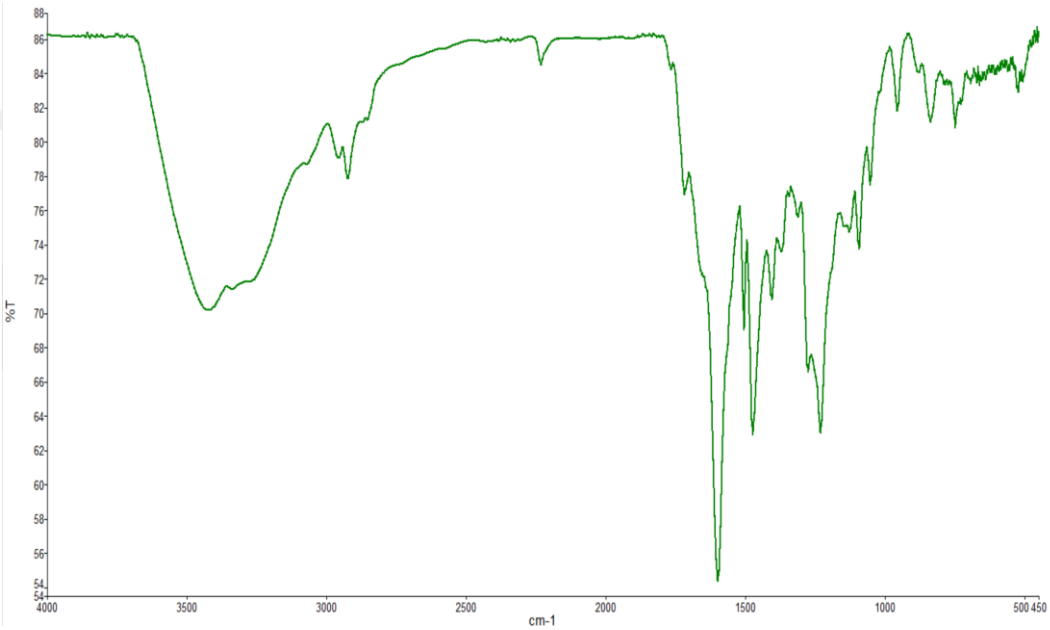


**Figure 3.123.** FT-IR spectrum of Cu(II)phthalocyanine.

- **UV–visible spectrum**

The UV–vis spectra of CuPc dissolved in DMF exhibited characteristic absorptions in the Q band region, between 600-700 nm. The Q band absorptions of the compounds correspond to the π-π* transition occurring between the HOMO and LUMO of the phthalocyanine ring. The compounds exhibited B band absorptions in the UV range 300-400 nm as a result of transitions from the lower π energy levels to the LUMO energy level. The UV–vis spectrum of the CuPc complex in DMF exhibits two absorptions in the Q band region at 610 as shoulder and 674 nm. As shown in **Figure 3.124.**

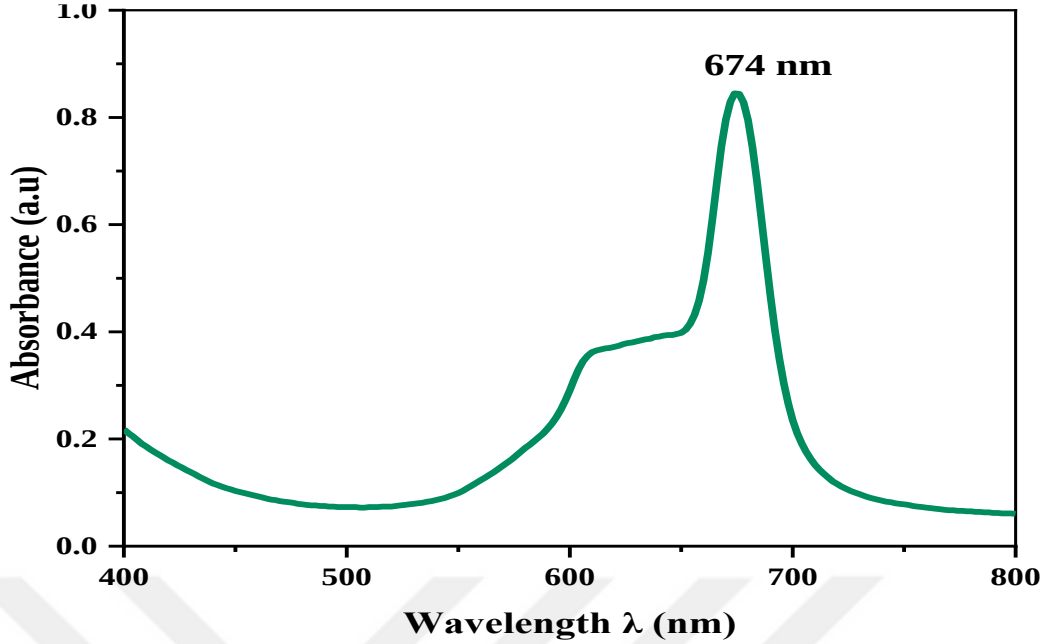


**Figure 3.124.** UV-visible spectrum of Cu(II)phthalocyanine.

- **Thermal analysis**

Based on TG and DTG studies, CuPc is thermally stable up to 350 °C, with an 8% mass loss attributed to the release of absorbed water from the complex's surface. The complex decomposition starts from 350 to 410 °C, resulting in a 65% mass loss. Additionally, the CuPc complex decomposes without melting, leading to a 76% total mass loss. The thermogram indicates that 24% of the residue remains after decomposition, as shown in **Figure 3.125.**

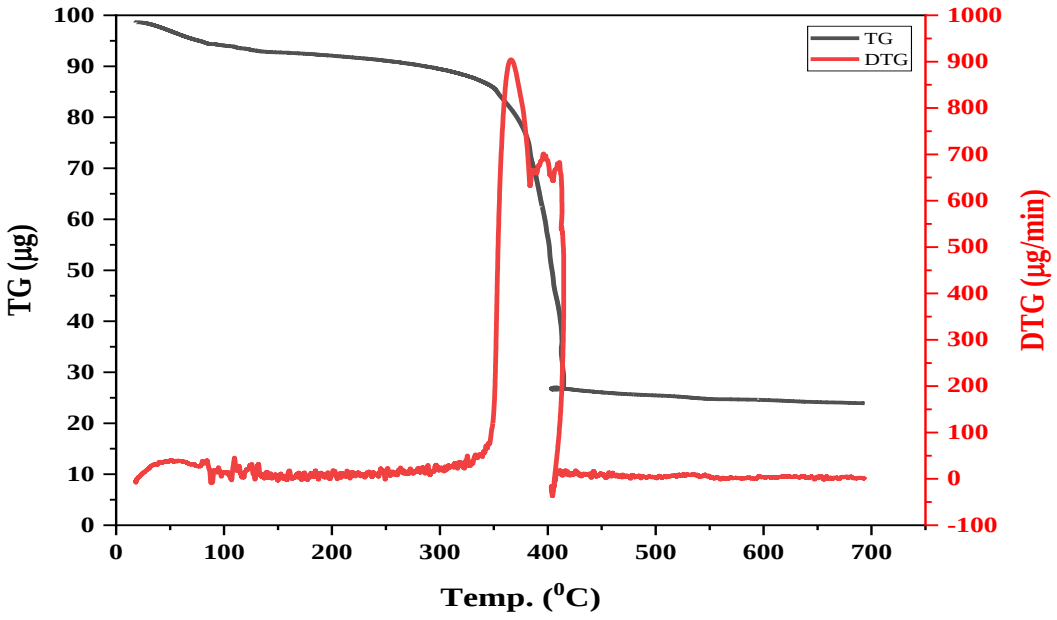


**Figure 3.125.** TG and DTG of Cu(II)phthalocyanine.

- **Electrochemical Properties**.

The electrochemical experiment of CuPc was performed using a GC electrode in DMF with TBAFB as the supporting electrolyte. CV and SWV techniques were used, and potentials were recorded in non-aqueous solutions relative to the ferrocene/ferrocenium couple (Fc/Fc+), which served as a pseudo reference electrode.

From **Figure 3.126,** and **Figure 3.127** it can be seen that the CuPc may undergo numerous reduction and oxidation reactions labelled as $R_1$, $R_2$, and $R_3$ on the electrochemical voltammogram of CuPc at -0.77, -1.10, and -1.45 V together with two oxidations wave $O_1$ and $O_2$ at 0.35 and 0.55 V respectively belong to phthalocyanine ring, which also has a reduction wave on copper metal labelled as Mr at -0.53 V. While removed of electron takes place from the HOMO energy level of phthalocyanine rings, the addition of electron goes to LUMO energy level. These redox reactions exhibited quasireversible behavior in terms of peak current and peak potential variations with scan rate.

The redox processes represented as $R_1$, $R_2$, and $R_3$ ascribed to Cu(II)Pc-2/Cu(II)Pc-3, Cu(II)Pc-3/Cu(II)Pc-4, and Cu(II)Pc-4/Cu(II)Pc-5, respectively. On the other hand, $O_1$ and $O_2$ correspond to oxidation processes: Cu(II)Pc-2/Cu(II)Pc-1 and Cu(II)Pc-1/Cu(II)Pc0, respectively.

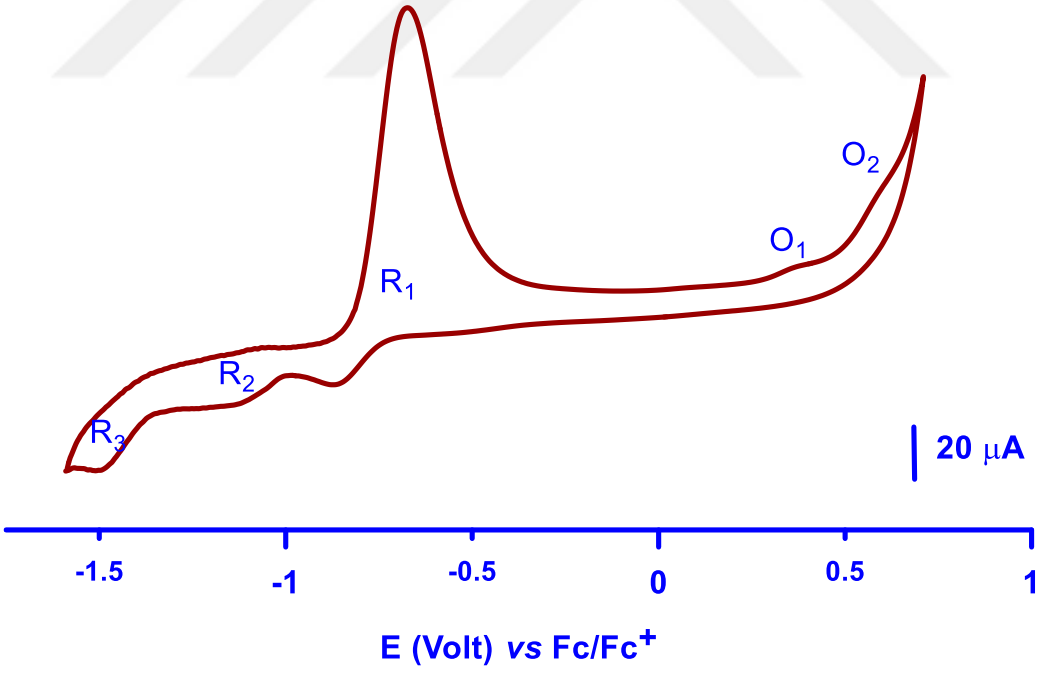


**Figure 3.126.** Cyclic voltammogram of Cu(II)phthalocyanine.

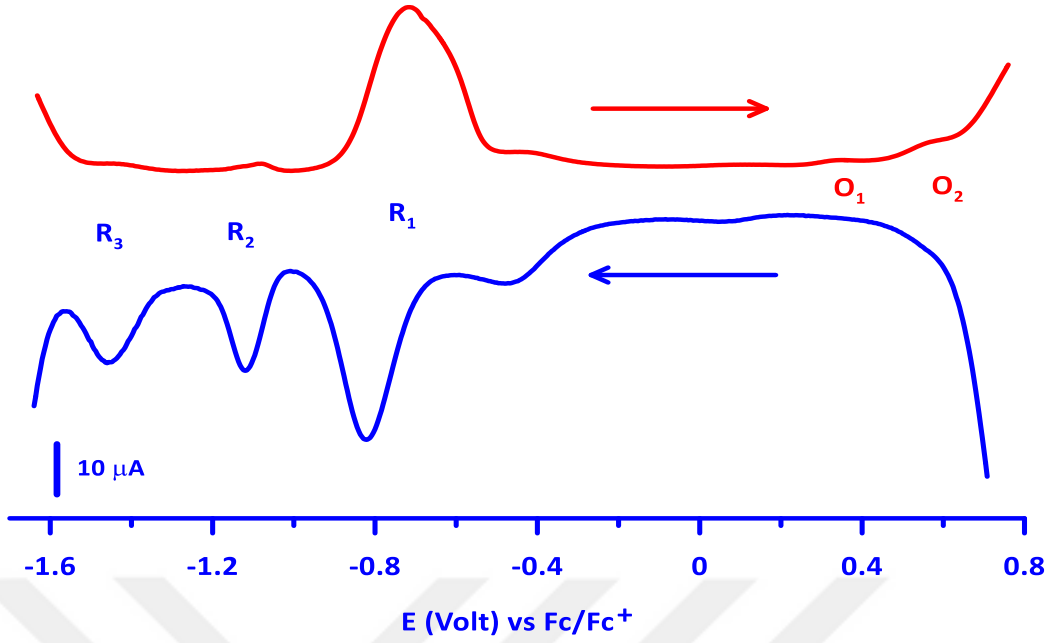


**Figure 3.127.** Square wave voltammogram of Cu(II)phthalocyanine.

## 3.26. 2,2',2'',2'''((2,9,16,23-tetrayltetrakis(oxy))tetrakis(benzene-4,1-diyl)) tetraacetamide Zinc phthalocyanine.

The Zinc phthalocyanine ZnPc was prepared by reacting 2-(4-(3,4-dicyanophenoxy) phenyl) acetamide with Zinc(II)acetate in DMF under an argon atmosphere. Cyclotetramerisation of four phthalonitrile ligands with Zn(II), afforded the green ZnPc complex, the molecular structure of the complex is shown in **Figure 3.128.**

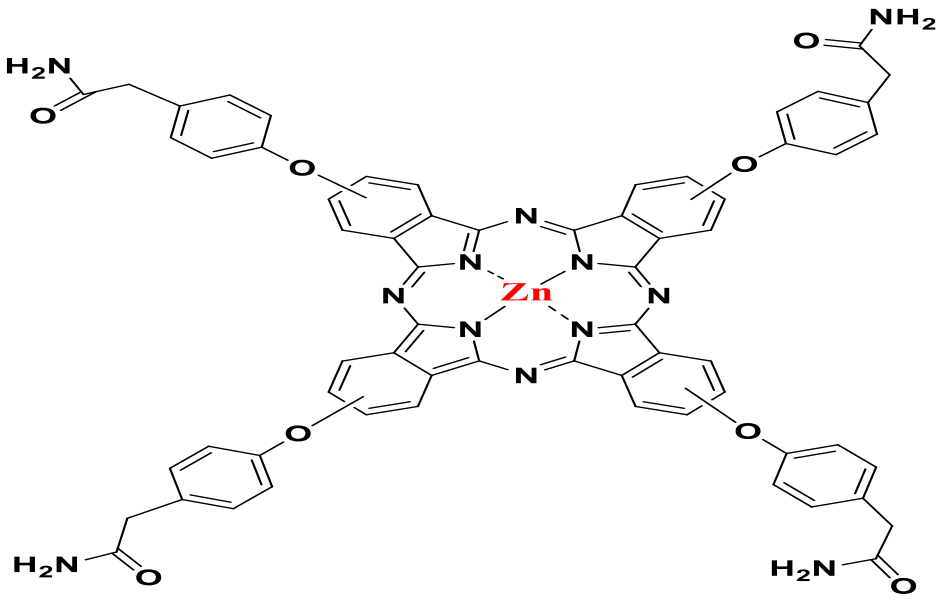


**Figure 3.128**. 2,2',2",2'"((2,9,16,23-tetrayltetrakis(oxy))tetrakis(benzene-4,1-diyl)) tetraacetamide Zinc phthalocyanine.

- **FT-IR Spectrum**

FT-IR spectra of the ZnPc given in **Figure 3.129** do not have the C≡N stretching vibration at 2233 $cm^{-1}$ indicating the formation of ZnPc without impurities of starting matarials. A weak peak corresponding to C-H bond vibrations was observed between 2976 $cm^{-1}$ and 2923 $cm^{-1}$. The aromatic C=C and C=N stretching vibrations were identified at 1608 $cm^{-1}$ and 1505 $cm^{-1}$, respectively. Aromatic C-H bending vibrations were found at 1410 and 1235 $cm^{-1}$. The band at 743 $cm^{-1}$ was attributed to C-C macrocycle ring deformation, and a characteristic C-O stretching vibration was observed at 1090 $cm^{-1}$.

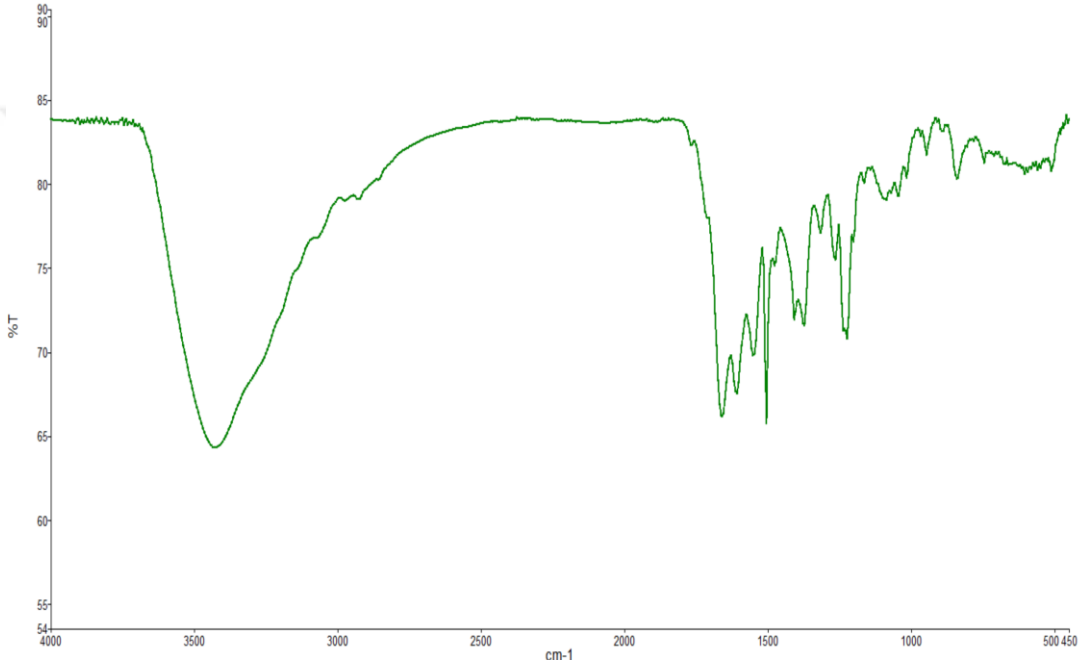


**Figure 3.129.** FT-IR spectrum of Zn(II)phthalocyanine.

- **UV–visible spectrum**

The UV–vis spectra of ZnPc dissolved in DMF exhibited characteristic absorptions in the Q band region, in between 600-700 nm. The Q band absorptions of the compounds correspond to the π-π* transition occurring between the HOMO and LUMO of the phthalocyanine ring. The ZnPc complex exhibited B band absorptions in the UV range at 350 nm as a result of transitions from the lower π energy levels to the LUMO. The UV–vis spectrum of the ZnPc complex in DMF exhibits Q bands at 610 and 680 nm, as well, as shown in **Figure 3.130.**

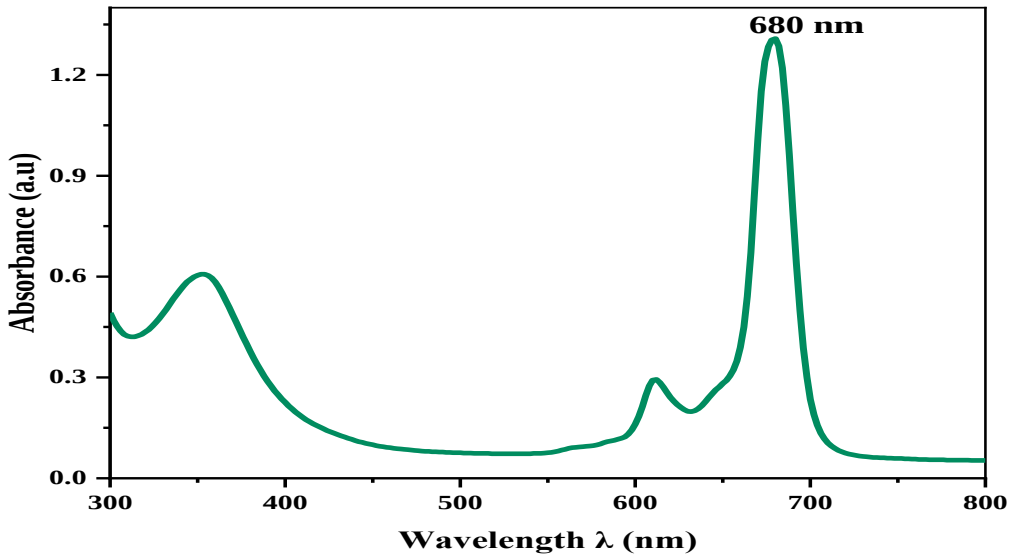


**Figure 3.130.** UV-visible spectrum of Zn (II)phthalocyanine.

- **Thermal analysis**

Based on TG and DTG studies, ZnPc is thermally stable up to 250 °C, with an 5% mass loss attributed to the release of absorbed water from the complex's surface. The complex decomposition starts from 250 to 420 °C, resulting in a 25% mass loss. The second stage happened from 420-610 °C, with reducing mass 55%. Additionally, the ZnPc complex decomposes without melting, leading to a 85% total mass loss. The thermogram indicates that 15% of the residue remains after decomposition, as shown in **Figure 3.131**.

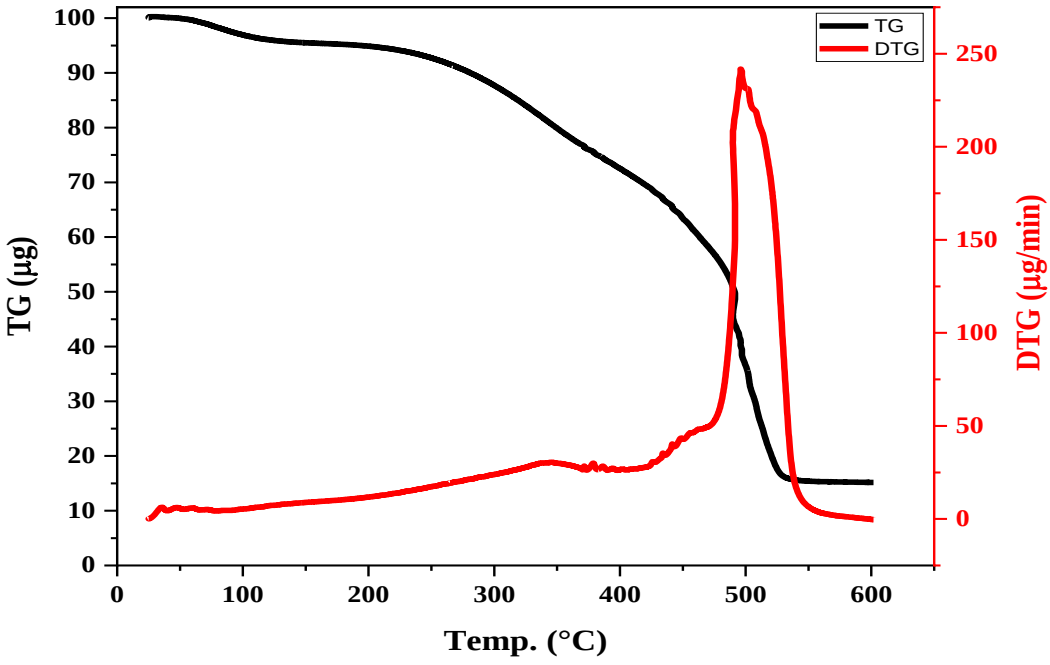


**Figure 3.131.** TG and DTG of Zn(II)phthalocyanine.

- **Electrochemical Properties**.

Electrochemical analysis of ZnPc was performed using a GC electrode in DMF with TBAFB as the supporting electrolyte. CV and SWV were techniques used, and potentials were recorded in non-aqueous solutions relative to the ferrocene/ferrocenium couple (Fc/Fc+), which served as a pseudo reference electrode.

According to **Figure 3.132,** and **Figure 3.133.** The ZnPc macrocycle moiety may undergo four reduction and two oxidation reactions. The electrochemical reduction waves labelled $R_1$, $R_2$, $R_3$, and $R_4$ on voltammogram at -1.34, -1.60, -1.83, and -2.12 Vs, and two oxidations wave $O_1$ and $O_2$ at 0.45 and 0.78 V respectively are all belong to phthalocyanine ring. The electrochemical molecule bandgap is equal to the difference in energy between these oxidation and reduction processes. These redox reactions of ZnPc exhibited reversible behaviour in terms of peak current and peak potential variations with scan rate.

The four redox processes $R_1$, $R_2$, $R_3$, and $R_4$ attributed to Zn(II)Pc-2/Zn(II)Pc-3, Zn(II)Pc-3/Zn(II)Pc-4, Zn(II)Pc-4/Zn(II)Pc-5, and Zn(II)Pc-5/Zn(II)Pc-6 respectively. $O_1$ and $O_2$ are corresponding to the two oxidation processes of ZnPc, specifically Zn(II)Pc-2/Zn(II)Pc-1, and Zn(II)Pc-1/Zn(II)Pc0 respectively.

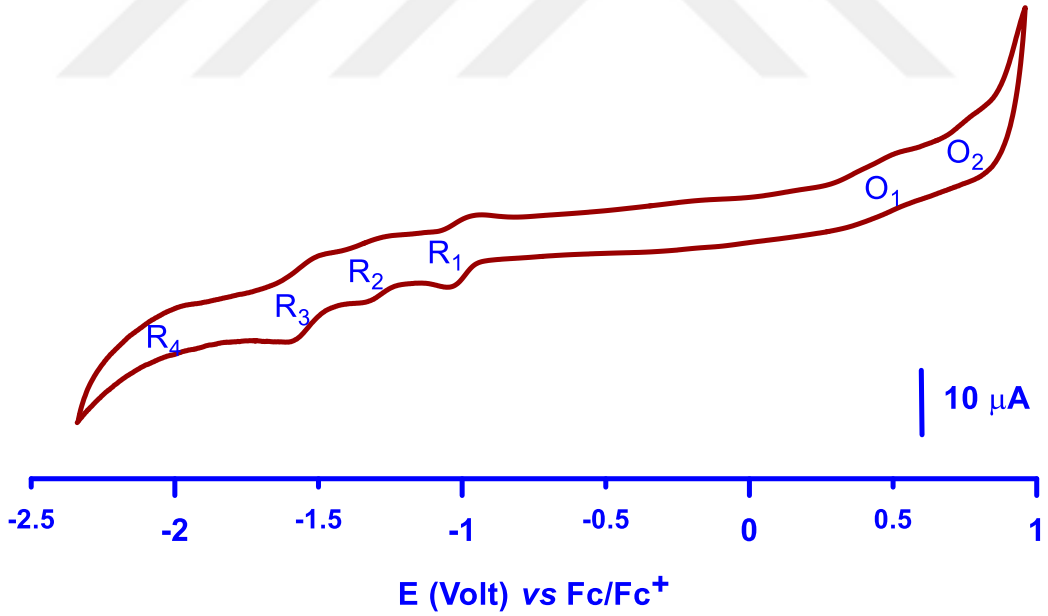


**Figure 3.132.** Cyclic voltammogram of zinc(II)phthalocyanine.

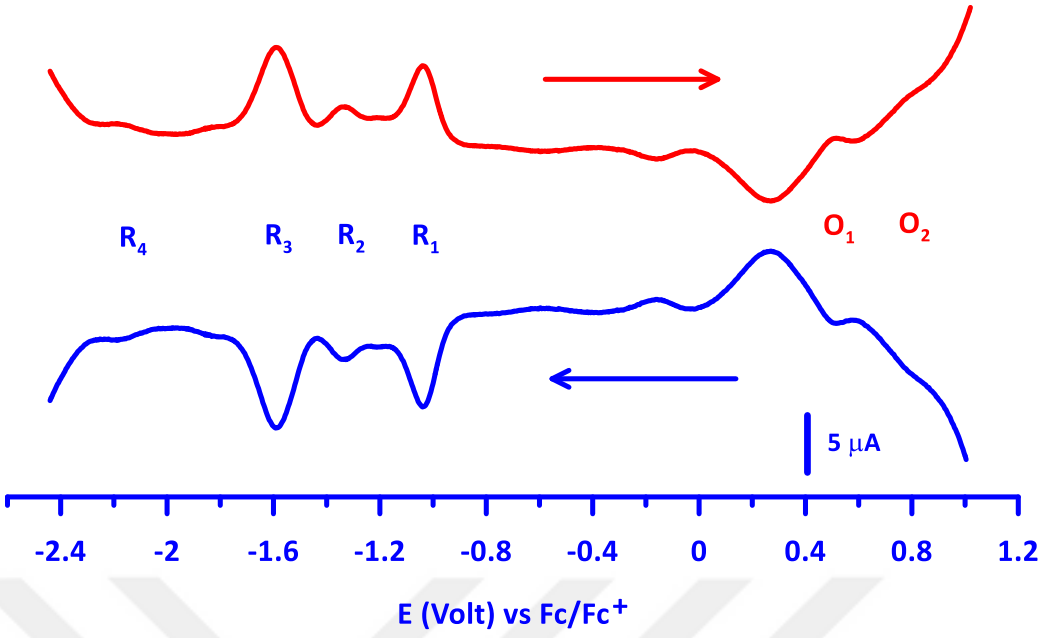


**Figure 3.133.** Square wave voltammogram of zinc(II)phthalocyanine.

# 4. CONCLUSION

This thesis discusses the synthesis of novel phthalocyanine compounds with symmetric structures, including 4-nitrophthalonitrile and three ligands that each have a unique structural substituent. The versatility of 4-nitrophthalonitrile as a synthetic precursor to a new class of phthalocyanines opens up possibilities for experimenting with different substituents to change the physical and chemical properties of synthesized phthalocyanine compounds.

After the synthesis of three new ligands, 18 metal phthalocyanine complexes and one metal-free phthalocyanine compound were obtained by combining three different ligands with acetate salts of Cr(II), Fe(II), Co(II), Ni(II), Cu(II), and Zn(II). Utilizing FT-IR, UV/visible spectroscopy, Thermal analysis (TG/DTG), and Electrochemistry (CV/SWV) techniques, the structures of the metal and metal-free phthalocyanine compounds were studied. The resulting data was used to describe the compounds and their properties. Witnessing the formation of phthalocyanine compounds via the use of their distinctive green color is the most fundamental and uncomplicated testing direction. All of the produced molecules being green is a telltale sign that phthalocyanine compounds were the ones that were created. It is also possible to tell that phthalocyanine compounds have formed when the C≡N peaks in the FT-IR spectra vanish.

The most of the synthesized phthalocyanine compounds that have very low solubility in general organic solvents, it was possible to get UV-visible spectra using DMF solvent which is the best solvent for the synthesized phthalocyanine compounds. These Pc compounds' UV/visible spectra showed the Q bond between 600-700 nm and the B bond from 350 to 500 nm in line with what has been reported in the literature.

All Pc complexes that were synthesized exhibit thermal stability up to 250 °C, but decomposition starts without a melting point, and all the decomposition is exothermic, according to the TG/DTG data. Because of the limitation of the experimental condition, residue after pyrolysis reaction is not conclusive to predict the metal oxides produced are comparable with the formula of phthalocyanine compounds.

Phthalocyanine compounds showed all the characteristic redox potentials in the electrochemical window of the solvent DMF, studied by CV and SWV techniques. The metal phthalocyanine complexes showed two oxidation potentials and four reduction potentials, which is typical for phthalocyanine complexes. There are also metal-related redox waves, also observed if the metal ion is redox active in the phthalocyanine compounds like Cr, Fe, Co, and Cu.

# REFERENCES


[1] Linert, W., Fukuda, Y., and Camard, A. (2001). Chromotropism of coordination compounds and its applications in solution, Coordination Chemistry Reviews, C Vol. 218 113-152.

[2] Trudu, F., Amato, F., Vaňhara, P., Pivetta, T., Peña-Méndez, E., and Havel, J. (2015). Coordination compounds in cancer: Past, present and perspectives, Journal of applied biomedicine, C Vol. 13 (2), pp: 79-103.

[3] Comba, P. (2000). Coordination compounds in the entatic state, Coordination Chemistry Reviews, C Vol. 200 217-245.

[4] Bailey, P.J. and Pace, S. (2001). The coordination chemistry of guanidines and guanidinates, Coordination Chemistry Reviews, C Vol. 214 (1), pp: 91-141.

[5] Lawrance, G.A., (2013). Introduction to coordination chemistry, John Wiley & Sons,

[6] Trofimenko, S., (1999). Scorpionates: the coordination chemistry of polypyrazolylborate ligands, World Scientific,

[7] Kettle, S.F.A., (2013). Physical inorganic chemistry: a coordination chemistry approach, Springer,

[8] McCleverty, J.A., (2003). Comprehensive coordination chemistry II, Elsevier Ltd,

[9] Alcarazo, M., Lehmann, C.W., Anoop, A., Thiel, W., and Fürstner, A. (2009). Coordination chemistry at carbon, Nature Chemistry, C Vol. 1 (4), pp: 295-301.

[10] Basolo, F., Johnson, R.C., and Carl, R., (1986). Coordination chemistry, Science reviews Northwood,

[11] Kraft, A. (2018). What a chemistry student should know about the history of Prussian blue, ChemTexts, C Vol. 4 (4), pp: 16.

[12] Comba, P. (1999). Strains and stresses in coordination compounds, Coordination Chemistry Reviews, C Vol. 182 (1), pp: 343-371.

[13] Mahmudov, K.T., Gurbanov, A.V., Aliyeva, V.A., Resnati, G., and Pombeiro, A.J. (2020). Pnictogen bonding in coordination chemistry, Coordination Chemistry Reviews, C Vol. 418 213381.

[14] Barata, J.F., Neves, M.G.P., Lacerda, P.S., Conceição, P., and Trindade, T. (2022). Quantum dot phthalocyanine non-covalent assemblies–A review, Dyes and Pigments, C Vol. 198 109931.

[15] Barth, J.V. (2009). Fresh perspectives for surface coordination chemistry, Surface Science, C Vol. 603 (10-12), pp: 1533-1541.

[16] Gao, H., Yu, R., Ma, Z., Gong, Y., Zhao, B., Lv, Q., and Tan, Z.a. (2022). Recent advances of organometallic complexes in emerging photovoltaics, Journal of Polymer Science, C Vol. 60 (6), pp: 865-916.

[17] Harmandar, K., Saglam, M.F., Sengul, I.F., Ekineker, G., Balcik-Ercin, P., Göksel, M., and Atilla, D. (2021). Novel triazole containing zinc (II) phthalocyanine Schiff bases: Determination of photophysical and photochemical properties for photodynamic cancer therapy, Inorganica Chimica Acta, C Vol. 519 120286.

[18] Günsel, A., Bilgicli, A.T., Barut, B., Taslimi, P., Özel, A., Gülçin, İ., Biyiklioglu, Z., and Yarasir, M.N. (2020). Synthesis of water soluble tetra-substituted phthalocyanines: Investigation of DNA cleavage, cytotoxic effects and metabolic enzymes inhibition, Journal of Molecular Structure, C Vol. 1214 128210.

[19] Köksoy, B., Akyüz, D., Şenocak, A., Durmuş, M., and Demirbaş, E. (2021). Novel SWCNT-hybrid nanomaterial functionalized with subphthalocyanine substituted asymmetrical zinc (II) phthalocyanine conjugate: Design, synthesis, characterization and sensor properties for pesticides, Sensors and Actuators B: Chemical, C Vol. 329 129198.

[20] Alosabi, A., Al-Muntaser, A., El-Nahass, M., and Oraby, A. (2022). Structural, optical and DFT studies of disodium phthalocyanine thin films for optoelectronic devices applications, Optics & Laser Technology, C Vol. 155 108372.

[21] Anderson, J.R. and Boudart, M., (2012). Catalysis: science and technology, Springer Science & Business Media,

[22] Keshipour, S. and Asghari, A. (2022). A review on hydrogen generation by phthalocyanines, International Journal of Hydrogen Energy, C Vol. 47 (26), pp: 12865-12881.

[23] Sakamoto, K. and Ohno-Okumura, E. (2009). Syntheses and functional properties of phthalocyanines, Materials, C Vol. 2 (3), pp: 1127-1179.

[24] Wan, X., Zhang, Z., Niu, H., Yin, Y., Kuai, C., Wang, J., Shao, C., and Guo, Y. (2021). Machine-learning-accelerated catalytic activity predictions of transition metal phthalocyanine dual-metal-site catalysts for CO2 reduction, The Journal of Physical Chemistry Letters, C Vol. 12 (26), pp: 6111-6118.

[25] Rak, J., Pouckova, P., Benes, J., and Vetvicka, D. (2019). Drug delivery systems for phthalocyanines for photodynamic therapy, Anticancer research, C Vol. 39 (7), pp: 3323-3339.

[26] Günsel, A., Atmaca, G.Y., Taslimi, P., Bilgicli, A.T., Gülçin, İ., Erdoğmuş, A., and Yarasir, M.N. (2020). Synthesis, characterization, photo-physicochemical and biological properties of water-soluble tetra-substituted phthalocyanines: antidiabetic, anticancer and anticholinergic potentials, Journal of Photochemistry and Photobiology A: Chemistry, C Vol. 396 112511.

[27] Demir, E., Silah, H., and Uslu, B. (2022). Phthalocyanine modified electrodes in electrochemical analysis, Critical Reviews in Analytical Chemistry, C Vol. 52 (2), pp: 425-461.

[28] Yenilmez, H.Y., Şahin, A.N., Altındal, A., and Bayır, Z.A. (2021). Photosensitive field effect transistor based on metallo-phthalocyanines containing (4-pentylphenyl) ethynyl moieties, Synthetic metals, C Vol. 273 116690.

[29] Yildirim, M.S., Alcay, Y., Yavuz, O., Atasen, S.K., Mermer, Z., Aribuga, H., and Yilmaz, I. (2022). Construction of anthraquinone functional zinc phthalocyanine sensor platform for ultra-trace amount of water determination in tetrahydrofuran and N, N-Dimethylformamide, Analytica Chimica Acta, C Vol. 1198 339531.

[30] Hurt, C., Brandt, M., Priya, S., Bhatelia, T., Patel, J., Selvakannan, P., Bhargava, S., Hong, Z., Wang, Z., and Li, X. (1984). Catalysis Science & Technology, Vol.

[31] Dursun, S., Akay, R.G., and Yazici, M.S. (2020). CVD graphene supported cobalt (II) phthalocyanine as cathode electrocatalyst for PEM fuel cells, International Journal of Hydrogen Energy, C Vol. 45 (60), pp: 34837-34844.

[32] De La Torre, G., Vazquez, P., Agullo-Lopez, F., and Torres, T. (1998). Phthalocyanines and related compounds: organic targets for nonlinear optical applications, Journal of Materials Chemistry, C Vol. 8 (8), pp: 1671-1683.

[33] Klyamer, D., Bonegardt, D., Krasnov, P., Sukhikh, A., Popovetskiy, P., Khezami, K., Durmuş, M., and Basova, T. (2022). Halogen-substituted zinc (II) phthalocyanines: Spectral properties and structure of thin films, Thin Solid Films, C Vol. 754 139301.

[34] Kaya, E.N., Köksoy, B., Yeşilot, S., and Durmuş, M. (2020). Purple silicon (IV) phthalocyanine axially substituted with BODIPY groups, Dyes and Pigments, C Vol. 172 107867.

[35] Sarıoğulları, H., Sengul, I.F., and Gürek, A.G. (2022). Comparative study on sensing and optical properties of carbazole linked novel zinc (II) and cobalt (II) phthalocyanines, Polyhedron, C Vol. 227 116139.

[36] Ömeroğlu, İ. and Durmuş, M. (2023). Water-soluble phthalocyanine photosensitizers for photodynamic therapy, Turkish Journal of Chemistry, C Vol. 47 (5), pp: 837-863.

[37] Saydam, S., Yılmaz, E., Bağcı, F., Yağlıoğlu, H.G., Elmalı, A., Salih, B., and Bekaroğlu, Ö., Synthesis, Characterization, Electrochemical, and Optic Limiting Properties of Novel CoII, CuII, and Double-Decker LuIII Phthalocyanines, 2009, Wiley Online Library.

[38] González-Rodríguez, D. and Bottari, G. (2009). Phthalocyanines, subphthalocyanines and porphyrins for energy and electron transfer applications, Journal of Porphyrins and Phthalocyanines, C Vol. 13 (04n05), pp: 624-636.

[39] Koçak, Ç.C. and Dursun, Z. (2022). Enhanced electrocatalytic oxidation of methanol on Au-Pt bimetallic particles modified copper phthalocyanine-carbon nanotube composite electrode, Materials Science and Engineering: B, C Vol. 275 115485.

[40] Günsel, A., Taslimi, P., Atmaca, G.Y., Bilgicli, A.T., Pişkin, H., Ceylan, Y., Erdoğmuş, A., Yarasir, M.N., and Gülçin, İ. (2021). Novel potential metabolic enzymes inhibitor, photosensitizer and antibacterial agents based on water-soluble phthalocyanine bearing imidazole derivative, Journal of Molecular Structure, C Vol. 1237 130402.

[41] Miles, J.R., Willis, M.R., and Jones, R.P. (2012). Photoconduction properties of some monomeric phthalocyanines and dibromoanthrone, Materials science in semiconductor processing, C Vol. 15 (1), pp: 61-72.

[42] Brilkina, A.A., Dubasova, L.V., Sergeeva, E.A., Pospelov, A.J., Shilyagina, N.Y., Shakhova, N.M., and Balalaeva, I.V. (2019). Photobiological properties of phthalocyanine photosensitizers Photosens, Holosens and Phthalosens: A comparative in vitro analysis, Journal of Photochemistry and Photobiology B: Biology, C Vol. 191 128-134.

[43] Zhao, F., Harnisch, F., Schröder, U., Scholz, F., Bogdanoff, P., and Herrmann, I. (2005). Application of pyrolysed iron (II) phthalocyanine and CoTMPP based oxygen reduction catalysts as cathode materials in microbial fuel cells, Electrochemistry communications, C Vol. 7 (12), pp: 1405-1410.

[44] Sorokin, A. and Kudrik, E. (2011). Phthalocyanine metal complexes: versatile catalysts for selective oxidation and bleaching, Catalysis Today, C Vol. 159 (1), pp: 37-46.

[45] Dini, D. and Hanack, M. (2004). Phthalocyanines as materials for advanced technologies: some examples, Journal of Porphyrins and Phthalocyanines, C Vol. 8 (07), pp: 915-933.

[46] Eu, S., Katoh, T., Umeyama, T., Matano, Y., and Imahori, H. (2008). Synthesis of sterically hindered phthalocyanines and their applications to dye-sensitized solar cells, Dalton Transactions, C Vol. (40), pp: 5476-5483.

[47] Köksoy, B., Akyüz, D., Şenocak, A., Durmuş, M., and Demirbas, E. (2021). Sensitive, simple and fast voltammetric determination of pesticides in juice samples by novel BODIPY-phthalocyanine-SWCNT hybrid platform, Food and Chemical Toxicology, C Vol. 147 111886.

[48] Günsel, A., Bilgiçli, A.T., Kandemir, C., Sancak, R., Arabaci, G., and Yarasir, M.N. (2020). Comparison of novel tetra-substituted phthalocyanines with their quaternized derivatives: Antioxidant and antibacterial properties, Synthetic metals, C Vol. 260 116288.

[49] Klipfel, N., Xia, J., Čulík, P., Orlandi, S., Cavazzini, M., Shibayama, N., Kanda, H., Igci, C., Li, W., and Cheng, Y.-B. (2022). Zn (II) and Cu (II) tetrakis (diarylamine) phthalocyanines as hole-transporting materials for perovskite solar cells, Materials Today Energy, C Vol. 29 101110.

[50] Yutronkie, N.J., King, B., Melville, O.A., Lessard, B.H., and Brusso, J.L. (2021). Attaining air stability in high performing n-type phthalocyanine based organic semiconductors, Journal of Materials Chemistry C, C Vol. 9 (31), pp: 10119-10126.

[51] Yabaş, E., Sülü, M., Saydam, S., Dumludağ, F., Salih, B., and Bekaroğlu, Ö. (2011). Synthesis, characterization and investigation of electrical and electrochemical properties of imidazole substituted phthalocyanines, Inorganica Chimica Acta, C Vol. 365 (1), pp: 340-348.

[52] Cranston, R.R. and Lessard, B.H. (2021). Metal phthalocyanines: Thin-film formation, microstructure, and physical properties, RSC advances, C Vol. 11 (35), pp: 21716-21737.

[53] Gamelas, S.R., Gomes, A.T., Faustino, M.A.F., Tomé, A.C., Tomé, J.o.P., Almeida, A., and Lourenço, L.M. (2020). Photoinactivation of Escherichia coli with water-soluble ammonium-substituted phthalocyanines, ACS Applied Bio Materials, C Vol. 3 (7), pp: 4044-4051.

[54] Luo, T., Nash, G.T., Xu, Z., Jiang, X., Liu, J., and Lin, W. (2021). Nanoscale metal–organic framework confines zinc-phthalocyanine photosensitizers for enhanced photodynamic therapy, Journal of the American Chemical Society, C Vol. 143 (34), pp: 13519-13524.

[55] Osati, S., Ali, H., and van Lier, J.E. (2015). Synthesis and spectral properties of phthalocyanine–BODIPY conjugates, Tetrahedron Letters, C Vol. 56 (16), pp: 2049-2053.

[56] Breloy, L., Yavuz, O., Yilmaz, I., Yagci, Y., and Versace, D.-L. (2021). Design, synthesis and use of phthalocyanines as a new class of visible-light photoinitiators for free-radical and cationic polymerizations, Polymer Chemistry, C Vol. 12 (30), pp: 4291-4316.

[57] van Staden, J.K.F. (2015). Application of phthalocyanines in flow-and sequential-injection analysis and microfluidics systems: A review, Talanta, C Vol. 139 75-88.

[58] Akin, M., Saki, N., Guzel, E., Orman, B., Nalbantsoy, A., and Kocak, M.B. (2022). Assessment of in vitro Cytotoxic, iNOS, Antioxidant and Photodynamic Antimicrobial Activities of Water-soluble Sulfonated Phthalocyanines, Photochemistry and Photobiology, C Vol. 98 (4), pp: 907-915.

[59] Gregory, P. (2012). Industrial applications of phthalocyanines, Journal of Porphyrins and Phthalocyanines, C Vol.

[60] Bekaroğlu, Ö. (2014). History, development, and a new concept of phthalocyanines in Turkey, Turkish Journal of Chemistry, C Vol. 38 (6), pp: 903-922.

[61] Gregory, P. (1999). Steamrollers, sports cars and security: phthalocyanine progress through the ages, Journal of Porphyrins and Phthalocyanines, C Vol. 3 (6-7), pp: 468-476.

[62] Arsalan, S. (2016). Phthalocyanines: Structure, synthesis, purification and applications, Batman Üniversitesi Yaşam Bilimleri Dergisi, C Vol. 6 (2/2), pp: 188-197.

[63] Mack, J. and Kobayashi, N. (2011). Low symmetry phthalocyanines and their analogues, Chemical reviews, C Vol. 111 (2), pp: 281-321.

[64] Sample, H.C. and Senge, M.O. (2021). Nucleophilic aromatic substitution (SNAr) and related reactions of porphyrinoids: Mechanistic and regiochemical aspects, European Journal of Organic Chemistry, C Vol. 2021 (1), pp: 7-42.

[65] Mori, S., Yoshiyama, H., Tokunaga, E., Iida, N., Hayashi, M., Obata, T., Tanaka, M., and Shibata, N. (2015). Design, synthesis, spectral investigations and biological activity of fluorinated phthalocyanine conjugated with galactose and comparison to its non-fluorinated counterpart, Journal of Fluorine Chemistry, C Vol. 174 137-141.

[66] Yazıcı, A., Dalbul, N., Altındal, A., Salih, B., and Bekaroğlu, Ö. (2016). Partition coefficient-Lewis basicity correlation in four dioxycyclobutenedion-bridged novel ball-type phthalocyanines, Synthetic Metals, C Vol. 212 25-30.

[67] McKeown, N.B., (1998). Phthalocyanine materials: synthesis, structure and function, Cambridge university press,

[68] Barut, B. and Demirbaş, Ü. (2020). Synthesis, anti-cholinesterase, α-glucosidase inhibitory, antioxidant and DNA nuclease properties of non-peripheral triclosan substituted metal-free, copper (II), and nickel (II) phthalocyanines, Journal of Organometallic Chemistry, C Vol. 923 121423.

[69] Gorduk, O., Gencten, M., Gorduk, S., Sahin, M., and Sahin, Y. (2021). Electrochemical fabrication and supercapacitor performances of metallo phthalocyanine/functionalized-multiwalled carbon nanotube/polyaniline modified hybrid electrode materials, Journal of Energy Storage, C Vol. 33 102049.

[70] Abuelwafa, A.A., Elnobi, S., Yamada, I., Shibata, N., and Soga, T. (2022). Studying the linear and nonlinear optical properties of trifluoroethoxy-coated zinc phthalocyanine ((4TFEO) 4-ZnPc) thin films, Optical Materials, C Vol. 123 111850.

[71] Koçyiğit, Ü.M., Taslimi, P., Tüzün, B., Yakan, H., Muğlu, H., and Güzel, E. (2022). 1, 2, 3-Triazole substituted phthalocyanine metal complexes as potential inhibitors for anticholinesterase and antidiabetic enzymes with molecular docking studies, Journal of Biomolecular Structure and Dynamics, C Vol. 40 (10), pp: 4429-4439.

[72] Klyamer, D., Bonegardt, D., and Basova, T. (2021). Fluoro-substituted metal phthalocyanines for active layers of chemical sensors, Chemosensors, C Vol. 9 (6), pp: 133.

[73] Güngör, S., Taşaltın, C., Gürol, İ., Baytemir, G., Karakuş, S., and Taşaltın, N. (2022). Copper phthalocyanine-borophene nanocomposite-based non-enzymatic electrochemical urea biosensor, Applied Physics A, C Vol. 128 (1), pp: 89.

[74] Ağırtaş, M.S., Altındal, A., Salih, B., Saydam, S., and Bekaroğlu, Ö. (2011). Synthesis, characterization, and electrochemical and electrical properties of novel mono and ball-type metallophthalocyanines with four 9, 9-bis (4-hydroxyphenyl) fluorene, Dalton Transactions, C Vol. 40 (13), pp: 3315-3324.

[75] Huang, C.-X., Li, G., Yang, L.-M., and Ganz, E. (2020). Ammonia synthesis using single-atom catalysts based on two-dimensional organometallic metal phthalocyanine monolayers under ambient conditions, ACS Applied Materials & Interfaces, C Vol. 13 (1), pp: 608-621.

[76] Kim, Y., Kim, D., Lee, J., Lee, L.Y.S., and Ng, D.K. (2021). Tuning the electrochemical properties of polymeric cobalt phthalocyanines for efficient water splitting, Advanced Functional Materials, C Vol. 31 (41), pp: 2103290.

[77] Yuan, J., Chen, S., Zhang, Y., Li, R., Zhang, J., and Peng, T. (2022). Structural regulation of coupled phthalocyanine–porphyrin covalent organic frameworks to highly active and selective electrocatalytic CO2 reduction, Advanced Materials, C Vol. 34 (30), pp: 2203139.

[78] Schmidt, A.M. and Calvete, M.J. (2021). Phthalocyanines: an old dog can still have new (photo) tricks!, Molecules, C Vol. 26 (9), pp: 2823.

[79] King, B., Melville, O.A., Rice, N.A., Kashani, S., Tonnelé, C., Raboui, H., Swaraj, S., Grant, T.M., McAfee, T., and Bender, T.P. (2020). Silicon Phthalocyanines for n-Type Organic Thin-Film Transistors: Development of Structure–Property Relationships, ACS Applied Electronic Materials, C Vol. 3 (1), pp: 325-336.

[80] Ouedraogo, S., Meunier-Prest, R., Kumar, A., Bayo-Bangoura, M., and Bouvet, M. (2020). Modulating the electrical properties of organic heterojunction devices based on phthalocyanines for ambipolar sensors, ACS sensors, C Vol. 5 (6), pp: 1849-1857.

[81] Carobeli, L.R., Meirelles, L.E.d.F., Damke, G.M., Damke, E., Souza, M.V.d., Mari, N.L., Mashiba, K.H., Shinobu-Mesquita, C.S., Souza, R.P., and Silva, V.R.d. (2021). Phthalocyanine and its formulations: a promising photosensitizer for cervical cancer phototherapy, Pharmaceutics, C Vol. 13 (12), pp: 2057.

[82] Ayaz, F., Yetkin, D., Yüzer, A., Demircioğlu, K., and Ince, M. (2022). Non-canonical anti-cancer, anti-metastatic, anti-angiogenic and immunomodulatory PDT potentials of water soluble phthalocyanine derivatives with imidazole groups and their intracellular mechanism of action, Photodiagnosis and Photodynamic Therapy, C Vol. 39 103035.

[83] Taslimi, P., Türkan, F., Güngördü Solğun, D., Aras, A., Erden, Y., Celebioglu, H.U., Tuzun, B., Ağırtaş, M.S., Günay, S., and Gulcin, I. (2022). Metal contained Phthalocyanines with 3, 4-Dimethoxyphenethoxy substituents: their anticancer, antibacterial activities and their inhibitory effects on some metabolic enzymes with molecular docking studies, Journal of Biomolecular Structure and Dynamics, C Vol. 40 (7), pp: 2991-3002.

[84] Nazeri, M.T., Javanbakht, S., Nabi, M., and Shaabani, A. (2022). Copper phthalocyanine-conjugated pectin via the Ugi four-component reaction: An efficient catalyst for CO2 fixation, Carbohydrate polymers, C Vol. 283 119144.

[85] Yıldız, B., Arslan, B.S., Güzel, E., Nebioğlu, M., Menges, N., Şişman, İ., and Şener, M.K. (2021). Non-aggregating zinc phthalocyanine sensitizer with bulky diphenylphenoxy donor groups and pyrazole-3-carboxylic acid anchoring group for coadsorbent-free dye-sensitized solar cells, Solar Energy, C Vol. 226 173-179.

[86] Wu, F., Yue, L., Cheng, K., Chen, J., Wong, K.-L., Wong, W.-K., and Zhu, X. (2020). Facile preparation of phthalocyanine-based nanodots for photoacoustic imaging and photothermal cancer therapy in vivo, ACS Biomaterials Science & Engineering, C Vol. 6 (9), pp: 5230-5239.

[87] Cranston, R.R., Vebber, M.r.C., Berbigier, J.n.F., Rice, N.A., Tonnelé, C., Comeau, Z.J., Boileau, N.T., Brusso, J.L., Shuhendler, A.J., and Castet, F.d.r. (2020). Thin-film engineering of solution-processable n-type silicon phthalocyanines for organic thin-film transistors, ACS Applied Materials & Interfaces, C Vol. 13 (1), pp: 1008-1020.

[88] Yue, Z., Ou, C., Ding, N., Tao, L., Zhao, J., and Chen, J. (2020). Advances in metal phthalocyanine based carbon composites for electrocatalytic CO2 reduction, ChemCatChem, C Vol. 12 (24), pp: 6103-6130.

[89] Kulu, I., Mantareva, V., Kussovski, V., Angelov, I., and Durmuş, M. (2022). Effects of metal ion in cationic Pd (II) and Ni (II) phthalocyanines on physicochemical and photodynamic inactivation properties, Journal of Molecular Structure, C Vol. 1247 131288.

[90] Matsuo, Y., Ogumi, K., Jeon, I., Wang, H., and Nakagawa, T. (2020). Recent progress in porphyrin- and phthalocyanine-containing perovskite solar cells, RSC advances, C Vol. 10 (54), pp: 32678-32689.

[91] Gürek, A.G., Sarıogulları, H., and Sengul, I.F. Comparative Study on Sensing and Optical Properties of Carbazole Linked Novel Zinc (Ii) and Cobalt (Ii) Phthalocyanines, Available at SSRN 4163894, C Vol.

[92] Praats, R., Käärik, M., Kikas, A., Kisand, V., Aruväli, J., Paiste, P., Merisalu, M., Leis, J., Sammelselg, V., and Zagal, J.H. (2020). Electrocatalytic oxygen reduction reaction on iron phthalocyanine-modified carbide-derived carbon/carbon nanotube composite electrocatalysts, Electrochimica Acta, C Vol. 334 135575.

[93] Latiff, N.M., Fu, X., Mohamed, D.K., Veksha, A., Handayani, M., and Lisak, G. (2020). Carbon based copper (II) phthalocyanine catalysts for electrochemical CO2 reduction: Effect of carbon support on electrocatalytic activity, Carbon, C Vol. 168 245-253.

[94] Yuen, A.P., Jovanovic, S.M., Hor, A.-M., Klenkler, R.A., Devenyi, G.A., Loutfy, R.O., and Preston, J.S. (2012). Photovoltaic properties of M-phthalocyanine/fullerene organic solar cells, Solar Energy, C Vol. 86 (6), pp: 1683-1688.

[95] Reji, R.P., Marappan, G., Sivalingam, Y., and Surya, V.J. (2022). VOCs adsorption induced surface potential changes on phthalocyanines: A combined experimental and theoretical approach towards food freshness monitoring, Materials Letters, C Vol. 306 130945.

[96] Ribeiro, C.P. and Lourenco, L.M. (2021). Overview of cationic phthalocyanines for effective photoinactivation of pathogenic microorganisms, Journal of Photochemistry and Photobiology C: Photochemistry Reviews, C Vol. 48 100422.

[97] de la Torre, G., Claessens, C.G., and Torres, T. (2007). Phthalocyanines: old dyes, new materials. Putting color in nanotechnology, Chemical Communications, C Vol. (20), pp: 2000-2015.

[98] Li, G., Lian, Z., Wan, Z., Liu, Z., Qian, J., Deng, Y., Zhang, S., and Zhong, Q. (2022). Efficient photothermal-assisted photocatalytic NO removal on molecular cobalt phthalocyanine/Bi2WO6 Z-scheme heterojunctions by promoting charge transfer and oxygen activation, Applied Catalysis B: Environmental, C Vol. 317 121787.

[99] Dahlen, M.A. (1939). The phthalocyanines a new class of synthetic pigments and dyes, Industrial & Engineering Chemistry, C Vol. 31 (7), pp: 839-847.

[100] Lessard, B.H. (2021). The rise of silicon phthalocyanine: from organic photovoltaics to organic thin film transistors, ACS Applied Materials & Interfaces, C Vol. 13 (27), pp: 31321-31330.

[101] Kenyon, R., Ink jet printing, in Chemistry and technology of printing and imaging systems1996, Springer. p. 113-138.

[102] Weiss, D.S. (2022). Organic Photoconductors: Photogeneration, Transport, and Applications in Printing, Photoconductivity and Photoconductive Materials: Fundamentals, Techniques and Applications, C Vol. 1 275-338.

[103] Weiss, D.S. (2016). The History and Development of Organic Photoconductors for Electrophotography, Journal of Imaging Science & Technology, C Vol. 60 (3), pp.

[104] Kumar, A., Mejjati, N.A., Meunier-Prest, R., Krystianiak, A., Heintz, O., Lesniewska, E., Devillers, C.H., and Bouvet, M. (2022). Tuning of interfacial charge transport in polyporphine/phthalocyanine heterojunctions by molecular geometry control for an efficient gas sensor, Chemical Engineering Journal, C Vol. 429 132453.

[105] Bıyıklıoğlu, Z. (2013). Electropolymerizable non-ionic and quaternized ionic titanium (IV) phthalocyanines and their electrochemistry, Dyes and Pigments, C Vol. 99 (3), pp: 727-732.

[106] Britannica, E., (2008). Britannica concise encyclopedia, Encyclopaedia Britannica, Inc.,

[107] Hohnholz, D., Steinbrecher, S., and Hanack, M. (2000). Applications of phthalocyanines in organic light emitting devices, Journal of Molecular Structure, C Vol. 521 (1-3), pp: 231-237.

[108] Ricciarelli, D., Meggiolaro, D., Ambrosio, F., and De Angelis, F. (2020). Instability of tin iodide perovskites: bulk p-doping versus surface tin oxidation, ACS Energy Letters, C Vol. 5 (9), pp: 2787-2795.

[109] Pashaei, B., Karimi, S., Shahroosvand, H., Abbasi, P., Pilkington, M., Bartolotta, A., Fresta, E., Fernandez-Cestau, J., Costa, R.D., and Bonaccorso, F. (2019). Polypyridyl ligands as a versatile platform for solid-state light-emitting devices, Chemical Society Reviews, C Vol. 48 (19), pp: 5033-5139.

[110] Nazeri, M.T., Javanbakht, S., Ramezani, M., and Shaabani, A. (2022). A facile and green synthesis of cobalt phthalocyanine-conjugated multiwall carbon nanotube by the Ugi reaction: As an efficient CO2 fixation catalyst, Journal of the Taiwan Institute of Chemical Engineers, C Vol. 136 104428.

[111] Kuzmina, E.A., Dubinina, T.V., Vasilevsky, P.N., Saveliev, M.S., Gerasimenko, A.Y., Borisova, N.E., and Tomilova, L.G. (2021). Novel octabromo-substituted lanthanide (III) phthalocyanines–Prospective compounds for nonlinear optics, Dyes and Pigments, C Vol. 185 108871.

[112] Borges-Martinez, M., Montenegro-Pohlhammer, N., Zhang, X., Galvez-Aranda, D.E., Ponce, V., Seminario, J.M., and Cardenas-Jiron, G. (2022). Fullerene binding effects in Al (III)/Zn (II) Porphyrin/Phthalocyanine photophysical properties and charge transport, Spectrochimica Acta Part A: Molecular and Biomolecular Spectroscopy, C Vol. 269 120740.

[113] Ng, K.K. and Zheng, G. (2015). Molecular interactions in organic nanoparticles for phototheranostic applications, Chemical reviews, C Vol. 115 (19), pp: 11012-11042.

[114] Lebedeva, N.S., Gubarev, Y.A., Vyugin, A.I., and Koifman, O.I. (2015). Investigation of interaction between alkoxy substituted phthalocyanines with different lengths of alkyl residue and bovine serum albumin, Journal of Luminescence, C Vol. 166 71-76.

[115] Farajzadeh, N., Atmaca, G.Y., Erdoğmuş, A., and Koçak, M.B. (2021). Comparatively singlet oxygen efficiency by sono-photochemical and photochemical studies of new lutetium (III) phthalocyanines, Dyes and Pigments, C Vol. 190 109325.

[116] Göksel, M., Durmuş, M., and Atilla, D. (2017). Synthesis and photophysicochemical properties of a set of asymmetrical peptide conjugated zinc (II) phthalocyanines bearing different fluorophore units, Inorganica Chimica Acta, C Vol. 456 95-104.

[117] Yurttaş, A.G., Sevim, A.M., Çınar, K., Atmaca, G.Y., Erdoğmuş, A., and Gül, A. (2022). The effects of zinc (II) phthalocyanine photosensitizers on biological activities of epitheloid cervix carcinoma cells and precise determination of absorbed fluence at a specific wavelength, Dyes and Pigments, C Vol. 198 110012.

[118] Yanık, H., Göksel, M., Yeşilot, S., and Durmuş, M. (2016). Novel phthalocyanine–BODIPY conjugates and their photophysical and photochemical properties, Tetrahedron Letters, C Vol. 57 (26), pp: 2922-2926.

[119] Zielichowska, A., Saczko, J., Garbiec, A., Dubińska-Magiera, M., Rossowska, J., Surowiak, P., Choromańska, A., Daczewska, M., Kulbacka, J., and Lage, H. (2015). The photodynamic effect of far-red range phthalocyanines (AlPc and Pc green) supported by electropermeabilization in human gastric adenocarcinoma cells of sensitive and resistant type, Biomedicine & Pharmacotherapy, C Vol. 69 145-152.

[120] Atmaca, G.Y., Karanlık, C.C., and Erdoğmuş, A. (2021). Measurement of improved singlet oxygen generations of indium chloride phthalocyanines by comparatively sono-photochemical and photochemical studies, Dyes and Pigments, C Vol. 194 109630.

[121] Macdonald, I.J. and Dougherty, T.J. (2001). Basic principles of photodynamic therapy, Journal of Porphyrins and Phthalocyanines, C Vol. 5 (02), pp: 105-129.

[122] Josefsen, L.B. and Boyle, R.W. (2008). Photodynamic therapy and the development of metal-based photosensitisers, Metal-based drugs, C Vol. 2008.

[123] Güzel, E., Günsel, A., Bilgiçli, A.T., Atmaca, G.Y., Erdoğmuş, A., and Yarasir, M.N. (2017). Synthesis and photophysicochemical properties of novel thiadiazole-substituted zinc (II), gallium (III) and silicon (IV) phthalocyanines for photodynamic therapy, Inorganica Chimica Acta, C Vol. 467 169-176.

[124] Maree, M.D., (1998). Synthesis and characterisation of a selection of phthalocyanines covalently bonded to water-soluble polymers and a ferrocenyl fragment, University of the Free State. Ph.D. thesis,

[125] Ishii, K. (2012). Functional singlet oxygen generators based on phthalocyanines, Coordination Chemistry Reviews, C Vol. 256 (15-16), pp: 1556-1568.

[126] Atmaca, G.Y., Aksel, M., Keskin, B., Bilgin, M.D., and Erdoğmuş, A. (2021). The photo-physicochemical properties and in vitro sonophotodynamic therapy activity of Di-axially substituted silicon phthalocyanines on PC3 prostate cancer cell line, Dyes and Pigments, C Vol. 184 108760.

[127] Terekhov, D.S., Nolan, K.J., McArthur, C.R., and Leznoff, C.C. (1996). Synthesis of 2, 3, 9, 10, 16, 17, 23, 24-octaalkynylphthalocyanines and the effects of concentration and temperature on their 1H NMR spectra, The Journal of organic chemistry, C Vol. 61 (9), pp: 3034-3040.

[128] Urbani, M., Ragoussi, M.-E., Nazeeruddin, M.K., and Torres, T. (2019). Phthalocyanines for dye-sensitized solar cells, Coordination Chemistry Reviews, C Vol. 381 1-64.

[129] de la Torre, G., Claessens, C.G., and Torres, T. (2000). Phthalocyanines: The need for selective synthetic approaches, European Journal of Organic Chemistry, C Vol. 2000 (16), pp: 2821-2830.

[130] Saraçoğlu, H., Güntepe, F., Yüksektepe, Ç., Çalışkan, N., and Saydam, S. (2011). Experimental and Ab initio computational studies on 4-(Benzhydryloxy) phthalonitrile, Molecular Crystals and Liquid Crystals, C Vol. 537 (1), pp: 111-127.

[131] Tylleman, B., Gbabode, G., Amato, C., Buess-Herman, C., Lemaur, V., Cornil, J., Gomez Aspe, R., Geerts, Y.H., and Sergeyev, S. (2009). Metal-free phthalocyanines bearing eight alkylsulfonyl substituents: Design, synthesis, electronic structure, and mesomorphism of new electron-deficient mesogens, Chemistry of materials, C Vol. 21 (13), pp: 2789-2797.

[132] Sorokin, A.B. (2013). Phthalocyanine metal complexes in catalysis, Chemical reviews, C Vol. 113 (10), pp: 8152-8191.

[133] Nemykin, V.N. and Lukyanets, E.A. (2010). Synthesis of substituted phthalocyanines, ARKIVOC: Online Journal of Organic Chemistry, C Vol.

[134] Raipiu, V., Wagner, L., R Raipiu, A., Ardeleanu, P., Amariupei, V., and Sorescu, A.-A. (2008). Synthesis and characterization of some phthalic acid derivatives precursors for phthalocyanine chromogens, Rev. Chim.(Bucharest, Rom.), C Vol. 59 973-978.

[135] De la Torre, G., Bottari, G., Hahn, U., and Torres, T. (2010). Functional phthalocyanines: synthesis, nanostructuration, and electro-optical applications, Functional Phthalocyanine Molecular Materials, C Vol. 1-44.

[136] Hunger, K., (2007). Industrial dyes: chemistry, properties, applications, John Wiley & Sons,

[137] Spesia, M.B. and Durantini, E.N. (2022). Evolution of phthalocyanine structures as photodynamic agents for bacteria inactivation, The Chemical Record, C Vol. 22 (4), pp: e202100292.

[138] Kingston, H.J., (2005). Polymers of Intrinsic Microporosity: Synthesis and Catalytic Properties, The University of Manchester (United Kingdom),

[139] Yakan, H., Çavuş, M.S., Güzel, E., Arslan, B.S., Bakır, T., and Muğlu, H. (2020). Phthalocyanines including 2-mercaptobenzimidazole analogs: synthesis, spectroscopic characteristics, quantum-chemical studies on the relationship between electronic and antioxidant properties, Journal of Molecular Structure, C Vol. 1202 127259.

[140] Hurley, T.J., Robinson, M.A., and Trotz, S.I. (1967). Complexes derived from 1, 3-diiminoisoindoline-containing ligands. II. Stepwise formation of nickel phthalocyanine, Inorganic chemistry, C Vol. 6 (2), pp: 389-392.

[141] Yang, C.H. and Chang, C.-t. (1982). Complexes derived from phthalonitrile. The intermediates to nickel phthalocyaninate, Journal of the Chemical Society, Dalton Transactions, C Vol. (12), pp: 2539-2540.

[142] Baumann, F., Bienert, B., Rösch, G., Vollmann, H., and Wolf, W. (1956). Isoindolenine als Zwischenprodukte der Phthalocyanin-Synthese, Angewandte Chemie, C Vol. 68 (4), pp: 133-150.

[143] Leznoff, C.C., Greenberg, S., Khouw, B., and Lever, A. (1987). The syntheses of mono-and disubstituted phthalocyanines using a dithioimide, Canadian journal of chemistry, C Vol. 65 (8), pp: 1705-1713.

[144] Wu, X., Vargas, M., Nayak, S., Lotrich, V., and Scoles, G. (2001). Towards extending the applicability of density functional theory to weakly bound systems, The Journal of Chemical Physics, C Vol. 115 (19), pp: 8748-8757.

[145] Ahmetali, E., Yıldız, B., Ahi, E.E., Durmuş, M., and Şener, M.K. (2022). Synthesis, photophysical and photochemical properties of unsymmetrical zinc (II) phthalocyanines bearing 8-hydroxyquinoline unit, Polyhedron, C Vol. 226 116111.

[146] Uchida, H., Reddy, P.Y., Nakamura, S., and Toru, T. (2003). Novel efficient preparative method for phthalocyanines from phthalimides and phthalic anhydride with HMDS, The Journal of organic chemistry, C Vol. 68 (22), pp: 8736-8738.

[147] Shaabani, A., Maleki-Moghaddam, R., Maleki, A., and Rezayan, A. (2007). Microwave assisted synthesis of metal-free phthalocyanine and metallophthalocyanines, Dyes and Pigments, C Vol. 74 (2), pp: 279-282.

[148] Tekintas, K., Kesmez, Ö., Bekircan, O., and Saka, E.T. (2022). Preparation, characterization and photocatalytic activity of novel 1, 2, 4-triazole based Cu (II) and Zn (II) phthalocyanines modified TiO2 nanoparticles, Journal of Molecular Structure, C Vol. 1248 131405.

[149] Farahmand, S., Ghiaci, M., and Razavizadeh, J.S. (2019). Copper phthalocyanine as an efficient and reusable heterogeneous catalyst for direct hydroxylation of benzene to phenol under mild conditions, Inorganica Chimica Acta, C Vol. 484 174-179.

[150] Konarev, D.V., Khasanov, S.S., and Lyubovskaya, R.N. (2014). Fullerene complexes with coordination assemblies of metalloporphyrins and metal phthalocyanines, Coordination Chemistry Reviews, C Vol. 262 16-36.

[151] Karabach, Y.Y., Kopylovich, M.N., Luzyanin, K.V., da Silva, M.F.C.G., Kukushkin, V.Y., and Pombeiro, A.J. (2017). Expanding the family of substituted-at-core nickel (II) phthalocyanines, Inorganica Chimica Acta, C Vol. 455 696-700.

[152] Demirbaş, Ü., Menteşe, E., Sökmen, B.B., Bayrak, R., and Akçay, H.T. (2018). Synthesis of some new Methoxy Bridged Benzimidazolyl-Substituted phthalocyanines as potent inhibitors of urease, Journal of Organometallic Chemistry, C Vol. 873 86-90.

[153] Bekaroğlu, Ö., (2010). Functional phthalocyanine molecular materials, Springer Science & Business Media,

[154] Jiang, J., (2010). Functional phthalocyanine molecular materials, Springer,

[155] Çimen, Y., Ermiş, E., Dumludağ, F., Özkaya, A.R., Salih, B., and Bekaroğlu, Ö. (2014). Synthesis, characterization, electrochemistry and VOC sensing properties of novel ball-type dinuclear metallophthalocyanines, Sensors and Actuators B: Chemical, C Vol. 202 1137-1147.

[156] Yabaş, E., Sülü, M., Dumludağ, F., Salih, B., and Bekaroğlu, Ö. (2018). Imidazole octasubstituted novel mono and double-decker phthalocyanines: Synthesis, characterization, electrical and gas sensing properties, Polyhedron, C Vol. 153 51-63.

[157] Li, J., Gryko, D., Dabke, R.B., Diers, J.R., Bocian, D.F., Kuhr, W.G., and Lindsey, J.S. (2000). Synthesis of thiol-derivatized europium porphyrinic triple-decker sandwich complexes for multibit molecular information storage, The Journal of organic chemistry, C Vol. 65 (22), pp: 7379-7390.

[158] Lu, G., Li, J., Jiang, X., Ou, Z., and Kadish, K.M. (2015). Europium Triple-Decker Complexes Containing Phthalocyanine and Nitrophenyl–Corrole Macrocycles, Inorganic chemistry, C Vol. 54 (18), pp: 9211-9222.

[159] Janczak, J., Kubiak, R., Richter, J., and Fuess, H. (1999). Bismuth triple-decker phthalocyanine: synthesis and structure, Polyhedron, C Vol. 18 (21), pp: 2775-2780.

[160] Lu, G., Li, J., Yan, S., He, C., Shi, M., Zhu, W., Ou, Z., and Kadish, K.M. (2015). Self-assembled organic nanostructures and nonlinear optical properties of heteroleptic corrole–phthalocyanine europium triple-decker complexes, Dyes and Pigments, C Vol. 121 38-45.

[161] Torres, T. (2006). From subphthalocyanines to subporphyrins, Angewandte Chemie International Edition, C Vol. 45 (18), pp: 2834-2837.

[162] Morse, G.E. and Bender, T.P. (2012). Boron subphthalocyanines as organic electronic materials, ACS Applied Materials & Interfaces, C Vol. 4 (10), pp: 5055-5068.

[163] Claessens, C.G., González-Rodríguez, D., and Torres, T. (2002). Subphthalocyanines: singular nonplanar aromatic compounds synthesis, reactivity, and physical properties, Chemical reviews, C Vol. 102 (3), pp: 835-854.

[164] Claessens, C.G., Gonzalez-Rodriguez, D., Rodriguez-Morgade, M.S., Medina, A., and Torres, T. (2014). Subphthalocyanines, subporphyrazines, and subporphyrins: Singular nonplanar aromatic systems, Chemical reviews, C Vol. 114 (4), pp: 2192-2277.

[165] Furuyama, T., Ogura, Y., Yoza, K., and Kobayashi, N. (2012). Superazaporphyrins: Meso-Pentaazapentaphyrins and One of Their Low-Symmetry Derivatives, Angewandte Chemie International Edition, C Vol. 51 (44), pp: 11110-11114.

[166] Furuyama, T., Sato, T., and Kobayashi, N. (2015). A bottom-up synthesis of antiaromatic expanded phthalocyanines: Pentabenzotriazasmaragdyrins, ie Norcorroles of superphthalocyanines, Journal of the American Chemical Society, C Vol. 137 (43), pp: 13788-13791.

[167] McKeown, N.B. (2000). Phthalocyanine-containing polymers, Journal of Materials Chemistry, C Vol. 10 (9), pp: 1979-1995.

[168] Achar, B., Fohlen, G., and Parker, J. (1982). Phthalocyanine polymers. II. Synthesis and characterization of some metal phthalocyanine sheet oligomers, Journal of Polymer Science: Polymer Chemistry Edition, C Vol. 20 (7), pp: 1785-1790.

[169] Kantekin, H., Dilber, G., and Bıyıklıoğlu, Z. (2008). A new polymeric phthalocyanine containing 16-membered tetrathia macrocyclic moieties by microwave irradiation: Synthesis and characterization, Journal of Organometallic Chemistry, C Vol. 693 (6), pp: 1038-1042.

[170] Kantar, C., Ağar, E., and Şaşmaz, S. (2008). The microwave-assisted synthesis and characterization of novel polymeric phthalocyanines containing resorcinarene, Dyes and Pigments, C Vol. 77 (3), pp: 487-492.

[171] Kantekin, H. and Bıyıklıoğlu, Z. (2008). Synthesis and characterization of new polymeric phthalocyanines substituted with pyridine through methyleneoxy bridges by microwave irradiation, Dyes and Pigments, C Vol. 77 (2), pp: 432-436.

[172] Kijo-Kleczkowska, A., Gnatowski, A., Szumera, M., Otwinowski, H., Kwiatkowski, D., and Suchecki, Ł. (2020). Effect of addition of coal sludge to polymeric material on thermal effects in analysis by TG/DTG/DSC methods. in E3S Web of Conferences. EDP Sciences.

[173] Gil, M., Podkościelna, B., and Mergo, P. (2017). TG/DTG/MS coupled methods for thermal analysis of new materials for optical fiber technology, Journal of International Scientific Publications: Materials, Methods and Technologies (Online), C Vol. 11 46-53.

[174] Grabowska, B., Skowron, M., and Kaczmarska, K. (2023). Polylactide Used as Filment in 3d Printing–Part 2: TG-DTG, DSC and DRIFT investigations, Journal of Casting & Materials Engineering, C Vol. 7 (4), pp: 41-48.

[175] Hajri, A., Touaiti, S., and Jamoussi, B. (2013). Preparation of Organic Zn-Phthalocyanine-Based Semiconducting Materials and Their Optical and Electrochemical Characterization, Advances in OptoElectronics, C Vol. 2013 (1), pp: 321563.

[176] Yabaş, E., Sülü, M., Dumludağ, F., Özkaya, A.R., Salih, B., and Bekaroğlu, Ö. (2012). Electrical and electrochemical properties of double-decker Lu (III) and Eu (III) phthalocyanines with four imidazoles and N-alkylated imidazoles, Polyhedron, C Vol. 42 (1), pp: 196-206.

[177] Attia, A.K., Ibrahim, M.M., and El-Ries, M.A.-N. (2013). Thermal analysis of some antidiabetic pharmaceutical compounds, Advanced pharmaceutical bulletin, C Vol. 3 (2), pp: 419.

# APPENDICES

## APPENDICES-1:

**Figure A 1.** The reaction of synthesized 4-nitrophthalimide.

**Figure A 2.** Filtration of 4-nitrophthalimide.

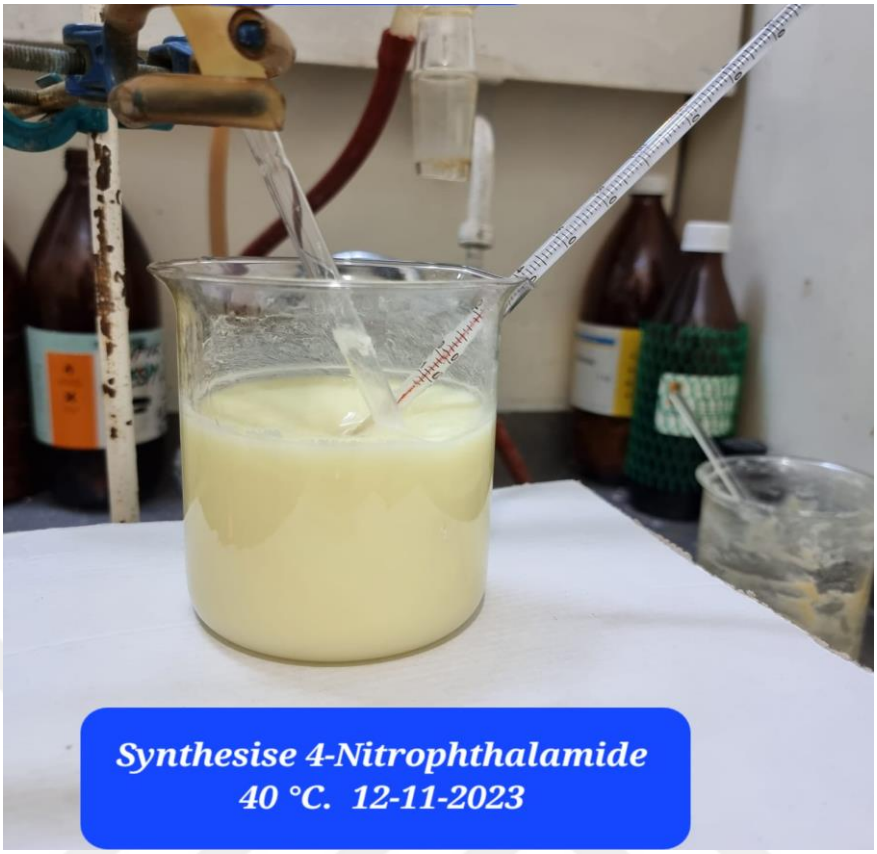


**Figure A 3.** Synthesize 4-Nitrophthalamide.

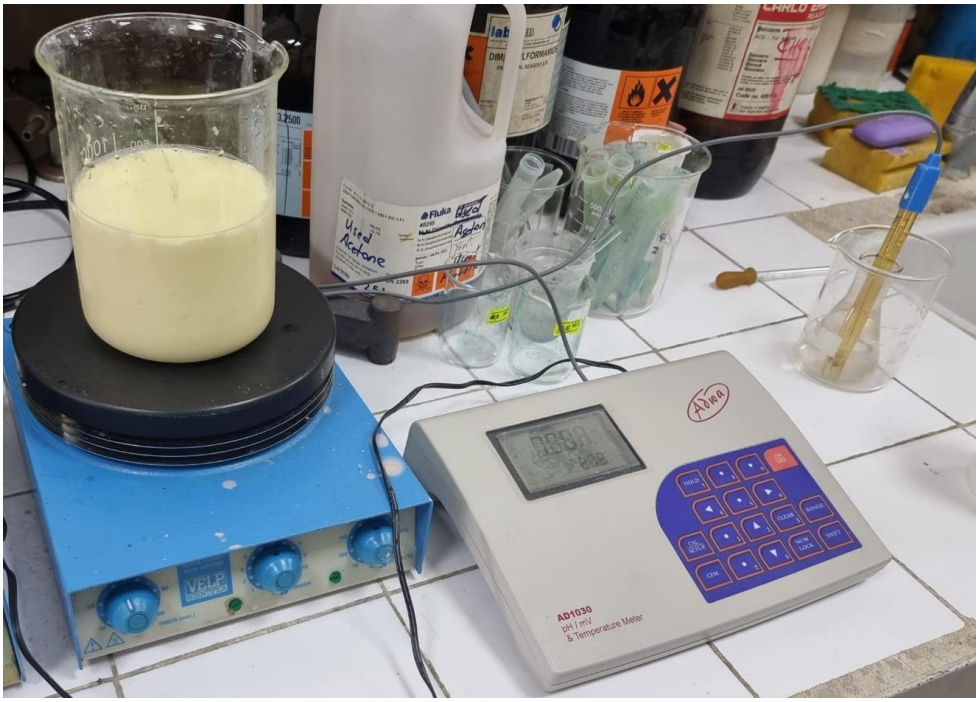


**Figure A 4.** Neutralization Mixture using PH Metter.

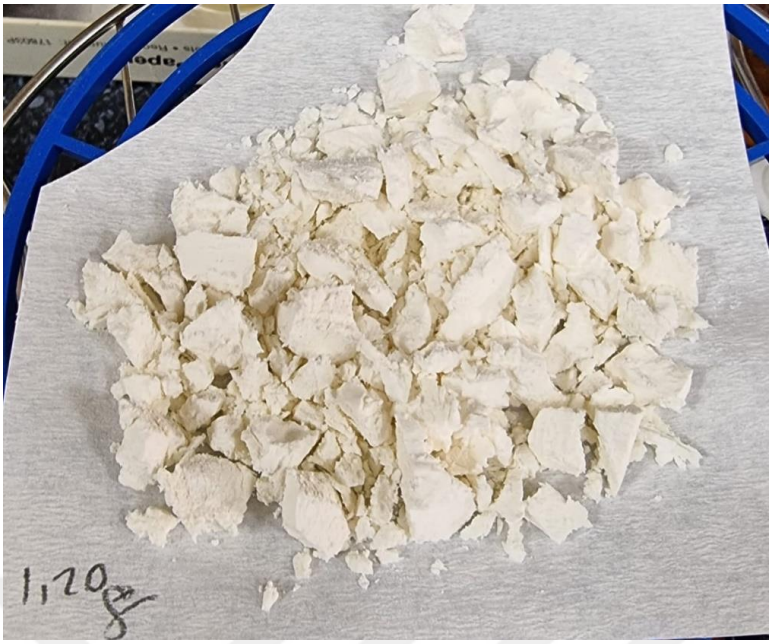


**Figure A 5.** 4- Nitrophthalonitrile result.


**Figure A 6.** Synthesize of Ligand 2-(4-(3,4- dicyanophenoxy)phenyl)acetamide.


**Figure A 7.** Continue reaction to synthesize CrPc and $H_2Pc$.


**Figure A 8.** Cooling down FePc and $H_2Pc$ complexes.

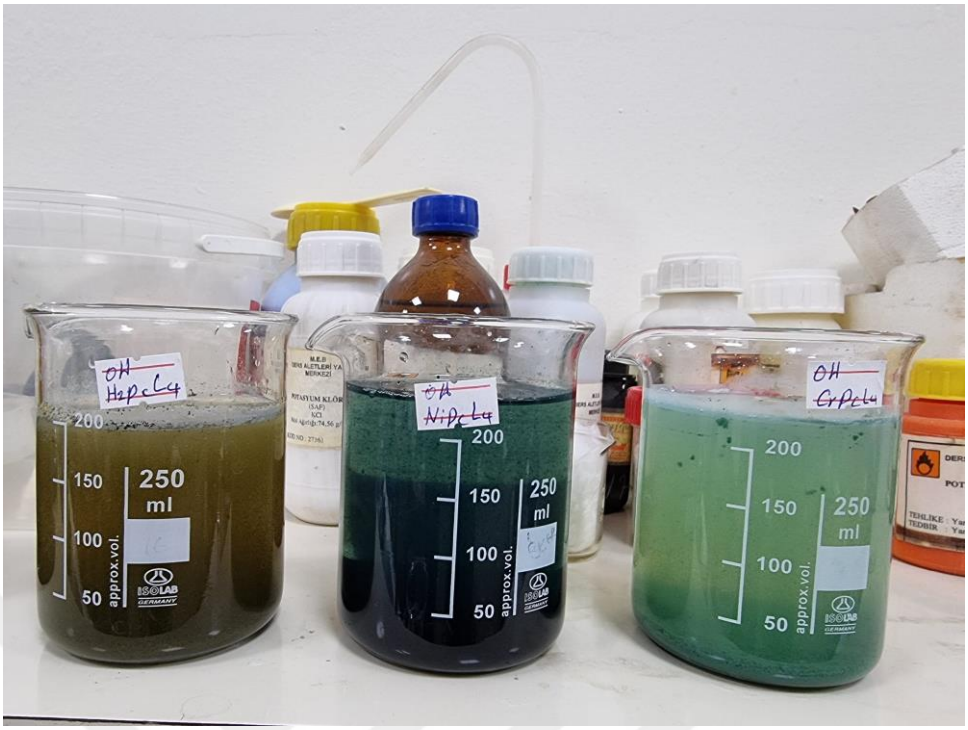


**Figure A 9.** Precipitating (CrPc, NiPc, $H_2Pc$) complexes in water.

**Figure A 10.** Part of samples ligand and Pc complexes.

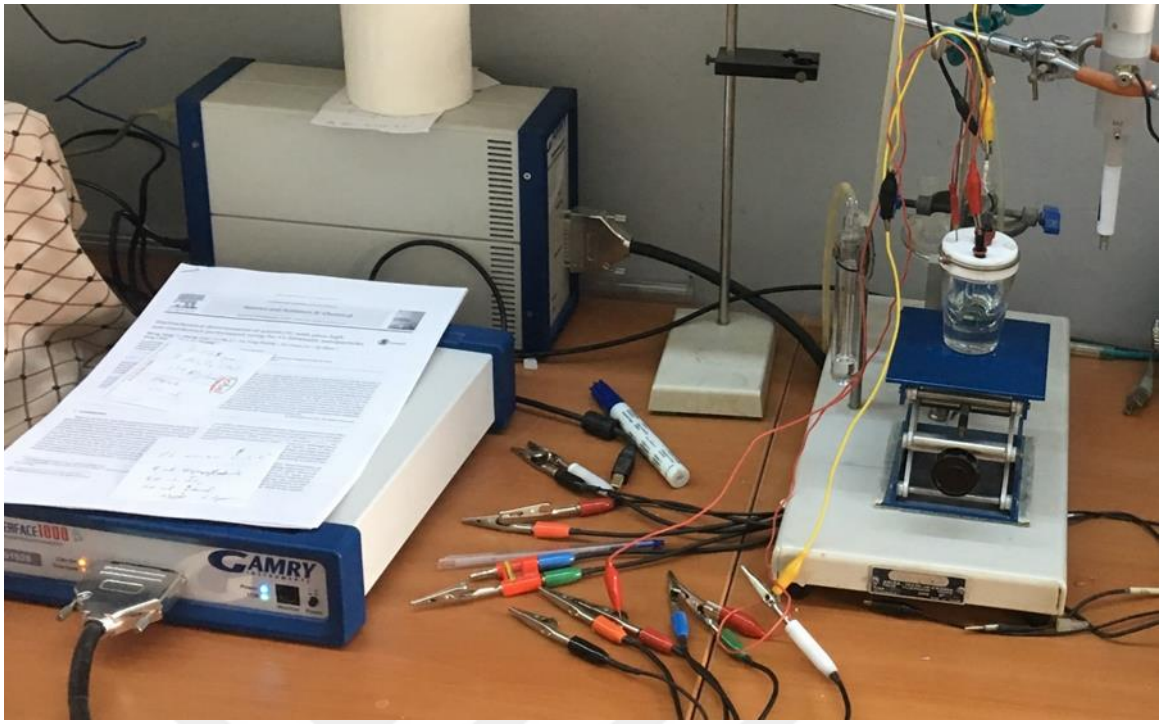


**Figure A 11.** The GAMRY instrumental to Voltametric analyzer (analysis CV and SWV).

**Figure A 12.** FT-IR Spectrophotometer, Perkin Elmer 1600.


**Figure A 13.** The UV visible spectrophotometer 1900 i.


**Figure A 14.** Pyris Diamond TG/DTA thermogravimetric/differential thermal analyzer.

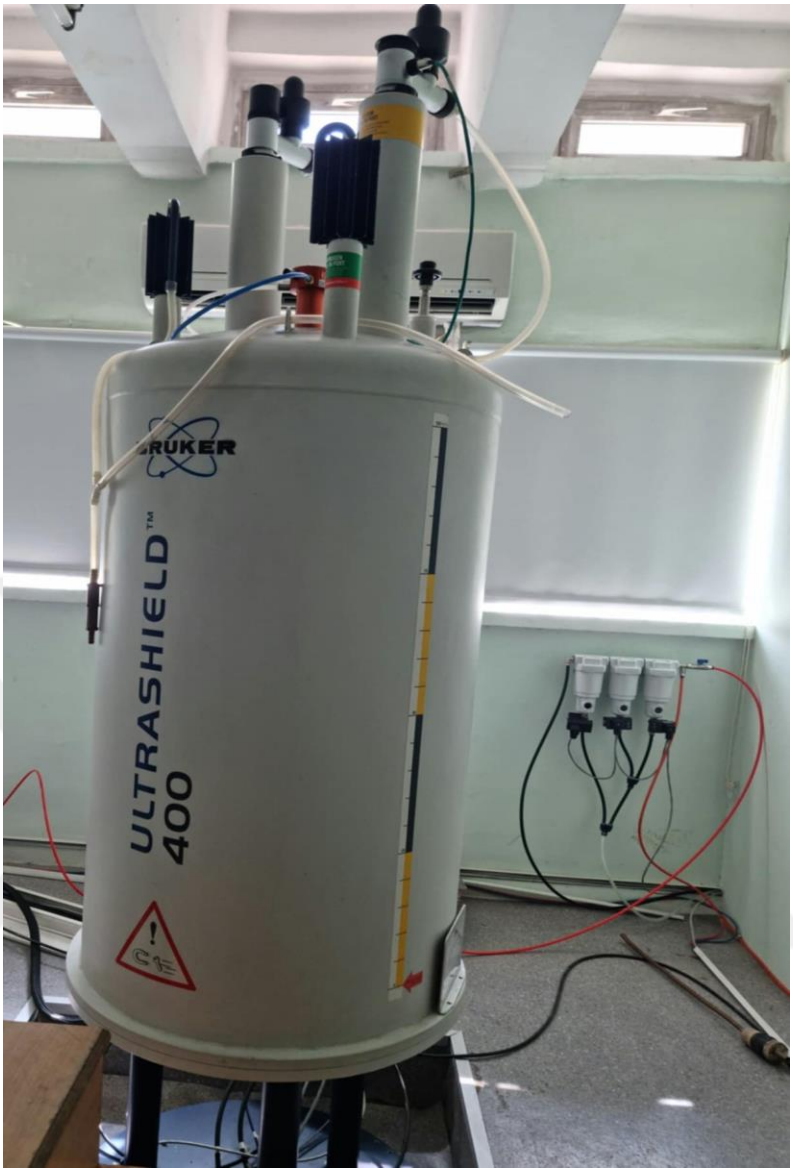


**Figure A 15.** Bruker advance III 400 MHz NMR spectrophotometer.

# CURRICULUM VITAE

**Othman Abdulrahman Hamad JUKL**

[redacted]

## ACADEMIC ACTIVITIES

**Paper:**

1. **Hamad, O.,** Kareem, R. O., & Kaygılı, O. (2023). Density Function Theory Study of the Physicochemical Characteristics of 2-nitrophenol. Journal of Physical Chemistry and Functional Materials, 6(1), 70-76.

2. **Hamad, O.** A., Kareem, R. O., & Omer, P. K. (2024). Properties, Characterization, and Application of Phthalocyanine and Metal Phthalocyanine. Journal of Chemical Reviews, 6(1).
3. **Jukl, O. A**. H., & Biryan, F. (2024). Synthesis of 4-Aminophenoxy Substituted Nickel Phthalocyanine Complex and Investigation of Electrochemical and Thermal Properties. MW Journal of Science, 1(2), 41-46.

**Proceedings:**

1. Participating in 7th International Conference on Physical Chemistry & Functional Materials 16-17 May 2024 Malatya Turgut Özal University Malatya / TÜRKİYE.
2. Participating in the 2nd International Palestra Scientific Research Congress on July 29-31, 2024, in Skopje, North Macedonia.